Trinity College Dublin
Coláiste na Tríonóide, Baile Átha Cliath
The University of Dublin

JURASSIC EVAPORITES AND DIAPIRISM ALONG THE SOUTHERN TANZANIAN CONTINENTAL MARGIN: IMPLICATIONS FOR PETROLEUM EXPLORATION

Maria Isabel Freitas da Silva Vucinic

A thesis submitted for the degree of Doctor of Philosophy

School of Natural Sciences

Department of Geology

2020

DECLARATION

I declare that this thesis has not been submitted as an exercise for a degree at this or any other university and it is entirely my own work.

I agree to deposit this thesis in the University's open access institutional repository or allow the library to do so on my behalf, subject to Irish Copyright Legislation and Trinity College Library conditions of use and acknowledgment.

_____

Maria Isabel Freitas da Silva Vucinic
2020

SUMMARY

One of the key issues for petroleum exploration along the entire Tanzanian margin is the extent of evaporite deposition and its diapirism. This leads to scenarios for the configuration and relative movement of conjugate fragments across East Africa. In Mandawa Basin, the separation from Africa provided restricted conditions for salt deposition in the Lower Jurassic, with the rise to continued deposition and sedimentation of anoxic marine shale and locally evaporites trigged by the evolution of the salt minibasin approximately in the Middle Jurassic.

In this study, the methodological approach of combining geological and geophysical techniques has been addressed to characterise the types of salt, the lithostratigraphy, and seismic sequences of the geological framework by variations through time in stratigraphy (source rocks) and structural geometry (salt diapirs). The provided legacy containing 2D seismic lines, geophysical well logs, well data were used as input data to re-access the onshore Mandawa salt basin. The workflow involved in importing the dataset, performed a quality check of the 2D seismic lines seismic attribute analysis horizon and fault interpretation, structural modelling, and depth conversion from the final 3D geocellular model from time to depth.

The identification of the lithological units has been carried out which helped to identify salt structures according to change in signal responses, lateral continuity, bedding sequences, and thickness surfaces. A well correlation in this thesis was performed resulting in seven zones defined in between the markers where four of them specifically may correlate to previous stratigraphic units proposed firstly by Shell in 1990 for the onshore Mandawa Basin: Mbuo Formation, Nondwa Formation, and Mtumbei Limestone Formation.

This study observed different types of salt of marine evaporite diapirism present in Mandawa Basin: halite, anhydrite and gypsum. Results in this study further suggest the existence of sequences of halite in most of the wells, such as Mbuo-1, Mihambia-1, East Lika-1, Mita Gamma-1, Mbate-1 and Mandawa-7. Another evaporite type as anhydrite salt has been identified interbedded with claystones and sandstones sediments in Milhambia-1 and East-Lika-1 wells. The salt in Mandawa Basin has been interpreted in this work as mostly autochthonous building up from the Lower Jurassic, below the

present-day shelf. In addition to the findings here, the appearance of an allochthonous detached salt sheet structure extending into the Lower Cretaceous strata in central Mandawa Basin suggests that the salt pillow originates from Upper Jurassic and with deposition during the Cretaceous.

The use of 2D restoration technique revealed that the salt layer and the overlapping layers had tabular geometry prior to extension followed by a rise of a diapir by reactive bearing to the formation of a graben associated with the extension of sedimentary overload.

Sequence stratigraphy analysis has also been carried out during this research according to the identification of reliable reflectors in conjunction with the well tops (markers) in the wells although poor quality in some areas was visible.

The 3D geocellular model shows the extensional block during the Lower Jurassic. A stratigraphic pinch out setting formed during restricted conditions triggered by the evolution of the mini-basin occurred approximately in the Middle Jurassic followed by a major Upper Jurassic transgression.

A lack of wells of the onshore Ruvuma Basin accessed in the present work poised ambitious to generate a detailed structural framework and a final model. Yet, in this thesis, a lithostratigraphy analysis was carried out making possible the characterisation of three horizons and two respective markers in a tentative equivalence of lithology and nomenclature from the Mandawa Basin with the Ruvuma Basin. Faults played a major control on sedimentation causing lateral changes. Continental clastic sandstones, marine shale siltstones interbedded with successions of non-deposition sandstones suggested transitional conditions during the Jurassic that widespread to three unconformity periods in the Lower Cretaceous. This work also presents a tentative well correlation based on well logs from one well in the Selous Basin. Five markers and respective seismic horizons have been named as the geological ages respectively with other studies.

CONFERENCE PRESENTATION

A work produced in this thesis has been presented to the scientific community during the course of this Ph.D. research as follows:

Vucinic, M.I.F.S. and Nicholas, C.J. (2019). The litho-stratigraphy and seismo-stratigraphy investigations along the Jurassic evaporites of the Tanzanian continental margin. European Geosciences Union General Assembly. Vienna, 2019 April.

ABBREVIATIONS

AAPG - American Association of Petroleum Geologists

AI – Acoustic Impedance

DFZ – Davie Fracture Zone

DT-E - Delta-T compressional after editing

EARS – East African Rift Systems

HST – High Stand Tract

LST – Low Stand Tract

m MD RT – meters Measure Depth Rotative Table

P-T conditions – Pressure and Temperature conditions

PSA - The Mandawa Production Sharing Agreement

RC – Reflection Coefficient

SEG - Society of Exploration Geophysicists

SSTVD – Subsea True Vertical Depth

STASS - Southern Trans-Africa Shear System

SWT – Seismic Well Tie

TDR – Time-Depth Relationship

TST – Transgressive Stand Tract

TOC – Total Organic Carbon

TVD – True Vertical Depth

VBM – Volume-Base Modelling

VOI – Volume of Interest

ACKNOWLEDGEMENT

I would like to express my sincere gratitude to my supervisor Dr. Christopher Nicholas for proposing this project where I could apply my professional expertise to academia. Chris has been supportive while also giving me space to undertake the research until the present form.

I am grateful to my sponsor, the Brazilian research program Science without Borders – CNPq created by the former president Dilma Rousseff.

Many thanks to my Confirmation Panel Professor Dr. David Chew and Professor Dr. Patrick Wyse Jackson for their suggestions conducting the research from the first stages.

This study would not have been accomplished without Schlumberger Company for providing the academic license for Petrel and PetroMod for the duration of this study.

I would like to thank Count Geophysics consultants who agreed to share the geophysical dataset from Dominion/TPDC, the technical discussions, and for the one day visit I had to the company's office in London.

Many thanks to my undergraduate professors, Sergio Citroni and Soraya Carelli, for their inputs in the last stages of the research.

Also, I want to thank Ms. Margaret Duncan (Mags) for all the positive support during the years we share the office in TTEC.

Many thanks to Trinity College Dublin, Geology Department technical and administrative staff so as my colleagues for their support and encouragement.

I want to thank the Dean of Graduate Studies for the granted an extension due to my maternity leave, also I am thankful to the Senior Tutor who helped me when I most needed a place for my son at TCD Day Nursery.

Finally, dedicated to the memory of my parents Ruth and Roberto, their encouragement in all the stages of my life; my parents-in-law, Miladinka and Bozidar, for their support from far but always present. My husband Luka for the kind and scientific support, insightful comments and suggestions, patience throughout the stages of this thesis. For the most important little person in my life, my dearest son Martin that had his big arrival during this fantastic Ph.D. years, thank you for showing me the meaning of life.

Table of Contents

List of Figures

LIST OF TABLES

CHAPTER 1

INTRODUCTION

The southern Tanzanian continental margin has been explored over the last 50 years. The Mandawa and Ruvuma basins of southern coastal Tanzania (Figure 1.1) record the pre-, syn- and post- Gondwana rift sedimentary fill both in outcrop, subsurface exploration wells, and seismic surveys. Whereas both basins are subject to active hydrocarbon exploration in the region due to the evidence of petroleum, both liquid and gaseous, evidenced by two gas discoveries and occurrence of oil seeps; the widespread Jurassic source rocks tend to be in the gas window (Nicholas *et al*. 2006; Nicholas *et al*. 2007, Hudson 2011; Hudson and Nicholas, 2014).

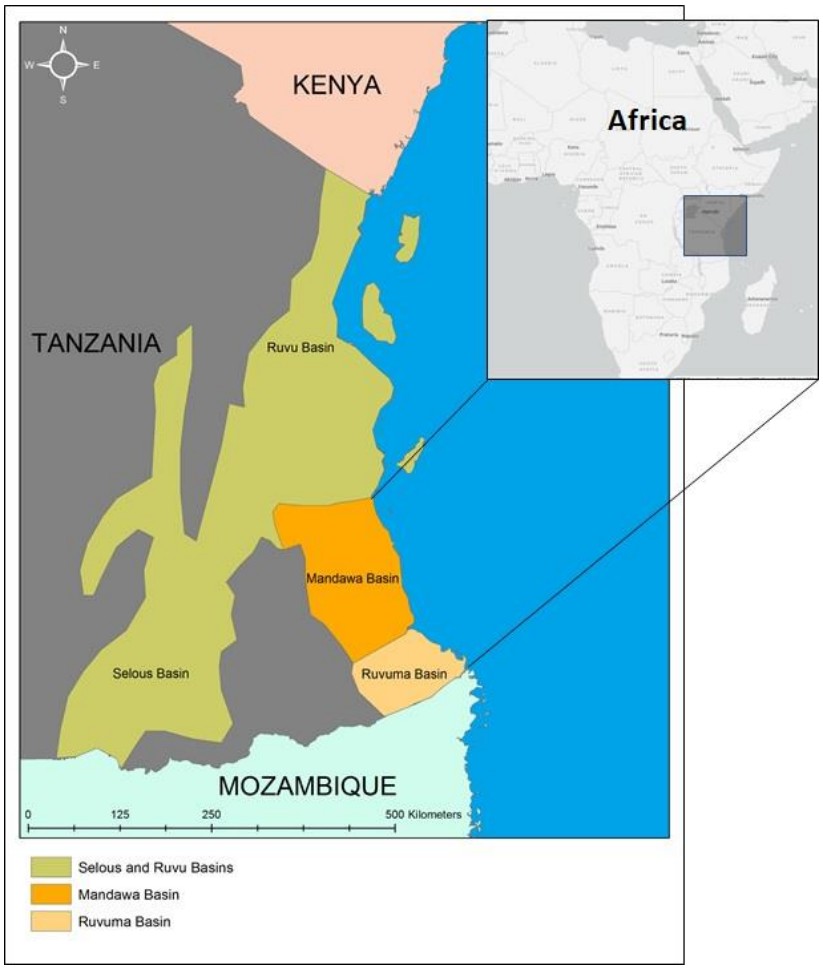

Figure 1.1 - Location of onshore Mandawa, Ruvuma and Selous Basins sedimentary basins of Tanzania (modified after Robertson/TPDC 1986; TPDC 2005; Hudson, 2010).

1.1 THESIS ORGANIZATION

To better structure and promote the reading of the work done, this thesis has been divided into thirteen chapters. These generally envisage the various phases of the project, being arranged in chronological order:

Chapter 1 – This chapter introduced the literature review in the context of this study stating the regional geological setting and structural evolution of Mandawa, Ruvuma and Selous in Tanzania and conjugate basins, Majunga and Morondava in Madagascar, the Davie Fracture Zone within the East African Basins; previous studies, the exploration history for petroleum in the cited basins, research questions, aim and fundamental objectives proposed at the beginning of the project.

Chapter 2 - This section presented the general data accessed to perform this work such as reports, well data, seismic data, shapefile, and the software supported for this research.

Chapter 3 – This chapter synthesized the methodologies that served as the basis for the analysis and interpretation of the available data.

Chapter 4 – The nine wells of the Mandawa Basin, one well in Ruvuma Basin and one representative well in Selous Basin and its formation descriptions and definitions are presented in this section.

Chapter 5 – The seismostratigraphic analysis with a description of the seismostratigraphic concept is referenced.

Chapter 6 – A set of suggested types os salt structures in seismic interpretation, the types of salts in Mandawa Basin are described based on geophysical well logs and external references;

Chapter 7 – This section presented the 3D geocellular model based on the structural framework with faults and a model without faults processed in Petrel software. Contains the horizons and faults interpreted, post-stack seismic attributes in the 2D seismic lines, depth conversion.

Chapter 8 - The discussion chapter comprised the main themes related to the research questions presented in Chapter 1 of this work.

Chapter 9 - Final conclusions of this dissertation. Some points of discussion are still to be explored in greater detail, with the prospect of future work focusing on the exploratory analysis of this marginal sector in Madagascar.

1.2 REGIONAL GEOLOGICAL IN THE CONTEXT OF THIS STUDY

The sedimentary basins classification in this thesis is considered in the morphotectonic groups of Karoo and East African Rift Valley Basins.

1.2.1 Karoo Rift Basins

The term Karoo has been cited to describe the sediments originally remaining from Karoo basin of South Africa of similar age, from Upper Paleozoic to Lower Mesozoic, across Gondwana (Kreuser *et al*., 1990; Duncan *et al*., 1997). According to Wopfner *et al*. (1994, 2002) the accumulation of Karoo successions in Africa was described as corresponding to two distinct regimes from southern and northern margins of Gondwana, classified as Pangean first-order cycle of supercontinent when it reached its maximum extent and breakup in terms of depositional sequence. The sedimentary fill lies unconformably on top of a metamorphic basement.

In Tanzania, Salman & Abdula (1995), Revees & de Wit (2000), and Chorowicz (2005) described two major rifting events of Karoo basin: an old rifting has been active since Permian and the later intra-continental rifting has been active since Miocene. In respect of Mandawa sub-basin, Kapalima (2003) mentioned that the Karoo rift sequence was formed by evaporitic sequence (anhydrite, gypsum, and halite) interbedded with shales, a which reflects the difference in rates of subsidence and sedimentary depositional environment. This evaporitic sequence developed significantly more rapidly in part of the basin marking a restricted marine onset (Mpanda, 1997).

The climate controls and tectonic events that took in place of Karoo basins of south-central Africa, determining the sedimentological and stratigraphic features. The preserved Karoo sequence (Figure 1.2) with up to 2–4 km in thickness and has been developed in cold arid climates in Upper Carboniferous–Lower Permian, during the foreland basin development in South Africa, as the climate became warmer and wetter in Upper Permian–Triassic times during the main Karoo rifting phase. The Lower Karoo sediments are characterised by glacial deposits, sandstones, and shales. In terms of

possible source, the Upper Permian coals and some thin organic-rich algal (oil-prone) shales occur along the southern rifts of Africa with important marine transgression events at the start of the Triassic in Madagascar which coincides with the initiation of the main Karoo rifting event (Catuneanu *et al.*, 2005).

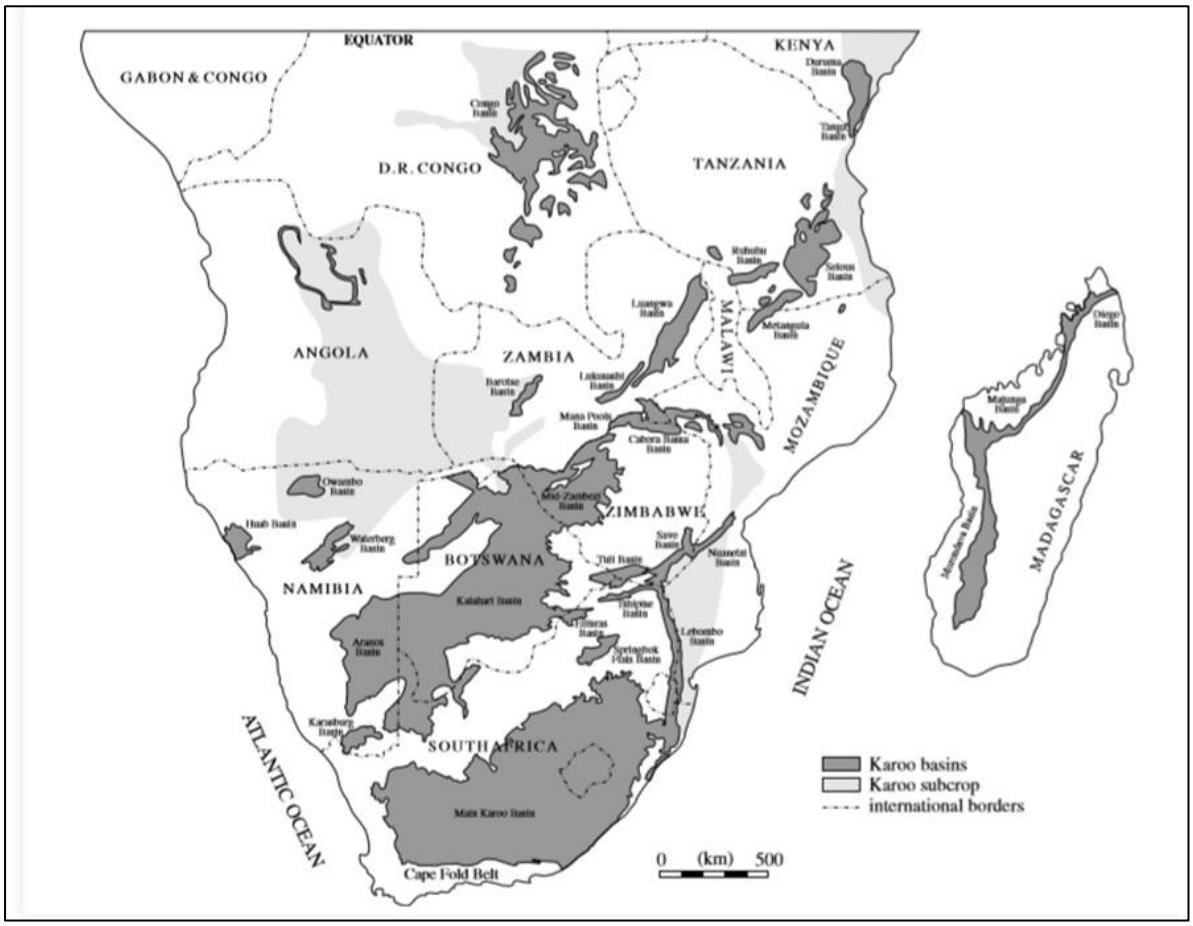

Figure 1.2 - The distribution of Karoo basins in south-central Africa (Johnson et al., 1996; Wescott and Diggens, 1998; Nyambe, 1999; Wopfner, 2002; Catuneanu et al., 2005).

1.2.2 East African Rift Valley Basins

The East African Rift System (EARS) is a major topographic feature in East Africa, composed by two branches: the eastern branch and the western branch separated by the East African Plateau (as an alternative to the Tanzanian plateau). The mechanisms that consider the timing rifting age, topography has been suggested and discussed by Wichura *et al.* (2010).

The EARS has developed above a mantle plume that started in southern Ethiopia and sourcing the volcanism in the region (Duncan and Richards, 1991; Ebinger and Sleep, 1998).

With regard to geological and geophysical data, Smith (1994) mentioned the presence of limited relief of fewer than 1000 m prior to the onset of volcanism in the EARS.

1.2.3 Coastal Basins

The coastal basin of Tanzania extends from the Kenyan border in the north to the Mozambican border in the south covering the Selous - Tanga and the Mandawa sub-basins becoming a continental shelf during the Aalenian – Bathonian (174 – 166 Ma) when the first marine transgression was bordered by the Tanga and Lindi faults (Mpanda, 1997). Geophysical (gravimetry) and geological (isopachs and structural features) data in the study of Sandwell and Smith (2009) and Said *et al.* (2015) corroborated to delineate the boundaries of the Tanzania coastal basin. The basin borders to the west by the Tanga and Mandawa faults which separate it from the basement. Towards the east, the basin is limited by a relatively low gravimetric feature parallel to the Davie Fracture Zone. The coastal basin is laterally adjacent to the Lamu Basin in the north and to the Ruvuma basin in the south.

1.3 REGIONAL TECTONIC SETTING AND DEVELOPMENT OF EAST AFRICAN BASINS

The evolution of the Mandawa Basin is a result of two rifting phases whose the first phase is referred as the Karoo rift during the Permo – Carboniferous, evolved to later episodes in the Lower Jurassic associated with the breakup of Gondwana continent, whereas the second phase of rifting resulted in thermal subsidence with the Mandawa Basin forming part of a failed rift arm (TPDC, 2005). The crustal extension in Lower Jurassic led to restricted shallow marine conditions with anoxic sediment deposition and the accumulation of thick sequences of oil-prone source rocks. Also in Lower Jurassic, tectonic activity led to new faulting and a period of halokinesis with evaporite deposits occurrence. Moreover, open marine conditions were set up until Middle Jurassic increasing the deposition of shallow marine clastic and carbonates gradually accumulated

before the development of a passive margin with deep marine claystones and turbidites in the late Cretaceous (Salman and Abdula, 1995; Reeves & de Wit 2000; Chorowicz, 2005).

A phase of tectonism in the Aptian reactivated salt movement and resulted in major listric faults in the 'post-salt' section. Deposition ceased in the salt basins during the Middle-Cretaceous whereas thick sediments continued to accumulate in the coastal basin (Salman and Abdula, 1995).

1.4 PREVIOUS STUDIES

1.4.1 Litho- and biostratigraphy studies

Many studies have deployed in the areas of litho- and biostratigraphic to establish relations of micropaleontology with stratigraphy, stratigraphic formations set through fossils, their ages and define them into biozones and found depositional systems as regards the discovery of Tendaguru fossil.

Descriptions of the biostratigraphy of the Mandawa basin can be found in Stewart *et al*. (2004); Bown (2005); Bown and Dunkley Jones (2006); Bown *et al.* (2008); Handley *et al.* (2008); Wade and Pearson (2008); Bown and Pearson (2009); Cotton and Pearson (2009), Berrocoso *et al.* (2010, 2012, 2015).

Additional biostratigraphic control is provided by calcareous nanofossils which are highly diverse and are indicative of a shelf to slope environment (Bown and Dunkley Jones, 2006; Bown *et al.*, 2008). The presence of common allochthonous shallow-water debris in the sites permits correlation with larger benthic foraminifer extinction events (Pearson *et al*., 2008).

Berrocoso *et al.* (2015) focused on the Middle- to Upper Cretaceous marine succession of southeastern Tanzania. According to the methods implemented in the coring analysis described in Berrocoso *et al.* (2010, 2012), the results demonstrate the predominance of excellent microfossil preservation and that upper Cretaceous succession is relatively thick and continuous. The previous cores drilled added to this work in reference were crucial to formally define a new unit, the Lindi Formation (Upper Albian – Coniacian), at the base of the Kilwa Group.

1.4.2 Geochemical analysis

TPDC contracted Robertson Research International Limited to evaluate the source rock potential of Tanzania using cuttings, cores and outcrop samples from the coastal basin area. Back then the employment of stratigraphic units had not been defined remaining unnamed and the usage of different names in the northern, central, and southern regions (Robertson and TPDC, 1986).

Kagya (1996) analysed the Mandawa basin generation based on the organic-rich samples from Mandawa-7 well and from his observations, he could recognize the influence of a hypersaline influence during deposition and a mix of organic marine and terrestrial input, involving a marine to estuarine depositional environment. He also concluded that the non-biomarker and biomarker maturity parameters used in his study indicate the source rock to be within the oil generation window. The author proved the existence of an effective source rock facies indicated by kerogen types II and III for a potential petroleum generation (Kagya, 1996).

More authors investigated the biomarker composition of sediments specifically in the Kilwa area in Tanzania. Van Dongen *et al.* (2006) demonstrated from the analysis that biomarker composition is dominated by the material of terrestrial and bacterial origin, indicating a marine setting of a higher plant input mostly stimulated by sedimentary microbial activity, including sulfate reduction.

Hudson (2011) analysed clays and shales trough Total Organic Carbon (TOC) and by Rock-Eval parameters. The use of organic geochemistry parameters (TOC analysis, S_1, S_2, and T_{max}) in 19 samples addressed the maturity and quality of source rocks. Using a similar method as Kagya (1996) in Mandawa-7 well, crossplot extracted from the analysis indicated that some samples are capable of generating gas represented by type III kerogen whether some may represent source rock that has generated oil in the basin with the presence of type II or III kerogen.

1.4.3 Paleoclimate studies

The last decade presented studies that cover climate models have been discussed among paleoclimate investigations to use the technique of isotope ratio ($\delta^{18}0$) of calcite to analyze through ancient oceans, the shells of fossil planktonic foraminifera and other organisms. However, the mismatch between data and models have raised questions about

the accuracy of much of the foraminifer data for quantitative climate reconstruction as further tropical deep-sea carbonates have been drilled and explored scientifically (Norris & Wilson, 1998; Schrag, 1999, Wilson & Norris, 2001; Pearson *et al*., 2001; Wilson *et al.*, 2002; Stewart *et al*. (2004); Pearson *et al.* (2007).

One of the detailed publications questioned the validity of data is that by Pearson *et al.* (2001). The work demarked for instance in the late Cretaceous and Eocene epochs to understand the geographical distributions of temperature-sensitive fossil organisms and the results of climate models with increased CO_2 levels. Presented new data from the exceptionally well-preserved foraminifer shells extracted from impermeable clay-rich sediments, which indicate tropical sea surface temperatures ranging between 28^{o}C and 32^{o}C.

Stewart *et al.* (2004) considered the theory of cool Miocene tropical temperatures. Based on $\delta^{18}0$ new isotopic data from three well-preserved foraminiferal assemblages, the research target to analyze tropical sea surface temperatures (SSTs) from early to Middle Miocene. A significant conclusion consists on the increase of temperature approximately of 10^{o}C that has been documented before from analysis found in several authors constraining diagenesis effects during burial deposition in the cold sea-floor environment (Killingley, 1983; Schrag *et al*., 1995; Norris and Wilson, 1998; Schrag, 1999; Wilson and Norris, 2001; Pearson *et al.* 2001; Wilson *et al*. 2002). Moreover, Stewart *et al.* (2004) proposed that new estimates presented are the result of exceptional shell preservation associated with impermeable hemipelagic clays not least suggested that the referred diagenetic effect is equally applicable to the Neogene foraminiferal isotope estimates (Norris and Wilson, 1998; Pearson *et al.*, 2001).

Pearson *et al*. (2007) estimated substantial temperature gradients, from the sea surface to seafloor and equator to poles, such as those required to sustain deep-water convection. However, the data also provide a new challenge to climate model studies, which is to replicate polar cooling through the Eocene while SSTs in the tropics may have remained constant or only slightly reduced. A nonlinear decline in heat transport by tropical storms in response to cooling could be one such mechanism.

1.4.4 Tendaguru studies

Despite the vast literature that is related to oil exploration, one of the most important and pioneer in outcrop investigations is the discovery of Tendaguru dinosaur fossils in the

early 1990s. Studies were conducted by the Museum für Naturkunde der Friedrich – Wilhelms – Universität Berlin (Humboldt – Universität) from 1908 to 1912. Later, in the 1920s, the British Museum of Natural History carried on further excavations (Schlüter, 1997).

The discovery of Tendaguru fossils in the early 1890s, during expeditions from the Museum für Naturkunde der Friedrich – Wilhelms – Universität Berlin and later by the British Museum of Natural History (Schlüter, 1997), was the first of many studies about litho-and biostratigraphy to establish the relations of micropaleontology with stratigraphic formations to define their ages, and define into biozones and depositional systems.

In the early 2000s, a new expedition by a joint project between the German – Tanzanian Tendaguru served as an approach to collect data of micro vertebrates, micro and macro invertebrates, plant fossils and new sedimentological and stratigraphical data. The focus was to apply these data in multidisciplinary research enlighten various unsettled points dissolved regarding the Tendaguru Beds such as depositional environment, structural reconstruction of paleoecosystems, and geological ages.

Among the scientific papers related to Tendaguru expedition Beds are Aberhan *et al.* 2002; Bussert *et al.* 2009; Bussert and Aberhan 2004; Heinrich *et al.* 2000; Janesch 1938; Russell *et al.* 1980; Sander 1999, 2000, Schrank 2005, 2010; Schuchert 1918, 1934). These studies are important to address the first stratigraphic analysis of the southern Mandawa.

1.5 EXPLORATION HISTORY OF THE MANDAWA BASIN, SOUTHERN TANZANIA

1.5.1 Tanzania

Tanzania is located in an area affected by major tectonic events commencing in the Permo – Triassic with the breakup of Gondwana and continuing to present-day. The development of the post - Gondwana East Africa Continental Margin is separated into two major phases, “rift and drift” (TPDC, 2005).

1.5.2 The Tanzania Drilling Project (TDP)

The Tanzania Drilling Project (TDP) involved an international partnership of scientists interested in using the thermally immature Tanzanian marine sediments of Cretaceous and Paleogene age for paleoclimate research (Pearson *et al.* 2006). The initiative provided drilling results of cores on areas of detailed investigation on Mandawa Basin around Kilwa to Lindi in the Ruvuma Basin.

The well first phase of the project took place in a deep marine shelf environment characterised by the existence of preserved microfossils ideal for geochemical analysis. Developed in two outcrop field trip sampling stages, results were published by Pearson *et al*. (2004) with the objective to summarize the lithostratigraphy, biostratigraphy, magnetostratigraphy, and organic geochemistry (Nicholas *et al*. 2006).

Drilling occurred between 2002 - 2005 provided valuable information to reconstruct the deposition environment in the Kilwa area and onwards to south Lindi in Ruvuma Basin (Pearson *et al*. 2006; Nicholas *et al*. 2006, 2007).

The second phase between 2007 and 2008 recovered samples along the Lindi area in southern Tanzania, on Upper Cretaceous sediments confirming the existence of a much more expanded and complete Upper Cretaceous sequence (Berrocoso *et al*. 2010, 2012) that was initially documented in Pearson *et al*. (2006) and Nicholas *et al*. (2006, 2007).

1.5.3 Petroleum System

By definition, a petroleum system comprises a pod of mature source rock and all genetical processes, source rock, reservoir rock, seal rock, migration paths all charged by source rock to occur in a proper timing and critical moment in order to generate oil and gas accumulations (Magoon and Dow, 1994).

Oil exploration projects and scientific studies along with governmental efforts have brought the continued discovery of hydrocarbons in Tanzania represented by gas fields, oil and gas show in boreholes, oil seeps, and bitumen outcrops (TPDC, 2005). The studies related to petroleum systems are summarized by many scientific studies, commercial reports and, unpublished TPDC's reports aimed at understanding the structural, stratigraphic evolution, and thermal history of the basin for petroleum exploration.

The study of Mpanju *et al*. (1991) concentrated in the western Rift Basin of Tanzania. It has been considered a significant interpretation for potential source rocks of the intracratonic basin Karoo coals. The analyses of four outcrop samples of Lower and Upper Permian age were collected to determine the richness, type, maturiry material, and hydrocarbon potential. All samples were conclusive to define they are rich in organic matter of types II and III kerogens, Vitrinite Reflectance ranging between 0.47% and 0.67% Ro where were recognized liptinite and vitrinite macerals mostly. The coals observed and carbonaceous samples were defined as capable of oil generation.

The organic geochemical characterisation of bitumen, seeps, rock extracts, and condensates from various areas of Tanzania was the study of Mpanju and Philp (1994). The study discussed also the attempts to correlate to presupposed source rocks and the nature of unusual seeps. From the results, the origin of bitumen was not clarified led a question. Biomarkers in a condensate in a particular area, Songo Songo, suggests the source rock containing type II/III kerogen however overall source rock potential quantified as poorly known.

The joint partnership between governments presented an overall of geochemistry and source rock potential of petroleum systems of East Africa passive margin covering basins in Kenya (Lamu basin), Tanzania basins, and Ruvuma basin in Mozambique (Maende and Mpanju, 2003).

There is limited information in the literature that is concerned with known oil seeps in Tanzania. The oil seeps are mainly based at Tundaua on the west coast of the Pemba Island, Wingayongo, at Msimbati near Mnazi Bay and in the Interior Rift Basins (TPDC, 2020).

Historically, research investigating the Pemba Island seep indicates that two separate sources are involved; a marine source, which has been correlated with Campanian-Maastrichtian shales. Nonetheless, the typing of the seep does not appear to be closely linked with oil shows from the nearby Pemba-5 well (TPDC, 2020).

Much of the available literature on seeps at Msimbati deals with the Mnazi Bay gas discovery indicated by two families of oil - one has been interpreted its generation process is from a carbonate source rock deposited in a strongly reducing environment - the other contains considerable terrestrial organic matter and biomarkers of Late Cretaceous or younger age (TPDC, 2020).

Detailed examination of oil seeps and slicks have been identified from the Interior Rift Basins. Previous research findings suggest that oil seeps were reported from Lake Tanganyika, as early as 1896, and in more recent times, project PROBE found an oil film on the lake. (TPDC, 2020).

At least two possible seeps are present in the Wingayongo area, around 70 km to the north of the Kianika area, in the Kisangire Block: at the northern flank of the Rufiji Trough shows unusual biomarker characteristics, which have been interpreted to be derived from a source rock deposited in a restricted carbonate, lacustrine environment. The Makarawe Shale (Bajocian) is a possible source of this seep (CoreLab/GHG, 2009; TPDC, 2020).

Besides, highly biodegraded tars are present in the Kipatimu Sandstone in Wingayongo-1 well. Attesting to the hydrocarbons at these localities are significantly altered by hydrothermal activity which has led to the deposition of a range of minerals at the site and has obstructed attempts to analyse the nature of the hydrocarbons and to determine their source (CoreLab/GHG, 2009).

There is a range of opinions regarding the source of the hydrocarbons in the highly biodegraded tars at Wingayongo hill and Wingayongo-1.

Detailed examination of Alconsult (1997) considered that the seepage could represent a mixture of thermogenic gas feeding a recent bacterial biomass (i.e. a "paraffin dirt"). CoreLab/GHG (2009) supported this view, stating that "it is now generally accepted that these are not natural oil seeps but are 'paraffin dirts' probably resulting from the action of thermogenic gases migrating to the surface and reacting with near-surface bacterial mats. The actual process of their formation is still a matter of discussion and although of academic interest they can discounted as evidence of an underlying oil accumulation."

Maende *et al*. (2008) suggested that samples from the Wingayongo oil seep are characteristic of altered (mainly evaporated), relatively immature to early mature oils, mixed with a highly mature biodegraded oil previously migrated to this seepage location.

Data from several studies have sampled and analysed the seep, as well as Mpanju and Philp (1994), Geomark Research Ltd. (2004), and Peters and Moldowan (2004).

GHGeochem Ltd. have reviewed the dataset in a proprietary report for Dominion Petroleum and taken together, these studies indicate that two separate and different seeps have been sampled, one from the Wingayongo "tar sands" (in the Lower Cretaceous

Kipatimu Sandstone) and a second from the Luhoi River (sampled by Texaco, some 5 km from Wingayongo) (De Wit *et al.*, 2015).

The data from the Luhoi seep are suggestive of degraded residual migrated hydrocarbons but the source of the material cannot be determined on the data available.

The tars in Wingayongo-1 are enriched in polar and asphaltic compounds and are severely depleted in saturated hydrocarbons which are almost exclusively hopanes (C28 bismorhopane, C30 hopane and C30 bisomorhopane). This highly restricted biomarker assemblage indicates that the source of the hydrocarbons is a sediment deposited in a restricted depositional environment such as a lagoonal or evaporitic setting. The bulk of the organic material at Wingayongo comprises pre-asphaltenes, which suggests geologically recent organic matter and that the petroleum products are a result of hydrothermal activity.

Apart from defining a petroleum system, Hudson (2011) examined the potential reservoir sandstones and potential source rocks of Mandawa basin prior to determine the chemical characteristics of the sandstones and a possible correlation and identification of sandstone units. The determination of potential source rocks, mostly referred to in the Nondwa Formation, was accomplished by Total Organic Carbon (TOC) and by Rock-Eval parameters to understand the stratigraphic relationship and petroleum system.

1.5.4 Tanzania as a petroleum province for exploration

In terms of oil exploration, a number of multinational petroleum companies have been in Tanzania at different times. The literature reveals that the first investigations commenced in the 1950s with British Petroleum (BP) after its concession rights. BP drilled six boreholes in 1956 on a 19 km extension along Mandawa salt core anticline. BP drilled some of the pioneer wells such as Pindiro-1 to test another salt cored surface anticline and Mandawa-7. The location of Mandawa-7 was established based on gravity and seismic data as well as geological field surveys. It penetrated the pre-salt for the first time and reached the Mbuo Formation. BP reported in 1958 oil fluorescence in Mandawa-7 proving the existence of good source rock, seal, and reservoir rocks along the stratigraphic column. However, the well was completed with no commercial discovery of hydrocarbons (Nicholas *et al*., 2007; Hudson & Nicholas, 2014). Nearly all shales and

mudstones penetrated in the well in deeper intervals yielded minor amounts of oil on soxhlet extraction (Spence, 1957; 1959).

Moreover, British Petroleum (BP) was the pioneer to produce a detailed geological map of the Mandawa area which served as the basis for more detailed maps of Mandawa basin.

Between the years 1971-82 the company Agip took over BP's relinquished area and held most of the Mandawa basin area and acquired 953 Km of six-fold geoflex seismic. Agip in 1979 drilled in the eastern part of the basin the well Kizimbani-1 (Upper Tertiary age sediments). Both the Lower Jurassic salt and the underlying Mbuo Formation were lacking in the well.

Later, Shell Petroleum Development Tanzania Limited (Shell PDT) herded most of Mandawa block and during the years 1987-88 acquired 1,685 Km of 48 fold dynamite seismic and obtained 6,433 gravity readings along the seismic lines. Shell drilled Mbuo-1 well to the basement located on the same salt anticline that was tested before by BP's Pindiro-1. Mbuo-1 is the only well entirely penetrated the stratigraphic section crossed deltaic sandstone reservoir beds intercalated with organic-rich black shales along the nearshore (TPDC, 2005).

After an extensive exploration campaign held by Shell, Dublin International Petroleum Limited proceeded the exploration signing a Production Sharing Agreement (PSA) over Mandawa and Rufiji basins in the late 1990s and drilled three new wells East Lika-1, Mbate-1 and Mita Gamma-1 before relinquished the area (TPDC, 2005; Hudson, 2011).

Between 2006 and 2011, the Mandawa basin was under the exploration license of TPDC/Dominion Petroleum Limited (Dominion) which acquired additional seismic data and reprocessed the legacy data for new interpretation before drilling the Mihambia-1 well and Kianika-1. Dominion relinquished the Mandawa basin in 2011 after unsuccessful drilling results (Hudson, 2011).

The discovery of gas in Songo Songo, Kilwa district in the Lindi region and Mnazi Bay in Mtwara is the only significant outcome of five decades of oil, and gas exploration efforts (TPDC, 2005).

1.6 EXPLORATION HISTORY OF THE RUVUMA BASIN, NORTHERN MOZAMBIQUE

1.6.1 Mozambique

Mozambique, located in southeast Africa, has a 2,500 km coastline with the Indian Ocean and a wide coastal plain that varies in width from 150 to 600 km. The major part of the country consists of undulating plateaus (Smelror *et al.*, 2006).

The sedimentary basin presented in this thesis, the Ruvuma basin has been investigated and described by European explorers since the early 1900s before the petroleum industry has been attracted to Mozambique. The first incursions to the region occurred by Dr. David Livingstone (1813 - 1873). Through mapping, he explored the River Ruvuma and discovered Lake Chilwa in Malawi and Lake Tananyika (Smelror *et al*., 2006).

Descriptions of the regional geology, stratigraphy, and tectonic evolution of these basins have been discussed in this present work however more detailed aspects were encountered for the northeastern part of Ruvuma basin as it is located in the border with Tanzania where most of the acquired data had been under analysis.

The development of East Africa, highlighting Mozambique has been an academic and commercial interest due to considerable resources attractiveness in hydrocarbon exploration.

Locally, Africa was the central portion of the Gondwana Supercontinent between the end of Precambrian – Ordovician orogeny, where it is exposed the major crystalline basement until present in coastal Africa, the North-South East Africa – Antarctica Orogenic Belt (Key and Revees, 2012). During the early Paleozoic occurred uplift and extension of Gondwana, creating numerous intracratonic Karoo rift, infilled by periglacial sediments of Carboniferous to Lower Permian age. The Karoo sediments are confined overlain by Lower Jurassic basalts (approximately 182 Ma). Smaller Triassic to Lower Jurassic half-grabens discordant to the Karoo rift-basins is filled predominantly of continental sediments intercalated with marine sediments (including the N'Gapa and Rio Mecole formations of coastal northern Mozambique) (Key *et al*., 2008; Revees, 2009; Key and Revees, 2012).

The evidence for the breakup of southwestern Gondwana has been investigated, and recognized volcanism episodes, tectonics, oceanic crust formation and basin development in southeastern Africa and conjugate Antarctic margin (Reeves, 2017). According to Rabinowitz *et al.* (1983), the Africa – Madagascar breakup took place circa 165 Ma, in the Middle Jurassic, followed by the southward motion of Madagascar and a hypothesis is that it has ended by the Lower Aptian (approximately 121 Ma) (Rabinowitz *et al*., 1983) or Middle Aptian (circa 118 Ma) (Bassias, 1992).

Although there is a general opinion on the first-order geological features of Gondwana (Viola *et al.,* 2008) ongoing discussions impact the Pan-African geological events, to reconstruct through models the tectonic history of its crustal fragments.

Descriptions of the timing of orogenesis in northern Mozambique are referenced in some geochronological researches (Jacobs *et al*., 2008; Viola *et al.,* 2008; Bingen *et al.,* 2009). In the last decades, studies focused to indicate the collision age that led to crustal thickening between Mesoproterozoic and Neoproterozoic tectonic blocks during the "Pan-African" orogeny for the final assembly (Pinna *et al.,* 1993; Meert, 2002; Boger and Miller, 2004; Jacobs and Thomas, 2004; Thomas *et al.,* 2010; Emmel *et al*., 2011).

As stated in Jacobs and Thomas (2004) and Thomas *et al*. (2010) the geology of northern Mozambique is made up of a collage of Meso- and Neoproterozoic crustal blocks which were finally juxtaposed during the "Pan-African" or "East-African Orogeny" – EAO (Stern, 1994) and which extends southwards into East Antarctica. Therefore, Viola *et al*. (2008) reported an improved understanding with new field structural observation obtained from an integrated regional-scale approach encompassing tectonic analysis supported by new high-resolution aeromagnetic and radiometric surveys, subdividing northern Mozambique into five megatectonic units on the basis of lithology, structure, and geochronology.

However, attempts to provide an explanation concerning the evolution of the amalgamation process led as a task in the matter that the collision of the many blocks involved may be better elucidated with a detailed conceptual model of the structural framework as proposed by Emmel *et al.* (2011) to explain the post-Pan-African Precambrian metamorphic basement cooling pattern in northern Mozambique. The methodology applied used combined dating methods comprising titanite, zircon, and apatite fission-track data which could provide arguments that support the analysis after

the Pan-African orogenesis (approximately 620 – 530 Ma) the Precambrian basement was subject to extensional tectonics and relative slow Lower Ordovician to Recent cooling. Basement rock cooling was mainly a response to Upper Paleozoic to Mesozoic rifting between Mozambique and East Gondwana during the opening of the Ruvuma and Mozambique sedimentary basins.

1.6.2 The Ruvuma Basin

In the literature, authors have been using the term Rovuma and Ruvuma to define the sedimentary basin situated in the southeastern coastal zone of Tanzania. Throughout this thesis, the term Ruvuma Basin is used to refer to the region named after the Ruvuma River, a river in the African Great Lakes region which forms most of its southern boundary with Mozambique (where it is known as Rovuma).

The Ruvuma basin is located on the border between Tanzania and Mozambique (Figure 1.3) where it lies in a north-northwest to south-southeast trending orogenic belt with a 400 km southern extension. The basement is characterised by Upper Proterozoic rocks of the Mozambique belt (Hancox *et al.* 2002; Smelror *et al.* 2006; Key *at al.* 2008). A bibliographical synthesis about the regional geology and tectonic has been successfully addressed by Balduzzi *et al*. (1992), Salman and Abdula (1995), Pearson *et al.* (2004), Nicholas *et al*. (2006, 2007), Key *et al.* (2008).

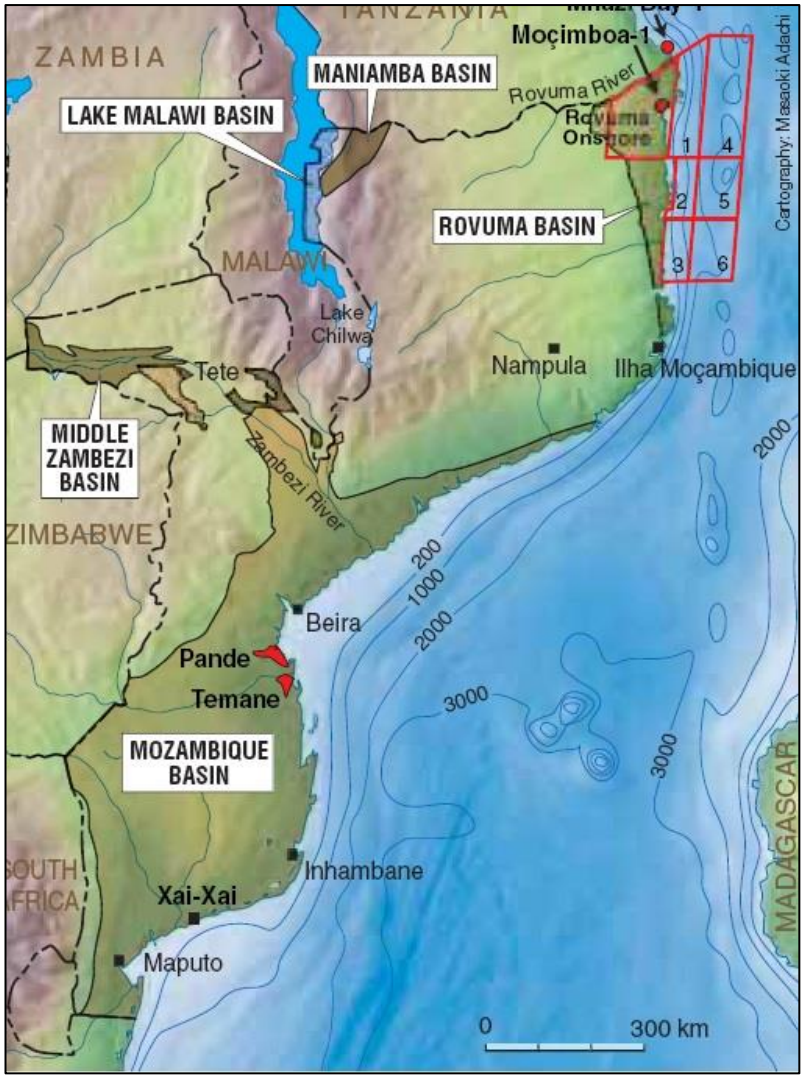

Figure 1.3 - Location of Ruvuma and Mozambique basins in Mozambique. Cartography: Masaoki Adachi (Smelror et al., 2006)

Diverse discussions regarding the breakup of the paleo-continent Gondwana are still not clear. From Permo – Jurassic age, the breakup timing has been postulated as a remarkable moment that affected the displacement of Gondwana sectors and the formation of a new oceanic crust in the Mozambique basin (Delvaux, 1989).

Nicholas *et al.* (2007) have observed potential tectonic mechanisms such as a Miocene inversion, strike-slip faulting, and periodic uplift of onshore southern Tanzania. Evidence of compression and transpression is suggested in Nicholas *et al.* (2007) through gravity data and seismic reflection analysis where a strike-slip movement faulting on the 'Ruvuma Plate' is compressing and shearing the southern coast of Tanzania against the Davie Fracture Zone (DFZ).

The Ruvuma basin began to preserve its actual configuration in the Lower Cretaceous due to a marine transgression flood in the eastern margin according to Nairn *et al.* (1991). A belt of Lower-Middle Cretaceous continental or transitional sediments parallel Karoo or Precambrian sediments to the west. To the east and upward, it grades into marine rocks which extend through Upper Cretaceous – Palaeocene – Eocene – Oligocene. It is suggested that Cretaceous sediments in Mozambique may overlie Karoo or post-Karoo igneous rocks or even the Precambrian basement (Catuneau *et al.*, 2005).

1.6.3 Stratigraphic framework of onshore Ruvuma Basin

The first modern tectonostratigraphic subdivision of northern Mozambique was published by Pinna *et al.* (1993).

Salman and Abdula (1995) described the stratigraphic framework that evolves in crystalline and metamorphic Precambrian rocks underlying the Karoo deposits, formed of continental terrigenous and coal-bearing formations from the Upper Carboniferous to the Lower Jurassic. The Karoo Group is topped by Post-Karoo sediments, continental, marine, and transitional, which are mostly eroded rocks of Karoo Group. At the base of the Post-Karoo section lies continental sediments, found in the southern part, known as "Red Beds Formation" from Upper Jurassic (?) – Lower Cretaceous. Overlain, there are marine, continental, and transitional facies between Lower Cretaceous and Cenomanian age. During the Cretaceous transgression, a marine sequence started to be distributed in the southern and central areas of the Mozambique basin, where also volcanic activities occurred. Later during Cenozoic age features characteristic of a passive margin emerged.

A summary of the lithostratigraphy is presented by Emmel *et al.* (2011) related to offshore basin while Key *et al*. (2008); Smelror *et al*. (2008) focused on the onshore basin. Hancox *et al*. (2002) particularly described the Maconde Formation stratigraphy in northern Mozambique (sediments from Macomia area were also referred to as the Maconde Formation) since it has been for many years a poorly understood Lower Cretaceous unit previously termed as Maconde Beds (Bornhardt, 1900; Flores and Noseda, 1961), proposed in the vicinity of Macomia, which presented a piece of new evidence for the Maconde Formation and a basinal marker horizon identified in its upper part that may represent tectonic uplift.

Several authors have successfully used outcrop data, reconstruction maps, seismic interpretation, and geochemical analysis in order to characterize the stratigraphic

provenance of the Ruvuma Basin. The first modern tectonostratigraphic subdivision of northern Mozambique was published by Pinna *et al*. (1993). A summary of the lithostratigraphy is presented in Salman and Abdula (1995) and Emmel *et al*. (2011) related to the offshore basin while Key *et al*. (2008) and Smelror *et al.* (2008) published studies focused in the onshore basin. Hancox *et al*. (2002) particularly focused in describe the Maconde Formation stratigraphy in northern Mozambique (sediments from Macomia area were also referred as the Maconde Formation) since it has been for many years a poorly understood Lower Cretaceous unit previously termed as Maconde Beds (Bornhardt, 1900; Flores and Noseda, 1961), in four sequence successions divided in eleven facies units proposed in the vicinity of Macomia, which presented new evidence defined on the basis of their architectural hierarchies, facies associations, and petrographic and palaeontological signatures, for the Maconde Formation and a basinal marker horizon was identified in its upper part that may represent tectonic uplift.

Salman and Abdula (1995) described the development of the Mozambique and Ruvuma Basins addressing the formation of the basins to the breakup of southwestern Gondwana and opening of the western part of the Indian Ocean. The study inferred the sediments based on seismic correlations with the Tanzanian Selous Basin indicating that the Ruvuma stratigraphic sequence was filled with crystalline and metamorphic pre – Cambrian age basement, continental terrigenous Karoo sediments, marine and lagoonal Jurassic deposits, and deltaic rocks of Cretaceous and Cenozoic age.

Nine lithostratigraphic formations of the Mesozoic – Cenozoic succession in the onshore part of the Ruvuma Basin in northern Mozambique have been related to the progressive break – up of the successions in Ruvuma Basin where onshore the coarse basin margin sediments above the unconformity are referred to as the Macomia Formation and the marine sediments, as the Pemba Formation. An Upper Cretaceous marine transgression was proposed as the origin of the Mifume Formation which comprises of marls or mudstones and calcareous sandstones (Salman and Abdula, 1995; Key *et al.*, 2008).

1.6.4 The Tanzania Drilling Project in Lindi Formation

The third phase of the Tanzanian Drilling Project (TDP) expedition synthesized the litho-, bio, and chemostratigraphy by coring six new discrete intervals of the Aptian – Albian (TDP Sites 36 and 38), Coniacian – Santonian (TDP Site 39) and Maastrichtian – Paleocene (TDP Site 37) in a total of 72.3 m sediments cored (Jiménez Berrocoso *et al.,* 2015). The study combined with previous samples cored between 2007 and 2008 in an area dominated by Middle - to Upper Cretaceous marine succession of southeastern Tanzania and northern Mozambique (Salman and Abdula, 1995; Jiménez Berrocoso *et al.,* 2010, 2012, 2014).

The preservation of planktonic and benthic foraminifera and calcareous nanofossils, especially that the new sites verify key lithological differences to the overlying units allowing to be proposed a new unit, the Lindi Formation, as the unit that forms the base of the Kilwa Group (Nicholas *et al*., 2006, Jiménez Berrocoso *et al.,* 2015). The proposed Lindi Formation underlies the Nangurukuru Formation (Nicholas *et al*., 2006) and includes the "separated stratigraphic unit", and extends the lower limit of the Kilwa Group from the Santonian to at least the Upper Albian (Jiménez Berrocoso *et al.,* 2015).

Due to similarity in dominant grain sizes between the Lindi Formation and the overlying Nangurukuru Formation, both units are dominated by clay and silt however a correlation boundary is difficult to be established (Nicholas *et al*., 2006; Jiménez Berrocoso *et al.*, 2010, 2012). The study provided conclusions that bring implications in respect of biostratigraphy, and petroleum geology. Jiménez Berrocoso *et al.* (2014) assumed that clay, and silt grained lithologies dominate the Lindi Formation being included in the Kilwa Group. Regarding the depositional setting, it came up with an apparent lateral continuity of the Lindi Formation and the consistent presence of a complete open marine across Coniacian – Santonian section and intervals within the Barremian – Middle Albian biota which indicates that the Lindi Formation was deposited in an outer shelf- upper slope setting that extended approximately 120 Km along the Tanzanian margin. For lithostratigraphy, the complete absence of bioturbation and relatively low % $CaCO_3$ but high organic carbon (up to 2.6% in the Turonian) indicates that this depositional setting experienced conditions of low energy most of the time and was located below the storm – wave base level.

1.6.5 Geochemical Analysis

Geochemical analysis has been a fully wide application in Ruvuma Basin in terms of characterisation of the geological history of East Africa Rift Valley System but also correlates with the provenance of oil seeps for petroleum exploration along the coastal margin between Mozambique and northern Tanzania in recent years.

The use of Rb – Sr data accompanied with the tectonostratigraphic model proposed a regional geological model involving three sequences: 1100 to 850 Ma (massive plutonic activity, limited deposition of supracrustal successions, granulite facies metamorphism, orthogneiss emplacement, and nappe tectonics during the Mozambican orogeny". The Mesoproterozoic crustal blocks were considered to be continuous across the Lurio Belt; 900 to 538 Ma (deposition of sediments (some units with a possible glacial affinity), correlated with the Katangan Supergroup of Zambia; ca. 550 Ma (Pan-African retrograde metamorphism and tectonics (including some thrusting) in an intracontinental environment (Pinna *et al.*, 1993).

Concerning petroleum exploration, commercial reports about regional geochemistry especially source rock generation is part of open discussion in oil companies and service companies whether under concessions or providing oil samples and well tests in Ruvuma Basin.

1.6.6 Petroleum systems

Based on a public domain report released in 2013, only a small number of wells have been drilled, consequently, the main potential source rocks remain undetected in the subsurface. Smelror *et al.* (2006) considered potential source rocks to be present in the syn-rift and early drift sequence throughout the basin.

The reservoir rocks in Ruvuma Basin contain several intervals of good quality, including Pliocene to Miocene sandstones, the Mnazi Bay gas field mainly covered by sandstone with good porosity and permeability and Msimbati gas field in the middle and north of the basin (Pereira-Rego *et al.,* 2012; Zongying *et at.,* 2013).

Seal rocks are composed of shale, mudstone, argillaceous limestone in addition to evaporites that occur in Mandawa, Ruvuma, and Somali basins (Salman and Abdula, 1995; Mbede, 1997; Smelror *et al*., 2006, Key *et al.,* 2008).

According to Smelror *et al.* (2006) traps are recognized in pre-rift fault blocks, stratigraphic traps in carbonates and Middle-Upper Cretaceous sands, and in young in Lower Tertiary basin.

1.7 EXPLORATION HISTORY OF THE SELOUS BASIN

The Selous Basin, also known as Luwegu Basin in Hankel (1987) – Figure 1.4, is configured as a NE-SW depocenter connecting the Ruvuma Basin in Mozambique, where extends northwards in a "Y-shaped" striking graben structure and represents the most extensive occurrence of Karoo rocks in East Africa, as described in Hankel (1987), Wright and Askin (1987), Catuneanu *et al.* (2005) and Langer *et al.* (2017).

Previous studies have subdivided the sedimentary sequence from five up to nine major lithostratigraphic units indicating Upper Permian to Lower Jurassic age for the Karoo Sequence (Besaire and Collignon, 1956; Hankel, 1987; Verniers *et al*., 1989; Catuneanu *et al*., 2005). The lithostratigraphic depositional sequences are covered in detail in Chapter 4.

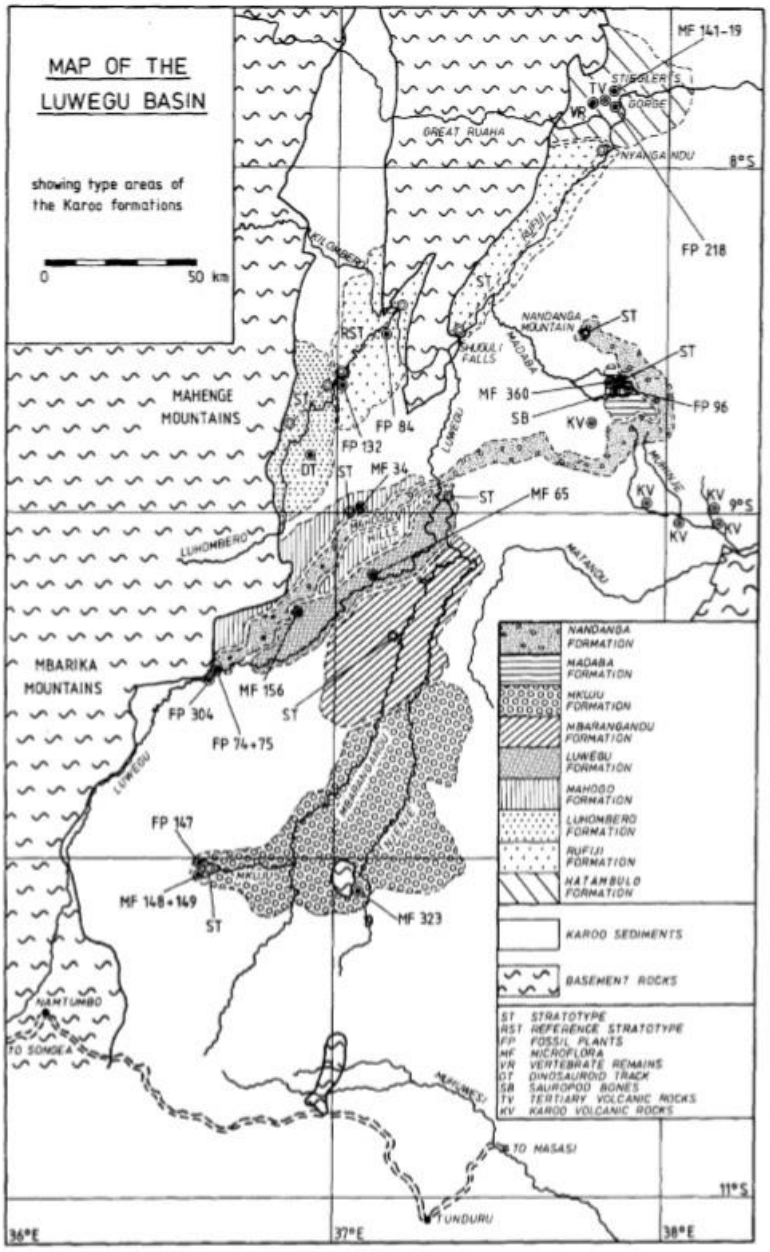

Figure 1.4 - A map representing the Karoo formations in the Luwegu (Selous) Basin (Hankel, 1987).

There has been oil and uranium prospection during the 1980s carrying out geological mapping, seismic acquisition, and drilling campaign of the Liwale-1 well, in the central part of the basin (Kreuser *et al*., 1990; Wopfner, 1994).

1.8 A COMPARISON WITH CONJUGATE BASINS IN MADAGASCAR

Madagascar is the fourth largest island in the world, and it is located east of East Africa in the Indian Ocean, in the centre of the Gondwana supercontinent (Figure 1.5). The island is separated by the Mozambique and Somali channels from the African continent. Its unique topography comprises of low topography and wide coastal plains at the western coast were formed by Late Palaeozoic-Cenozoic sedimentary basins. Adjacent, the highlands in the central-eastern part were assembled by uplifted crystalline basement rocks. On the east coast, the coastal plain is narrow, and the highland rises. During its assembly in the Neoproterozoic-Early Cambrian crustal fragments collided and amalgamated Madagascar trigging to the dislocation of Gondwana. Compression gave rise to high orogenic belts (Pan-African Orogen) throughout the supercontinent (Stern, 1994; Krabbendam and Barr, 2000; Meert, 2002; Geiger, 2004). In the sequence, the orogenic belts conducted to the extension and translation during the later Gondwana break-up (Pili *et al.*, 1997; Piqué *et al.*, 1999; Emmel *et al.*, 2004b).

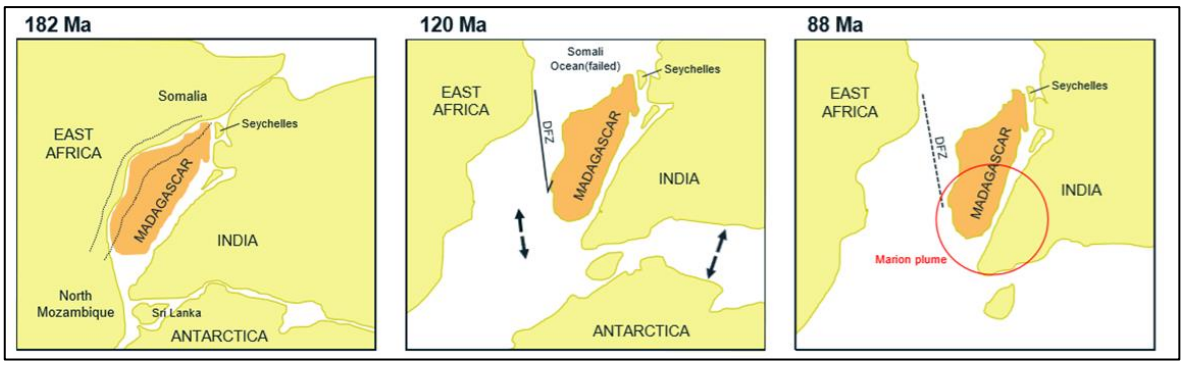

Figure 1.5 - The tectonic history showing the central position for Madagascar within reassembled Gondwana and the disruption and dispersal process occurred the disintegration of Gondwana and led to the present situation of Madagascar as the fourth largest island in the world positioned in the Indian Ocean. Modified after (Reeves, 2014) in Trater (2017).

Due to the opening of the Atlantic rift, Madagascar has a continuous Precambrian sedimentary record rich in organic matter for oil & gas exploration in its three main western sedimentary basins: Ambilobe, Mahajanga, and Morondava (Wescott and Diggens, 1997; Pique *et al.*, 1999).

There are studies that have proposed that the extensional Somalia Margin is conjugate to Majunga Basin (NW of Madagascar), whereas the transform Tanzania - North Mozambique margin is conjugate to Morondava Basin, southwest of Madagascar (Coffin & Rabinowitz, 1988; Reeves, 2014; Klimke & Franke (2016).

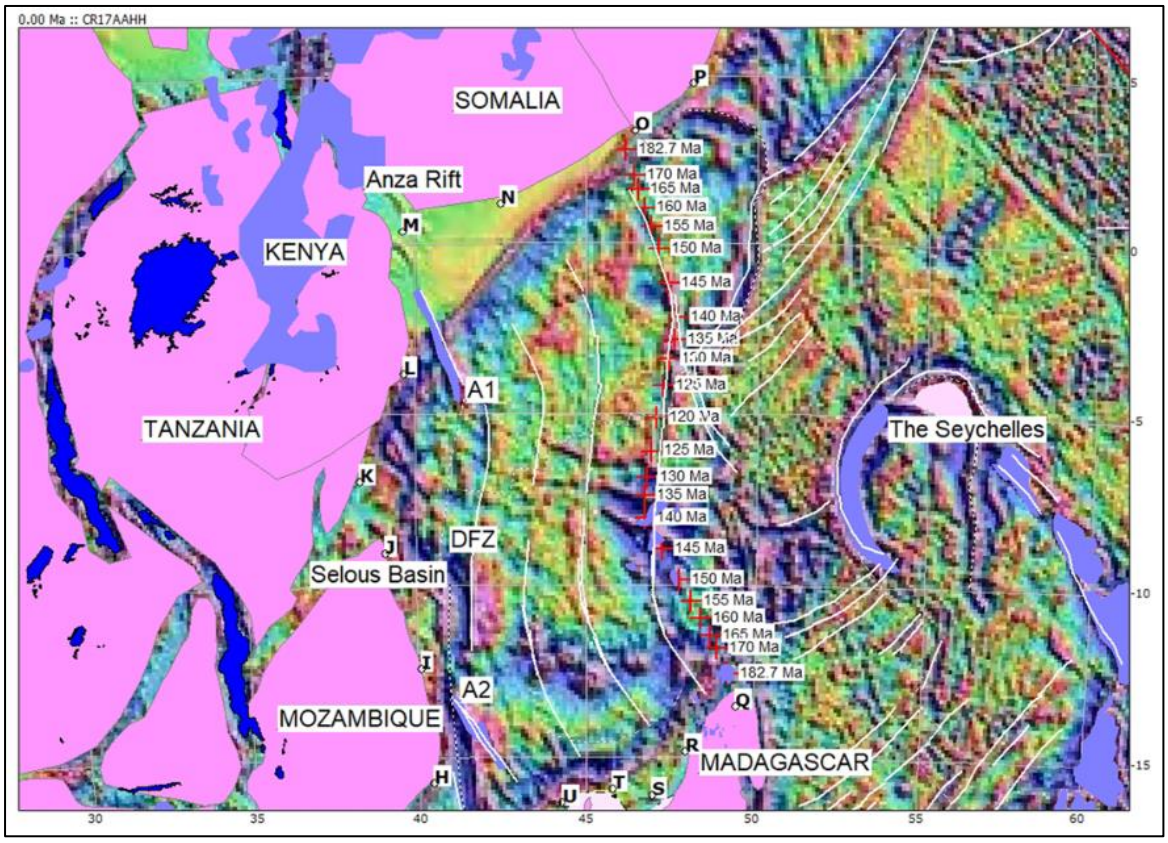

Figure 1.6 - Ocean floor topographic data in ocean gravity images in detail (Smith and Sandwell, 1997; Sandwell et al., 2014) for Africa–Antarctica corridor, with locations for the interpreted positions of the mid-ocean ridge at intervals for the modelCR17AAHH in Reeves (2017).

A recent model (CR17AAHH), created by palaeogeographic reconstruction, described the early phases of the Gondwana disruption; the tectonic development of the western Indian Ocean ensemble was described in four regimes by Reeves *et al.* (2016), and to explain how the global constraints of an all-Gondwana assembly (Figure 1.6). At 182.7 Ma aligns the contours of the southern margin of the Selous Basin in Tanzania with those of the southernmost margin of the Morondava Basin in Madagascar. Most of the crust extended during the Karoo stayed below the Morondava Basin in Madagascar, much less along the Tanzania – Kenya margin (Reeves, 2017). The research also suggested that some earlier stretching, most likely in a NE–SW direction through sinistral strike-slip on the Southern Trans-Africa Shear System (STASS) (Reeves *et al*., 2016) which demonstrably underwent sinistral strike-slip movement during the Karoo stages (Catuneanu *et al*., 2005).

It continued into stretched elements of the full-thickness Precambrian crust we envisage lying between Madagascar and Tanzania-Kenya in a pre-Karoo reassembly possibly found 200 km or more outboard of the present-day Precambrian outcrop in Tanzania and Madagascar (Reeves, 2017).

1.8.1 Morondava Basin

The interest in a reconnaissance of the Morondava basin started in the 1950s when the first geological maps were produced, and the first hydrocarbon investigations initiated.

The Morondava Basin is located on the west coast of Madagascar, about 400 km from the east coast of the African continent. It covers an area of about 220,000 km^2, extending into deep water. The offshore part of the basin is relatively unexplored, but the presence of an active hydrocarbon system is indicated by gas shows in some of the wells; by gas chimneys and brightening on seismic data, and by a geochemical sampling of sea-bottom sediments (Roberts *et al*., 2018).

The Morondava Basin is part of the divergent margin along the western part of Madagascar that developed in response to the Karoo Rift Phase (Permian-Triassic) and the subsequent separation of Madagascar from East Africa during the Lower Cretaceous. The basin extends from onshore (east) to offshore (west) where water depths reach 3,000 meters and it is bounded to the west by the Davie Fracture Zone in oceanic crust, to the east by the Precambrian basement of Madagascar, and to the northeast by a structural high that separates it from the Majunga Basin (Geiger *et al.,* 2004).

The geology of the Morondava Basin can be described into mega sequences, primarily the Paleogene/Neogene Post Rift; the Upper Cretaceous Post Rift; the Upper Jurassic to Lower/Middle Cretaceous Syn Rift; and the Karoo Rifted Terrain (Permian to Lower Jurassic) (Bassias *et al.,* 2015; Tari and Rock, 2016; Roberts *et al*., 2018).

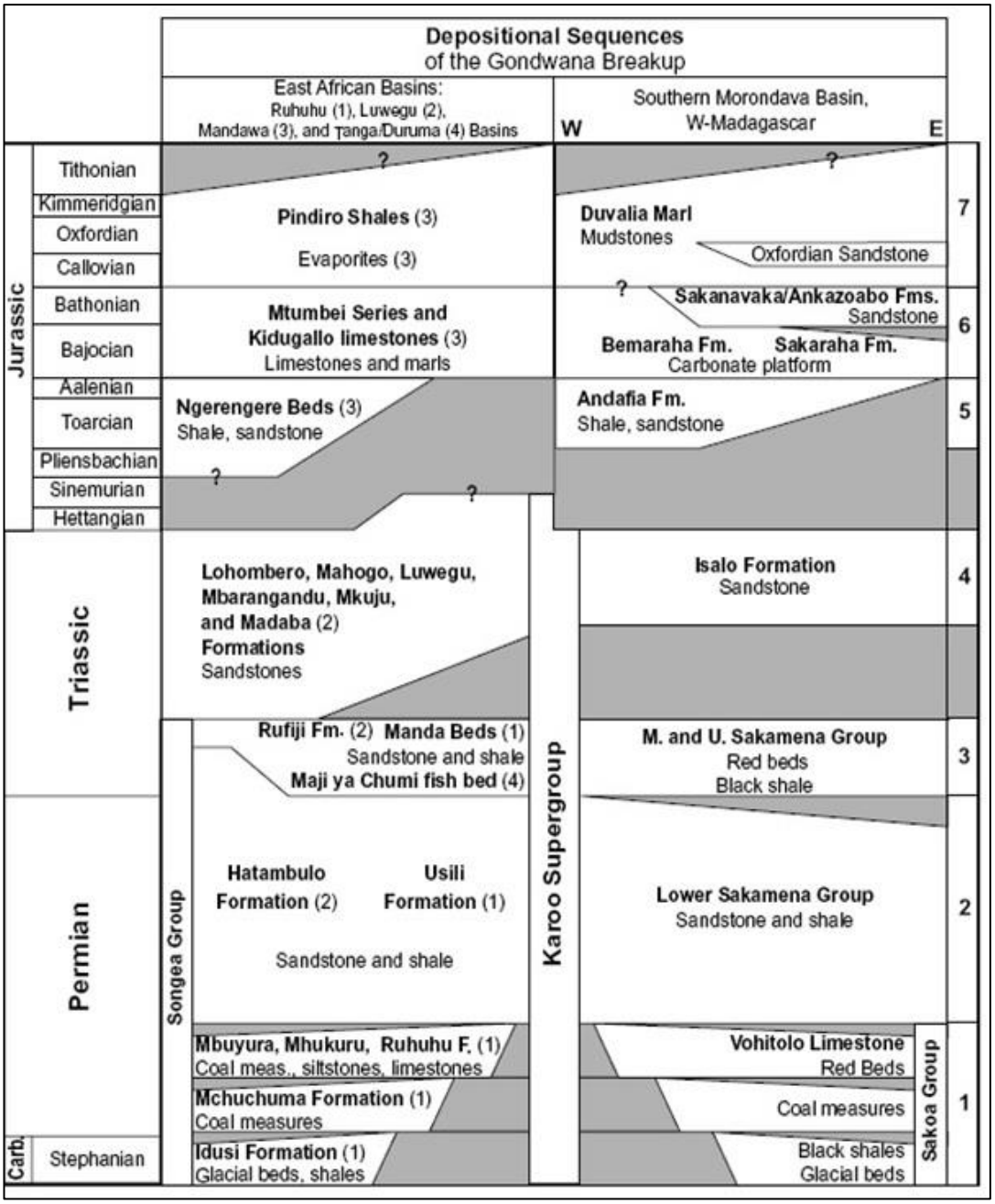

Figure 1.7 - A correlation between the depositional sequences in the East African Basins (left) compiled from Hankel (1994), Kreuser (1995), and Wopfner (1994, 2002) and southern Morondava Basin (right) from Geiger et al. (2004).

Besairie (1972) used depositional sequences to define the southern Morondava basin, limited in successive stratigraphic groups during the deposition of the Karoo Supergroup (Figure 1.7); the sequences consist of the Sakoa and Sakamena groups and the Isalo Formation. Clark (1998); Wescott and Diggens (1997, 1998); Piqué *et al*. (1999) reappraised the sedimentological and stratigraphical configuration for Karoo sequences.

Geiger *et al*. (2004) reviewed and subdivided the Jurassic depositional sequences to correlate Mandawa Jurassic depositional sequences compiled from Kreuser (1995).

The major NW–SE striking gravity features in Africa, align with similar features in Madagascar (Fig. 1.8) (Piqué *et al*., 1999; Geiger, 2004; Geiger *et al*., 2004). Different onshore and rift trends and pre-existing Precambrian structural grains include major onshore shear zones, for example, NW-SE oriented Aswa and Cupa Shear Zones and the NE-SW oriented South Trans African Shear System (STASS). The offshore margin is segmented into normal fault-controlled segments (Somalia offshore and conjugate Majunga in Madagascar), oblique-slip or pull-apart (Kenya-North Tanzania offshore), and transform segment (South Tanzania-North Mozambique) (Sinha *et al*., 2019).

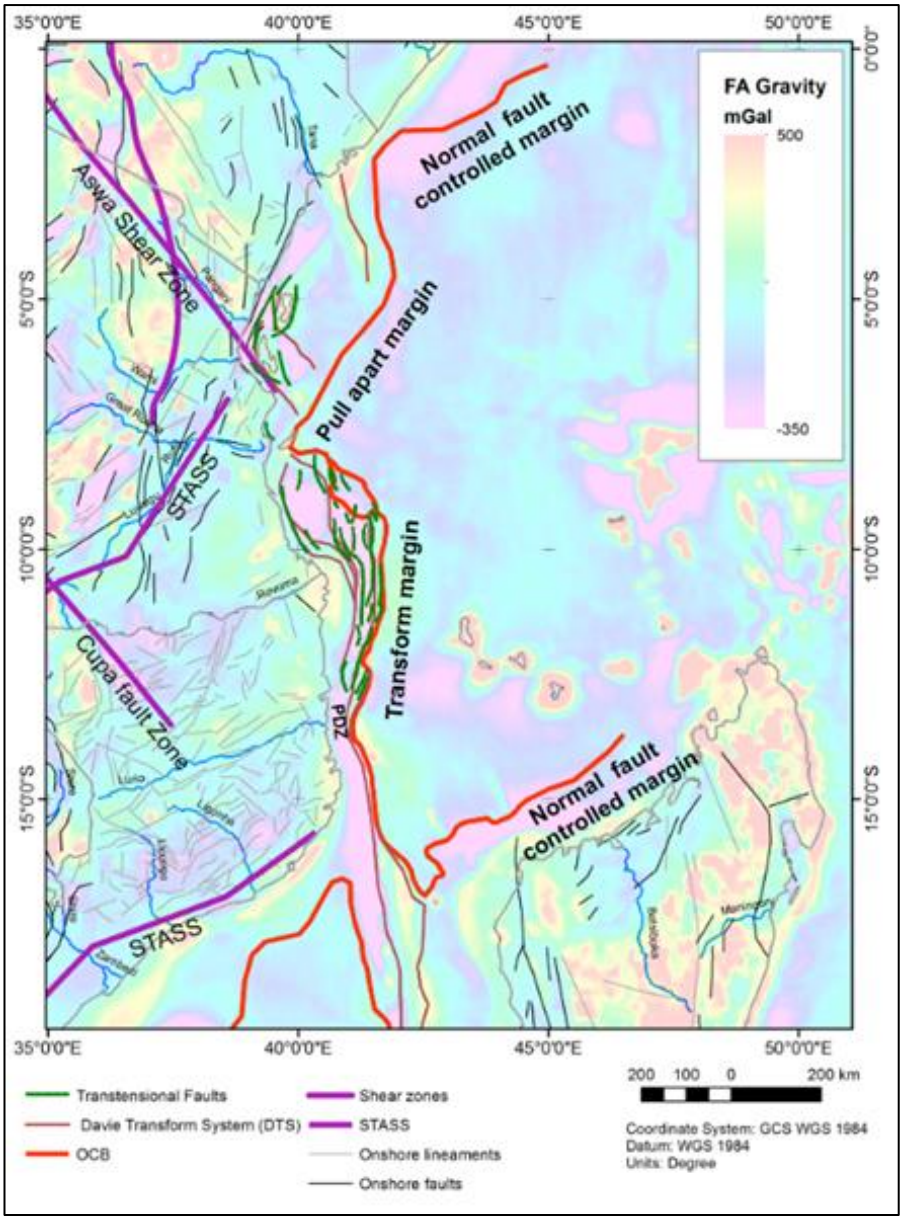

Figure 1.8 - The tectonic element map of the East Africa onshore and offshore (modified after Commission for the Geological Map of the World, 1990; Rapolla et al., 1995; Tanzania Petroleum Development Corporation Promotion Brochure, 2009). Backdrop: Free-air gravity map (Sandwell et al., 2014).

1.8.2 Davie Fracture Zone

The Davie Fracture Zone has been observed as a linear oceanic fracture zone, a prominent morphological feature in the Mozambique Channel linked with the breakup between Eastern and Western Gondwana (Figure 1.9). It is characterised by a zone of N-S trending gravity low anomaly bounded to the east by gravity high anomaly striking across the continental margin of Mozambique and Madagascar (Coffin and Rabinowicz, 1987; Geiger *et al.*, 2004; Müller *et al.*, 2008; Reeves *et al.*, 2016).

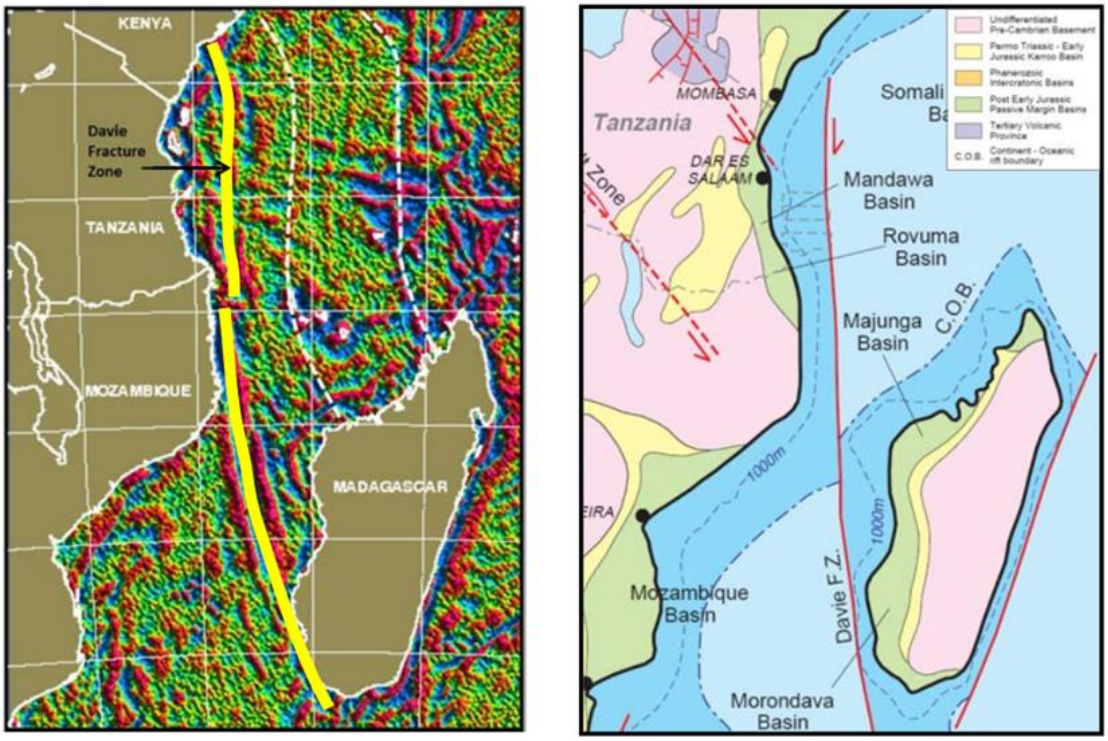

Figure 1.9 - Tectonic and regional gravity interpretation (left) across the Davie Fracture Zone (right) (Higgins and Sofield, 2011).

The ridge was discovered by Heirtzler and Burroughs (1971) and proposed that the Davie Ridge represents the expression of a transform fault resulting from the relative southward motion of Madagascar with respect to Africa after observing bathymetric elevation in the Mozambique Channel. The feature was then termed the Davie Fracture Zone by Scrutton (1978).

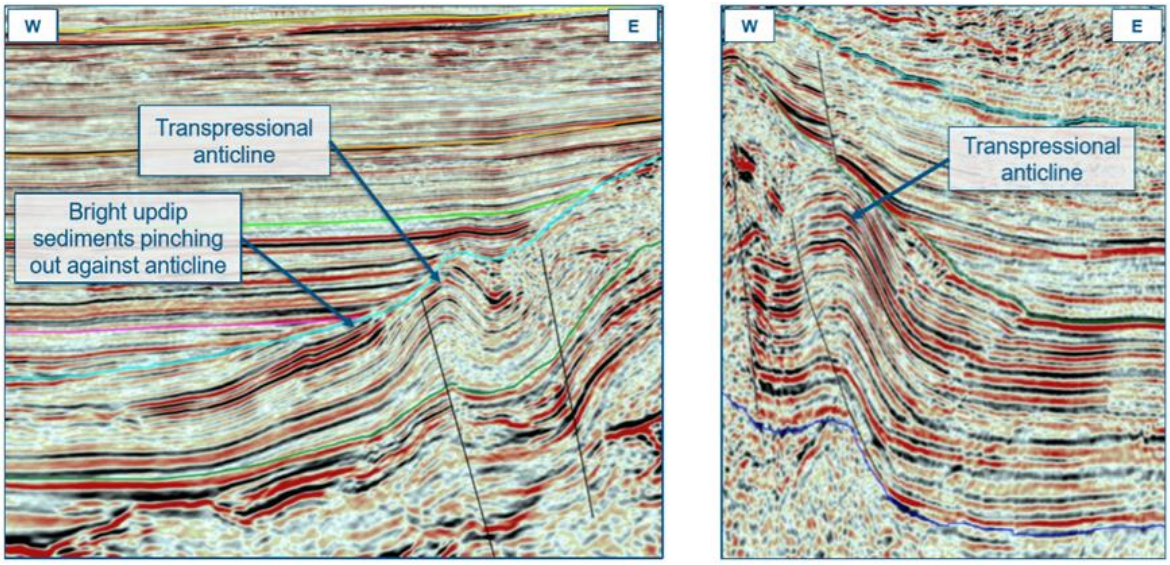

Figure 1.10 - Transpressional structures on the flanks across the Davie Fracture Zone interpreted in seismic lines (Tranter, 2017).

A number of studies have been carried out to describe the origin and evolution of the Davie Fracture Zone, its provenance and influence in the tectonic processes (Figure 1.10), and its correlation to onshore tectonic features (Reeves and de Wit, 2000; Schettino & Scotese, 2005; Reeves, 2009; Gaina *et al*., 2013; Reeves *et al*., 2016; Reeves *et al*., 2016; Reeves, 2017; Sinha *et al.*, 2019).

1.8.3 Majunga Basin

The Majunga basin is located in the north-western quadrant of Madagascar (Figure 1.11). Herein the Majunga basin is defined as extending between the crystalline basement outcrops at the eastern margin of the basin, the Bekodoka basement high in the Cap St. Andre area in the southwest to similar basement exposures along the Ampasindava Peninsula to the northeast. The 3,000 m isobath is arbitrarily taken to be the seaward limit of the basin. The stratigraphy appears to be significantly different between the onshore and shelf as it is known from well and outcrop data, and the deep-water domain, where it is inferred from the new seismic data. The following brief description of the stratigraphic column is therefore highly generalized, and it reflects geology seen in the onshore part of the Majunga Basin (Jeans and van Meerbeke, 1995).

Figure 1.11 - Reconstruction from Reeves et al. (2002) in Banks (2008) highlighting the Majunga Basin (in red).

In terms of stratigraphy to correlate to the salt studied in the present work, thick sequences of continental clastics and occasional coals began to accumulate in the graben areas (Figure 1.12). The Sakoa, Sakamena, and Lower Isalo (Isalo I) formations represent the initial flux of clastics into Karroo rift basins (Jeans and van Meerbeke,1995; Tari *et al.*, 2004).

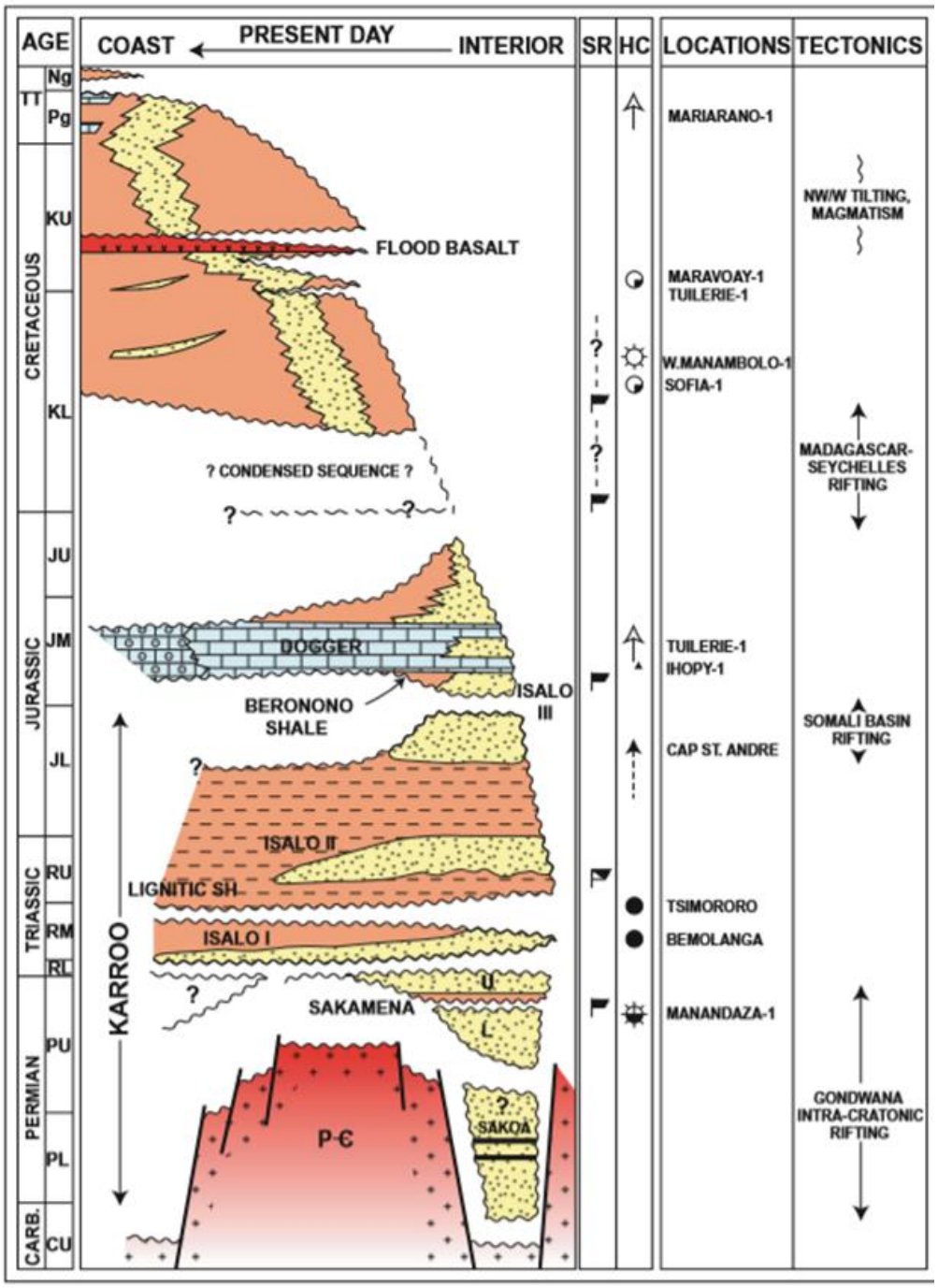

Figure 1.12 - Stratigraphy of the onshore Majunga basin from Jeans and van Meerbeke (1995).

Unconformably overlying these sediments is the Upper Isalo (Isalo II). The upper part of the Isalo (Isalo III) succession also contains some gypsum, probably age equivalent with the massive salt that is seismically imaged in the deep-water offshore (Tari *et al.*, 2004). Lalaharisaina and Ferrand (1994) suggested that salt was not found in the onshore Majunga basin, neither in outcrops nor in boreholes. Its presence under the shelf was inferred from the existence of detached fault blocks at the coastline. Further work of Banks *et al*. (2008) suggested through seismic geometries (Figure 1.13), that the salt basin extends onshore.

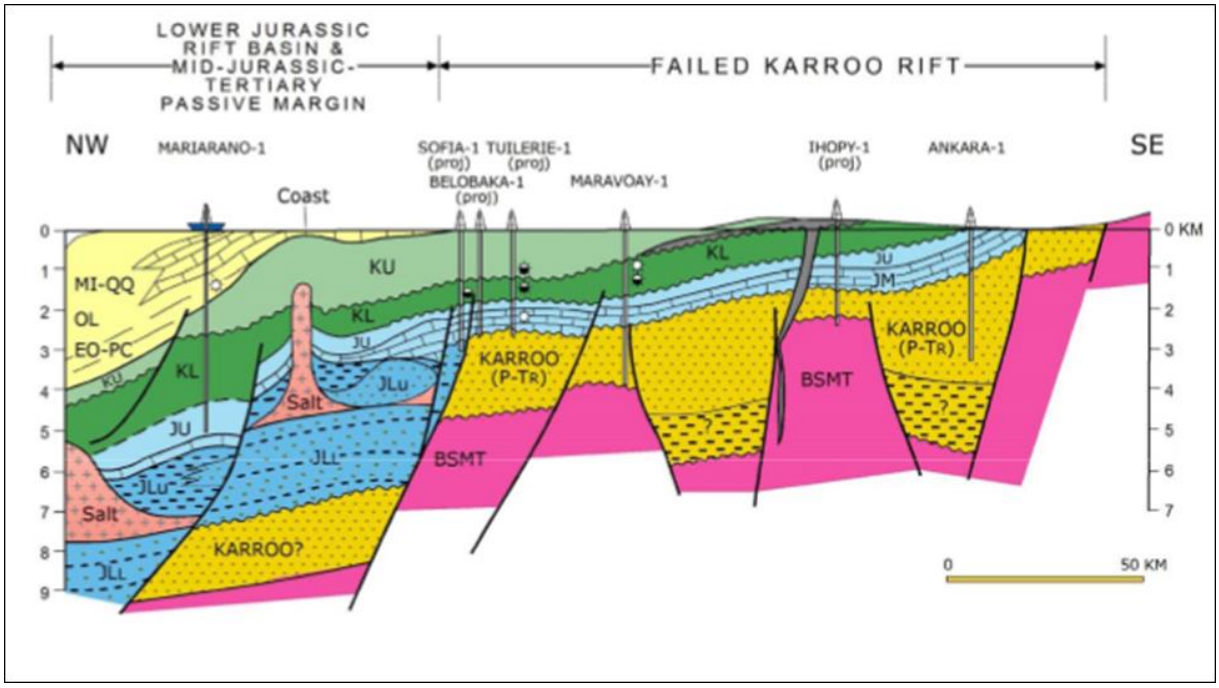

Figure 1.13 - A cross-section NW-SE suggesting Jurassic salts in the coastal extending onshore in the Majunga Basin (Banks, 2008).

Dirkx (2016) mentioned the Majunga Basin as a Jurassic salt basin characterised by allochthonous salt diapirs and canopies (Figure 1.14). It is also mentioned in (Davison & Steel, 2017), that a Toarcian salt is present in the rift section of the Mandawa Basin and is interpreted on seismic in the offshore part of the Majunga Basin, possibly of similar age.

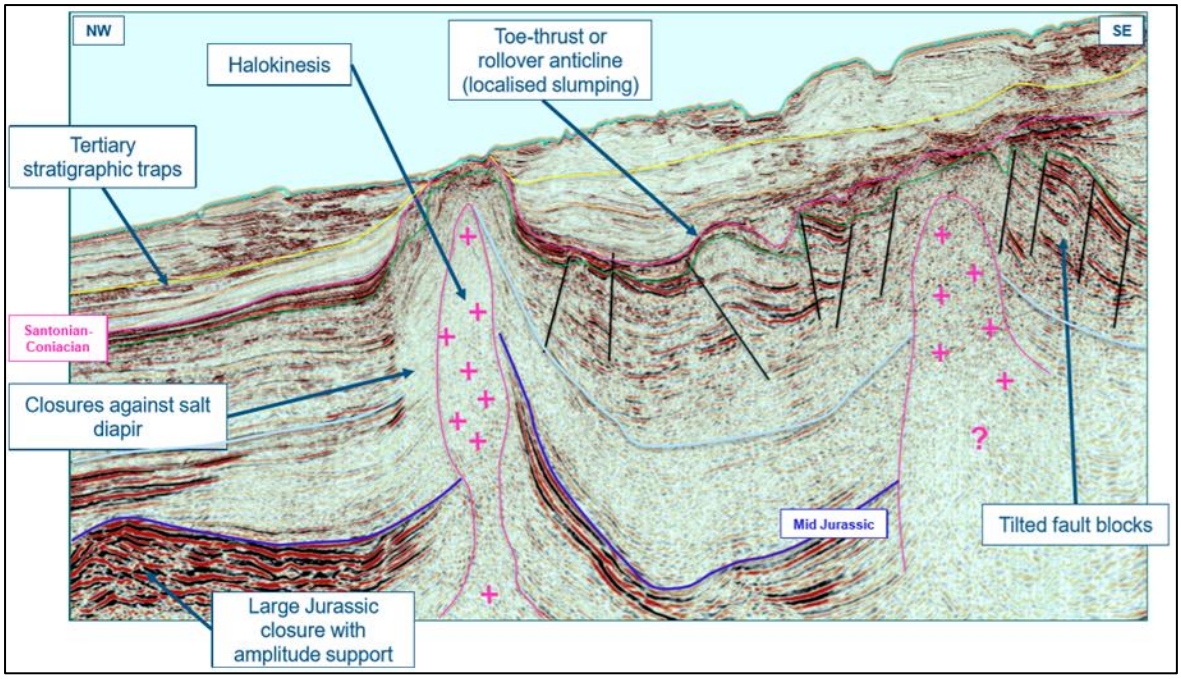

Figure 1.14 - Majunga Basin described as a Jurassic salt basin with the presence of allochthonous salt diapirs and canopies Dirkx (2016).

1.9 RESEARCH QUESTIONS

The questions addressed by this research were:

- **What were the different types of salts present in the southern coastal Tanzanian basins?**
- **When did marine evaporite diapirism take place, how many episodes of the movement were in place, and when did diapirs breach the palaeo-land surface?**
- **How did the basin sedimentation respond to the lithostratigraphy caused by diapirism?**
- **How did marine evaporite diapirism breach previous traps or were new trap geometries created in younger layers?**
- **How did halokinesis influence the thermal evolution across the Mandawa Basin, thereby affecting seal and hydrocarbon generation and migration?**
- **Were the evaporitic strata in Kizimbani-1 well linked to the Nondwa Formation, or were they a younger evaporitic event?**
- **How did the lateral migration of shallow salt uplift in the Mandawa Basin and did it extend to the Ruvuma and Selous basins?**
- **How did the seismic attributes contribute to the identification and interpretation of seismic horizons, faults to produce the 3D geocellular model?**
- **Could the well logs and seismic data be used to estimate the total amount of basinal extension of diapirism?**
- **Would revise the model of the geological evolution of the Mandawa Basin indicate the diapirism extension to the conjugate basins in Madagascar?**

1.10 AIM AND OBJECTIVES FOR THE PRESENT STUDY

This research aimed to re-evaluate the Mandawa and Ruvuma basin evaporites along the Tanzanian continental margin and possibly correlate to analogue basins in Madagascar. It addressed a regional synthesis covering geological and geophysical well data sets used in the processes of seismic interpretation, isopach maps, lithostratigraphy analysis, 2D restoration sequences, seismic attributes, time-depth conversion, and a 3D geocellular model to re-assess the salt basin.

CHAPTER 2

DATA ACCESSED

2.1 REPORTS

The database received for this research is a historical database containing the legacy of wells drilled from oil companies since the 1950s in Mandawa Basin (Figure 2.1). TPDC/Dominion Petroleum Limited (Dominion) was last under the exploration license from 2006-2012. The company relinquished the area of Mandawa block after unsuccessful drilling exploration. From 2012 on, the entire database remained without use, even though the wells have proved a good capacity of source generation. Count Geophysics Limited acquired the right to have the geophysical database comprising seismic and well data of the eleven wells (Mandawa, Ruvuma, and Selous basins), daily drilling reports, and maps entitled in this study. The company ceded the database for academic use as well as consultants agreed to act as advisors on this project.

The well data have been used for stratigraphic studies, structural and thickness maps and the geophysical dataset have been used for tie seismic with wells, seismic attributes for salt structure analysis, time-depth conversion, regional structural model in-depth studies.

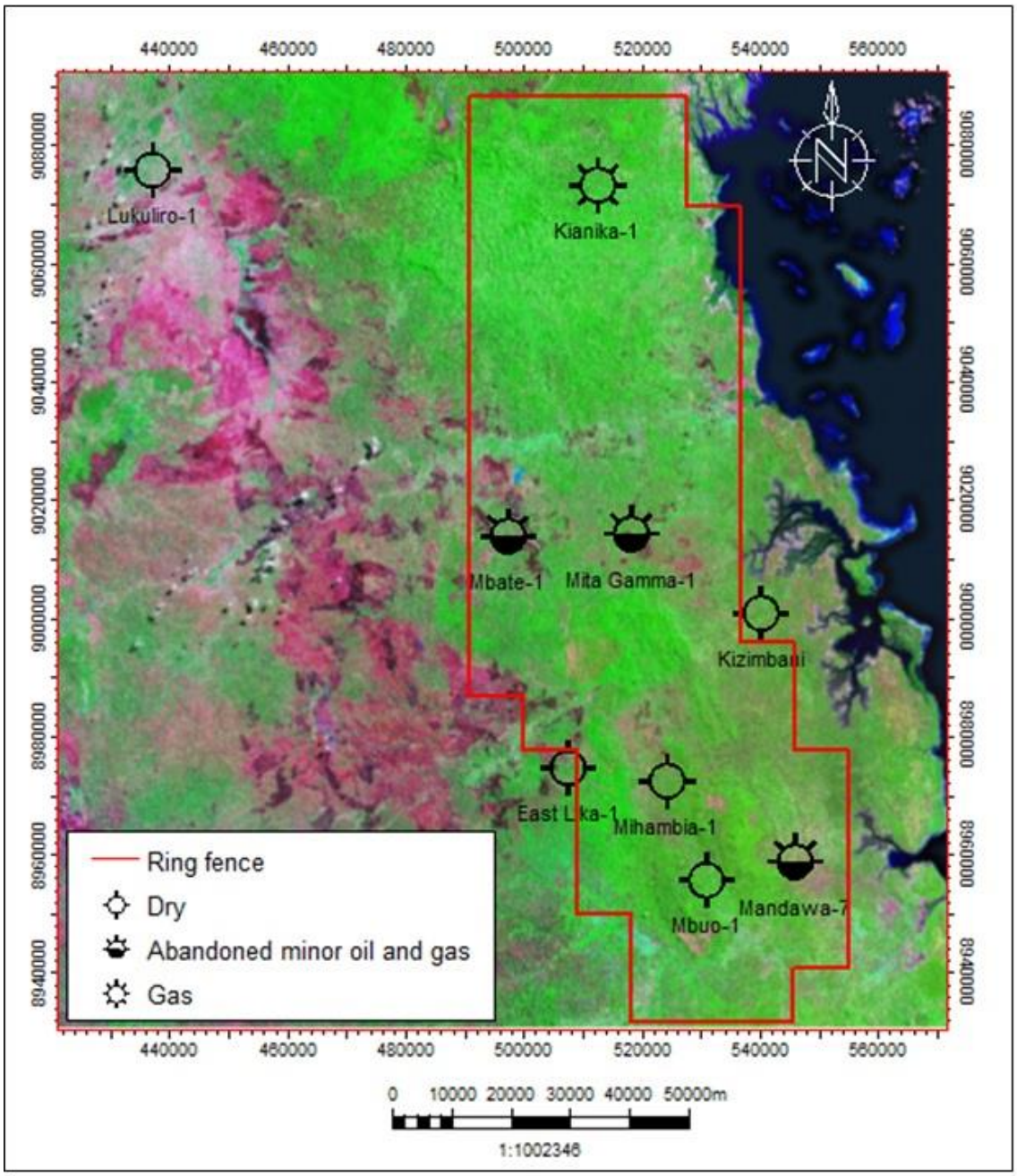

Figure 2.1 - Map of Mandawa PSA block containing the main wells of this study: Mihambia-1 (dry), Mbuo-1 (dry), East Lika-1 (dry), Mandawa-7 (abandoned), Kizimbani-1 (dry), Mita Gamma-1 (abandoned), Mbate-1 (abandoned), Kianika-1 (gas).

2.2 WELL DATA

2.2.1 Well logs – LAS files

Well logs were imported in a standard file format known as Log ASCII Standard (LAS) used to exchange geophysical wireline well log information along a wellbore (see Appendix 2.2.1). To establish a conventional geological model, the wells presented were normalized to metric depth, well header values are according to industry-standard format as well as colour patterns to represent well log curves in tracks.

Well logs: Standardized from feet to meters only the sonic logs remain in μs/ft.

Well tops (markers): Markers were defined after performed well correlation resulting in facies lithologies of Mandawa Basin. They bound between geological units as seen in the borehole. They can then be used during the model building phase as an additional control of the positions of the model horizons. This ensures that horizons match the observed horizon data in the well location (Schlumberger, 2018).

2.2.2 Well heads

There are twelve exploration wells used as control wells in the area of study, four of which fall outside Mandawa exploration block (Figure 2.2). Well heads provided the X, Y, Z coordinates of each well in UTM with offset (Rotary Table or Kelly Bushing) . The information available in reports were: Total Depth (TD), Kelly Bushing (KB) and UTM coordinates for all wells. The well data content is summarized in Appendix 2.2.2.

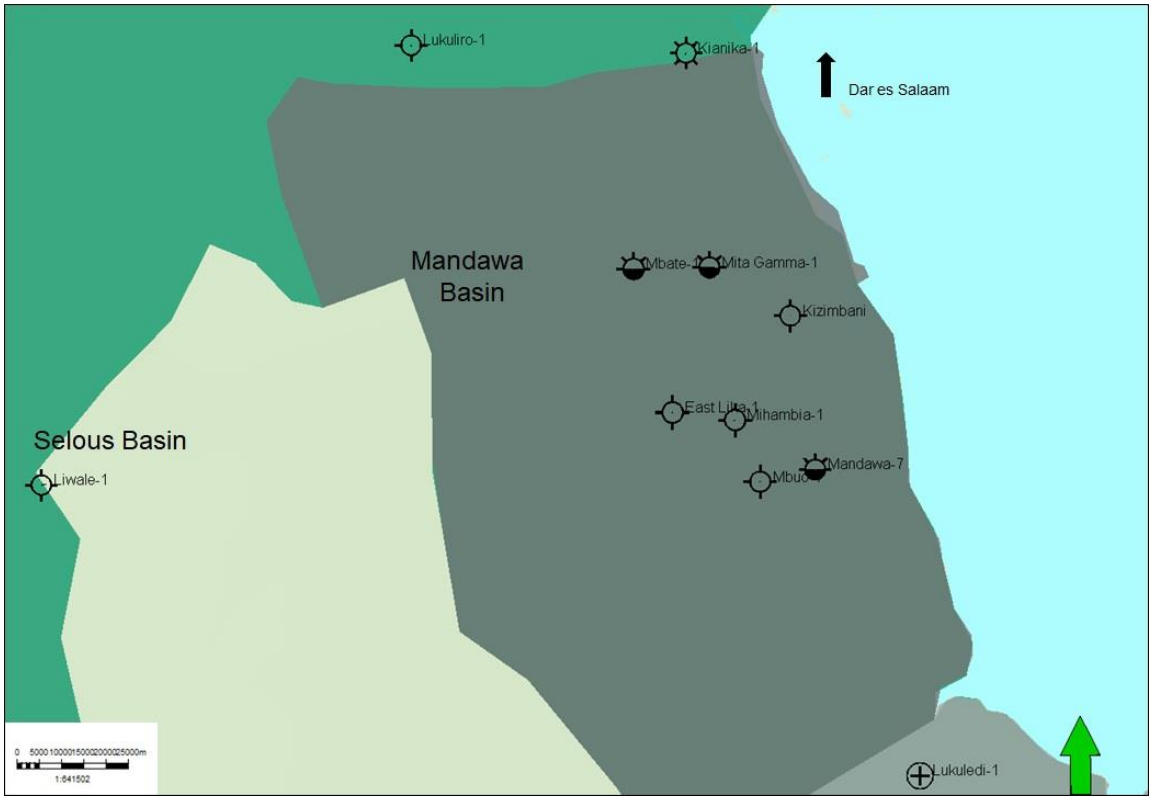

Figure 2.2 - Location of wells for this study in the southern Tanzanian continental margin.

2.2.3 Checkshots

A checkshot is conditioned to the first seismic arrival at the receiver giving the travel time. They are time/depth pairs for a borehole obtained by analyzing the first seismic arrival for known depths in the borehole. Checkshots are used to obtain a time-depth relationship for the borehole and are essential for generating synthetic seismograms and are used to scale an integrated sonic log (Schlumberger, 2018). Checkshot data content is summarized in Appendix 2.2.3 to the related wells.

2.3 SEISMIC DATA

2.3.1 2D seismic lines

To manipulate seismic data, it is important to comprehend specific input data: seismic survey, checkshots, and the polarity of the data. The oil industry developed several standardized formats allowing the data sharing between different software. SEG-Y is one of the most important and is used in exporting and importing. SEG is acknowledged as the Society of Exploration Geophysicists and it is one of the most recognized geophysical societies worldwide for the petroleum industry.

The existing set of 252 2D seismic lines in SEG-Y format distributed along the Mandawa, Selous and Ruvuma basins and wells respectively (Figures 2.3, 2.4, 2.5 and 2.6) for this study distributed in inlines and crosslines with a bin spacing of 50 m (see Appendix 2.3.1) has been previously interpreted by oil companies and consultants (Hudson, 2011).

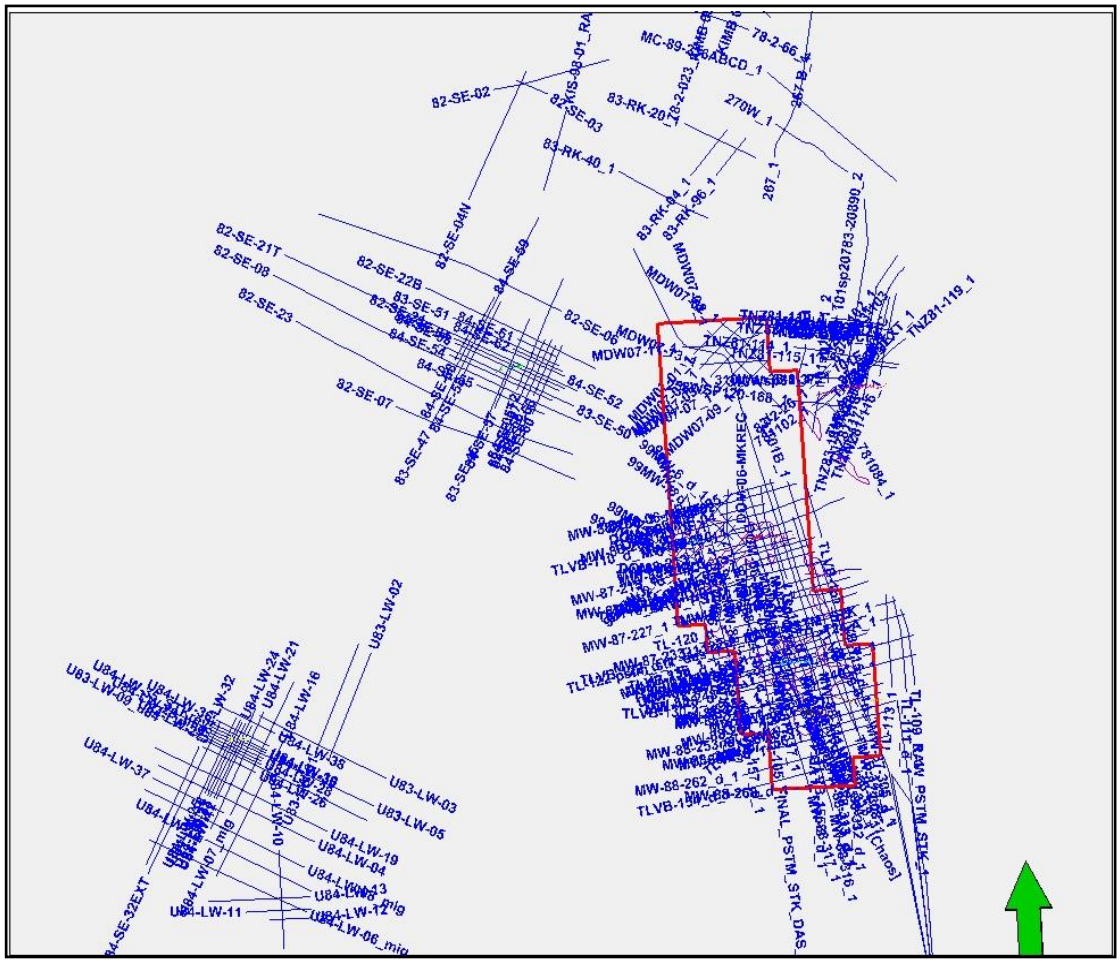

Figure 2.3 - Representation of the 252 2D seismic lines covering Mandawa Basin (red ring fence on right) and Selous Basin (left).

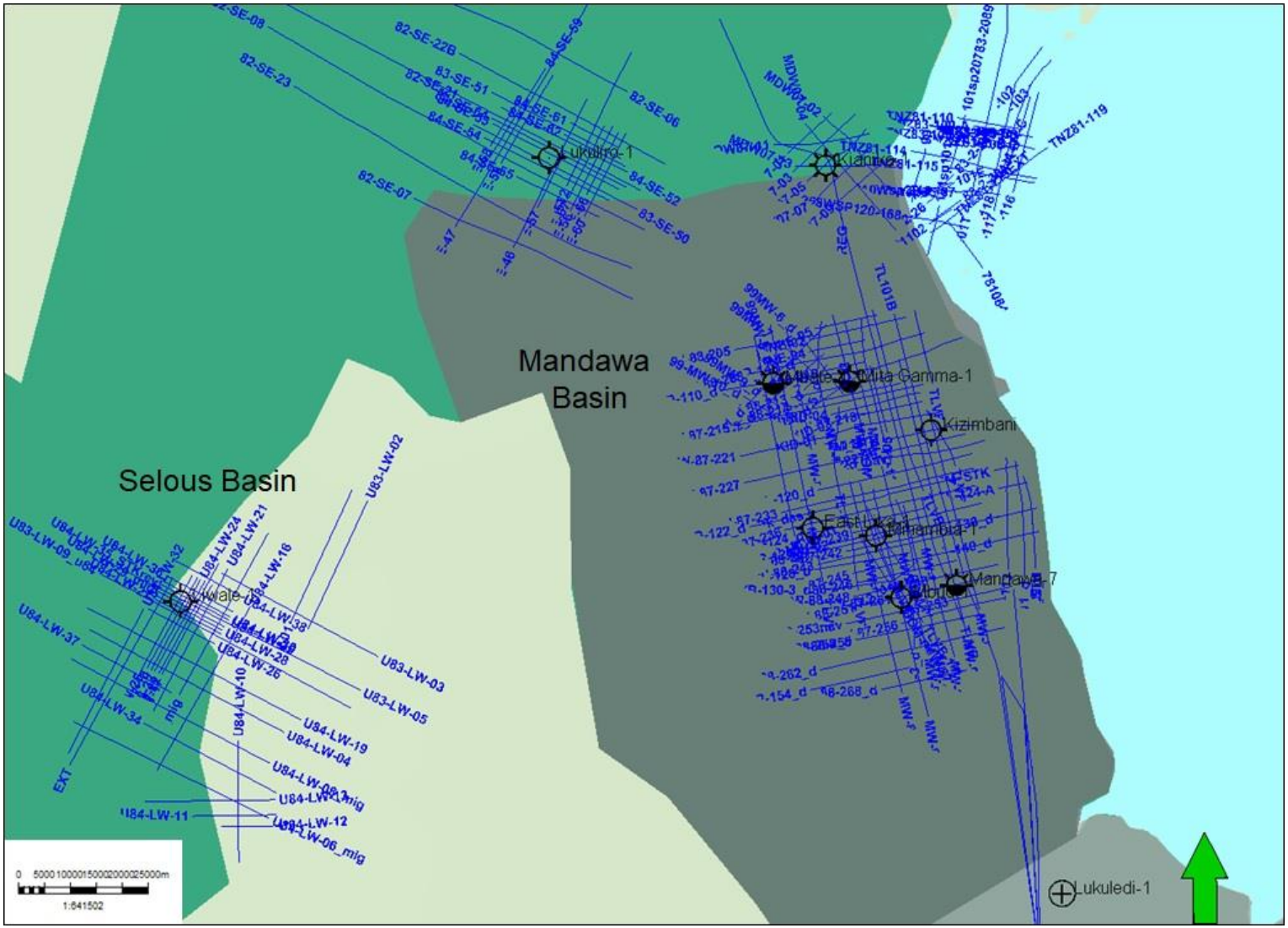

Figure 2.4 - A view of the wells accessed in this study in the Tanzanian onshore basins.

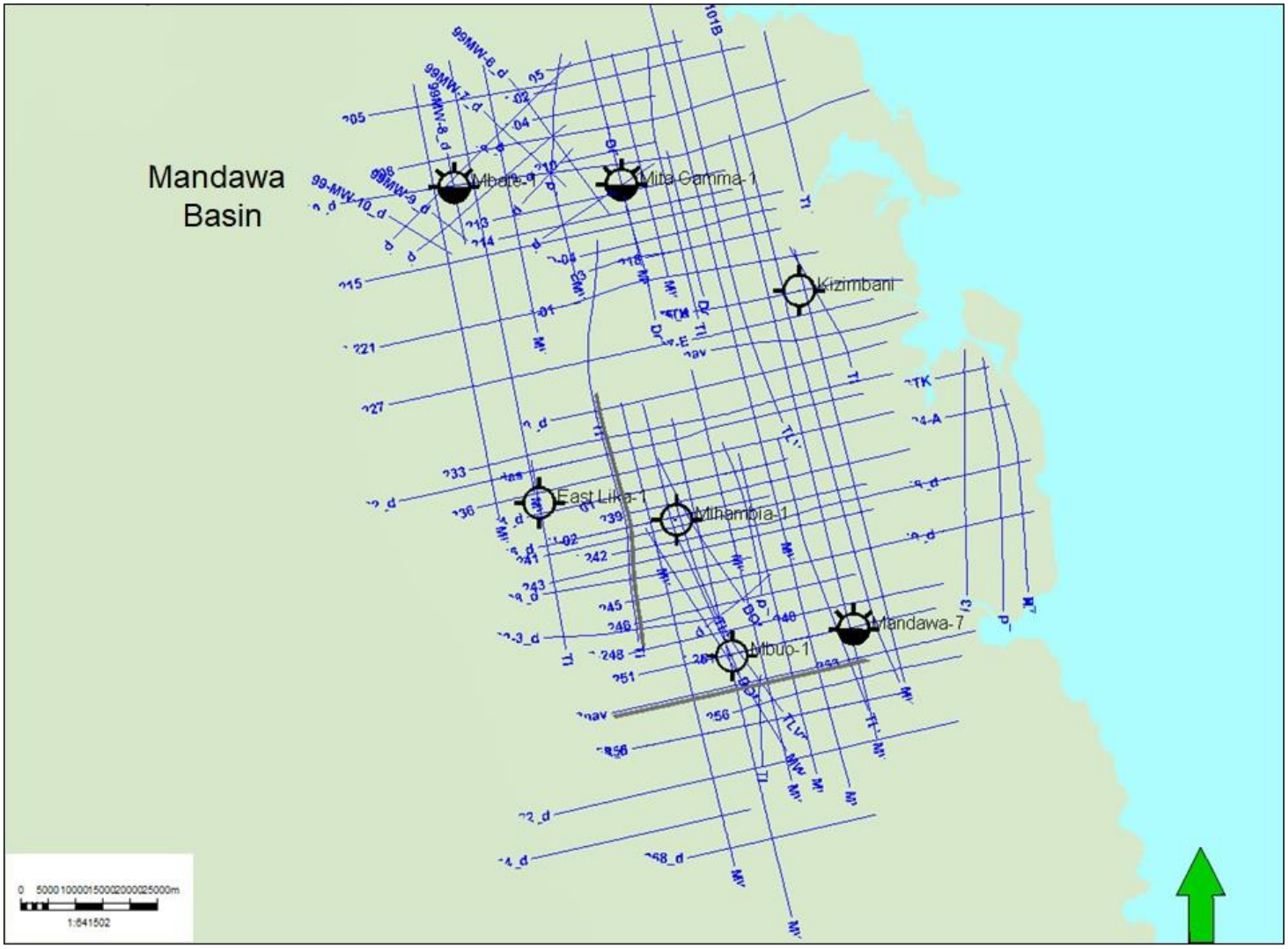

Figure 2.5 - The 2D seismic lines in Mandawa Basin analysed in this study and the wells (from north to south: Mbate-1, Mita Gamma-1, Kizimbani-1, East Lika-1, Mihambia-1, Mbuo-1, Mandawa-7).

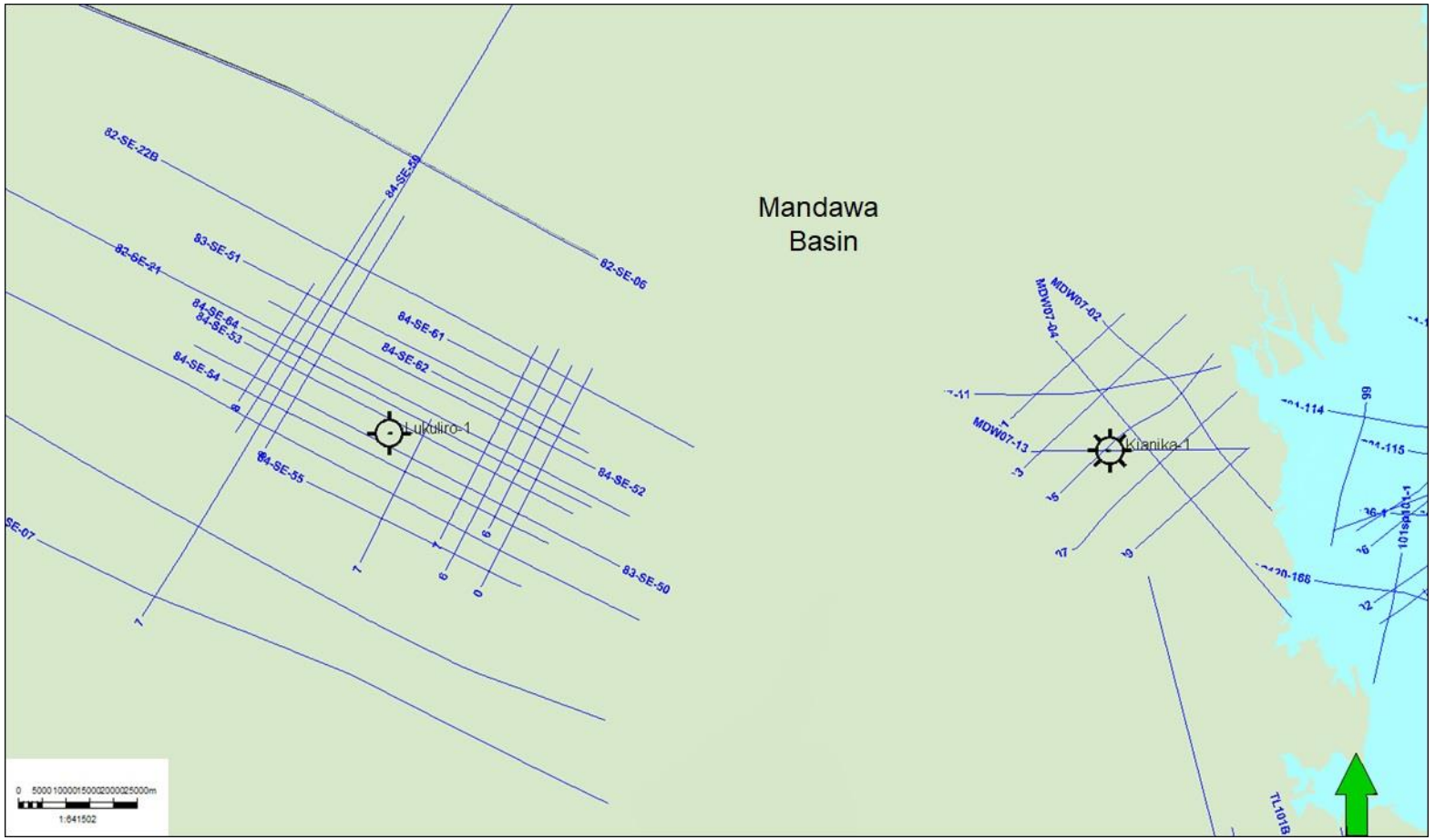

Figure 2.6 - The wells Lukoliro-1 (left) and Kianika-1 (right) and 2D seismic lines accordingly outside Mandawa PSA, Tanzania.

2.3.2 Reprocessed 2D seismic lines

The input 2D seismic line data of this study were processed in different decades, with the oldest processed being replaced by newer ones. The last reprocessing campaigns took place during 2006 and 2008. During 2006, Dominion acquired 494.7 km of 2D seismic data in the Mandawa and Kisangire PSAs, part of which included a regional line DOM-06-MKREG, which crossed the north Mandawa area and connected existing seismic data in the Kisangire and south Mandawa blocks (Figure 2.7). Further 2D seismic data was acquired across this area to delineate this structure in 2007 and 2008. About 67 2D lines were reprocessed in 2006 covering Mandawa and Kisingire areas in a total of 2064 km according to the 2D Seismic Reflection Survey by IMC Geophysics International Limited on behalf of Dominion Petroleum Limited to provide supplementary data in areas where data had previously been acquired. In 2008 a new reprocessing has been carried out by Fugro Seismic Imaging Limited in the north Mandawa area covered 226 km containing information about the lines to target for interpretation in this study - MDW07-01, MDW07-02, MDW07-03, MDW07-04, MDW07-05, MDW07-07, MDW07-09, MDW07-11 and MDW07-13. In this manner, the 2D lines correspond to the ending of a deSpike substitute in the interpretation process to the PSTM lines. The lines beginning with the initials MIH are from the Mihambia area, whilst the lines KID are from Kidumba and KIS lines are from Kisingire.

The processing flow has been divided into two paths. One brute stack without deconvolution (called 'basic' version) and brute stack with deconvolution and some noise filter reduction applied (called 'refined' version). Either basic or refined version was applied only for MNE and KREG lines in block. Otherwise, brute stack used was deconvolution with spike deconvolution and Final Stack.

Mandawa Block:

1 Transcription from SEG-Y to ProMAX
2 Raw data QC
3 2D CMP binning geometry and trace data QC
4 Trace edit
5 First break suppression value
6 Elevation statics
    a) final datum elevation: 0 m (MSL)
    b) replacement velocity: 2200 m/s
    c) math method: shotholes using uphole info

7 True amplitude recovery (TAR) with spherical divergence correction ($1/TV^2$)
8 Spiking/predictive deconvolution
   a) type of deconvolution: zero phase spiking
   b) operator length: 80
   c) white noise: 0.1
9 Moveout stretch muting interactively picked from corrected shots
10 2D CMP interactive velocity every 1250 m
11 2D CMP stack
12 Automatic residual statics surface consistent correction
13 Time invariant equalization
14 F-X deconvolution
15 Final stack

Changes in shot and receiver locations were annotated based on the information available in the observer's log. Some errors were found in geometrical spreading and traces. A basic tracing mute to remove the effect of NMO stretch and high amplitude first break refraction energy was applied. muting in gather pre-processing were shallower than stacked mute.

Some deconvolution tests were taken all the way through to the stack stage for better comparison of the result. Deconvolution with predictive varies gaps, varies operator length, varies design window, and white noise 0.1% were tested and displayed. For Mandawa lines spiking deconvolution was used to achieve quick stack data.

The time variant filter was used to suppress noise lying outside frequency range of desired reflection data. The applied filter was linearly interpolated between control times. Narrow bandpass and wide bandpass filters were tested on the data to obtain the final filter parameters.

Analysis of these filter panels led to design of the time variant filter. Once high cut filter limiting was selected, a low cut filter test was run on the data having those high cuts applied, and a final filter selected.

Static corrections were applied to seismic data to compensate for the effect of variations in elevations, weathering, thickness, weathering velocity with reference to a datum.

Elevation static were applied at this stage to reduce travel times to a common datum level, and also the daily elevation static stacks to monitor stack data quality at the target horizon (s).

Figure 2.7 - Seismic acquisition on land in Mihambia in 2006. Dynamite in shot holes in subsurface in the line Mih-4 was used to generate acoustic waves (Hudson, 2011).

Since acquiring the Mandawa Block, Dominion has built a large legacy database comprising all the geological and seismic data previously acquired by other operators (BP, Agip, Shell, Tanganyika), and has also acquired 730 km of new 2D seismic lines. Dominion has carried out a detailed exploration evaluation of the Mandawa Block, and initially focused on the plays not evaluated by previous operators, in particular, the Mihambia Formation post - Nondwa salt play, which was evaluated with the Mihambia

-1 well (Figure 2.8). Dominion has also carried out extensive surface geological mapping in the block, building on earlier work by BP and Shell (Hudson, 2011).

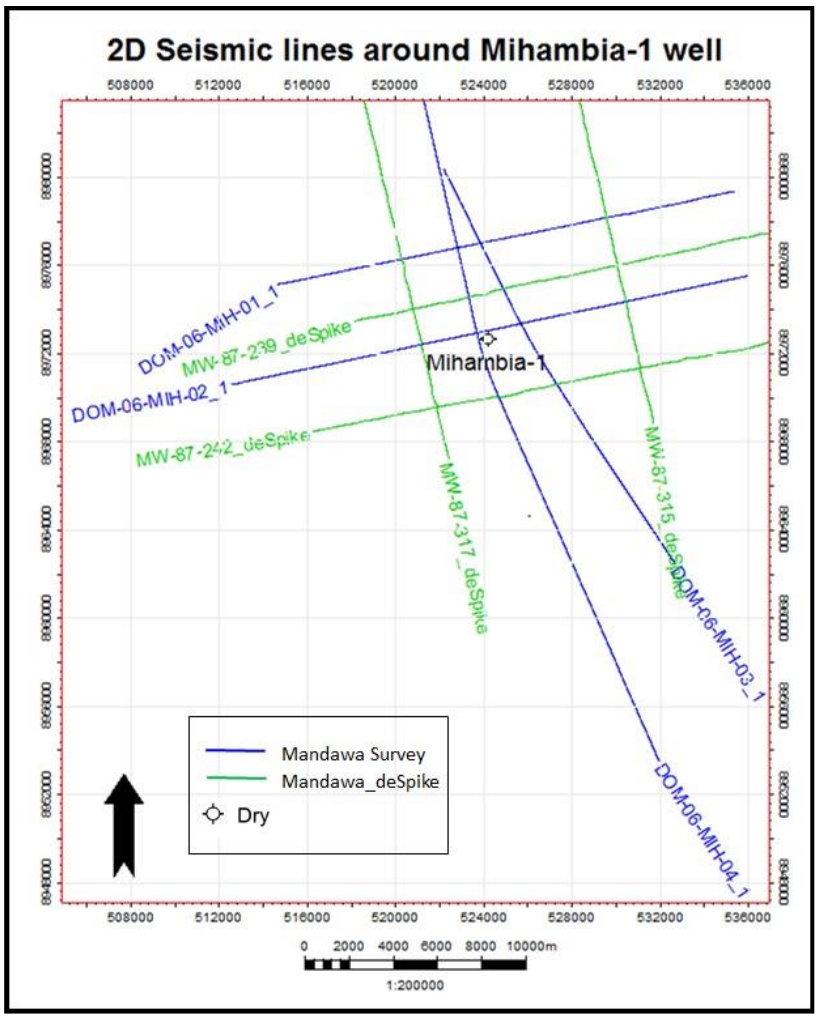

Figure 2.8 - Example of processed 2D seismic lines around Mihambia-1 well Blue colour lines are from the original Mandawa Survey; green colour lines were reprocessed with the suffix "deSpike" to classify them.

2.4 SHAPEFILE

2.4.1 Coordinates datum

Geological and geophysical interpretation involves the creation of earth models whose response describes observed data from geophysical recordings, well logs, and cores.

Coordinate system: Geographic Coordinate Reference System (CRS): WGS 84

Projection: Former Arc 1960/ UTM Zone 37S (Universal Transverse Mercator).

Unit: International Meters

Ellipsoid: Clarke 1880 (RGS)

The Arc 1960 geodetic datum references the Clarke 1880 (RGS) ellipsoid and the Greenwich prime meridian. It encompassed the older local projection survey data in Tanzania such topographic base maps used in the field surveying. Petrel software has a catalog that allows uses to find and select the appropriate Coordinate reference system bond to a geodetic transform (Georepository, 2016). The transform defines the conversion from the coordinate system's datum to the WGS84 datum. In the software Petrel, Tanzania is storaged in the UTM 84 Zone 37S.

2.4.2 Area of Mandawa Block

Additional data such as the ring-fence for Mandawa PSA block in shapefile format (see Appendix 2.4), markers, previously interpreted faults, and horizons were also received as reference data.

2.5 SOFTWARE

In this study the software Petrel versions 2015 to 2018 (software platform property of Schlumberger) has been adopted. Petrel E&P Platform combines multidisciplinary workflows from exploration (geophysics application) to geological modelling, petroleum engineering and drilling. Although this software, produced by Schlumberger Limited, was developed for reservoir modelling in previous decades it gained more attention among Oil & Gas professionals with a demand to expand the workflow to add geophysical functionalities.

From this perspective, Petrel was chosen to be used in this study as it has a complete set of applications. Before conducting to the objectives of this thesis, it was necessary to import geological data (data management), perform quality check the dataset of 2D seismic lines, well logs to perform the stratigraphic framework, geophysics, structural and the final geocellular model. Regardless of its workflow, Petrel is able to receive and import data previously interpreted in miscellaneous commercial exploration and modeling software packages.

As Petrel has its own dynamic to import data, in order to define the best functionality of all data collected, the methodology of this study follows four steps: set the coordinate system (1), import well head (2), geophysical well logs (3), import well tops (markers) (4), and the seismic survey (5).

CHAPTER 3

METHODOLOGY

3.1 THEORETICAL BACKGROUND

Most of the world's petroleum occurs in sedimentary rocks. The location of petroleum reserves requires an understanding of the nature of the rocks in which the reserves occur, and well logs are one of the primary sources for such data. Effective seismic interpretation requires correlating seismic data with well data (Adcock, 1993). At the current stage of seismic exploration technology, 2D and 3D seismic surveys have demonstrated their efficiency and reliability as methodologies and concepts have been tested and constantly improved since the advent of onshore oil drilling. In particular, 2D seismic surveys are used to build structural frameworks of the subsurface with a certain degree of reliability (Omar *et al.*, 2006; Filippova *et al*., 2011). However, in complex structural settings, this technique has proven to be insufficient and thus should mainly be used at the initial stage of field exploration to reveal promising exploration targets and to provide an initial estimate of their potential as hydrocarbon-bearing reservoirs (Filippova *et al.*, 2011).

Well logs (see Table 3.1) are defined as a continuous record and as described by Jarvis (2006) compute the physical measurements of a petrophysical property in a formation within the confined space of a borehole along with its depth. Nonetheless, there are issues involved in measuring these petrophysical properties in well data across an entire borehole. During wireline runs in the field, the data are not recorded throughout the wellbore since it is a costly operation for companies that reduce it to certain sections, frequently measured in target zones already determined. Added to this fact, it is common to receive corrupted or tainted data. According to Asquith and Gibson (1982) logs help to define physical rock characteristics such as lithology, porosity, pore geometry, and permeability in order to identify productive zones, to distinguish between oil, gas, or water in a reservoir, and to estimate hydrocarbon reserves. Rider (2002) discussed that geophysical logs act as records of radioactive properties, whilst acoustic logs (as a function of depth) are typical of each lithology.

Table 3.1. Types of well logs and its properties and functionalities (Cant, 1992).

Log	Property measured	Units	Geological interpretation
Spontaneous potential	Natural electric potential (relative to drilling mud)	Millivolts	Lithology, correlation, curve shape analysis, porosity
Conventional resistivity	Resistance to electric current flow (1D)	Ohm-metres	Identification of coal, bentonites, fluid types
Micro resistivity	Resistance to electric current flow (3D)	Ohm-metres and degrees	Borehole imaging, virtual core
Gamma ray	Natural radioactivity (e.g., relater to K, Th, U)	API units	Lithology (including bentonites, coal), correlation, shape analysis
Sonic	Velocity of compressional sound wave	Microseconds/metre	Identification of porous zones, tightly cemented zones, coal
Neutron	Hydrogen concentration in pores (water, hydrocarbons)	Per cent porosity	Porous zones, cross plots with sonic and density for lithology
Density	Bulk density (electron density) (includes pore fluid in measurement)	Kilograms per cubic metre (g/cm^3)	Lithologies such as evaporites and compact carbonates
Dipmeter	Orientation of dipping surfaces by resistivity changes	Degrees (azimuth and inclination)	Paleoflow (in oriented core), stratigraphic, structural analyses
Caliper	Borehole diameter	Centimetres	Borehole state, reliability of logs

In this thesis, a geophysical and geological analysis has been performed to create a 3D geocellular model that delineates the lithostratigraphy analysis, a simplified stratigraphical sequence, and salt tectonics of the Mandawa Basin, southern Tanzania.

3.2 GEOPHYSICAL WELL LOGS USED IN THIS STUDY

This section involves a suite of the most used continuous geophysical well data (Figure 3.1) in a qualitative analysis of the well-log data involved through its well-logs signatures such as Caliper (CALI), Gamma-Ray (GR), Sonic log (Δt), Density (RHOB), Neutron (NPHI) and Resistivity (ILD and ILM) (Glover, 2012). A petrophysical characterisation to define potential lithological lateral variation and the Seismic Well Tie process added to auxiliary well logs such as ΔT-E (Delta-E Corrected after editing) and ΔT-E-Corrected (Delta-E Corrected after editing).

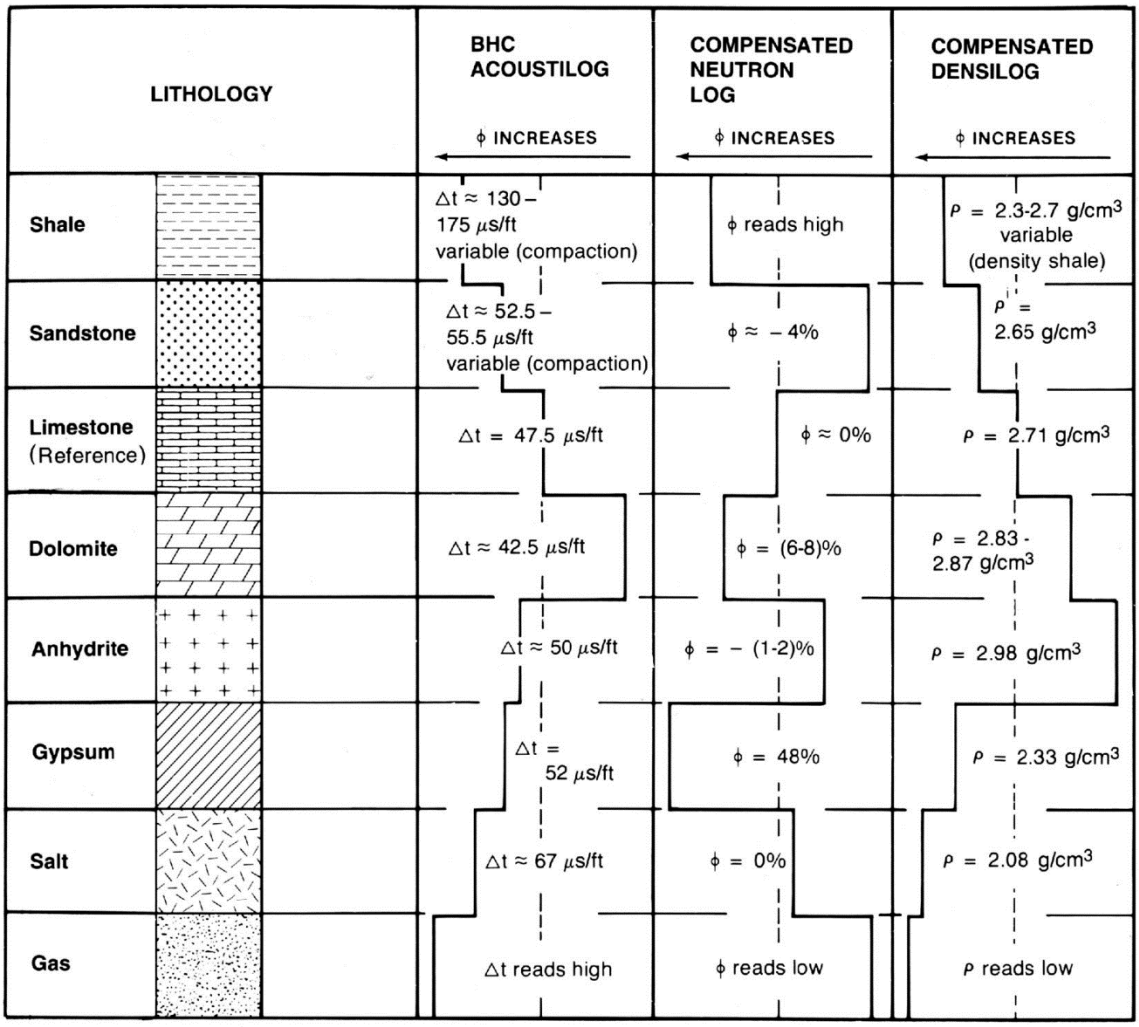

Figure 3.1 - Well logging from several rock lithologies according to acoustic, neutron and density logs. Extracted from Glover (2012).

3.2.1 Gamma-Ray

Natural radiation of unstable elements consists primarily of alpha, beta, and gamma rays but it is practical to measure only the gamma radiation in a wellbore (Atlas, 1982). The gamma ray log (GR) measures the natural radioactivity transmitted by unstable elements ^{238}U, ^{232}Th and ^{40}K whereas the spectral suite measures these three elements separately (Rider, 2002).

The official unit of gamma ray measurement in the log is the API but can also be plotted on a linear scale of 0-100% shale. The gamma ray log detects the shale content due to their radioactivity shales, giving a high GR log record while sands and carbonates exhibit low reading except in cases of radioactive sands due to zircon, glauconite, etc (Atlas, 1982; Rider, 2000). In this matter, gamma ray log is applied to lithology identification providing evidence of reservoir rocks as distinguished from shales, shale content, formation evaluation, alternative log when the Spontaneous Potential (SP) log cannot recognize mud filtrate resistivity in a well. It highlights the importance of gamma ray log in delineating the low radioactivity of non-radioactive evaporites as halite, anhydrite, and gypsum (Atlas, 1982).

The index of gamma ray is determined using the formula below from Schlumberger (1974):

$$\mathrm{GR} = \frac{GR_{\log} - GR_{min}}{GR_{max} - GR_{min}}$$

Where:

V_{sh} = Shale volume

GR_{log} = Gamma ray log reading

GR_{max} = Gamma ray log reading in shale zone

GR_{min} = Gamma ray log reading in clean sand zone

3.2.2 Sonic or Acoustic log (Δt)

A sonic log is a type of acoustic log also classified as a porosity log, that measures the slowness displaying traveltime of a compressional sound known as P-waves versus depth (Figure 3.2). It is typically recorded by pulling a tool on a wireline up the wellbore. The

tool emits a sound wave that travels from the source to the formation and back to a receiver (Schlumberger, 2017).

For Asquith and Gibson (1982), and Atlas (1982) the interval transit time (Δt) or "slowness" of the wave in microseconds per foot (μs/ft) is the reciprocal of the velocity of a P-wave in feet per second, which is diagnostic for lithological identification, porosity, compaction, stratigraphic correlation, overpressure and as input data for the synthetic seismogram generation.

The sonic log is diagnostic for certain rocks as coals and evaporites for this study, which have a constant, well-recognized velocity and transit time.

Lithology (matrix)	V_{ma} (ft/sec)	Compressional Δt_{ma} (μsec/ft)	Shear Δt_{ma} (μsec/ft)
Sandstone			
Unconsolidated	17,000 or less	58.8 or more	93
Semiconsolidated	18,000	55.6	92.9
Consolidated	19,000	52.6	92.9
Limestone	21,000	47.6	
Dolomite	23,000	43.5	72
Shale	6,000 to 16,000	167 to 62.5	
Salt (halite)	15,000	67	116
Coal			
Lignite	7,150	140	
Bituminous	8,300	120	
Anthracite	9,500	105	
Granite	20,000	50	
Minerals			
Calcite	22,000	46	89
Quartz	18,000	51	74
Evaporites			
Anhydrite	20,000	54	98
Gypsum	19,000	53	
Trona		65	
Iron Minerals			
Limonite		57	103
Pyrite		38	59
Siderite		44	85
Hematite		46	72
Micas			
Biotite		51	224
Muscovite		47	79

Figure 3.2 - Velocity (V) and transit time (Δt) values of the most common lithologies (after Carmichael, 1982).

3.2.3 Caliper

The caliper log (CALI) is a tool normally measured mechanically that records the diameter and shape of a borehole along the drilling depth. Notice that wellbores are usually irregular, this well log tool quantifies hole diameter at multiple locations through a vertical profile, as an example of new tools that obtain with accuracy a well shape and orientation (Schlumberger, 2017).

The scale is prompt measured in inches (in) which is the pattern in use for bit size measurements. Feature points for a caliper tool mainly are to determine hole diameter along with the presence of other logs, evaluate cementing and well-completion operations, a qualitative indication of both the condition of the wellbore and quantify the mud necessary to in place prior hole stability (Schlumberger, 2017).

3.2.4 Resistivity

As resistivity is defined as the ability of a substance to impede the flow of an electrical current, in subsurface exploration, resistivity logs are a type of electric logs essential information evaluation in a well (Asquith and Gibbon, 1982; Schlumberger, 1991). Hence, measure the resistivity of a formation accompanied by porosity and water resistivity is important in the manner to establish the hydrocarbon saturation versus water relationship; depending on the difference in resistivity between rocks filled with hydrocarbon content and rocks filled with formation water content. Resistivity is called true resistivity (R_t) and expressed in units of ohm.meters^2 or meter, displayed in logarithmic scale from 0.2 to 2000 ohm.m, in order to capture very low readings in measurement curves (Schlumberger, 1991).

To facilitate the readings during well correlation in this study, the well log curves used during wireline runs in Mandawa block were dual induction curves referred to as Deep Induction Resistivity (ILD) and Medium Induction Resistivity (ILM).

3.2.5 Density

The formation density log can be defined as gamma ray density log (Rider, 2002) or usually on its abbreviations RHOB, RHOZ, and DENS and it measures the bulk density of the formation. As defined by Schlumberger Well Services Inc. (1989) it detects gas-bearing zones, determines hydrocarbon density, evaluates shaly sand reservoirs and complex lithologies, and a reliable method to identify evaporites in well logs. They

bombard the formation with radiation and measure how much radiation returns to a sensor (see Table 3.2 from Glover, 2012). Rider (2002) corroborated by mentioning the functionality of density log for calculation of seismic to create a synthetic seismogram along with the seismic velocity extracted from acoustic log to produce acoustic impedance as input data in the forward modeling process.

Scaled in units of density, gm/cc, or km/km^3, density log is frequently used scales are a range of 2.0 to 3.0 gm/cc or 1.95 to 2.95 gm/cc across two tracks for common lithologies.

Table 3.2. Matrix densities used in the density porosity with the apparent density read by the tool against the actual bulk density (Glover, 2012).

Compound	Composition	Actual Bulk Density, ρ_b	2 Z/A	Effective Electron Density, ρ_e	Apparent Bulk Density, ρ_a
Quartz	SiO_2	2.654	0.9985	2.650	2.648
Calcite	$CaCO_3$	2.710	0.9991	2.708	2.710
Dolomite	$CaCO_3.MgCO_3$	2.870	0.9977	2.863	2.876
Anhydrite	$CaSO_4$	2.960	0.9990	2.957	2.977
Sylvite	KCL	1.984	0.9657	1.916	1.863
Halite	NaCl	2.165	0.9581	2.074	2.032
Gypsum	$CaSO_4.2H_2O$	2.320	1.0222	2.372	2.351
Anthracite (low)		1.400	1.030	1.442	1.355
Anthracite (high)		1.800	1.030	1.852	1.796
Coal (Bituminous)		1.200	1.060	1.272	1.173
Coal		1.500	1.060	1.590	1.514
Pure Water	H_2O	1.000	1.1101	1.110	1.000
Salt Water	200,000 ppm NaCl	1.146	1.0797	1.237	1.135
Oil	$(CH_2)_n$	0.850	1.1407	0.970	0.850
Methane	CH_4	ρ_m	1.247	$1.247\rho_m$	$1.335\rho_m$-0.188
Gas	$C_{1.1}H_{4.2}$	ρ_g	1.238	$1.238\rho_g$	$1.325\rho_g$-0.188

The density value is the result of the collision between artificial gamma rays and electrons in the formation using a source of ^{60}Co or ^{137}Cs. Tittman and Wahl (1965) and Asquith and Gibson (1982) named this phenomenon as Compton, the scattered gamma rays (absorbing low energy) that arrives at the detector is an indication of formation Density.

Porosity from the density log is calculated using the equation (Schlumberger, 1991):

$$\phi_{Den} = \frac{\rho_{ma} - \rho_b}{\rho_{ma} - \rho_f}$$

Where:

ϕ_{Den} = Apparent density porosity

ρ_{ma} = Matrix density

ρ_b = Bulk density log reading

ρ_f = Fluid density

3.2.6 Neutron

Asquith & Gibson (1982) described the neutron log (abbreviated as NPHI, PHIN, or φN) as a porosity log that is applied to measure the hydrogen nuclei concentration in a formation. The basic measurement noticed as the oldest type of logs has been summarized among authors as measure the amount of Gamma Ray capture following artificial stimulation by bombarding run of fast neutrons. The latest sources measure the amount of epithermal and thermal energy of hydrogen and rock after bombardment (Atlas, 1982; Keary *et al.*, 2002). The logging device is a non-contact tool that emits neutrons from a source. Emitted neutrons collide with nuclei of the formation and lose some of their energy. Maximum energy loss occurs when emitted neutrons collide with hydrogen atoms because a neutron and a hydrogen atom have almost the same mass. Therefore, most neutron energy loss occurs in the part of the formation that has the highest hydrogen concentration.

In thick evaporite successions, a neutron log can distinguish between various evaporite salts (see Table 3.3) on the basis of water of crystallization (Rider, 1996). Gypsum is the most common of the evaporites containing water of crystallisation. In a neutron-density (NPHI-RHOB) crossplot, several hydrated salts have high neutron-log values and characteristic tightly-clustered apparent bulk densities, which separates them from other anhydrous evaporites such as salt or anhydrite, which contain no water and hence have NPHI values near zero (Warren, 2018).

Table 3.3. Neutron log values of some evaporites (Schlumberger, 1989).

Mineral	Composition	Neutron log value T
Carnalite	KClMgCl2.6H2O	60
Gypsum	CASO4.2 H2O	60
Kainite	MgSO4KCl.3H2O	60
Polyhalite	K2SO4Mg(SO4)4.2H2O	25
Halite	NaCl	-3
NaClAnhydrite	CASO4	-2
Sylvite	KCl	-3

The density – neutron log is a combination log (Figure 3.3) that simultaneously records neutron and density porosity. Porosities may differ on the logs according to the matrix density used by the logging program to calculate porosity is different from the actual formation matrix density; gas is present in the formation pore space and shale/clay is present in the formation (Alberty, 1994).

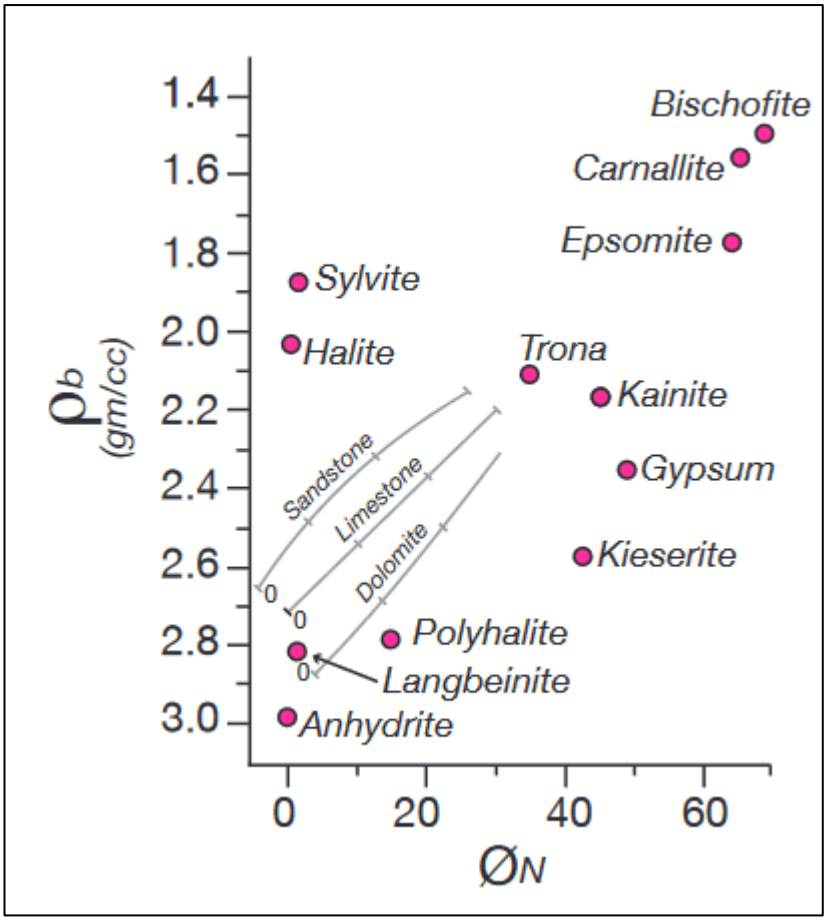

Figure 3.3 - Crossplot of neutron (NPHI Ø) versus density (RHOB gm/cc) for a variety of evaporite salts. Also shown are the typical field lines for most sandstones, limestones and dolomites with variable porosities (Warren, 2018).

3.3 SEISMIC REFLECTION METHOD

Seismic data is produced by sending artificial energy into the earth and recording its response. In the early days, waves were generated by detonating in shallow wells. Nowadays different range of frequencies for wave generation is created by vibrations (Bartucz, 2009).

The purpose of analyzing seismic reflections is the identification of stratigraphic sequences in seismic data. Avseth *et al.* (2005) concluded that mapping geological structures in seismic data requires picking and tracking main horizons and its major discontinuities and also identify major faults. The main objectives are to outline the subsurface framework and distinguish horizons and its discontinuities extend or vary laterally and vertically according to fluctuations at the sea level.

3.4 POLARITY AND PHASE OF THE DATA IN WAVELET EXTRACTION

It is important to understand the shape of the wavelet to be extracted especially the dominant part of it that has a contrast of acoustic impedance (White and Simm, 2002).

A minimum phase wavelet has short time duration and a concentration of energy at the start of the wavelet with possible symmetrical and asymmetrical shapes while a zero-phase wavelet has shorter symmetry beneficial property with a maximum at time zero duration, usually the most used wavelet it is a more accurate data condition (Brown and Abriel, 2014).

Ricker wavelet is a very commonly used type of wavelet defined by its dominant frequency as zero-phase wavelet having an equivalent minimum-phase that allows being formulated (Schlumbeger, 2018).

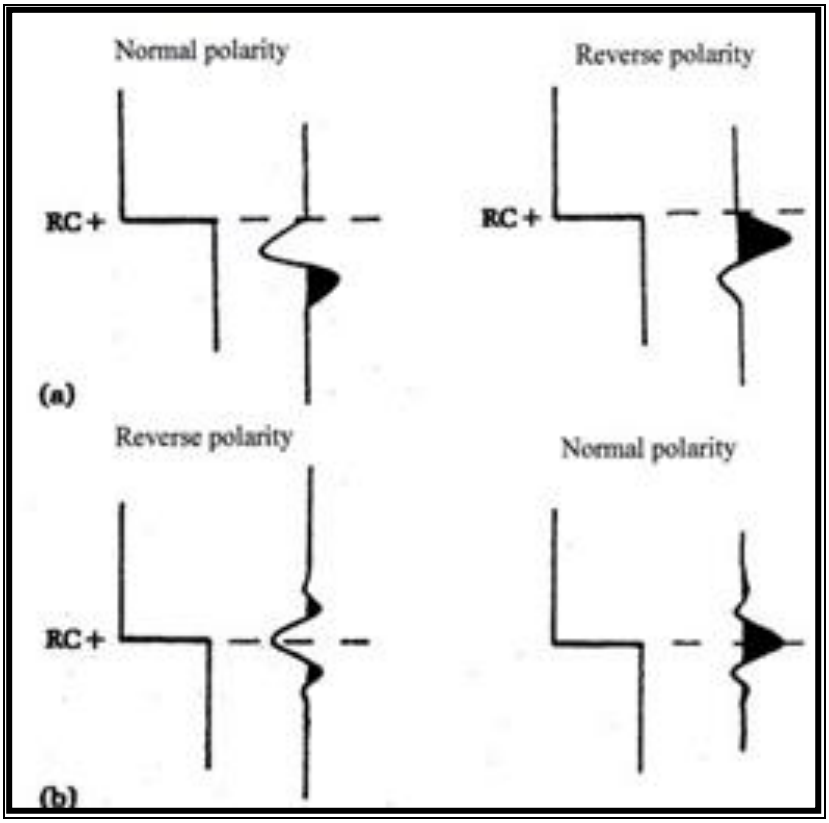

Figure 3.4 - Representation of phase and normal and reverse polarities after Sheriff (1995).

The Society of Exploration Geophysicists (SEG) by the SEG Technical Standards Committee adopted many years ago the standard polarities for land and marine surface-seismic conventions, stating that early refraction from vertical component first arrivals into a source breaks downward for the display of minimum-phase and zero-phase

wavelets, known as SEG normal polarity (Thigpen *et al*., 1975). This definition does not easily transfer to zero-phase wavelets, thus there is no universal normal for zero-phase processed polarity. The convention for polarity is widely used for many geophysicists interpreters but it is still not well understood (Figure 3.4) since processed polarity on within a region of the world (American or European convention) has a distinguish preference and important input data that needs to be stated as interpreter correlates and tie data in order to recognize bright or dim spots in the study. American polarity standard is defined as if signal arises from a reflection that indicates an increase in acoustic impedance, the polarity is, by convention, positive and is displayed as a peak whilst European polarity standard refers to decrease in acoustic impedance is represented by a white through in acoustic impedance (Simm and White, 2002; Brown and Abriel, 2014; Schlumberger, 2017).

3.5 THE SEISMIC WELL TIE CONCEPT

In the geophysical literature, several authors contribute to the advent of Seismic Well Tie workflow. In particular, Walden and White (1984), White (1997), White and Hu (1998), White and Simm (2002), White and Simm (2003) Edgar and van der Bann (2011) and Cubizolle *et al.* (2015) address the advance and importance on the Seismic Well Tie process to seismic interpretation. Nowadays, service oil companies demand time to reproduce new and more accurate algorithms and tools in the software, creating an interactive environment in order to compare synthetic seismograms that best represent the subsurface events. However, it is notable that the final result of the whole process was highlighted by Lindseth (1979) as a first approach to establish the difference in acoustic impedance between seismic events, a particular action in seismic interpretation that ties time and depth domains data creating the synthetic seismogram.

The American Association of Petroleum Geologists (AAPG) defines the Well Seismic Tie as a bridge to go from seismic “wiggles” to the rocks that produced the “wiggles” and the interpretation of the subsurface geology. As the techniques encompassing the Seismic Well Tie are widely known for geophysicists, White and Simm (2003) outlined a tutorial paper commonly adapted and followed by service companies and has been used in this study:

- Edit and calibrate the sonic and density logs;
- Review and assess the seismic data
- Construct the well log synthetics sequences required
- Run pilot analysis of the well data
- Estimate the wavelet, with diagnostic checks on its accuracy

3.5.1 Sonic Calibration

Spikes are often undesirable in data because they represent data that is either erroneous or that is outside the log resolution (Handerson, 2011). In this thesis, it was necessary to remove spikes of Sonic log in order to perform the Sonic Calibration as input for Seismic Well Tie (Schlumberger, 2017; 2018). The first well tested was Mihambia-1 using the well log DT-E (Delta-T compressional after editing) where spikes were encountered in the whole well mainly at the top of the log compromising the further analysis combined with Acoustic Impedance. After sonic correction, the well log was addressed as DT calibrated sonic log.

The colour scheme for seismic interpretation follows the blue-white-red or European standard data polarity where the colour blue gives a negative amplitude reflection (Figure 3.5).

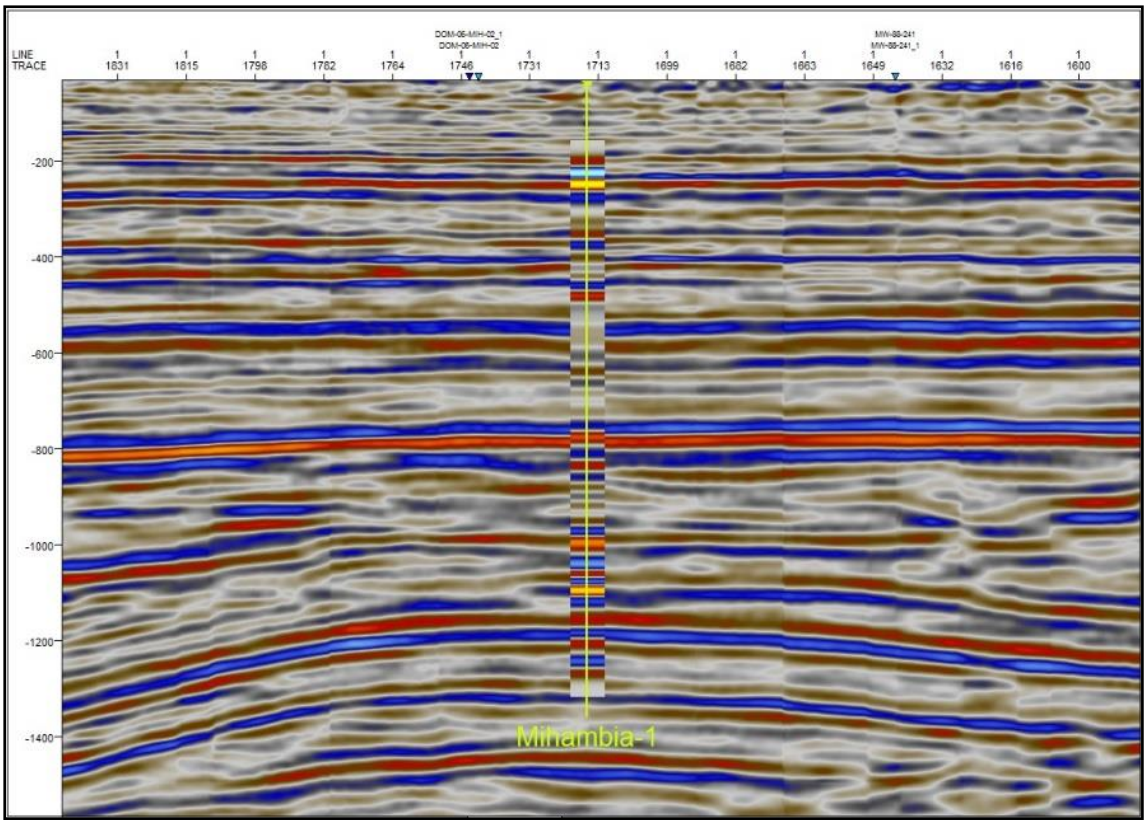

Figure 3.5 - The Reflection coefficient rectangle in DOM-06-MIH-04_1 2D seismic line.

3.6 SYNTHETIC SEISMOGRAM

Generating a synthetic seismogram is a way to predict the seismic response of the Earth (Schlumberger, 2017). The velocity data extracted from the sonic log combined with another log as density is used to tie the seismic data (in time domain) with a well (in depth domain) producing acoustic impedance, the difference interface between two rock layers creating a synthetic seismic trace, represented by the formula (Schlumberger, 2017; 2018):

$$Z\ (AI) = \rho .\ V$$

Where:

Z (AI) = Acoustic Impedance

ρ = density of medium

V = velocity of medium

This trace closely approximates to a trace from a seismic line that passes close to the well in which the logs were acquired. That is the principle of synthetic seismogram generation by convolving the reflection coefficient resulted from the sonic and density logs along with an ideal or real wavelet to the reflections as a matter of correlating with seismic data, defining the seismic "wiggle" traces (Schlumberger, 2017). Thus, it involves the geological and seismic events for the purpose of constructing a Time-Depth Relationship (TDR). By definition, the Reflection Coefficient (RC) is the ratio of the amplitude of the reflected wave to the incident wave, or how much energy is reflected. The following equation defines the reflection coefficient (RC) in terms of AI for the normal incidence of a seismic pulse at an AI boundary (Shuey, 1985):

$$RC = \frac{v_2\rho_2 - v_1\rho_1}{v_2\rho_2 + v_1\rho_1}$$

Where:

RC = Reflection Coefficient

ρ_1 = Density of Medium 1

ρ_2 = Density of Medium 2

V_1 = Velocity of Medium 1

V_2 = Velocity of Medium 2

To summarise, the synthetic seismogram is created by convolving the reflectivity series and the wavelet to model how acoustic energy reflects from the various layers of the subsurface aiming to enhance the further step of interpreting geophysical data when picking the reflection events (seismic horizons), part in previously established from markers in well logs correlation with seismic reflectors. Synthetics also is used to define if a target seismic reflector (horizon) is a peak or a through according to major reflections. Moreover, a good quality synthetics depends on the processed data such as seismic and well log quality added to a representative wavelet extracted.

3.6.1 Wells performed Synthetic Seismogram

The wells in Mandawa Basin displayed particular synthetic characteristics due to their scattered positions in the Mandawa Block, however the same patterns of reflections and amplitude were observed in the wells. The Lukuledi-1 in the Ruvuma Basin and the

Liwale-1 in Selous Basin also were analysed synthetics were produced respectively to be able to perform the horizon interpretation process.

The .las files acquired from wireline services were imported into Petrel software. The wells whose calibrated sonic and density log were associated, Petrel automatically generated a computed acoustic impedance and reflectivity coefficient for each well such as Mbuo-1, East Lika-1, Mihambia-1, and Mita Gamma-1. Other wells as Mbate-1, Mita Gamma-1, Kizimbani-1, Kianika-1, Lukoliro-1, Lukuledi-1 (in Ruvuma Basin), and Liwale-1 (in Selous Basin) had missing sections of logs, in particular the sonic log, where a complete log is required to perform the synthetics process. The use of the log estimator was necessary to generate logs from other logs using standard formulas. For those wells mentioned the estimation process of Density to/from Sonic extracted the sonic log from the density that Petrel uses the Gardner's Approximation formula (Schlumberger, 2018).

Density to/from Sonic (Gardner's Approximation) by Schlumberger (2018):

$$Density = C.Sonic^{x}$$

Where:

C and x are constants

Wavelets were extracted from the seismic section to convolve with the resulted impedance logs and to produce the synthetic trace for comparison within the seismic section. Through the Wavelet toolbox in Petrel, wavelets were extracted using the analytical method of Ricker stated as a zero-phase wavelet commonly convolved with a reflectivity trace to generate a synthetic seismogram. The main input is the central frequency. The frequency and phase spectrums are purely a function of the frequency input (Schlumberger, 2018). Four different frequency intervals of reflections to examine the effect of attenuation were taken: Ricker 15 Hz for Mbuo-1 and Mihambia-1; 20 Hz for Mita Gamma-1; 25 Hz for East Lika-1, Liwale-1 in Selous Basin, Lukoliro-1, Lukuledi-1 in Ruvuma Basin, Mbate-1 and Ricker 30 Hz in Kianika-1. The length used was the default of 128 ms.

Figure 3.6 represents the output track representation for the Synthetic Seismogram in Mihambia-1 well in particular: Depths in the well (TVD) and (SSTVD), Acoustic Impedance, Reflection Coefficient, DOM-06-MIH-04_1 crossline, Synthetic Seismogram generation, Interval Velocity, Output Interval Velocity, and Drift. A time

shift was solved doing a manual bulk shift of 10 ms according to seismic reflectors and well matching the horizons in the blue troughs.

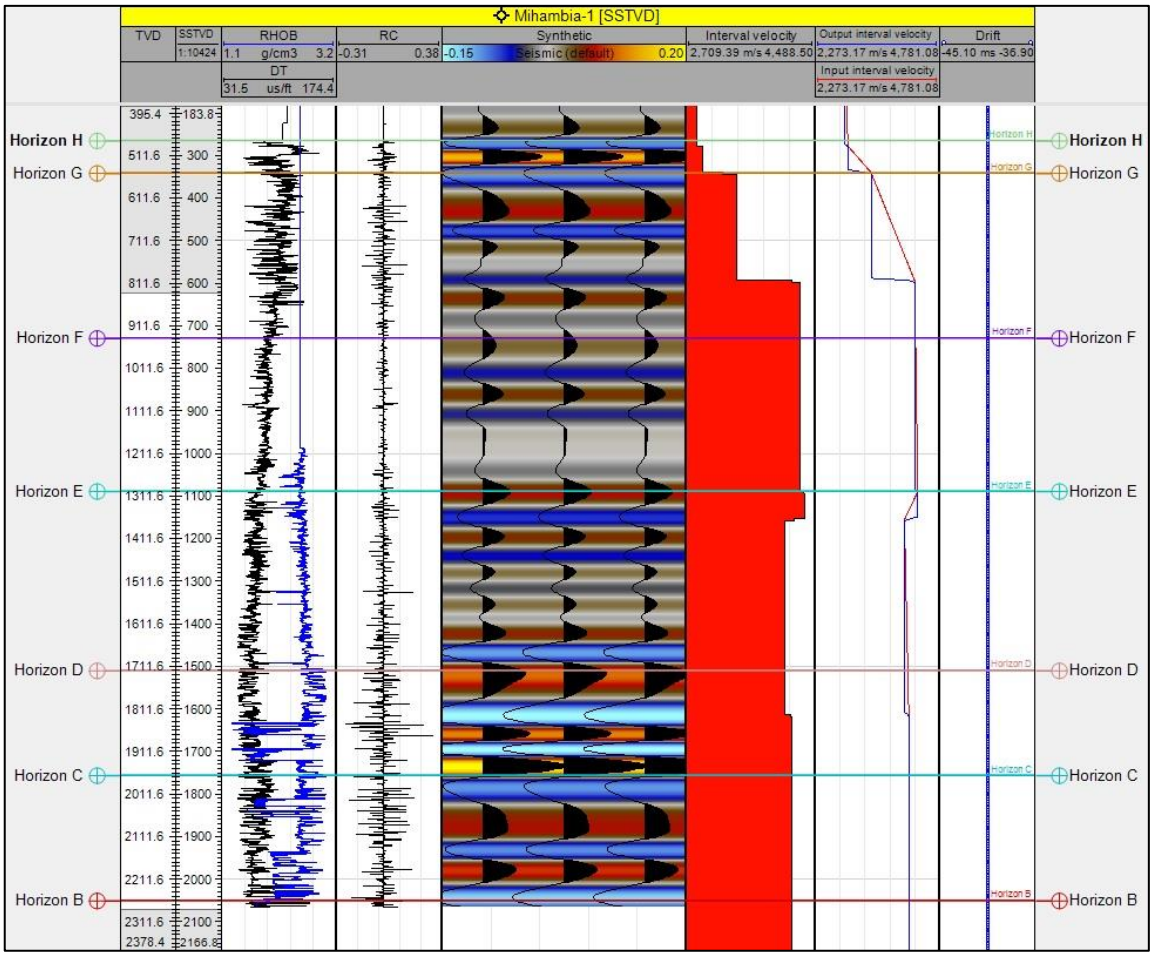

Figure 3.6 - Example of the Synthetic seismogram for Mihambia-1 well tying seismic with markers (well tops).

The synthetics from all Mandawa Basin wells closely correlate with one another. For Mita Gamma-1, the synthetic has been inserted into the seismic data 99-MW-4_d at the well location. The seismic data has been shifted by 10 ms to shorter times to tie with the synthetic seismogram (Figure 3.7). East Lika-1 has been inserted the into seismic TLVB-157_d (Figure 3.8); the synthetic for Lukoliro-1 (Figure 3.9) was calibrated to the seismic line 83-SE-46; the seismic line 88-MW-251 (Figure 3.10) was extracted to perform the synthetics in Mbuo-1 well; Mbate-1 had the seismic line 99MW-8_d extracted for the synthetics (Figure 3.11); extracted the seismic line MDW07-13 for Kianika-1 (Figure 3.12); the line TL-116_d for Kizimbani-1 (Figure 3.13); Liwale-1 has been inserted into

the seismic line U83-LW-05 (Figure 3.14) and Lukuledi-1 was inserted in the TL-101A_d-1 seismic line (Figure 3.15).

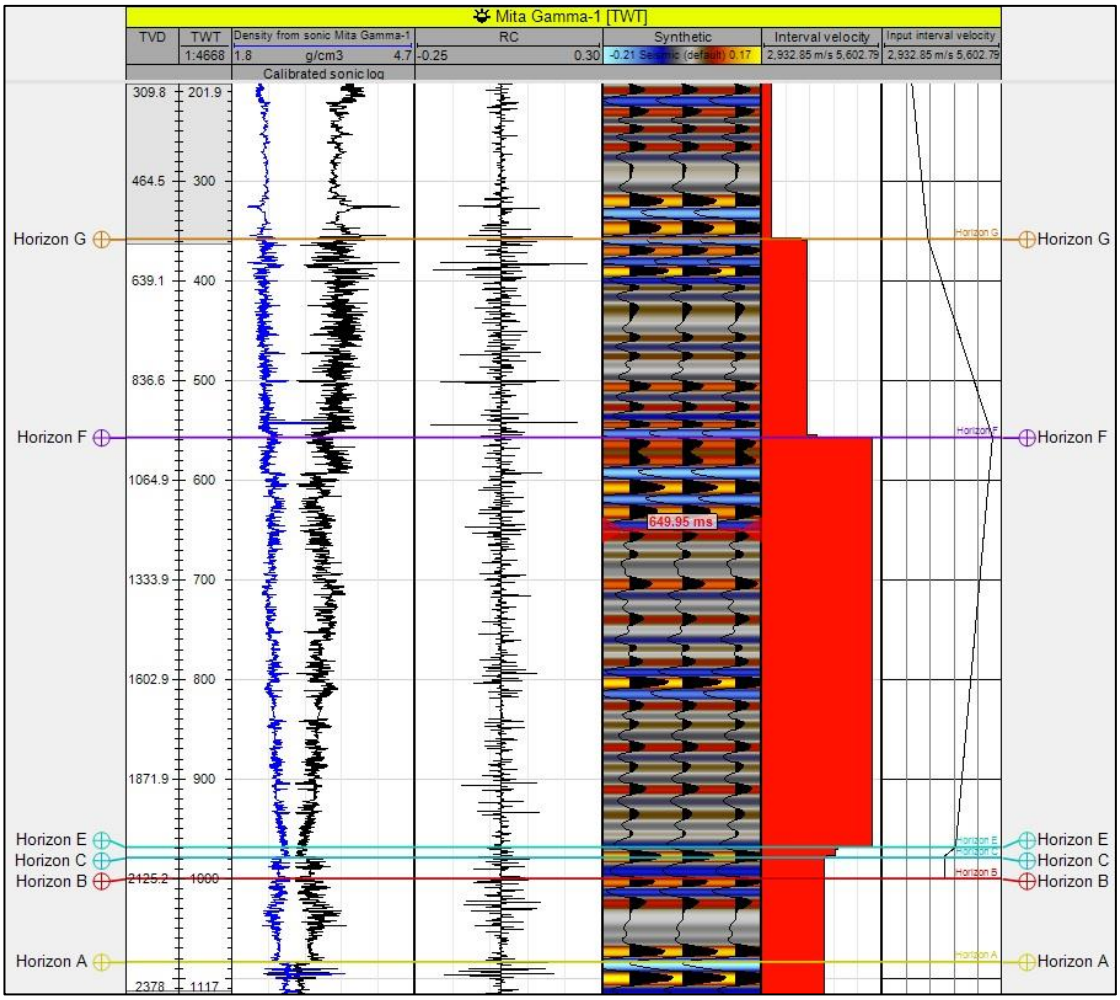

Figure 3.7 - Synthetic Seismogram for Mita Gamma-1 well. Display of acoustic impedance, traces, well logs, well tops and a zero-phase wavelet.

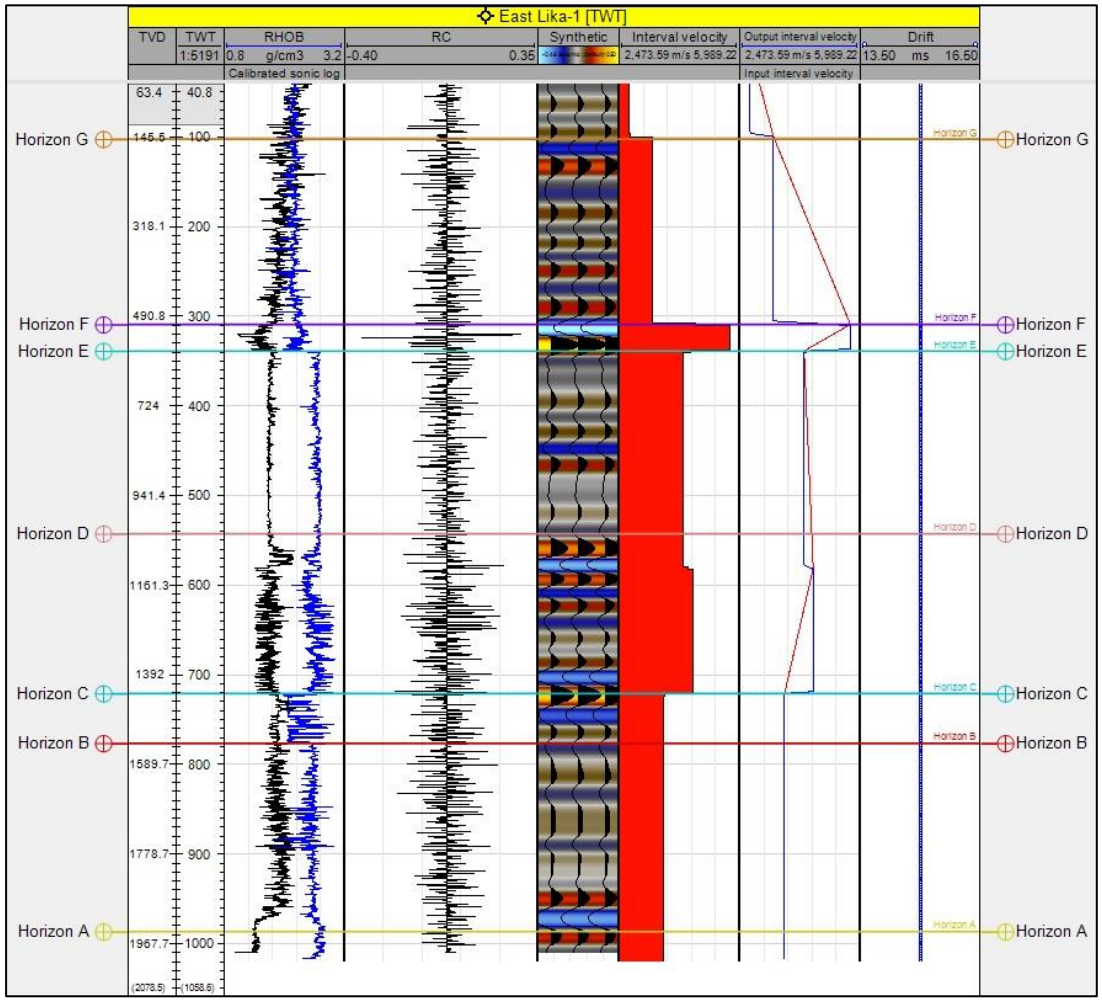

Figure 3.8 - Synthetic Seismogram for East Lika-1 well. Display of acoustic impedance, traces, well logs, well tops and a zero-phase wavelet.

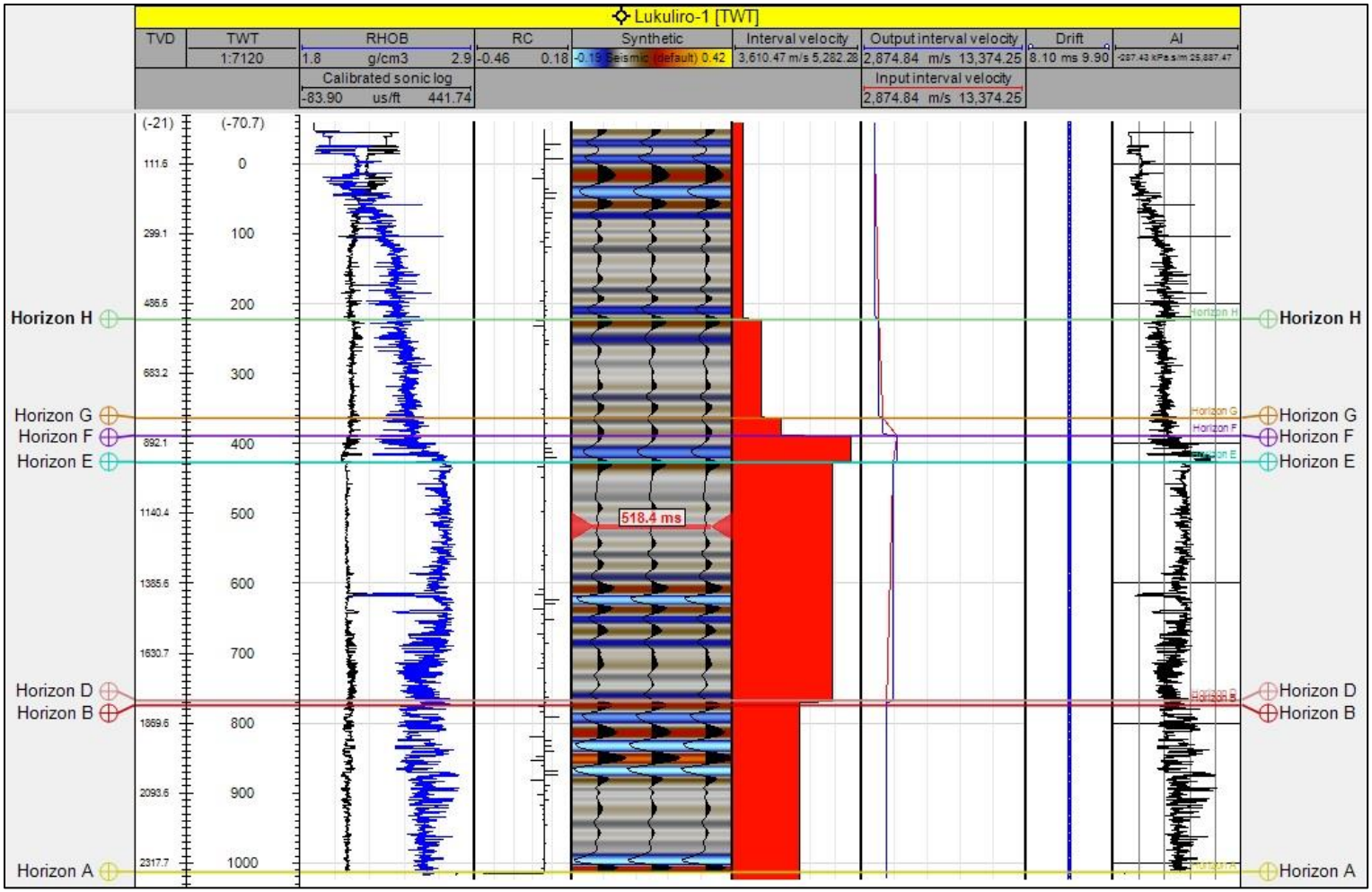

Figure 3.9 - Synthetic Seismogram for Lukoliro-1 well. Display of acoustic impedance, traces, well logs, well tops and a zero-phase wavelet.

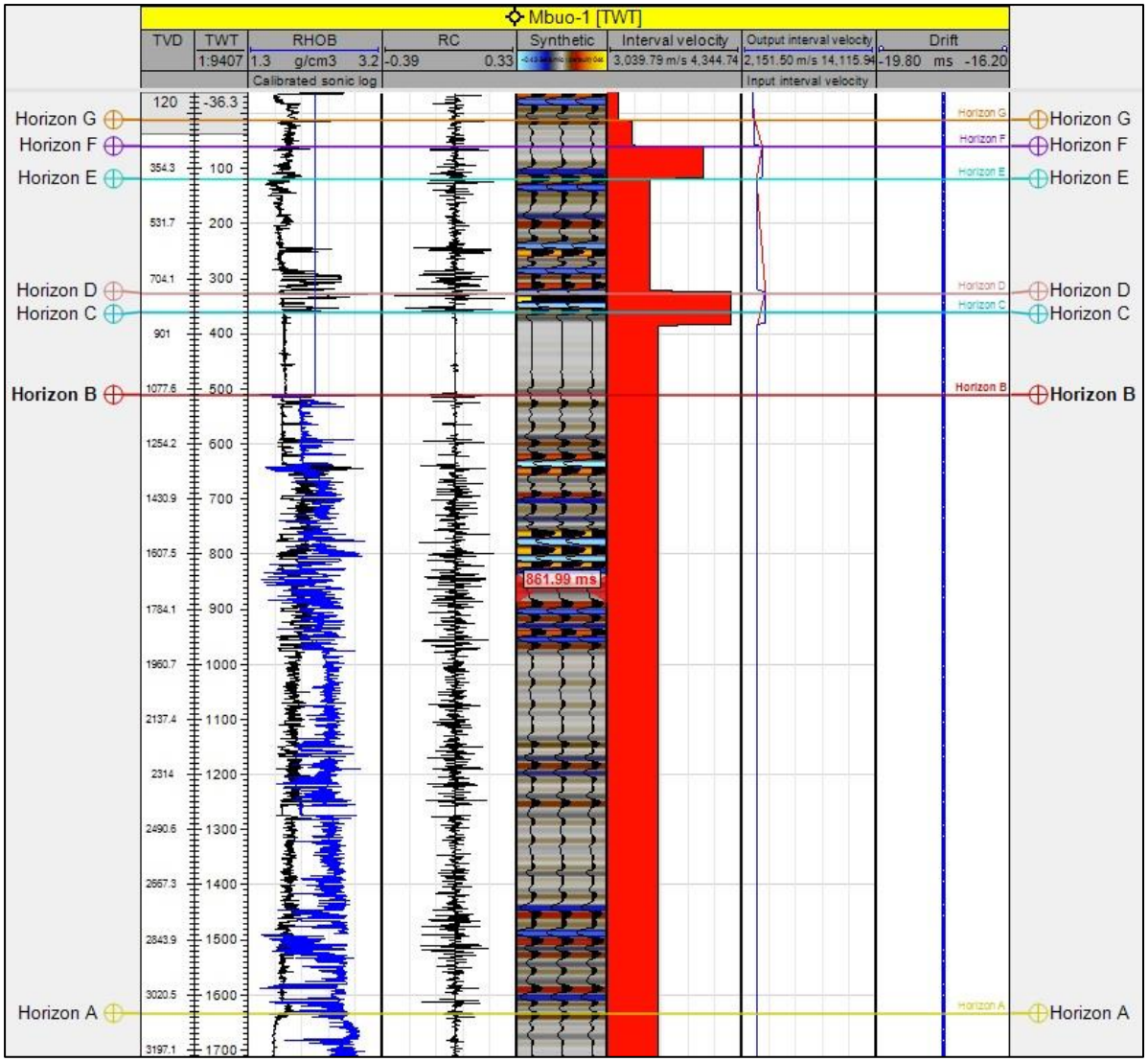

Figure 3.10 - Synthetic Seismogram for Mbuo-1 well. Display of acoustic impedance, traces, well logs, well tops and a zero-phase wavelet.

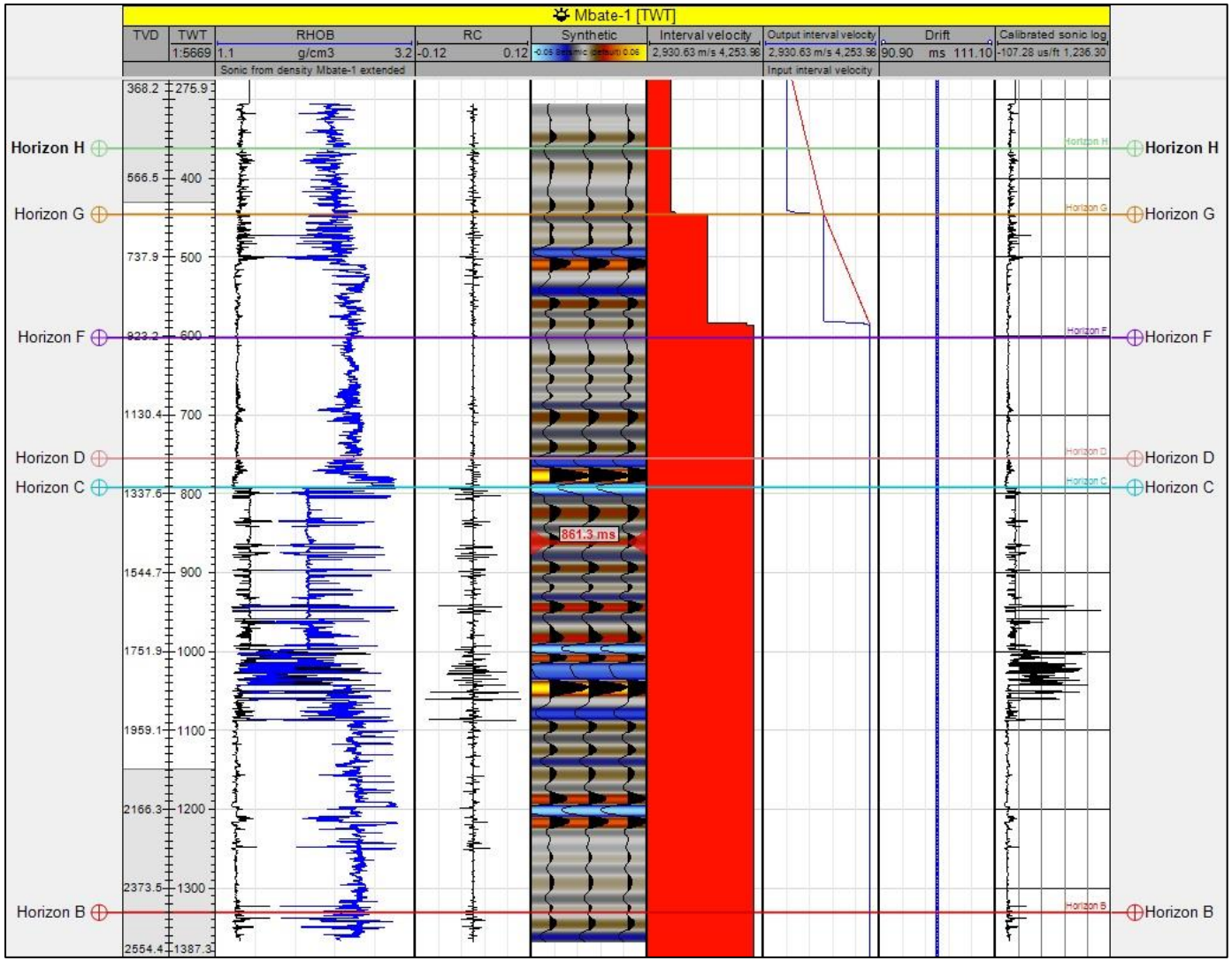

Figure 3.11 - Synthetic Seismogram for Mbate-1 well. Display of acoustic impedance, traces, well logs, well tops and a zero-phase wavelet.

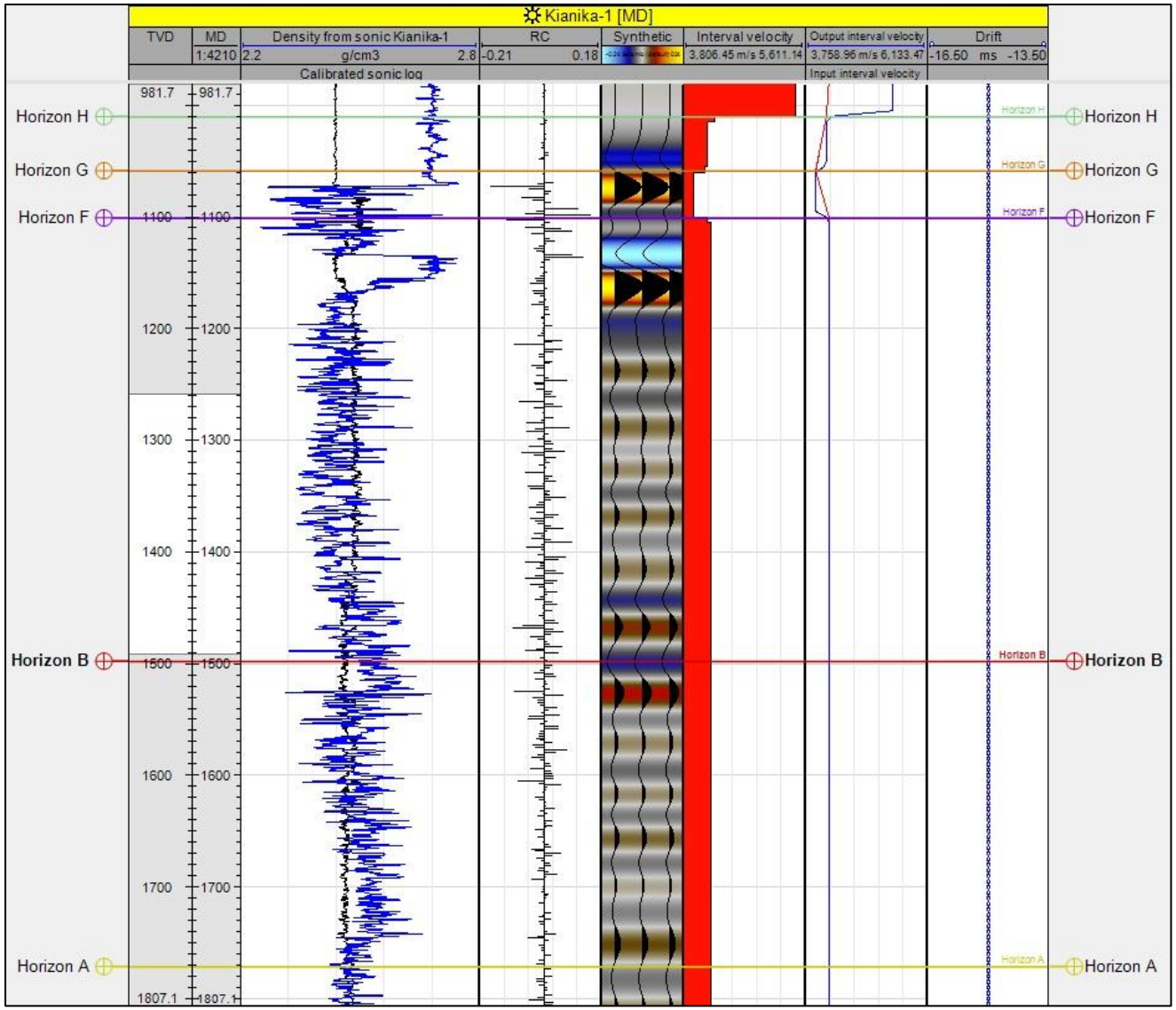

Figure 3.12 - Synthetic Seismogram for Kianika-1 well. Display of acoustic impedance, traces, well logs, well tops and a zero-phase wavelet.

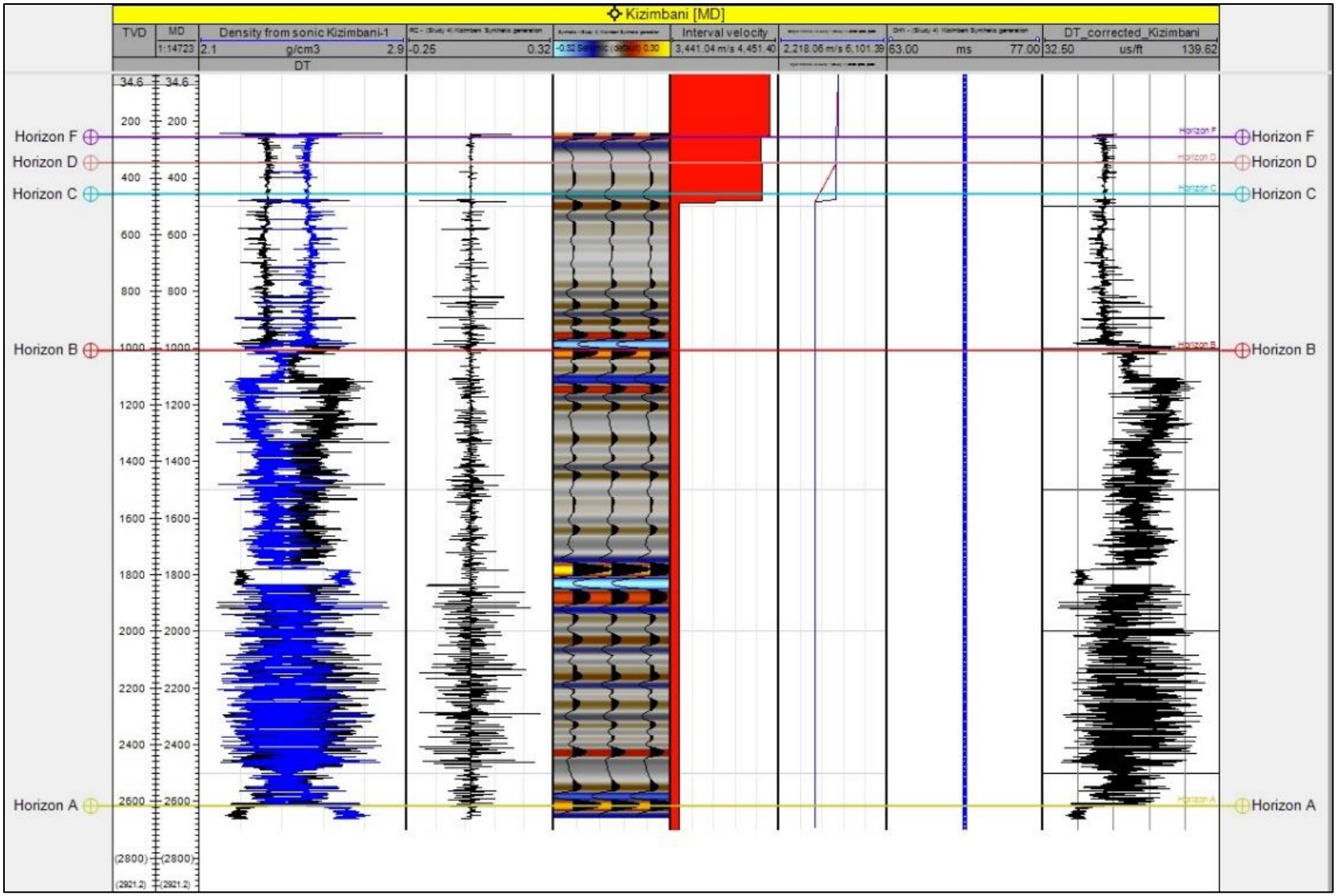

Figure 3.13 - Synthetic Seismogram for Kizimbani-1 well. Display of acoustic impedance, traces, well logs, well tops and a zero-phase wavelet.

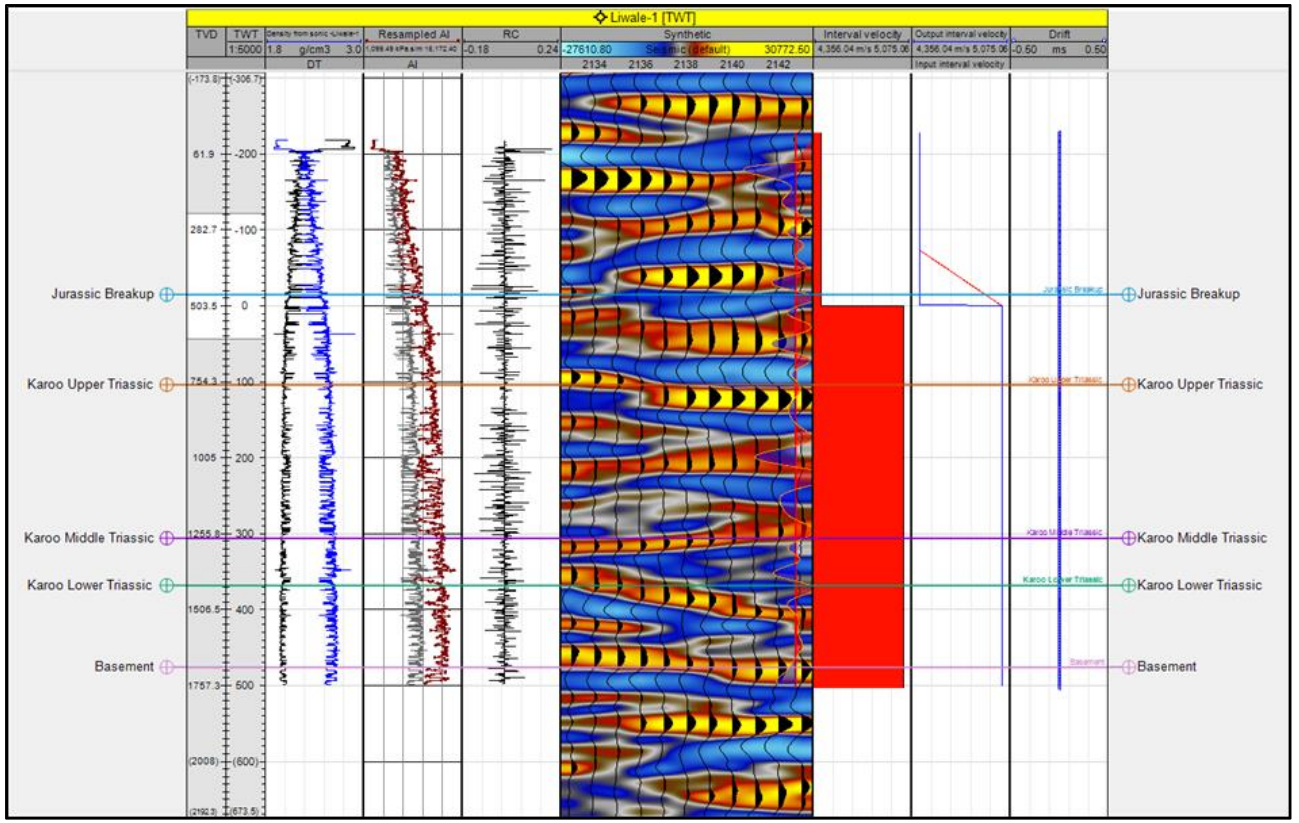

Figure 3.14 - Synthetic Seismogram for Liwale-1 well. Display of acoustic impedance, traces, well logs, well tops and a zero-phase wavelet.

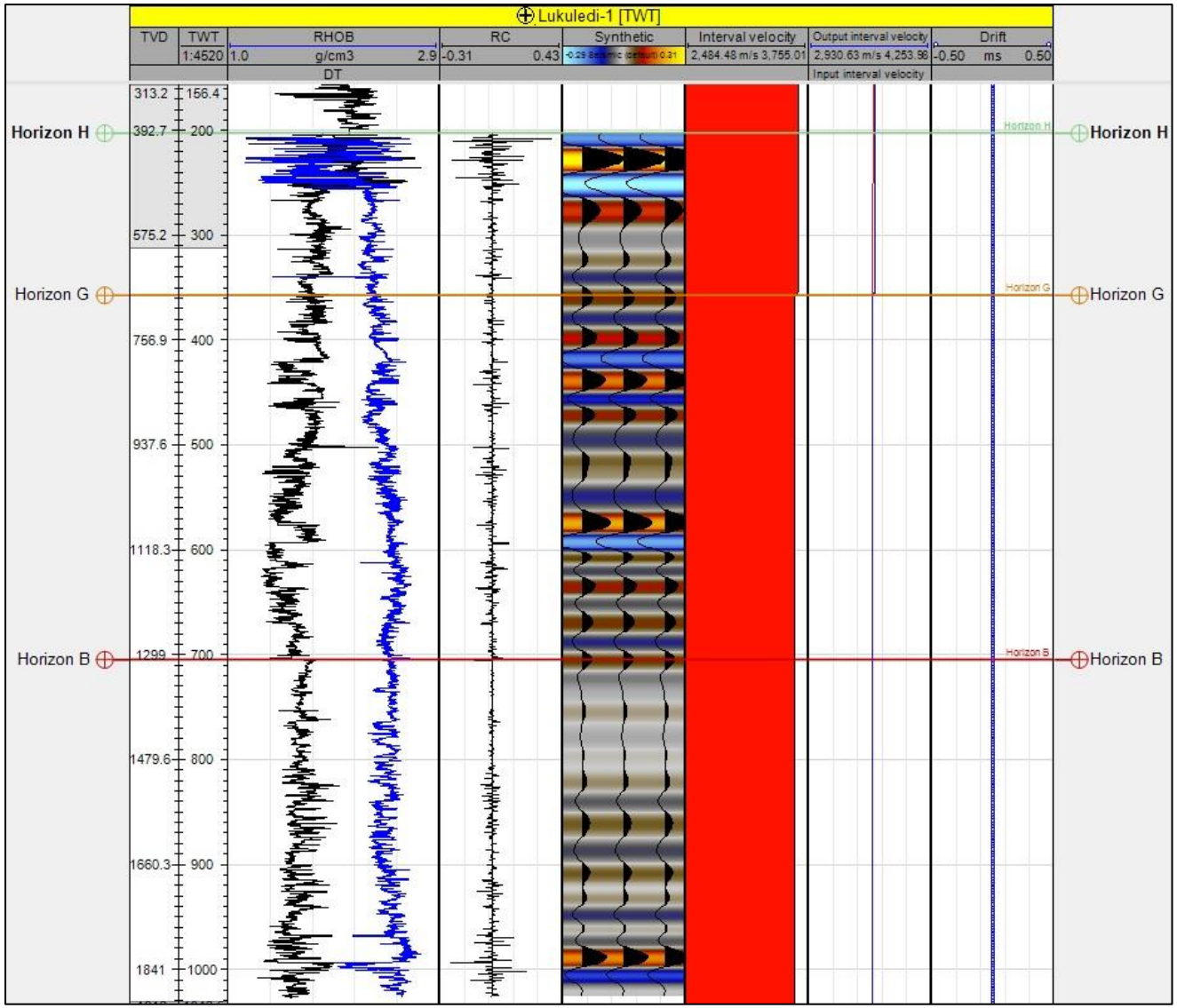

Figure 3.15 - Synthetic Seismogram for Lukuledi-1 well. Display of acoustic impedance, traces, well logs, well tops and a zero-phase wavelet.

CHAPTER 4

THE WELLS OF THE MANDAWA BASIN, RUVUMA BASIN, AND SELOUS BASIN

4.1 MANDAWA BLOCK

Each exploration well described in this chapter has been done by following unpublished well reports from service companies.

4.1.1 Mihambia-1

Located 300 km south of Dar es Salaam, the Mihambia-1 well was Dominion Oil & Gas Limited's first well the in the onshore Mandawa PSA. It is located 16 km to the ESE of the East Lika-1 well and NNW of the Mbuo-1 well. In the picture 4.1 Mihambia-1 is located at Easting 524,182.67 and Northing 8,972,728.4 reached a total depth of 2,508 m MD RT on the 2D seismic line DOM-06-MIH-04 (SP 2529).

Mihambia-1 exploration well was the targeted well to interpret the Middle Jurassic transgressive marine claystones and sandstones of the Mihambia Formation. The Mihambia sandstones were suggested to be the potential reservoirs of the Mandawa Basin and constitute the primary objective of the well. Several units had been assigned to the Mihambia Formation, where seismic horizon D was defined as the prospect for the well drilling. The shallow marine sands and limestones of the Mtumbei Formation were considered a secondary target where seismic interpretation showed structural closure.

The well results showed the Mihambia Formation sandstones to be present at the well location. Due to the large washout over the interval, wireline logs could not fully evaluate the nature of the sands however the resistivity showed unambiguously no shows over this interval as well as no shows in the Mihambia-1 well.

The Mihambia Formation was interpreted to represent the salt rock, the Nondwa Formation, distinguished the first appearance of anhydrite from the first appearance of halite.

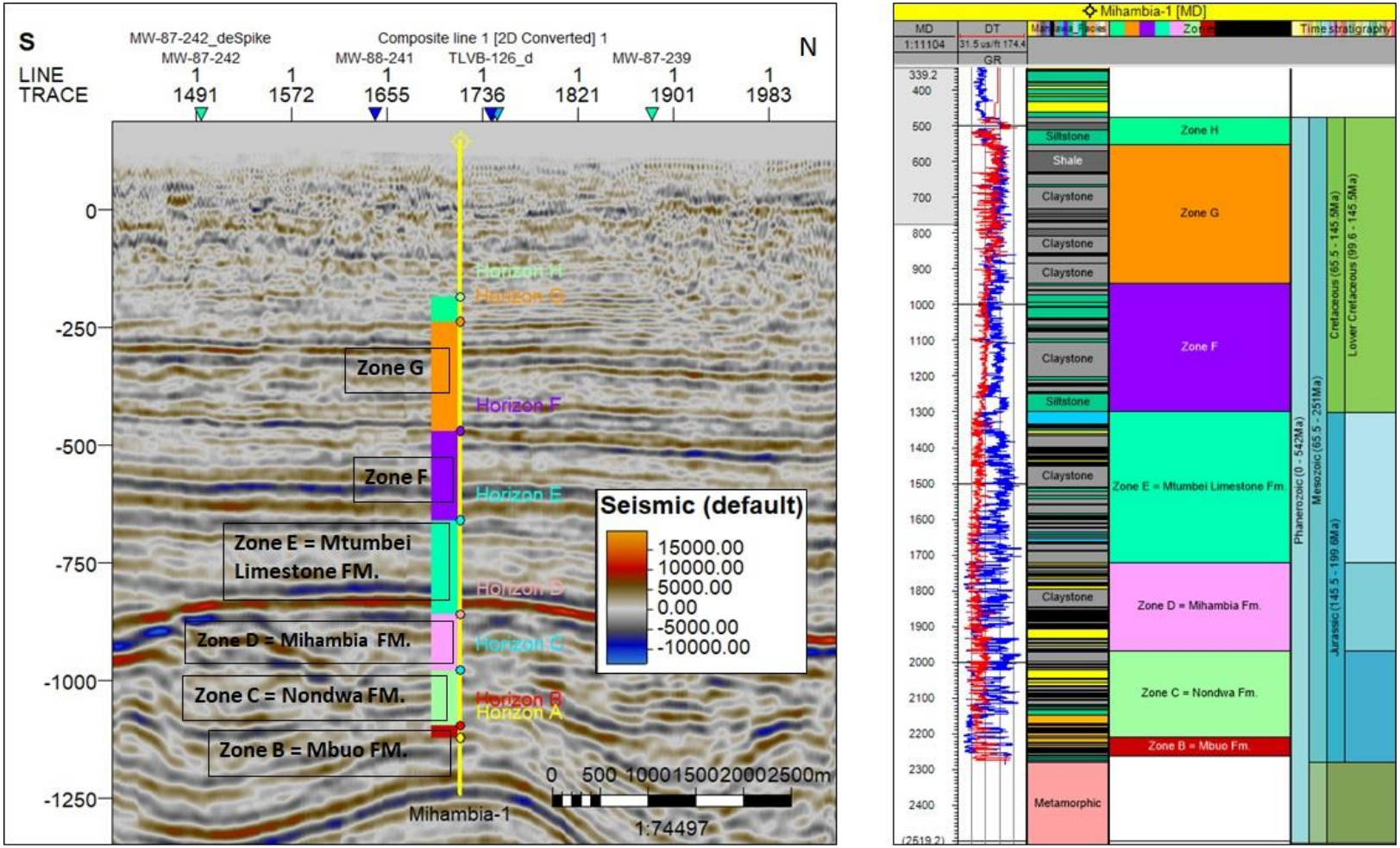

Figure 4.1 - ***The zones distributed along Mihambia-1 well in the 2D seismic line (left) and the correlation of DT and GR logs, lithostratigraphy, zones and associated ages (right).***

4.1.2 Mbuo-1

Mbuo-1 was a wildcat well driller on the 2D seismic line 88-MW-251 (SP 1465) in southeastern Tanzania, under coordinates Easting 590.829 and Northing 8,955.956 (Figure 4.2). The major objectives for drilling this well were the sandstones in the pre-mobile salt: the Lower Jurassic Nondwa Formation. The drilling program for this well had composed of formation evaluation from 0 m to 3,313 m total depth mainly of halite and anhydrite. In addition to formation evaluation and conventional mud logging, automatic real-time data monitoring was carried out.

During the logging run, results showed as shallower than prognosis penetrating the top salt of the evaporite. The sediments above the top salt were interpreted as water-bearing and comprise of unconsolidated siltstone underlain by a thick claystone sequence with interbedded evaporites. A few areas of sand were interpreted at the base of the clastic objective beneath the evaporites. The sandstones are composed by high micaceous and either tight or water-bearing. They suggest overly the metamorphic basement. Claystones within the evaporite sequence were identified as potential source rocks based on the Seismic Well Tie process.

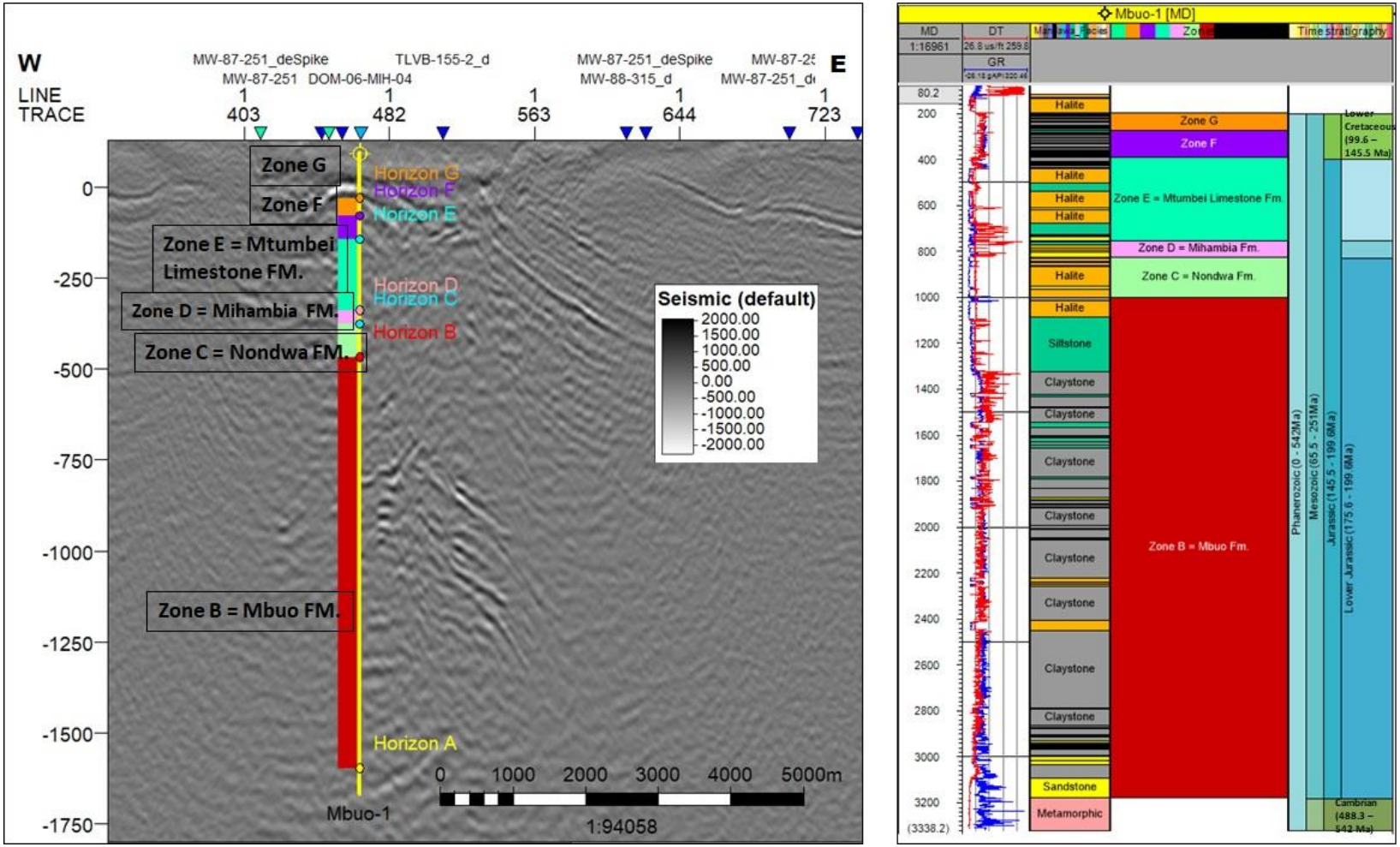

Figure 4.2 - The zones distributed along Mbuo-1 well in the 2D seismic line (left) and the correlation of DT and GR logs, lithostratigraphy, zones and associated ages (right).

4.1.3 Mbate-1

Mbate-1 was a wildcat well drilled on the seismic line 99MW-8_d (SP 280) in the Mandawa Basin, southern east Tanzania, in the UTM 497.250 E and 9,014.200 S – Figure 4.3. The major targets were the sandstones of the pre-mobile salt within the Lower Mbuo and basal sand formations and as a secondary objective the Upper Mbuo Formation. The well reached a total depth of 3,087 m MD RT reaching the Zone B - Mbuo Formation.

According to the drilling campaign results, the oil generated in the basin suggested being far from the present location as the capillary pressure due to low permeability among the salt layers.

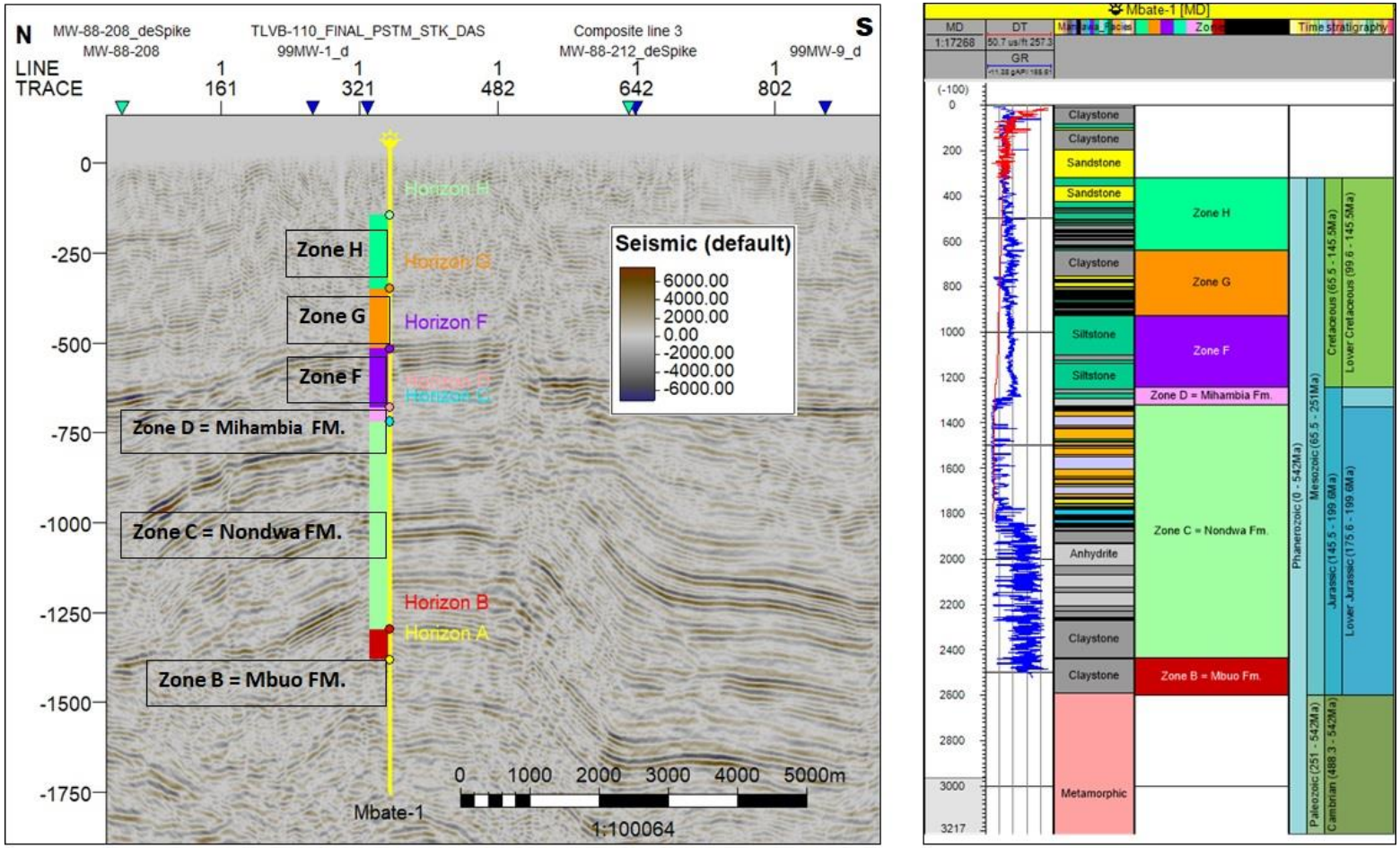

Figure 4.3 - ***The zones distributed along Mbate-1 well in the 2D seismic line (left) and the correlation of DT and GR logs, lithostratigraphy, zones and associated ages (right).***

4.1.4 Mandawa-7

Mandawa-7 well (Figure 4.4) was located on the Mandawa Anticline, southern Tanzania under UTM coordinates Easting 545.857 and Northing 8,959.104, 2D seismic line MW-87-251 (SP 1670). The third deep test well was drilled by British Petroleum /Shell Africa located in the Mandawa Anticline, initially named Pindiro Shales of the Middle Jurassic age with a total depth of 4,065 m MD RT.

The literature provided by Shell named the Pindiro Shales as composed of interbedded, limy shales, anhydrite, and gypsum. The Upper Pindiro Evaporites were mainly described as salt with subordinate shale and anhydrite ranging the age from the Triassic to the Lower Jurassic. The Lower Pindiro Evaporites have been described as of anhydrite, siltstones suggesting from Triassic age.

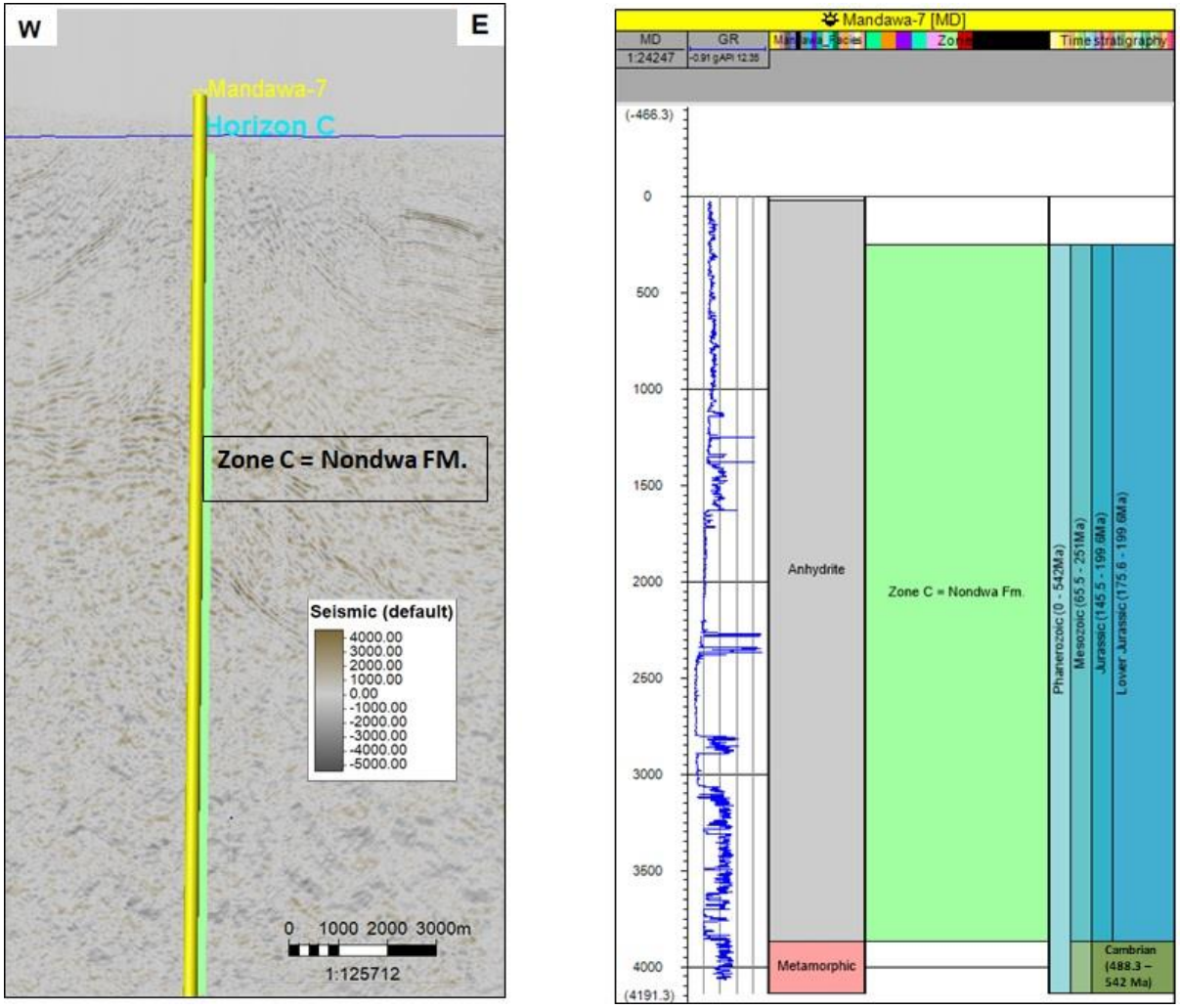

Figure 4.4 - ***The zones distributed along Mandawa-7 well in the 2D seismic line (left) and the correlation of GR log, lithostratigraphy, zone and associated ages (right).***

4.1.5 East Lika-1

East Lika-1 was designed to test one of several structures culminations and leads on the Masasi Platform, west of the deep Mandawa Basin (Figure 4.5). Dublin International Petroleum (Tanzania) drilled the well located on UTM 607.431 E and 8,974.961 N in the 2D seismic line TLVB-157_d (SP 1900). This well focused in combining in one area, the proven source in Mbuo-1 and Mandawa-7, together with the assumed potential to be a reservoir under the basement. The main target was the Lower Mbuo sandstone with the well reaching a total depth of 2,000 m MD RT. A secondary objective was to test the syn-rift hydrocarbon source Upper Mbuo Formation suggested to be sand-rich derived mainly from the south and partially from the west of Mandawa Basin.

The interpreted stratigraphy according to the geophysical well logs suggested that open marine facies are related to the shallower layers, specifically between water bottom to proximally 500 m. In the sequence, progresses to the appearance of the Mtumbei Limestones between 600 m and 1,000 m. Accordingly, more proximal facies containing evaporites (anhydrite and halite) fairly mixed with claystone and sandstones are noticed in the depth of 1,100 m to 1,800 m. Underneath, comprises the consolidated metamorphic basement reaching the total depth of 2,000 m MD RT.

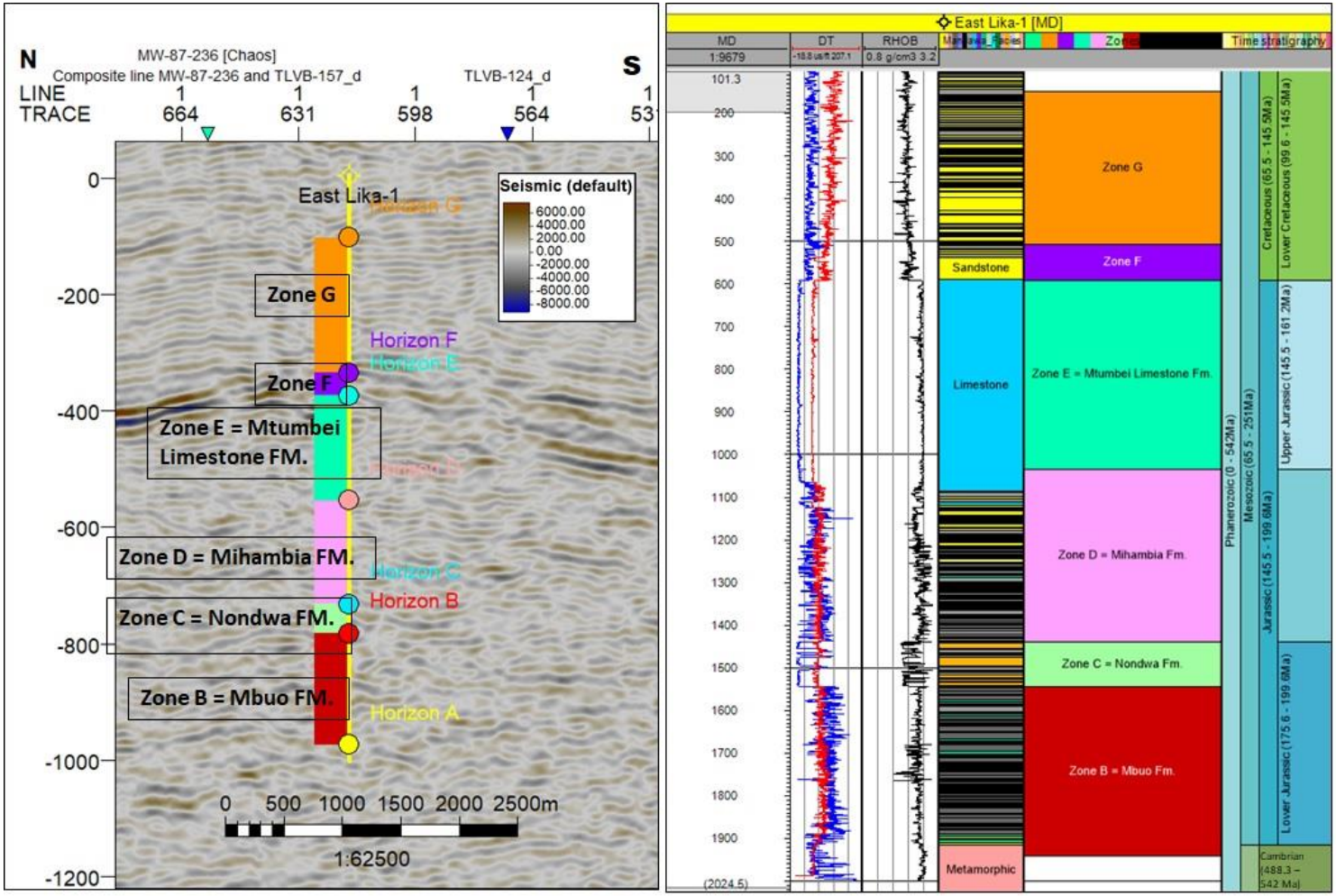

Figure 4.5 - *The zones distributed along East Lika-1 well in the 2D seismic line (left) and the correlation of DT, GR and RHOB logs, lithostratigraphy, zones and associated ages (right).*

4.1.6 Mita Gamma-1

Mita Gamma-1 was located in the Mandawa Block of the Kilwa district of southeastern Tanzania, 312 km south of Dar es Salaam, and was planned as a vertical wildcat well (Figure 4.6). The location is according to the 2D seismic line 99-MW-4_d (SP 1420) and UTM Easting 518.126 Northing 9,014.547 had the primary objective to test the crest in the pre-evaporite sequence, were thought to be fluvially derived sandstone reworked from an older Karoo and basement origin or a possible reef body developed on the crest of the basement high. A further possibility of penetrating pre-rift Karoo rather than basement was postulated. This well reached the total depth of 2,390 m MD RT.

Stratigraphically, this well showed claystone and sandstone interbeds, limestone, siltstone, and minor appearance of anhydrite and halite beds.

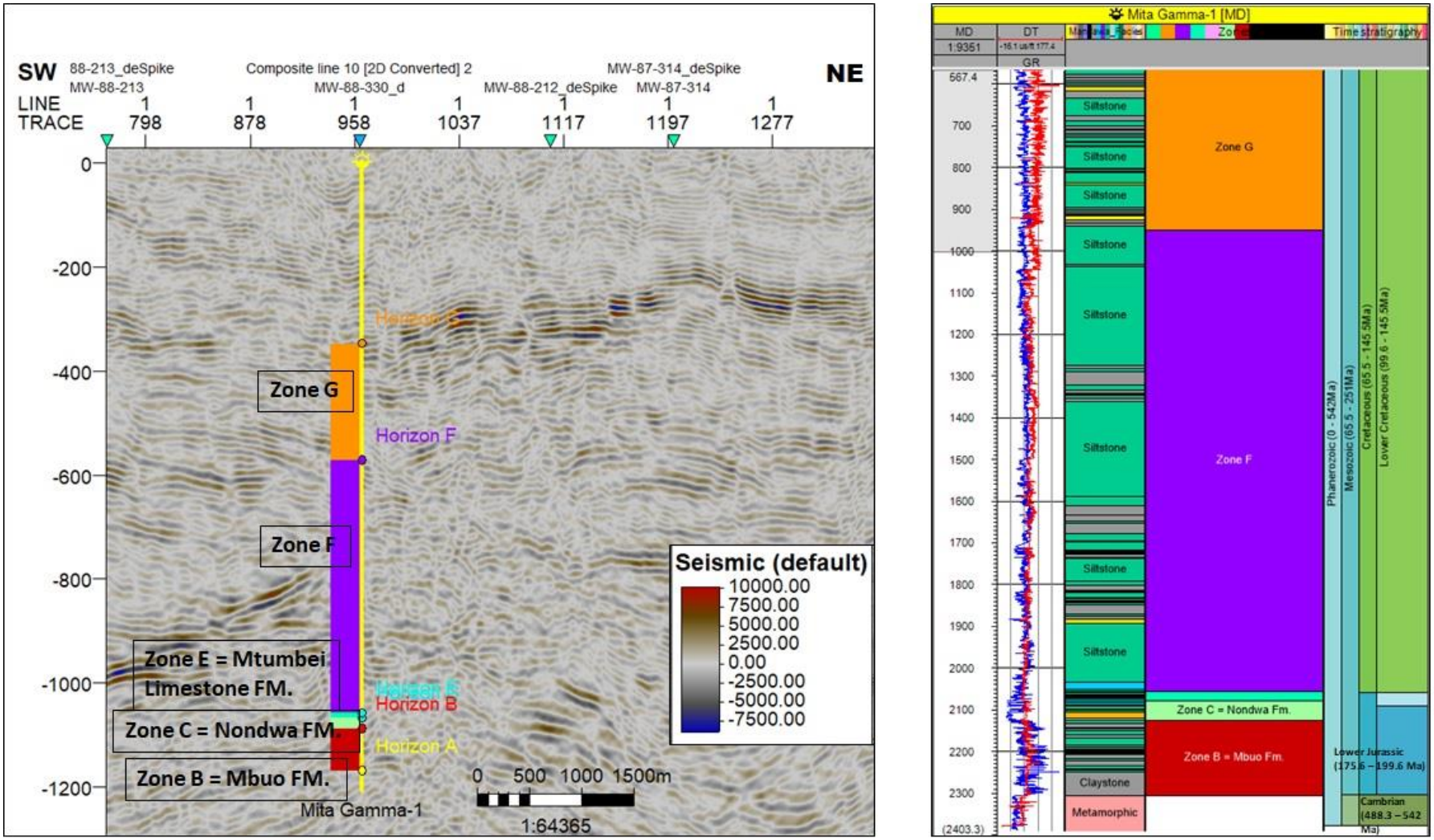

Figure 4.6 - ***The zones distributed along Mita Gamma-1 well in the 2D seismic line (left) and the correlation of DT and GR logs, lithostratigraphy, zones and associated ages (right).***

4.1.7 Kizimbani-1

Kizimbani-1 was the third wildcat drilled by AGIP (Africa) Ltd., Tanzania Branch, onshore in the Mandawa Basin. The well lied on the 2D seismic line TL-116_d (SP 535), UTM Easting 540.110 and Northing 9,001.125, on the northern border of the Mandawa Basin, where the salt section suggested to have pontential thickness and magnetometric and gravimetric surveys showed a structural high of the basement which may have developed during the Mesozoic (Figure 4.7). This well had a target to check the oil possibilities of Karoo Formation below the salt complex.

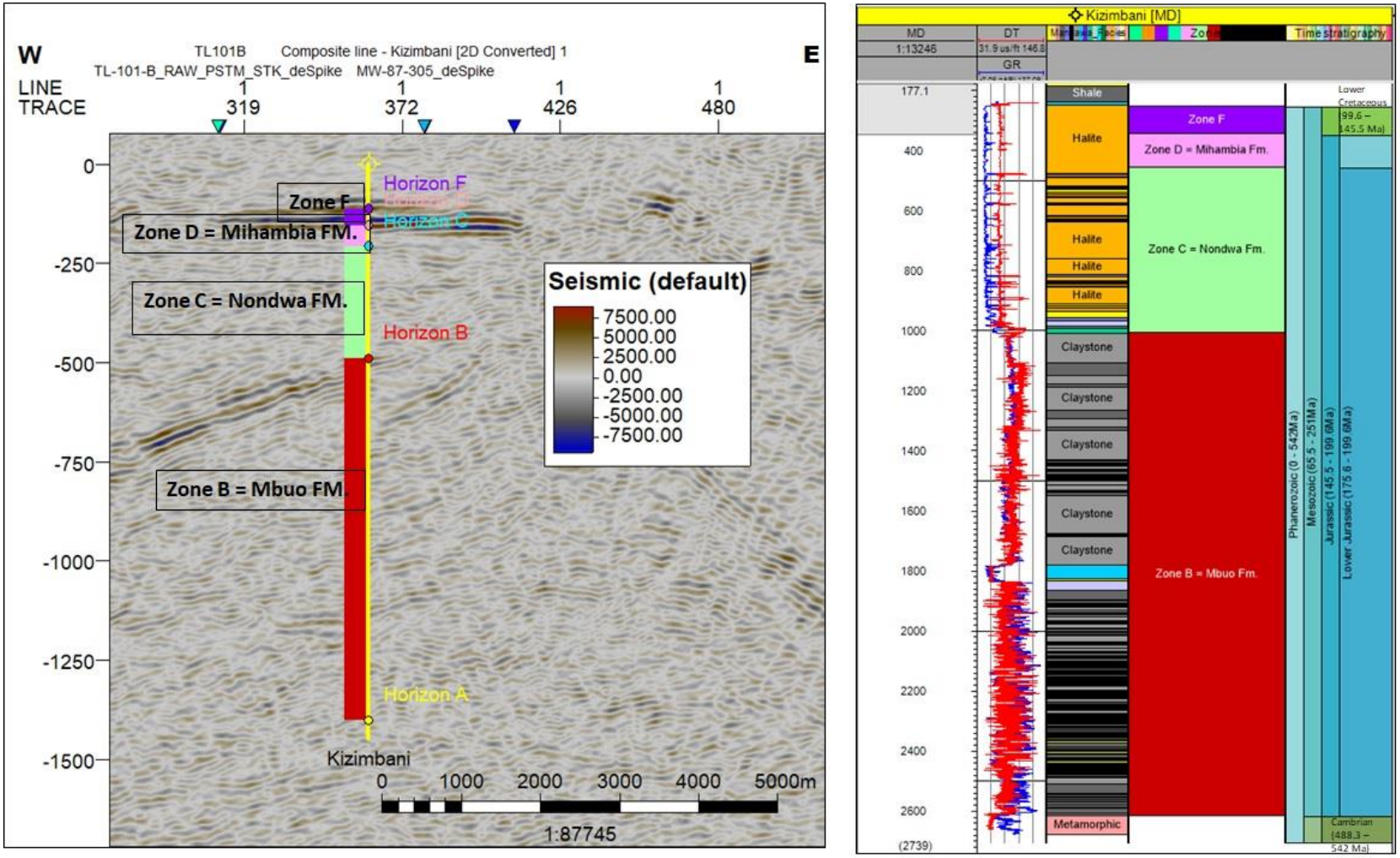

Figure 4.7 - The zones distributed along Kizimbani-1 well in the 2D seismic line (left) and the correlation of DT and GR logs, lithostratigraphy, zones and associated ages (right).

4.1.8 Kianika-1

The proposed surface location of the Kianika-1 well lied at SP 493 on seismic line MDW07-13, coordinates Easting 512.437.06, and Northing 9,073.565.96 (Figure 4.8). This well was positioned on the crest of the Kianika structure. The Kianika Structure is fault-bounded on all sides, with a major easterly dipping basin bounded fault on its western side, and appears to be cored by a long-standing basement high.

During the drilling program, the target was suggested as the Middle Jurassic Mtumbei Formation carbonate play, described by Shell as oolitic or reefal facies. It is known that only Lukoliro-1 had previously tested this play in Tanzania, targeting the Mtumbei Limestone, but did not encounter hydrocarbons in this unit. This well spudded a total depth of 2,922 m MD RT below ground level.

There has been considerable uncertainty between identified seismic horizons and their equivalence to lithostratigraphic and lithological units in Kianika-1. This is due to the lack of nearby wells, limited and difficult seismic ties to distant offset wells, which are in the central part of Mandawa Block and regarding published studies as the latest correlates to Hudson (2011) referring to the north of Mandawa Basin. The nearest wells, Mita Gamma-1 and Mbate-1, are around 60 km to the south. The nearest well to the west is Lukuliro-1, which is around 75 km distant.

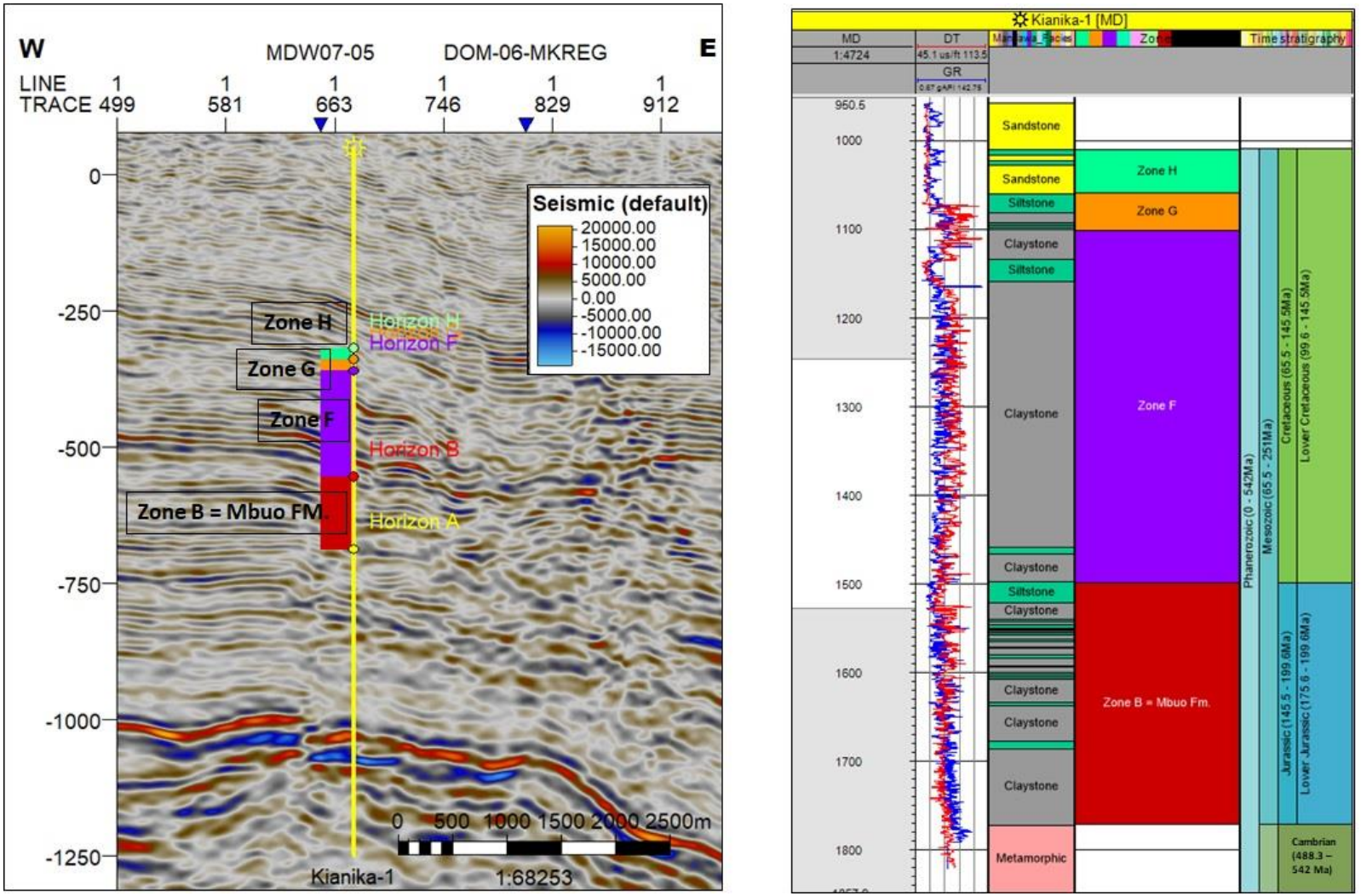

Figure 4.8 - ***The zones distributed along Kianika-1 well in the 2D seismic line (left) and the correlation of DT and GR logs, lithostratigraphy, zones and associated ages (right).***

4.2 OUTSIDE MANDAWA BLOCK

4.2.1 Lukoliro-1

According to Shell, Lukoliro-1 was drilled to test the Jurassic developed in a fault block within the Lukoliro Embayment. The well was interpreted to the closest 2D seismic line 84-SE-53 (SP 2643) away 1,3 km from where the well was proposed and reached a total depth of 2,367 m MD RT (Figure 4.9).

In Lukuliro-1 well, the recovered lithology was mainly limestone, with a thin unit of sandy dolomite. Three sedimentary facies were identified in Lukuliro -1, from core and wireline log data; limestone – peloid, oncoid, ooid grainstone facies, limestone – peloid packstone facies and sandy dolomite facies. The grainstone facies comprises the best potential reservoir rock and is interpreted as representing low relief carbonate sand shoals in a shallow subtidal to the intertidal zone.

The cored interval of Mtumbei Limestone in Lukuliro -1, between 1,141.32 m and 1,150.16 m, had poor overall reservoir properties. The maximum porosity and permeability, found in grainstone facies, are 15% and 1mD respectively. Measured permeability in the core only rarely exceeds 0.01mD. Shell quoted log porosities in the Mtumbei Limestone in the Kisangire-1 well of around 4% (at a depth of around 1850 m). Log interpretation, however, revealed the formations to be water-beared except to a very calcareous and tight interval containing gas.

In the Lukuliro-1 well, the potential porosity was found to have been infilled by calcite cement, which had been precipitated from phreatic pore waters. This is the main diagenetic process that has reduced porosity in the Mtumbei Limestone, and has infilled intergranular, intragranular and mouldic pores, at relatively shallow burial depths in this well before significant compaction. Dolomitisation has also occurred but is restricted to the sandy dolomite facies interval. The final diagenetic process to have affected the limestone in the well was a minor dissolution of some oolitic grains and mostly occured in grainstones that have some intergranular porosity, which allowed the passage of late-stage leaching pore waters.

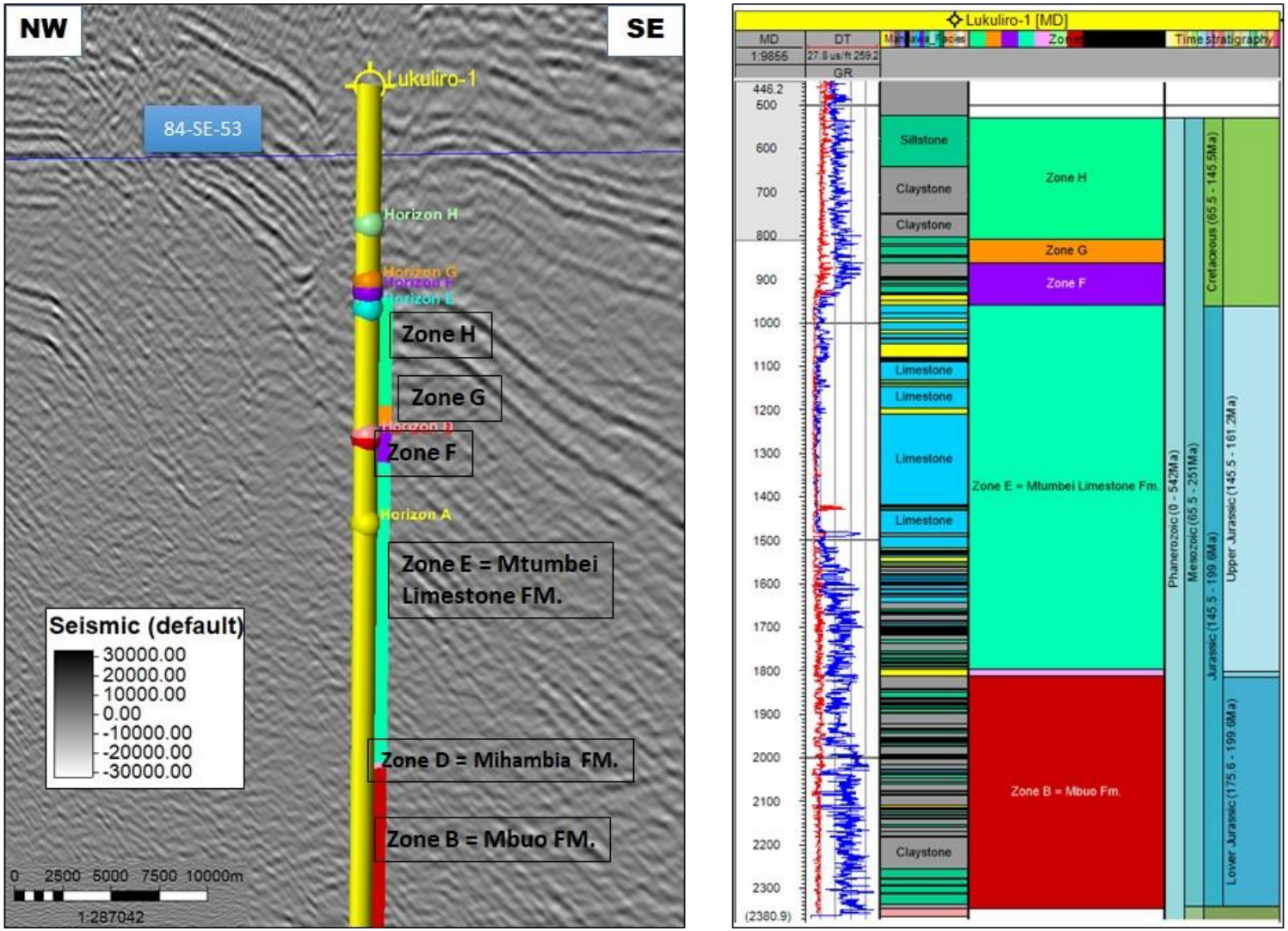

Figure 4.9 - *Seismic amplitude section from Lukoliro-1 well through NW-SE (left). Stratigraphic column of Lukoliro-1 (MD) with reference zones and ages (right).*

4.2.2 Lukuledi-1

The Lukuledi was the first well to be drilled by Texaco Exploration Tanzania Inc. in the Ruvuma Basin PSA, 16 km south-southwest inland rift valley to the northwest, between the Ruvuma and Rufiji rivers in the Lindi District (Figure 4.10). It tested a postulated fault trap on the eastern flank of the anticlinal according to the seismic available, the closest 2D seismic line, TL-101A_d-1 (SP 1501) which stands 2,2 km from the well whose coordinates are UTM Easting 572.953 and Northing 8,876.193. The Lukuledi-1 proved to have a massive source potential of the Karoo deposits in the basin.

In summary, the well tested the reservoir rocks, source rocks, and maturity, seal rocks and geothermal gradient. The primary reservoir objective was the Permian-Triassic continental Karoo sands just above the basement. A secondary reservoir objective targeted the Middle-Upper Jurassic carbonates and sandstones. These sandstones have been affected by moderate levels of compaction and development of authigenic clays.

Texaco had a primary play to achieve the block faulted Triassic Karoo continental reservoir rocks, sourced and sealed by overlying Lower Jurassic oil-prone shales and salt. A secondary play targeted the Middle-Upper Jurassic carbonates and sandstones reservoirs interbedded with source/seal shales of similar age. The well was spudded at 1,894 m MD RT total depth as rocks were described as from the Cretaceous age.

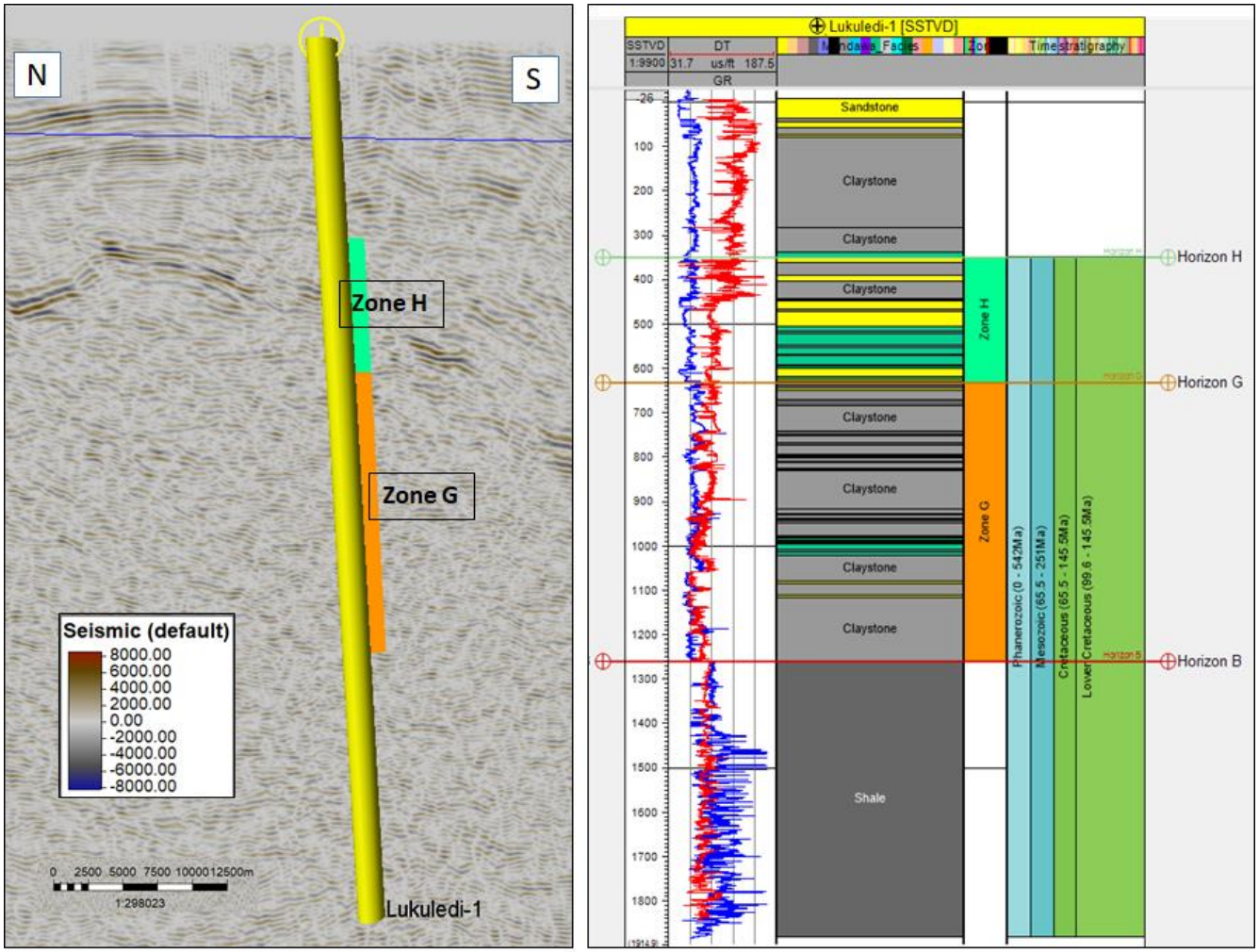

Figure 4.10 - The zones distributed along Lukuledi-1 well in the 2D seismic line (left) and the correlation of DT and GR logs, lithostratigraphy, zones and associated ages (right).

4.3 RUVUMA BASIN STRATIGRAPHY TERMINOLOGY

The stratigraphic development of the Ruvuma Basin is related to the progressive breakup of southwest Gondwana (Salman and Abdula, 1995). However, the most up-to-date lithostratigraphy (Figure 4.11) has been proposed in Key *at al.* (2008) based on a fieldwork project carried out in 2005 and information from published papers and unpublished reports and Smelror *et al.* (2006).

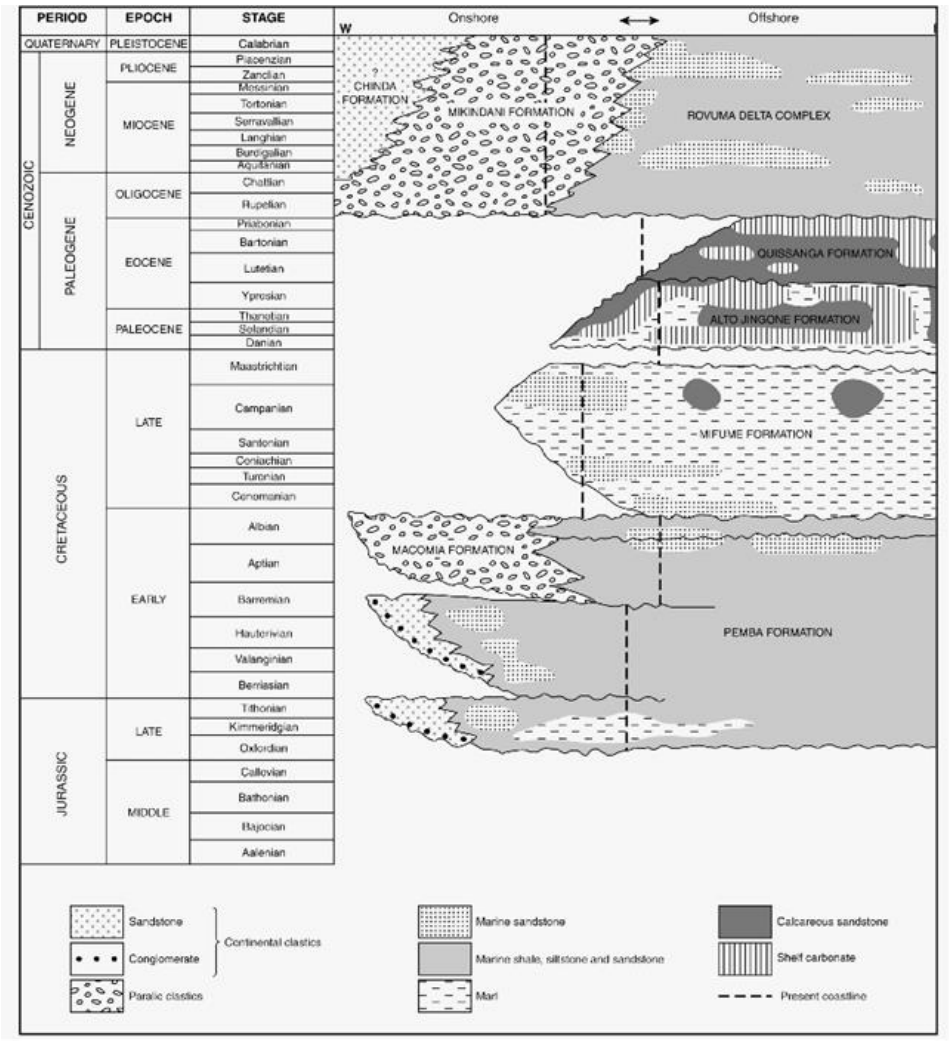

Figure 4.11 - Lithostratigraphic scheme for the onshore Ruvuma Basin. The Macomia Formation equivalent to the Horizon G – Zone G and Horizon H – Zone H in this thesis. From Lonropet SARL (2000), Smelror et al. (2008), and Key et al. (2008).

The stratigraphic nomenclature uses local place names in northern Mozambique and southern Tanzania as the formal names of the revised lithostratigraphic units.

The number of wells drilled in the onshore Ruvuma Basin was not ambitious to generate detailed subsurface maps. Due to limited dataset available to perform a conceptual interpretation of Lukuledi-1 well, no more than three horizons and two respective markers have been mapped in a tentative equivalence of lithology according to previous lithostratigraphic formations in the onshore part of the Rovuma Basin in northern Mozambique (Hancox *et al*., 2002; Smelror *et al*., 2008; Key *et al*., 2008). Faults played a major control on sedimentation causing lateral changes and nomenclature from the Mandawa Basin with the Ruvuma Basin were summarized:

4.3.1 The red marker at 398 m MD attributed to Horizon B – Mbuo Formation

This section is composed mostly of continental clastic sandstones, marine shale siltstones and claystones likely to be equivalent to the N'Gapa Formation of undefined age (Jurassic) as described in Key *et al*. (2008).

4.3.2 The orange marker at 678 m MD attributed to Horizon G – Zone G

Deposits of continental clastic sandstones and marine shale siltstones likely to be equivalent to Pemba Formation (Upper Jurassic – Lower Cretaceous) according to Key *et al*. (2008).

4.3.3 The green marker at 398 m MD attributed to Horizon H – Zone H

The Horizon H – Zone H lies the Horizon G – Zone G mainly as a thick succession of siltstones and sandstones with shales interbedded mapped as equivalent to the Macombia Formation of Lower Cretaceous age (Hancox *et al*., 2002; Key *et al*., 2008).

Periods of non-deposition suggested transitional conditions during the Jurassic that widespread to three unconformity periods in the Lower Cretaceous.

4.4 SELOUS BASIN STRATIGRAPHY TERMINOLOGY

As mentioned in Chapter 1, the Karoo deposits in the southern margin of the Selous Basin, southern Tanzania, correlate to those of Upper Triassic to Lower Jurassic age in the central portion of the basin. From field observations, various authors have described lithostratigraphic units corresponding to different depositional environments (Hankel, 1987; Kreuser *et al.*, 1990, Wopfner, 1994) in five depositional sequences initiated with the Carboniferous glacial beds upward coarsening sequences of basal sandstone of coal bedded on the basement marked the second tectonic event (Verniers *et al*., 1989). The third tectonic event was carried out during a predominantly humid climate during a coal deposition. The margin of the Selous Basin commenced at the time of the fourth succession episodes of tectonism and erosion carried out to a hiatus slumped onto Permian/Triassic boundary (Catenuanu *et al*., 2005). The Karoo rift sequence is defined by fluvialite sandstones resting on basal conglomerate (Kapilima, 2003).

Based on biostratigraphic investigations (micro floras, macro floras, fossil woods, vertebrates) the Karoo formations have been related to chronostratigraphic units from Upper Permian to Lower Jurassic. The study of Hankel (1987) described the stratigraphy of the Karoo Supergroup of the Selous Basin described ages, units, adapted lithofacies, and paleontology respectively (Figure 4.12).

AGE		UNIT	THICK-NESS	LITHOFACIES	PALAEONTOLOGY
LOWER JURASSIC	Liassic	NANDANGA FORMATION	300 m	Braided stream deposits; Conglomeratic and very coarse grained, arcosic, friable, buff coloured sandstones	Fossil woods Macroflora 104
				major unconformity	
		MADABA FORMATION	300 m	red beds: Meandering river deposits; Fining-upward cycles of multicoloured sandstones, siltstones and mudstones	Classopollis chateaunovi Microflora Sauropod remains Macroflora 96
UPPER TRIASSIC	Rhaetian	MKUJU FORMATION	200 m	red beds: Braided stream deposits; mainly coarse grained, white, feldspathic, partly calcareous sandstones with intercalations of red siltstones	Polypodiisporites ipsviciensis Microflora Macroflora 147
	Norian	MBARANGANDU FORMATION	250 m	Braided stream deposits; Laterally not persistent cycles of mainly medium and coarse grained, grey, yellow and greenish sandstones with calcareous concretions	Indeterminable plant fragments
		LUWEGU FORMATION	200 m	red beds: Fluviolacustrine flood plain deposits; mainly red siltstones with thin interbedded, white and greenish, fine grained, flaserbedded sandstones	Minutosaccus crenulatus Microflora Samaropollenites speciosus Microflora
	Carnian	MAHOGO FORMATION	300 m	Braided stream deposits; Laterally not persistent cycles of mainly medium and coarse grained, yellow and greenish grey sandstones with a characteristic spotted appearance; rare intercalations of siltstones	Staurosaccites quadrifidus Microflora Macroflora 75 Macroflora 74
MIDDLE TRIASSIC	Ladinian	LUHOMBERO FORMATION	1400 m	Braided stream deposits; Laterally not persistent cycles of mainly medium and coarse grained, grey and yellow sandstones; thin intercalations of siltstones and mudstones	Dinosauroid track
	Anisian				
LOWER TRIASSIC	Scythian	RUFIJI FORMATION	2100 m	Braided stream deposits; Laterally persistent cycles of mainly medium and coarse grained, grey and greenish grey sandstones with intercalations of siltstones and mudstones	Macroflora 132 Macroflora 84
UPPER PERMIAN		HATAMBULO FORMATION	900 m	Deltaic-lacustrine deposits: Ruaha Member: fluviodeltaic sandstones Sumbadzi Member: lacustrine black shales Pangani Member: deltaic, coarse sandstones Kidani Member: fluviodeltaic sandstones	Guttulapollenites hannonicus Microflora Macroflora 218 Reptile remain

Figure 4.12 - The stratigraphic table of the Karoo Supergroup in the Selous Basin in Hankel (1987).

Dominion Petroleum Limited awarded the PSA in the Selous Basin in the middle 2000s. The basin was described as under exploration since the first exploration work carried out by Shell in the middle 1980s. After that, several studies were carried out including geological field work, the study of available well data, photogeological work, the study of limited aeromagnetic and gravity data, acquisition of seismic and drilling two wells. The Jurassic sediments of Mandawa do not extend into Selous (Dominion, 2006).

4.4.1 Liwale-1

Liwale-1 was a wildcat well drilled in southern Tanzania Easting 337.629.40 and Northing 8,957.110.66 in the 2D seismic line U83-LW-05 (SP 3170), northwest of the town of Liwale, 200 km of the Rufiji River (Figure 4.13). This well was drilled to evaluate the nature and extension of the Karoo sandstones and to determine if there were any potential source rocks in the region reaching a total depth of 1761 m.

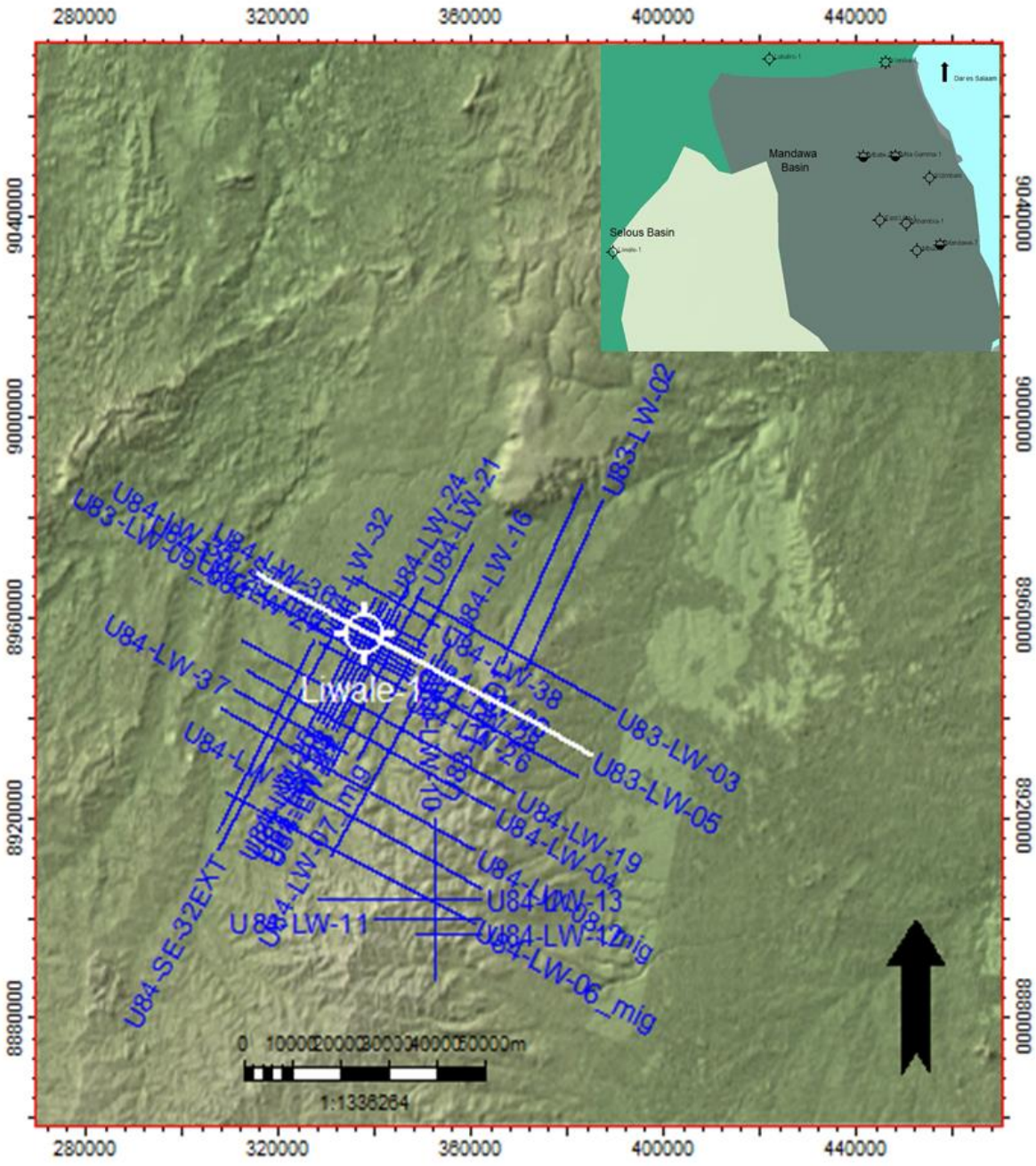

Figure 4.13 - The location in the southern portion of Tanzania where the 2D seismic lines transect gathering the surroundings of Liwale-1 well where in white is highlighted line U83-LW-05 interpreted for seismic well tie.

4.5 FORMATION DESCRIPTION AND DEFINITIONS OF THE SELOUS BASIN

To address a comprehensive lithostratigraphy in this thesis, five markers (see Appendix 4.5) and respective horizons based on well logs (Gamma Ray, Sonic, Porosity, and Density) in the Liwale-1 well have been interpreted (Figure 4.14), named as the geological ages with combining studies of Hankel (1987) and Catenuanu *et al*. (2005), shown in the Figure 4.15, in order to avoid misleading interpretation and the biostratigraphy classification attributed in previous studies.

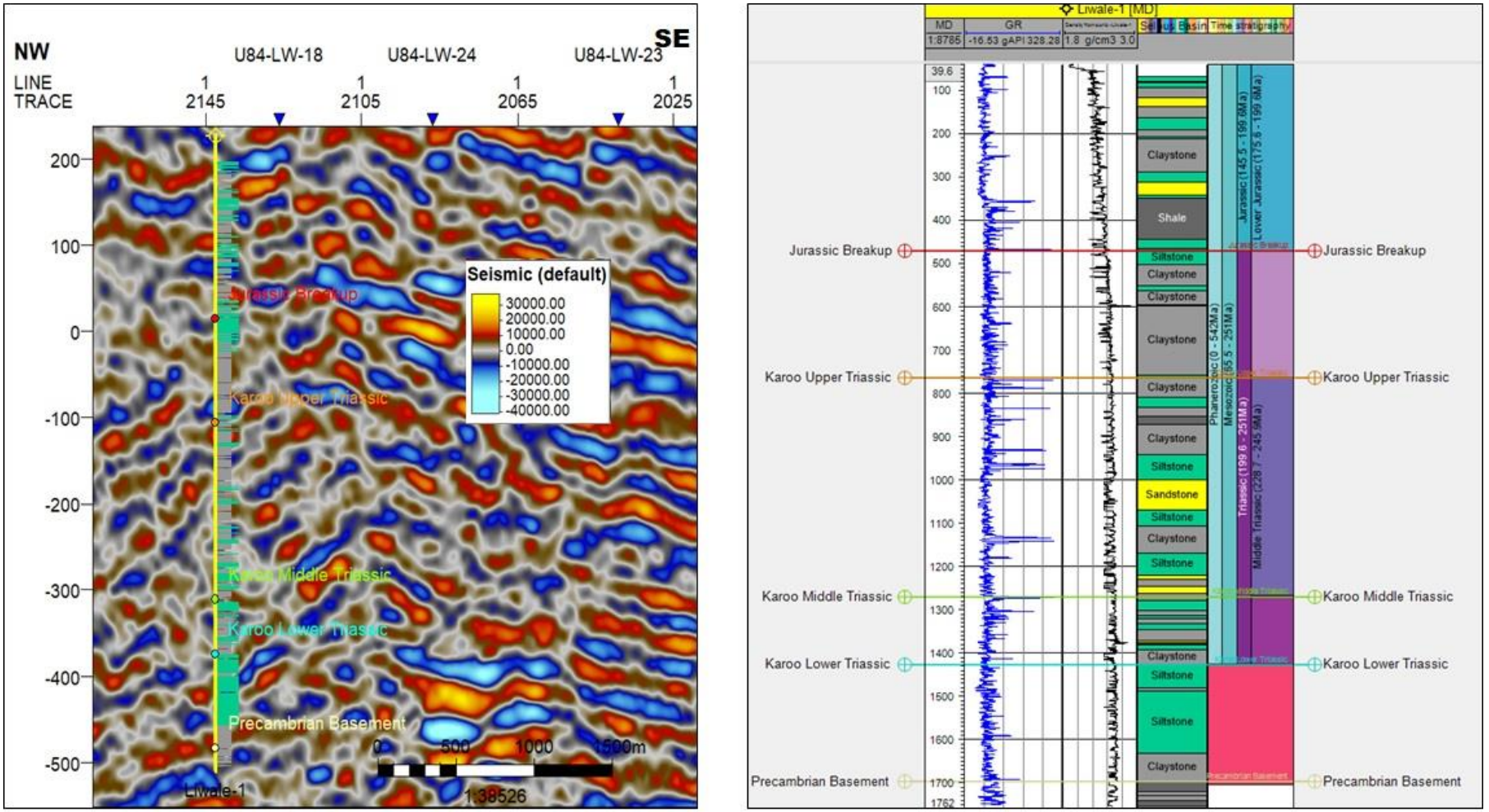

Figure 4.14 - ***The zones distributed along Liwale-1 well in the 2D seismic line U84-LW-18 (left) and the correlation of DT and GR logs, lithostratigraphy, zones and associated ages (right). The 2D seismic line U83-LW-05 where well tops corresponding from base to top to Precambrian Basement, Karoo Lower Triassic, Karoo Middle Triassic, Karoo Upper Triassic and the Jurassic Breakup were interpreted in Liwale-1 well.***

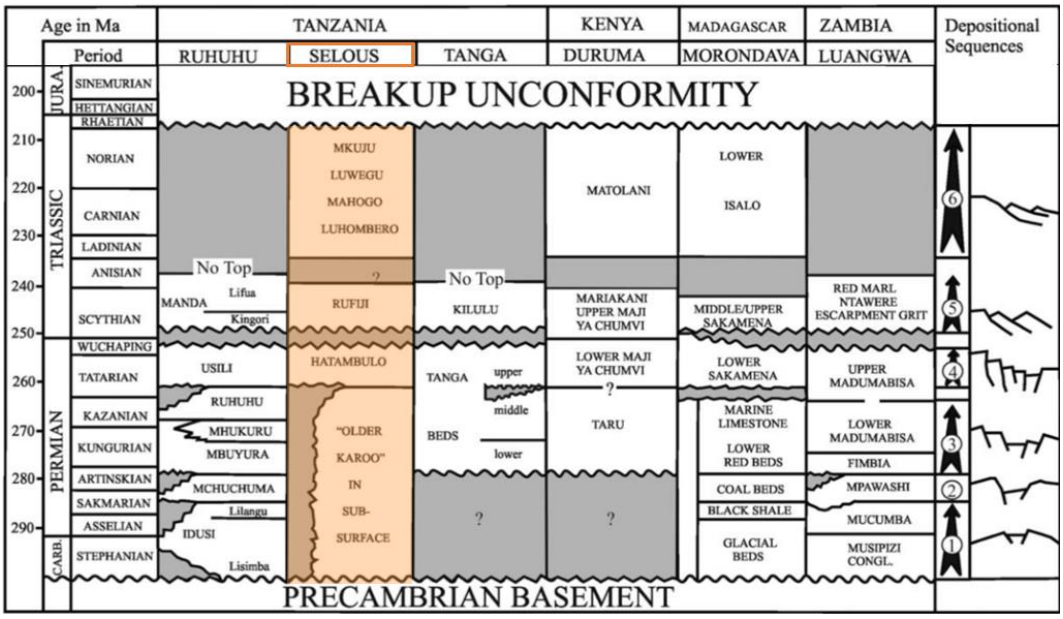

Figure 4.15 - Stratigraphic chart of the Selous Basin (highlighted in orange) and correlative basins. Adapted from Catenuanu et al. (2005).

4.5.1 The light beige marker at 1700 m MD attributed to Precambrian Basement

The Selous section suggests the presence of glacigene Karoo deposits. The first major tectonic pulse occurred prior to the onset of coal deposition (Catuneanu *et al*., 2005).

4.5.2 The blue marker at 1427 m MD attributed to Karoo Lower Triassic

Claystone, siltstone, thin basal limestone have been observed as Lower Triassic Karoo deposits in this thesis however these deposits may correlate to the deltaic-lacustrine deposits build up mainly by feldspathic sandstones and black shales of the Hatambulo Formation according to Hankel (1987) and Catuneanu *et al.* (2005).

4.5.3 The green marker at 1269 m MD attributed to Karoo Middle Triassic

Fluvial deposits build up mainly by coarse sandstones interbedded with siltstones and claystones potentially correspond to the Luhomero Formation formalized in Hankel (1987).

4.5.4 The orange marker at 764 0 MD attributed to Karoo Upper Triassic

Consists of fluvial sandstones, siltstones, and siltstones. Possibly correlates the Lower Triassic Rufiji Formation bedded by fluvio-lacustrine flood plain siltstone deposits of the

Luwegu Formation described in Catuneanu *et al.* (2005). The Upper Karoo successions in the majority of eastern African Karoo basins ceased by a major unconformity carried out by the beginning of breakup leading to the separation between Africa and Arabia; Madagascar and India.

4.5.5 The red marker at 471 m MD attributed to Jurassic Breakup

Siltstones and claystones have been interpreted interbedded suggesting equivalence of the Mabada Formation in Hankel (1987). The hiatus around the Permian – Triassic boundary is observed in all Tanzanian Karoo basins and in Mozambique (Wright and Askin, 1987).

4.6 MANDAWA BASIN STRATIGRAPHY TERMINOLOGY

Lithostratigraphy deals with the lithology of strata and with their organization into units based on lithological character (Hedberg, 1976).

Oil companies have adopted the terminology for stratigraphy units for central Mandawa formations proposed by Shell Petroleum Tanzania Limited (Shell PDT) in 1990 based on fieldwork, drilling activities, and seismic interpretation to define lithology and ages across the north and south Mandawa Basin (Figure 4.16). Nicholas *et al.* (2006) published the associated stratigraphy of the coastal Mandawa. Yet, terminologies were difficult to associate as studies were unpublished or outdated. To address the absence of published geological data covering the central Mandawa Basin, fieldwork has been done by Hudson (2011) which investigated the stratigraphy of north, south, and coastal Mandawa proposing a reviewed stratigraphic framework and a geological - structural map of the Mandawa Basin.

In respect of the Karoo lithofacies in Mandawa Basin, they were described as more distinct and more varied due to differences in the subsidence rates within half grabens. To the south at Mandawa evidence of marine incursion is more obvious as early Karroo clastics are followed by transitional continental to marine beds then lagoonal shales and evaporitic sequence of Triassic age (Mbede and Dualeh, 1997).

In this chapter, the proposed lithological nomenclature for the geological markers (well tops/markers – Appendix 4.6) and formation zones formations and their boundaries,

lithostratigraphic framework, and evolution of formations are addressed to abstain from the previous stratigraphic nomenclature adopted by oil companies due to misreading upon decades of petroleum exploration. Geological ages were defined according to the International Chronostratigraphic Chart (ICS, 2019) associating formations to series/epoch and stage/age.

The colours were chosen to represent the well trajectory, well names, and well symbol in the maps or well sections in this thesis were defined as:

Dark (black) background: yellow or white well trajectory, well names and well symbol.

Light (white) background: black or red well trajectory, well names, and well symbol.

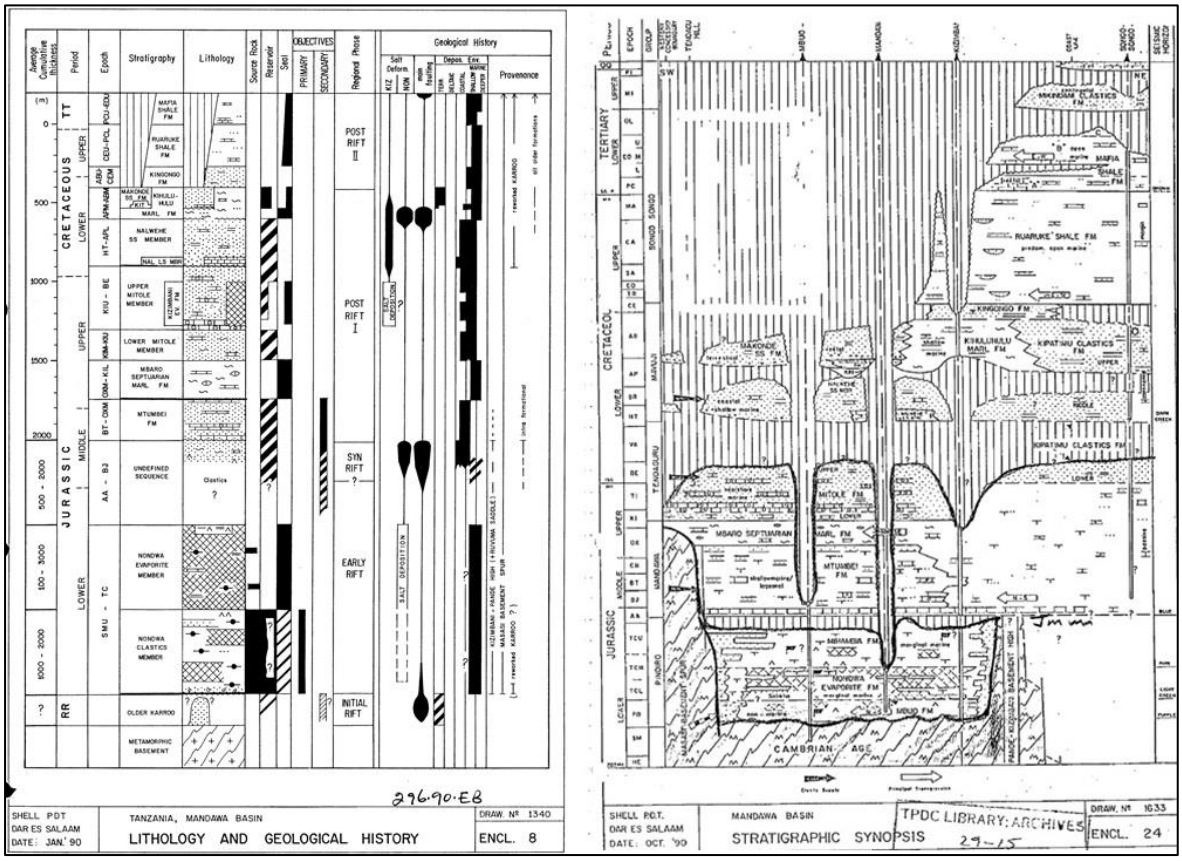

Figure 4.16 - Stratigraphic definitions formulated by (left) and the stratigraphic synopsis (right) for the Mandawa Basin (Shell, 1990).

These geological markers (Figure 4.17) were defined and bounded in stratigraphic order marked by stratal thickness changes across salt structures and most normal listric faults and reverse faults, from the oldest to the youngest, according to the responses seen from the geophysical well logs, such as Sonic D*T*, Gamma Ray GR, Density RHOB, and

Porosity NPHI: Horizon A, Horizon B, Horizon C, Horizon D, Horizon E, Horizon F, Horizon G and, Horizon H (see Appendix 4.4).

Figure 4.18 presents the seven zones defined in between the markers where four of them specifically may correlate to previous stratigraphic units proposed firstly by Shell in 1990 for the onshore Mandawa Basin, Mbuo Formation, Nondwa Formation and, Mtumbei Limestone Formation. From the lowermost to the uppermost, the zones are comprehending as Zone B - Mbuo Formation (Fm.), Zone C - Nondwa Formation (Fm.), Zone D - Mihambia Formation (Fm.), Zone E - Mtumbei Limestone Formation (Fm.), Zone F, Zone G and Zone H (see Appendix 4.7). The Horizon A, as the basement is not classified as a zone in Petrel as it is the lowermost layer.

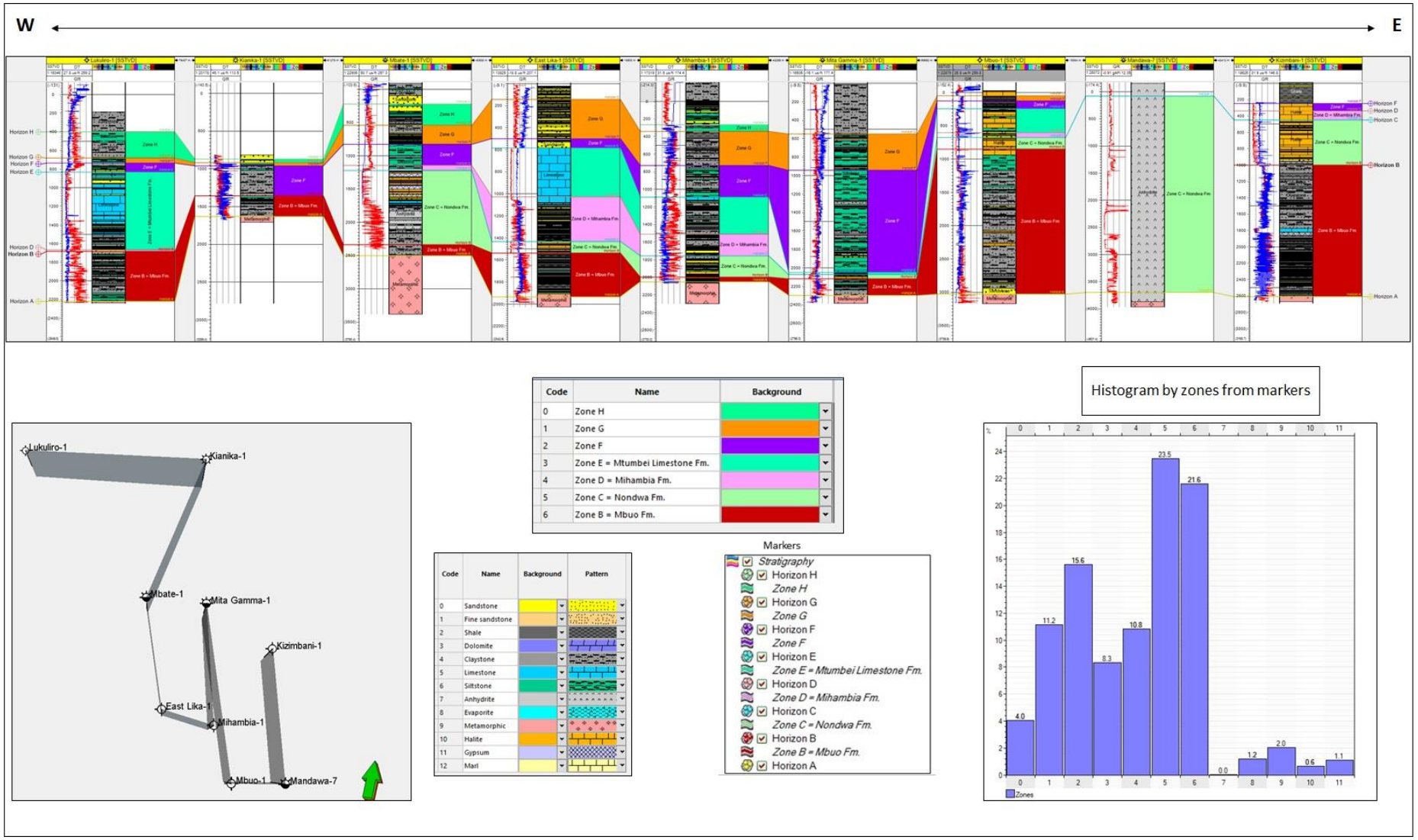

Figure 4.17 - Well correlation (W-E) within wells in Mandawa Basin (Lukoliro-1, Kianika-1, Mbate-1, East Lika-1, Mita Gamma-1, Mihambia-1, Mbuo-1, Kizimbani-1 and Mandawa-7, cross-section view in Petrel, code for zones and lithologies and histogram by zone from markers (well tops).

4.6.1 Horizon A – Metamorphic Basement

Horizon A = Metamorphic Basement occurs as the basement of the sedimentary strata in the Mandawa basin (Hudson, 2011).

The radiometric date of the bottom hole sample of the basement from Kizimbani-well using K/Ar is 537 ± 7, approximately Precambrian/Cambrian age (Balduzzi *et al.* 1992).

4.6.2 Horizon B – Mbuo Formation

The Horizon B = Mbuo Formation comprises of siliciclastic rocks (claystone interbedded with siltsones, sandstones, and shales) deposited unconformably over the Metamorphic Basement during Lower Jurassic. The formation occurs and varies in thickness in almost all the wells correlated and interpreted in this thesis in the Mandawa Basin with the exception of Mandawa-7. Sandstone beds were interpreted in central to the south of Mandawa Block alternating with claystones and shales suggesting to be a potential source rock. To the south of the block in Kizimbani-1 well, limestone (approximately 46 m) and a thin bed of gypsum (nearly 30 m) have been interpreted using geophysical well logs.

This unit has been previously addressed using several names including Nondwa shales (Mandawa-7), Mbuo sandstone (Mbuo-1), Mbuo Claystone (Mbuo-1), Mbuo Lower (East Lika-1), Mbuo Upper (East Lika-2) (Hudson, 2011).

4.6.3 Horizon C – Nondwa Formation

This Lower Jurassic evaporitic rock formation was deposited over the Mbuo Formation. Although the formation is known to contain proven source rocks, these organic-rich claystones are interbedded with halite beds, gypsum, and anhydrite of variable thickness. Due to its excellent sealing properties, this evaporitic unit may, therefore, prevent hydrocarbon migration from the source rocks into the post salt section.

Seismic interpretation revealed that the thick Lower Jurassic salt basin, known from wells in south and central Mandawa East Lika-1, Mbuo-1, Mbate-1, Mihambia-1, thin unit in Mita Gamma-1, Mandawa-7 and Kizimbani-1), does not extend the full length of the Mandawa. This may represent the northern limit of the Mandawa Basin and appears to coincide with the location of a major WNW – ESE oriented transfer fault.

The Lukuliro-1well in the north of Mandawa does not contain the Horizon C – Nondwa Formation source rock unit, therefore there is a northern limit to this section to the east

and south of these wells. The location of this northern limit is not at present known due to the general lack of well penetrations in the north Mandawa.

Outcrop rocks occur as shales interbedding to selenitic gypsum, anhydrite, granular limestones, and dolostones (Hudson, 2011).

4.6.4 Horizon D – Mihambia Formation

The Horizon D = Mihambia Formation corresponds to the siliciclastic of a dominantly sandy unit with minor claystones and limestone stringers and marginal marine rock formation from Lower Jurassic to Middle Jurassic deposited over the Nondwa Formation. The formation was interpreted in the subsurface from north to south Mandawa by Lukoliro-1 (approximately 16 m), Mbate-1, East Lika-1, Mihambia-1, Mbuo-1, and Kizimbani-1 wells of variable thickness. The base of the Horizon D = Mihambia Formation characterizes the of lithology from the evaporites to sandstone with an occasional pack of halite (approximately 100 m) seen in Kizimbani-1 ascending to open marine facies – shales and limestones deposits.

4.6.5 Horizon E – Mtumbei Limestone Formation

The Horizon E - Mtumbei Limestone Formation constitutes of sandy dolomite and shallow marine limestone formation of Middle to Upper Jurassic deposited over the Horizon D = Mihambia Formation.

In wells that have penetrated the Horizon E = Mtumbei Formation clastics, this unit comprises fine to coarse-grained sandstones, of possible fluvial-deltaic origin. The sandstones within the Horizon E - Mtumbei Formation are considered to have moderate reservoir potential. Some wells as East Lika-1, Kizimbani-1, Mbuo-1, Mihambia-1 and Mita Gamma-1 suggest the occurrence of a sandstone unit.

Two wells in the Mandawa PSA block, Lukuliro-1, and Mita Gamma-1, have previously targeted the Mtumbei Limestone Formation. Lukuliro-1 did not encounter hydrocarbons in this unit, although oil shows have been found in Mita Gamma -1 in the Mtumbei Limestone.

Previous studies in Lukuliro -1, the Mtumbei Limestone Formation was cored, the recovered lithology being mainly limestone, with a thin unit of sandy dolomite. Three sedimentary facies were identified in Lukuliro -1, from core and wireline log data; limestone – peloid, oncoid, ooid grainstone facies, limestone – peloid packstone facies

and sandy dolomite facies. The grain-supported carbonate facies was interpreted as representing low relief carbonate sand shoals.

The well log interpretation in this study suggests that the carbonate rock facies section in the well represents the margins of a laterally more extensive sand shoal. A no matrix grain-supported facies was probably deposited in slightly deeper water than the shallow marine limestone, where facies can be regarded as the background sedimentation of the shallow subtidal shelf. The interval of Horizon E - Mtumbei Limestone in Lukuliro -1, between 1141.32 m and 1150.16 m, was interpreted as poor overall for reservoir properties.

4.6.6 Horizon F – Zone F

The Horizon F - Zone F is addressed as interbedded claystones, siltstones and shales overlying unconformably the Mtumbei Formation. The formation occurs and varies in thickness in almost all the wells correlated and interpreted in this thesis in the Mandawa Basin with the exception of Mandawa-7.

Upper Jurassic to Lower Cretaceous in most Tanzania wells is of apparent source rock potential and have TOC contents ranging from 1 to 11%. Data from the Songo Songo-5 well shows that despite good to very good TOC contents the pyrolysate yields are at best only moderately good and are, notably, mostly poor. (Core Lab/TPDC, 2009). Outcrop observations registered this formation developed in a lagoonal environment where siliciclastic mud, fine carbonates and plant debris interacts (Hudson, 2011).

4.6.7 Horizon G – Zone G

Represented by an open marine shore from Lower Cretaceous with rapid deposition of claystone package at the base of Horizon G - Zone G. The formation is penetrated by Lukoliro-1, Kianika-1, Mbate-1, East Lika-1, Mihambia-1, Mita Gamma-1 and Mbuo-1 wells varying in thickness.

4.6.8 Horizon H – Zone H

The Horizon H - Zone H is represented by tightly interbedded shales, siltstones, and sandstones laid down in a shallow open marine environment from Lower Cretaceous.

The shales and sandstones dominate the unit gradding to be generally in both directions, indicating a rapid deposition of the clastic rocks occurring in the Lukoliro-1, Kianika-1, Mbate-1, and Mihambia-1 wells.

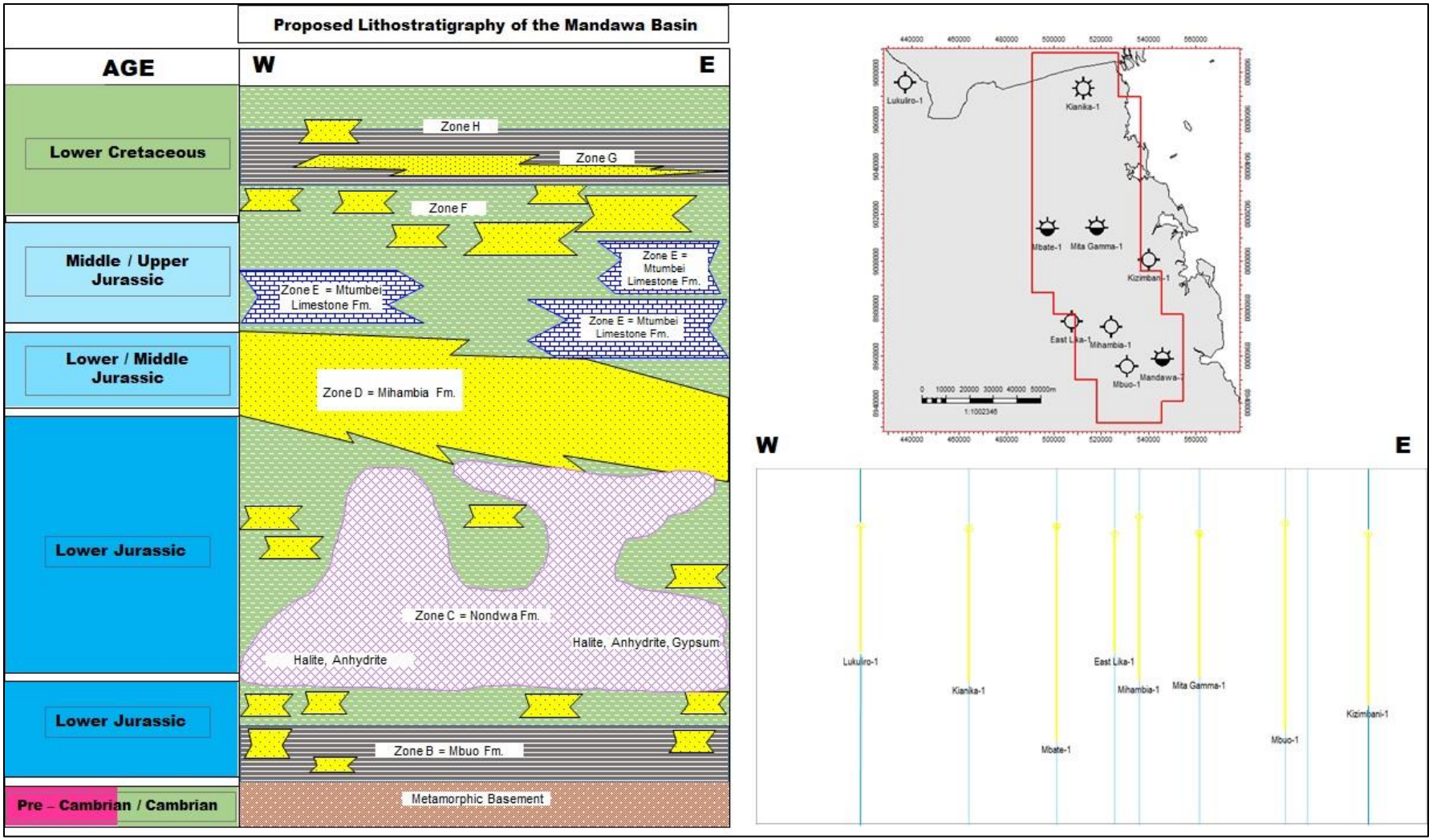

Figure 4.18 - *Proposed Lithostratigraphy of the Mandawa Basin. The subsurface units (left) have been established according to geological logs, geophysical logs and seismic profiles. The map shows the location of the wells (top) and their view in cross-section (right). Adapted from Copestake (2008).*

CHAPTER 5

SEQUENCE STRATIGRAPHY ANALYSIS

5.1 SEQUENCE STRATIGRAPHY CONCEPT

In the literature, sequence stratigraphy has been investigated, described and, understood throughout the decades. During the 1970s, studies were published focusing on the relationship of sedimentation and unconformities, the appearance of argumentation towards changes in the sea level leading to emerging the studies of seismic stratigraphy.

Sequence stratigraphy, unlike lithostratigraphy, provides a chronostratigraphic framework for the correlation and mapping of syndepositional facies. It is also useful for predicting stratigraphic and geometric relationships and facies distribution which is important in exploration, and reservoir characterisation. Sequence stratigraphy is based on seismic stratigraphy, biostratigraphy, chronostratigraphy and sedimentology, but not necessarily on lithostratigraphy (Emery and Myers, 1996). Essentially the term has been used to describe the rock relationships within a chrono-stratigraphic framework of repetitive sequences, subdivided into systems tracts, genetically related strata and by the stacking patterns of parasequence sets and parasequences bounded by marine-flooding surfaces alternating erosion or non-deposition, or their correlative conformities the sequence stratigraphy of formations observed in the field (Emery and Myers, 1996; Wagoner *et al.,* 1987).

5.1.1 Sequence stratigraphy framework

The sequence stratigraphy framework provides the genetic context in which event-significant surfaces and the strata they separate and placed into a coherent model that accounts for all temporal and spatial relationships of the facies that fill a sedimentary basin (Catenuanu, 2006). Three main sequence stratigraphic models are routinely used to analyze the sediment fill history of a basin. These three models are similar in terms of their use of correlative chronostratigraphic surfaces to study stratigraphy in a time-dependent framework. They differ, however, in their placement of boundaries between discrete stratigraphic intervals. For example, in the depositional sequence model (Mitchum *et al.,* 1977; Vail *et al.,* 1977; Posamentier *et al.,* 1988), sequences are bound by surfaces that reflect the transition from a regressive phase to a transgressive phase,

and are composed of a subaerial unconformity in many up-dip positions and correlative marine conformities in more distal positions; genetic stratigraphic sequences (Galloway, 1989) in contrast are bound by maximum flooding surfaces that mark the transition from an overall transgression to a regression.

Stratal terminations are defined by the geometric relationship between strata and the stratigraphic surface against which they terminate and are best observed at larger scales, particularly on 2D seismic lines and in large-scale outcrops. The main types of stratal terminations are described by truncation, toplap, onlap, downlap, and offlap (Catuneanu, 2002). Sequence stratigraphy deals with the 'packing and wrapping' of sedimentary successions in the response to relative sea-level changes and fluctuations in sediment supply to the basin.

Sequence: a sequence represent one cycle of deposition bounded by non-marine erosion, deposited during one significant cycle of fall and rise of relative sea level.

System tracts: a linkage of contemporaneous deposition systems, where a depositional system is a three-dimensional assemblage of lithofacies, genetically linked by active (modern) or inferred (ancient) processes and environments.

Transgressive system tracts (TST): system tracts that develop during a relative sea-level rise and when accommodation volume is increasing faster than the rate of sediment supply.

Maximum flooding surface (MFS): a surface that marks the end of the transgressive system tract, a point where progradation begins.

High stand system tracts (HST): is the youngest system tract in a sequence. It represents the progradational system deposited after maximum transgression and before a sequence boundary.

5.1.2 Types of stratal terminations

The types of stratal terminations (Figure 5.1) are characterised according to geometric relationship strata and the stratigraphic boundaries of depositional sequences against which they terminate (Mitchum and Vail, 1977; Mitchum *et al*., 1977; Posamentier *et al.*, 1988, Emery and Myers, 1996).

The morphology in stratigraphic interpretation includes the identification of conformal, onlapping, offlapping, hummocky, and chaotic reflector packages, ideally integrated within a sequence stratigraphic framework (Chopra and Marfurt, 2016).

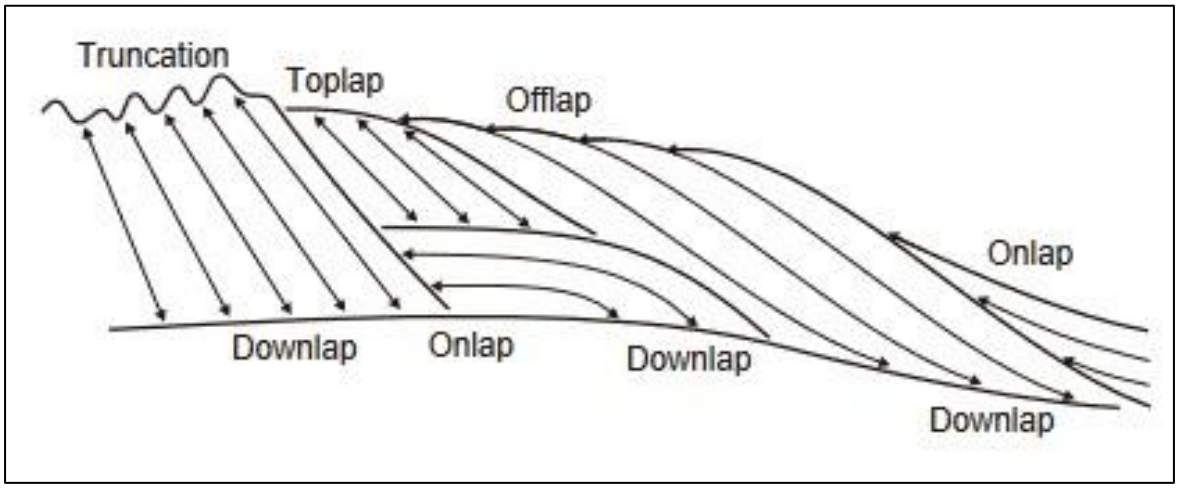

Figure 5.1 - Types of stratal terminations (Myers, 1996).

Truncation: termination of strata against an overlying erosional surface. Toplap may develop into truncation, but truncation is more extreme than toplap and implies either the development of erosional relief or the development of an angular unconformity. They are used to describe the stacking patterns of stratal units and to provide criteria for the recognition of various surfaces and system tracts (Posamentier *et al*., 1988).

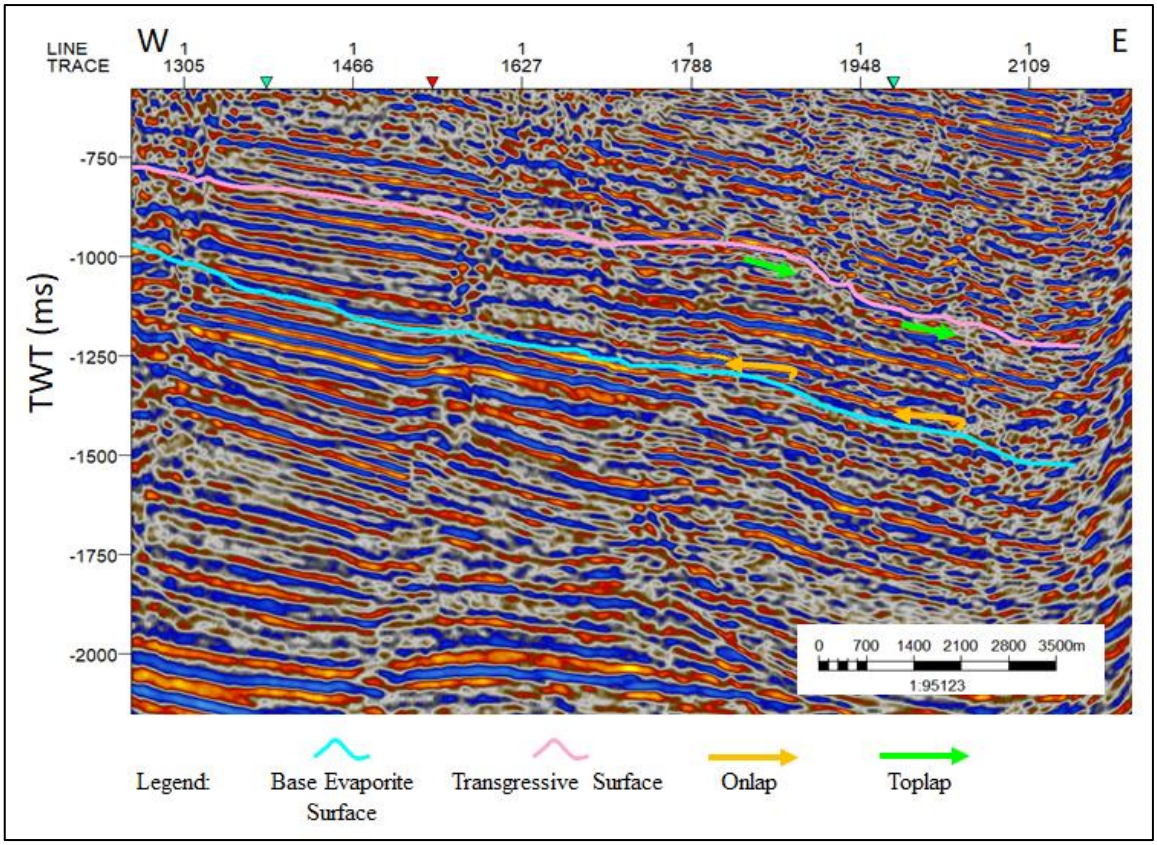

Figure 5.2 - Toplap and onlap features observed in a seismic 2D line from Mandawa Basin. High amplitude and continuous reflector overlie the Base Evaporite Surface reflector.

Toplap: termination of inclined strata (clinoforms) against an overlying lower angle surface, mainly as a result of non-deposition (sediment bypass), ± minor erosion. Strata lap out in a landward direction at the top of the unit, but the successive terminations lie progressively seaward. The toplap surface represents the proximal depositional limit of the sedimentary unit (Catunenau, 2006). In seismic stratigraphy, the top set of a deltaic system (delta plain deposits) may be too thin to be "seen" on the seismic profiles as a separate unit (thickness below the seismic resolution). In this case, the top set may be confused with toplap (Figure 5.2).

Onlap: termination of low-angle strata against a steeper stratigraphic surface. Onlap may also be referred to as lap out, and marks the lateral termination of a sedimentary unit at its depositional limit. Onlap types of stratal terminations may develop in marine, coastal, and nonmarine settings (Catuneanu, 2006; Catuneanu *et al.* (2009) (Figure 5.3).

Marine onlap: develops on continental slopes during transgressions slope aprons (Galloway, 1989; healing-phase deposits, Posamentier and Allen, 1993), when deep-water transgressive strata onlap onto the maximum regressive surface.- coastal onlap:

refers to transgressive coastal to shallow-water strata onlapping onto the transgressive (tidal, wave) ravinement surfaces.- fluvial onlap: refers to the landward shift of the upstream end of the aggradation area within a fluvial system during base-level rise (normal regressions and transgression), when fluvial strata onlap onto the subaerial unconformity.

Offlap: the progressive offshore shift of the updip terminations of the sedimentary units within a conformable sequence of rocks in which each successively younger unit leaves exposed a portion of the older unit on which it lies. Offlap is the product of base-level fall, so it is diagnostic for forced regressions (Catuneanu, 2006).

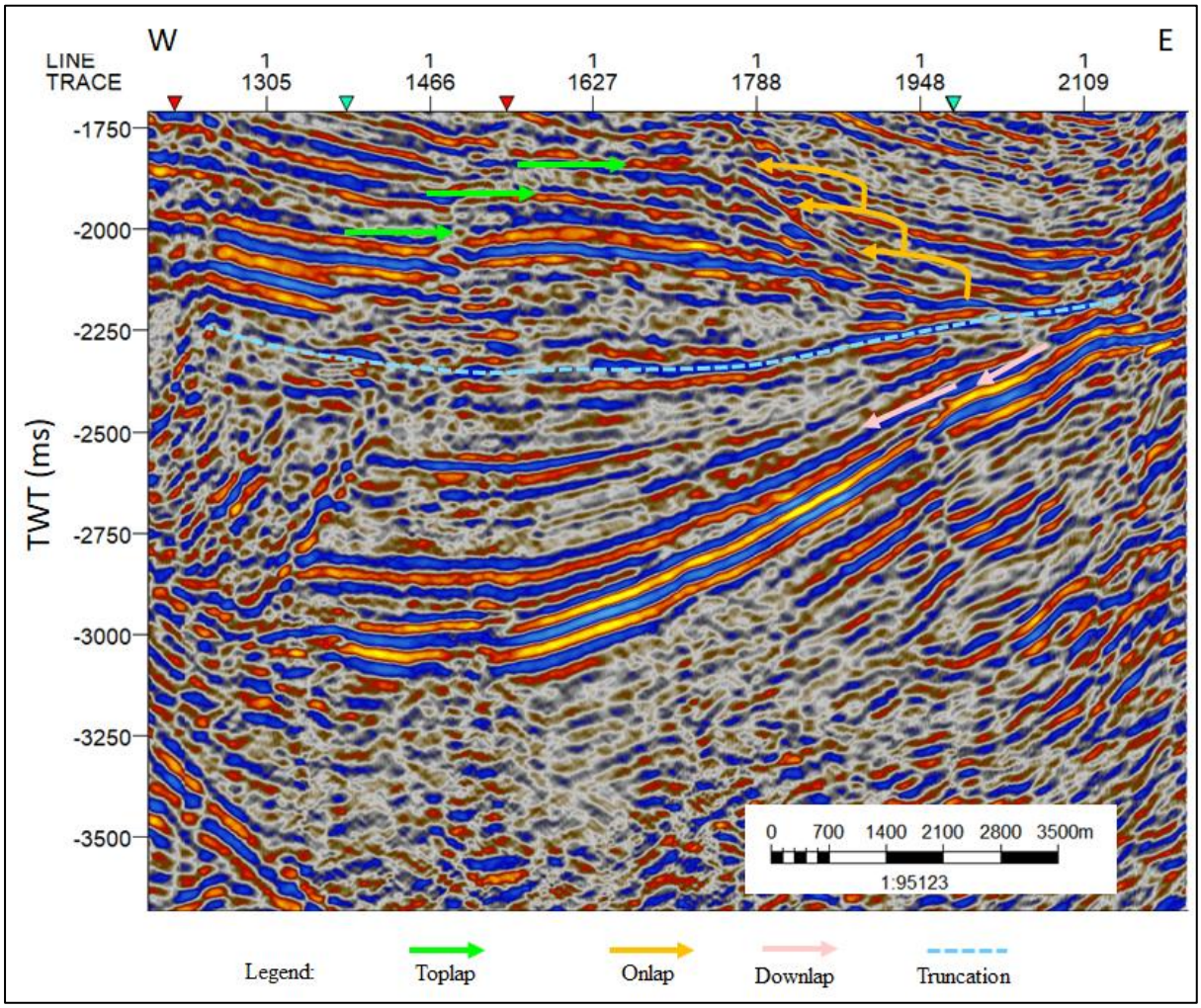

Figure 5.3 - Seismic modelling terminations mapped: toplap, onlap, downlap and truncation.

Downlap: termination of inclined strata against a lower-angle surface. Downlap may also be referred to as baselap, and marks the base of a sedimentary unit at its depositional limit. Downlap is commonly seen at the base of prograding clinoforms, either in shallow-marine or deep-marine environments. It is uncommon to generate downlap in non-marine

settings, excepting for lacustrine environments. Downlap, therefore, represents a change from marine(or lacustrine) slope deposition to marine (or lacustrine) condensation or non-deposition (Catuneanu, 2006).

Stratigraphic surfaces mark shifts through time in depositional regimes and are created by the interplay of base-level changes and sedimentation.

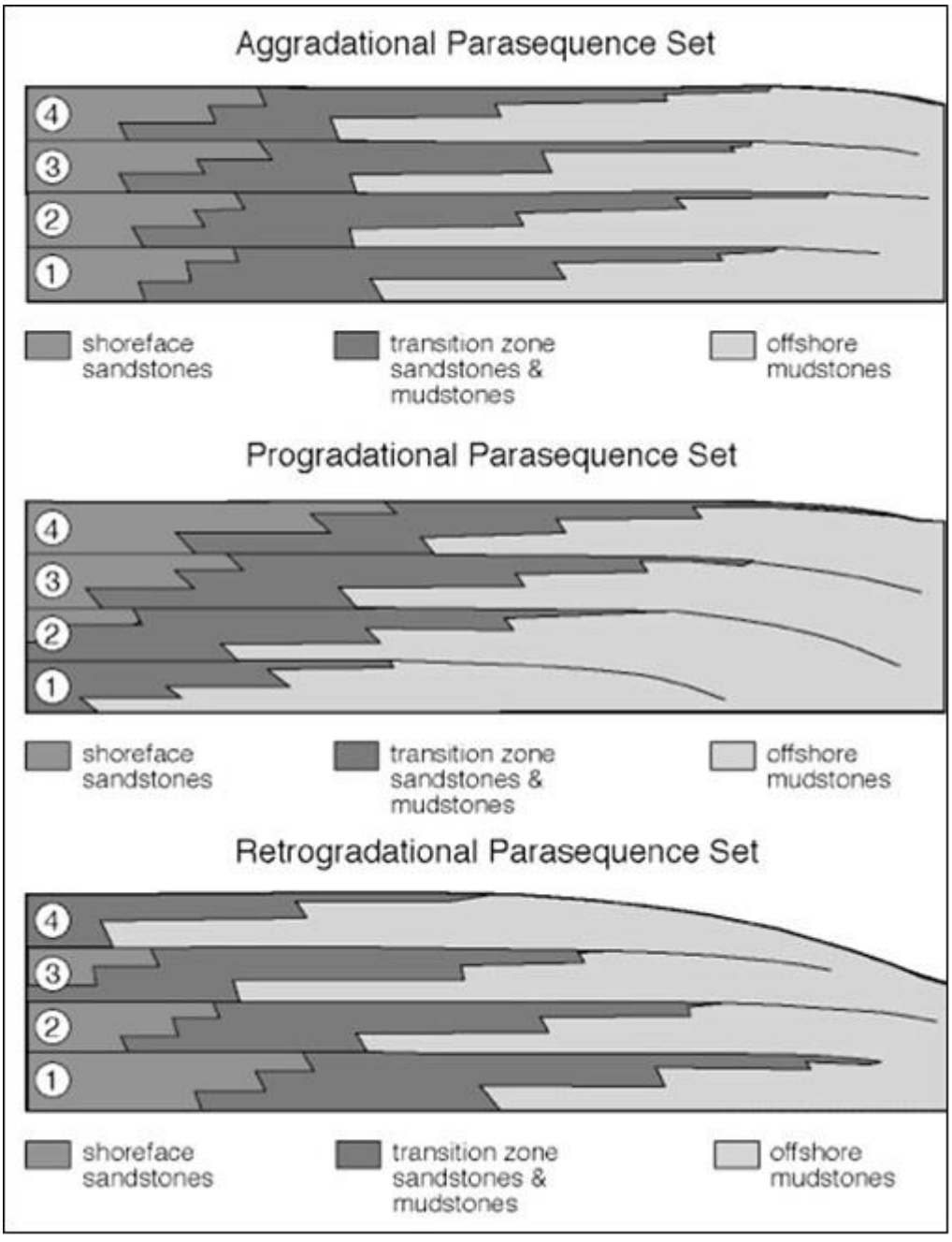

Figure 5.4 - Progradational, Retrogradational and Aggradational patterns (Van Wagoner et al., 1988).

5.2 HIERARCHY OF SEQUENCES – CYCLE DURATION

The hierarchy system based on cycle duration (Vail *et al.*, 1977; Mitchum and Van Wagoner, 1991; Vail *et al.*, 1991) considers essentially eustasy responsible to sequence generation at any order of stratigraphic cyclicity (see Table 5.1). A cycle of relative or eustatic change of sea-level that has a duration on the order of 100 to 200 million years is known as a first-order cycle (Mitchum, 1977). Using the concept of stratigraphic base level, deposition of non-marine strata above a subaerial unconformity is essencially described. With an increase in accommodation space and continuing siliciclastic sediment influx into an area, aggradational and progradational processes remain active. Different levels in the hierarchy of sedimentary cyclicity (Haq *et al*., 1988; Vail *et al.*, 1991) have been assigned to orders, defined based on their perceived durations; those of concern to us here are: large-scale cycles, with durations approximating to stages and thought to represent some 10 my (so-called 2nd-order, or transgressive-regressive facies cycles) and medium-scale cycles, approximating to ammonite zones or subzones and representing approximately 0.5 to 3 my (so-called 3rd-order or sequence cycles). Lithologic cycles also occur at smaller scales described as 4th order.

Table 5.1. The duration of stratigraphic cycles marks the hierarchical order cycles (modified from Vail *et al*., 1991).

Hierarchical order	Duration (My)
First order	50+
Second order	3 – 50
Third order	0.5 – 3
Fourth order	0.08 – 0.5
Fifth order	0.03 – 0.08
Sixth order	0.01 – 0.03

The past decade aggregated the advent of sophisticated models describing the architecture of depositional sequences in response to relative sea-level change (Posamentier *et al*., 1988; Posamentier and Vail, 1988; Sarg, 1988; Galloway, 1989; Van Wagoner *et al.*, 1990; Vail *et al.*, 1991; Tucker, 1991; Posamentier *et al.*, 1992). However, doubt still exists as to whether the sequence stratigraphy of any basin is primarily a response to eustatic or regional sea-level fluctuation, or even whether the genesis of a given

depositional sequence was necessarily governed by sea-level change at all (Galloway, 1989; Miall, 1991; Schlager, 1992).

5.3 SEISMIC FACIES UNITS

Seismic facies analysis of units (Figures 5.5 and 5.6) uses the geological interpretation of the parameters to recognize and describe the deposition environment. This description considers the internal configuration and parameters such as amplitude, continuity, and frequency (Vail *et al*., 1977).

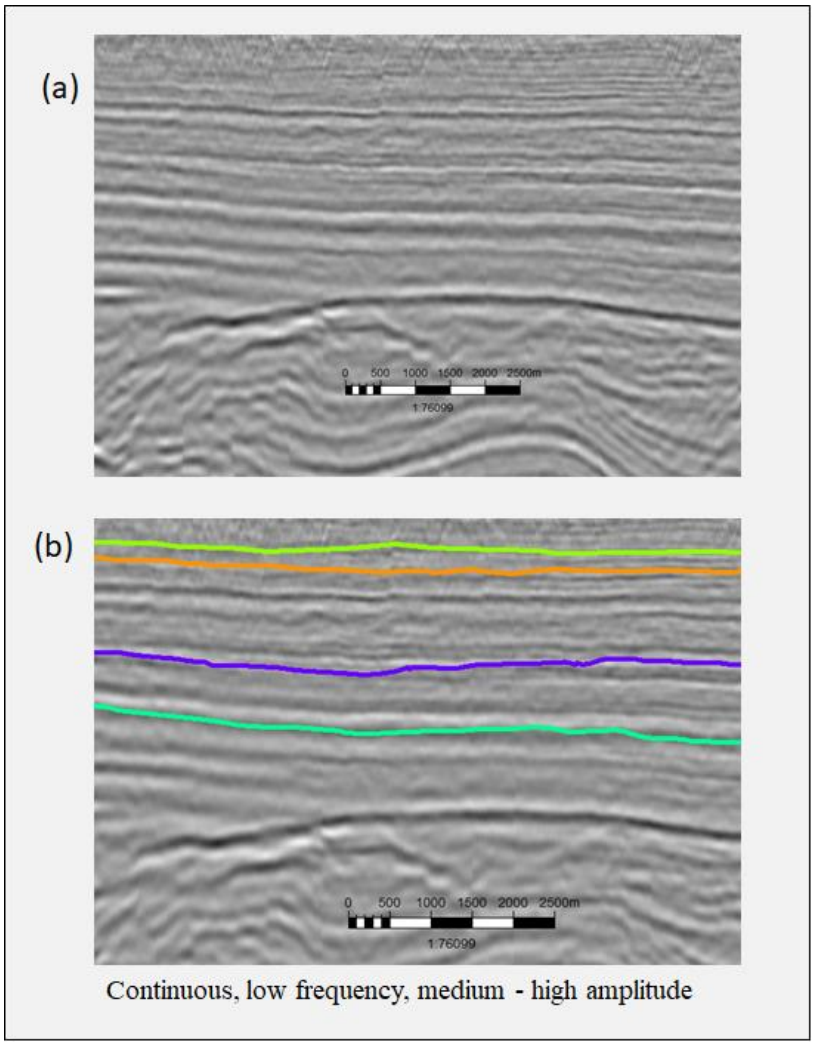

Figure 5.5 - Seismic reflection characteristics (a) not interpreted and in (b) continuous, low frequency, medium-high amplitude facies units.

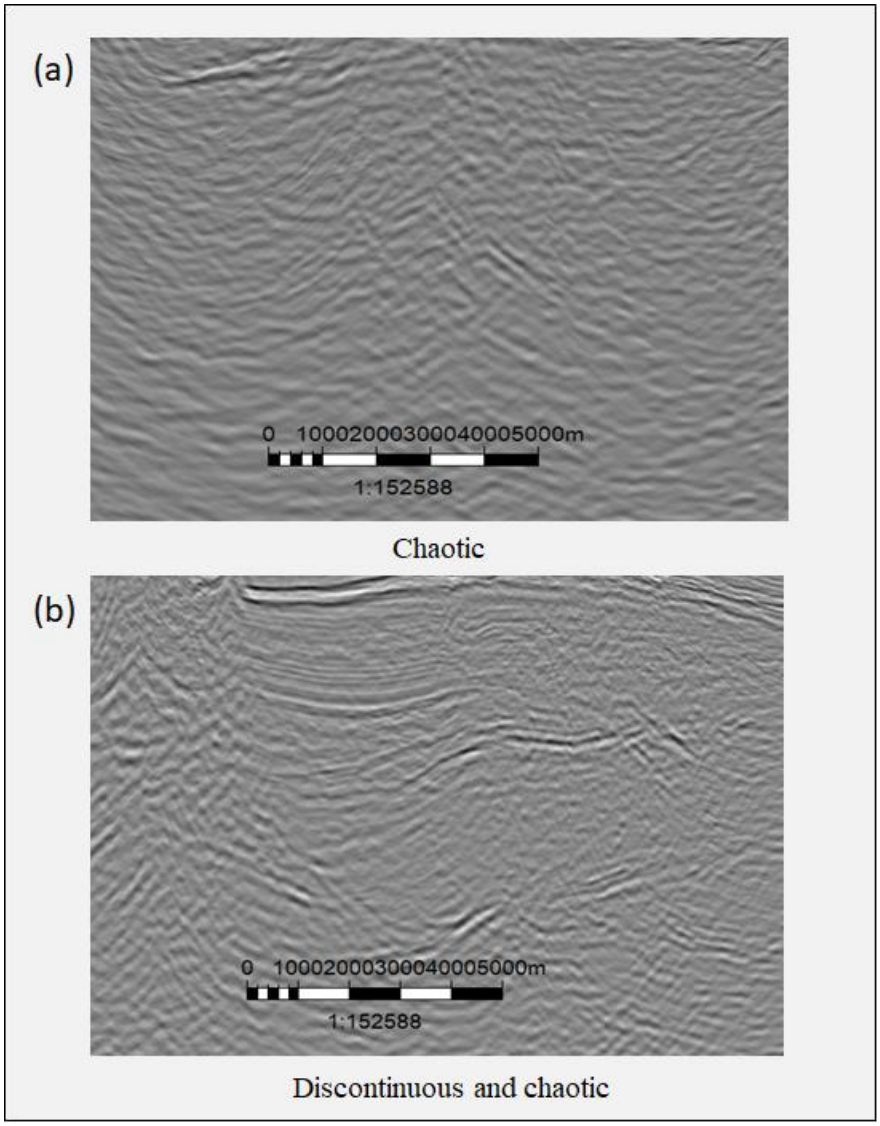

Figure 5.6 - Facies units mapped in (a) chaotic and in (b) discontinuous and chaotic.

5.4 SEQUENCE STRATIGRAPHY ANALYSIS OF THE MANDAWA BASIN

Identification and correlation of stratigraphy sequence (Sansom, 2016) and well biostratigraphic database has been outlined in the Tanzanian southern coast and offshore basins (Hudson, 2011).

The study of nature of seismic sequences in this thesis carried out as a simplified Mandawa Basin area sequence stratigraphy potentially divided the strata into eight seismic sequences in accordance with the pattern of stacked seismic units based on on high amplitude reflections and its geometry. The profiles selected for regional seismic stratigraphic analysis are oriented in NE-SW, running from shelf to the deep offshore

area. Sequence boundaries were identified by truncation, onlap, toplap, and downlap stratal terminations based on the seismic resolution dataset and area of extension.

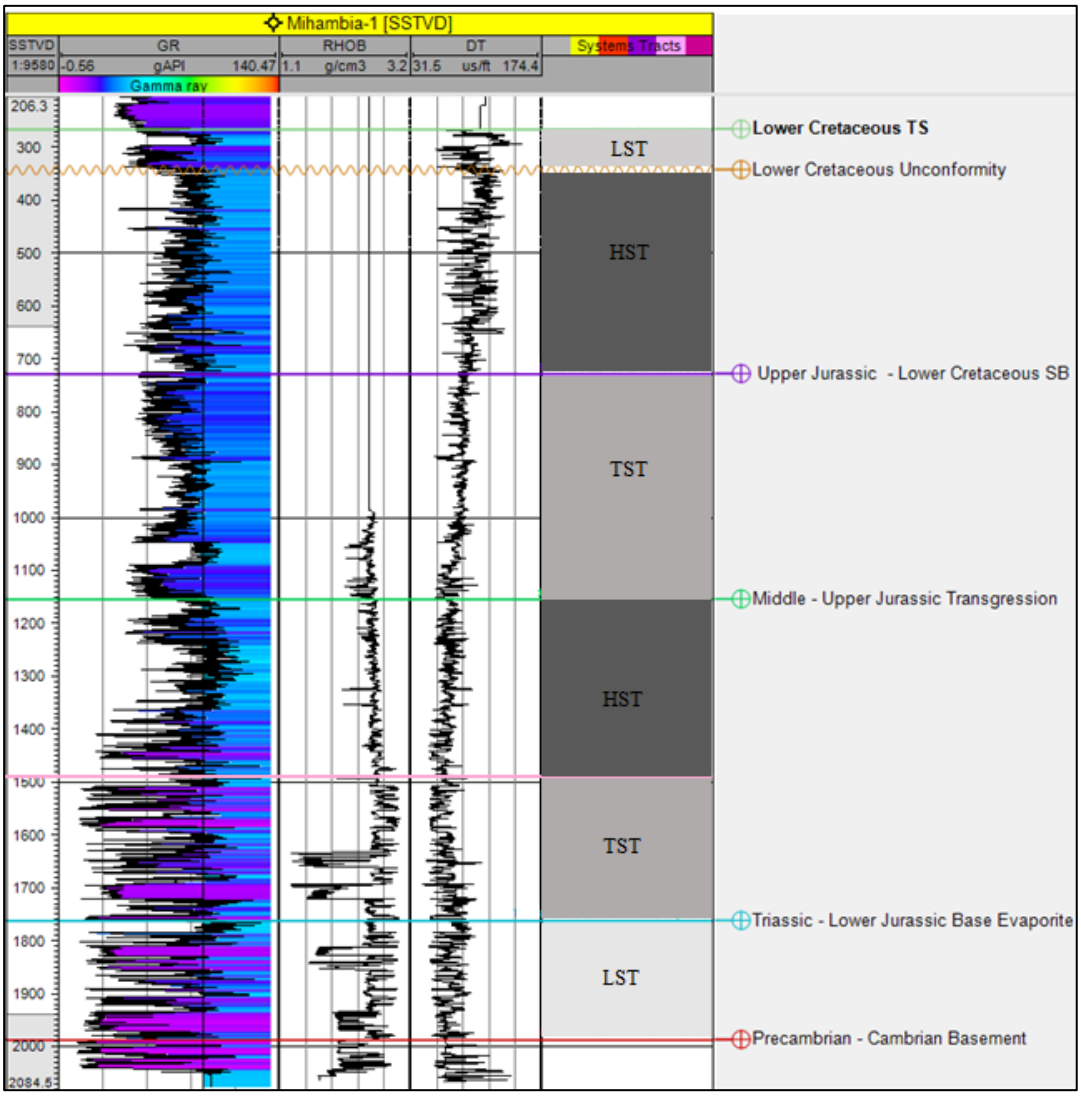

Figure 5.7 - Interpreted the stratigraphic system tracts and depositional sequences according to geophysical well logs in Mihambia-1 well, Mandawa Basin (LST – low stand system tract, TST- transgressive system tract, HST- high stand system tract).

The system tracts interpreted in Figure 5.7 were based on lowstand system tract (LST) as an overall regressive stratigraphic unit of metamorphic basement. A claystones package interbedded evaporite filling into the basin to transgressive (TST) which showed low gamma ray and the sharp boundary was recognized as a retrogradational parasequence set bounded. Upward sandstones marked the high system tract (HST) was recognized as prograding unit bounded and associated overlying limestone indicates a gradual change from clastic to carbonate establishing the composite sequence scale. The stacking pattern of several siltstone and sandstone established the composite sequence set.

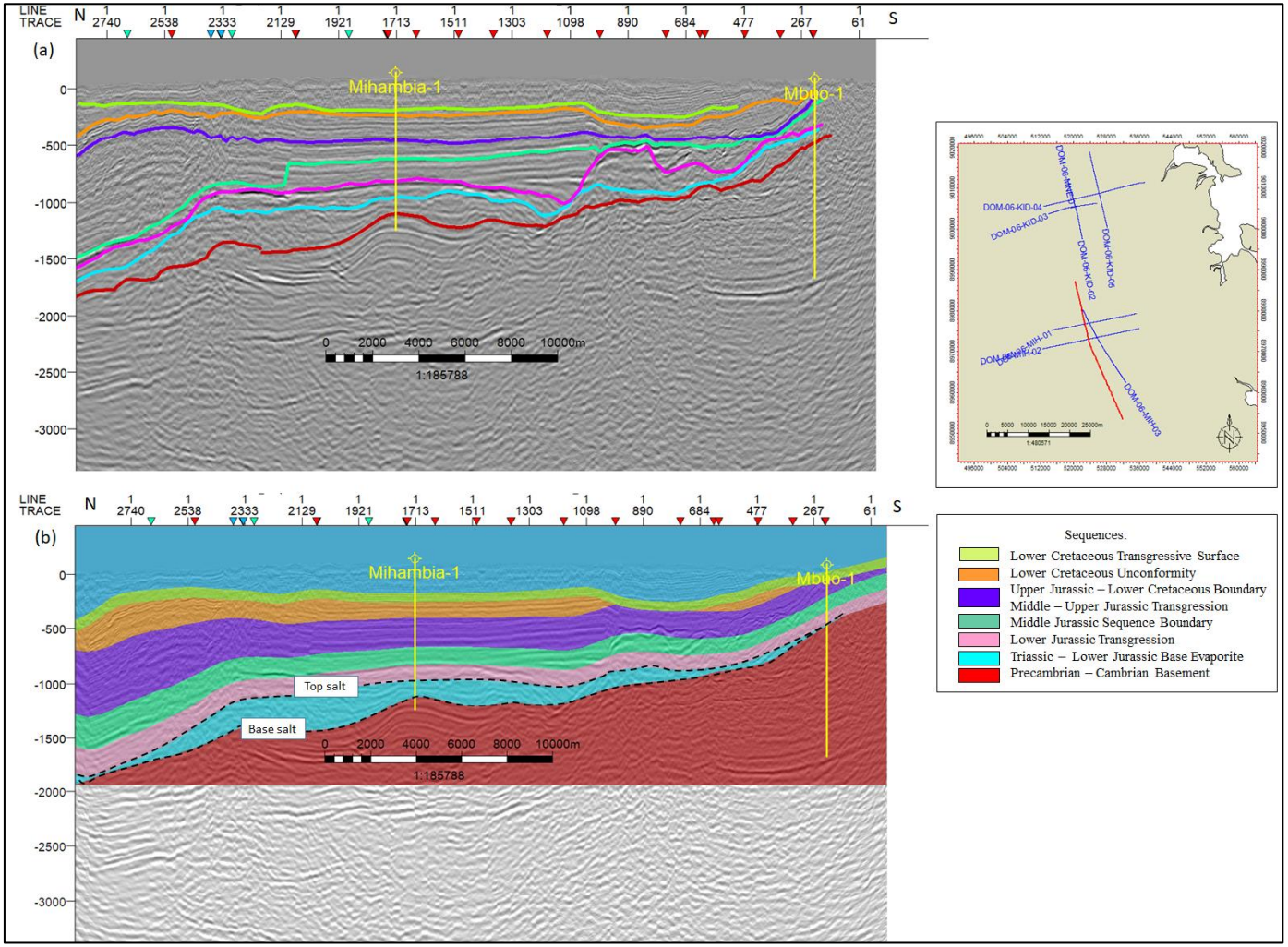

Figure 5.8 - A seismic sequence interpreted in DOM-06-MIH-04 composite line illustrating in (a) depositional sequence of reflectors and (b) depositional sequence in stratigraphic condition.

The sequence stratigraphy of the onshore Mandawa Basin (Figure 5.8) was interpreted as the base of Lower Jurassic Transgression represented by a continuous and high amplitude doublet, above which the reflections become low and wide. This doublet is possible to be correlated to lithologic contrast between evaporite of the Horizon C – Nondwa Formation and the overlying sandstone of the Horizon D – Mihambia Formation which falls close to the top of the Mtumbei Limestone where this is developed. But over Kianika-1 well, there is a separation of around 400 m between the Horizon D – Mihambia Formation and the Horizon E – Mtumbei Limestone. The top of Middle – Upper Jurassic Transgression is represented by continuous and low amplitude seismic reflectors that may correspond to the limestone of the Horizon E – Mtumbei Limestone Formation described in Chapter 4 equates to a limestone development, implying that this level corresponds to the top of the Middle – Upper Jurassic Transgression. The lithological nature interval is uncertain, however, and the lack of well penetrations in north Mandawa means that there is a little lithological calibration of the seismic to help establish a lithological prognosis for this part of the stratigraphic succession. The overlying bright seismic markers correspond to the Upper Jurassic – Lower Cretaceous Boundary, as siltstones and claystones of the Horizon F – Zone F were mapped. The appearance of an unconformity that marked the Lower Cretaceous has been mapped by the bright reflectors, Horizon G – Zone G, corresponding to the border between limestones and clastics as claystones bedding in Mandawa Basin. However, the continuation southward in Lukuledi-1 well in Ruvuma Basin could be the same unconformity or to the deposits of similar age of the Kilwa Group possibly the Lower Cretaceous Unconformity Horizon H – Zone H (Hudson, 2011; Hudson and Nicholas, 2014).

5.4.1 Precambrian - Cambrian Basement

Top Basement was penetrated by four wells (Mbuo-1, East Lika-1, Mita Gamma-1 and, Kizimbani-1) in the Mandawa basin Top Basement is a distinct unconformity between crystalline metamorphic and igneous rocks and overlying non-metamorphic sediments. The basement in well penetrations is metamorphic gneiss, which was dated radiometrically as 537±7 MyBP using K/Ar (Balduzzi *et al.*, 1992).

5.4.2 Triassic – Lower Jurassic Base Evaporite

Base Main Evaporite is a bounding surface forming the base of one major halite and/or anhydrite that developed during Triassic interval (Middle part of the Toarcian – Pliensbachian in previous interpretations). Core Lab/TPDC (2009) suggested the surface to have developed as the result of a regional event with high evaporite sedimentation rates, possibly as a result rifting event in a marginal marine basin. Horizon B – Mbuo Formation to Horizon C – Nondwa Formation.

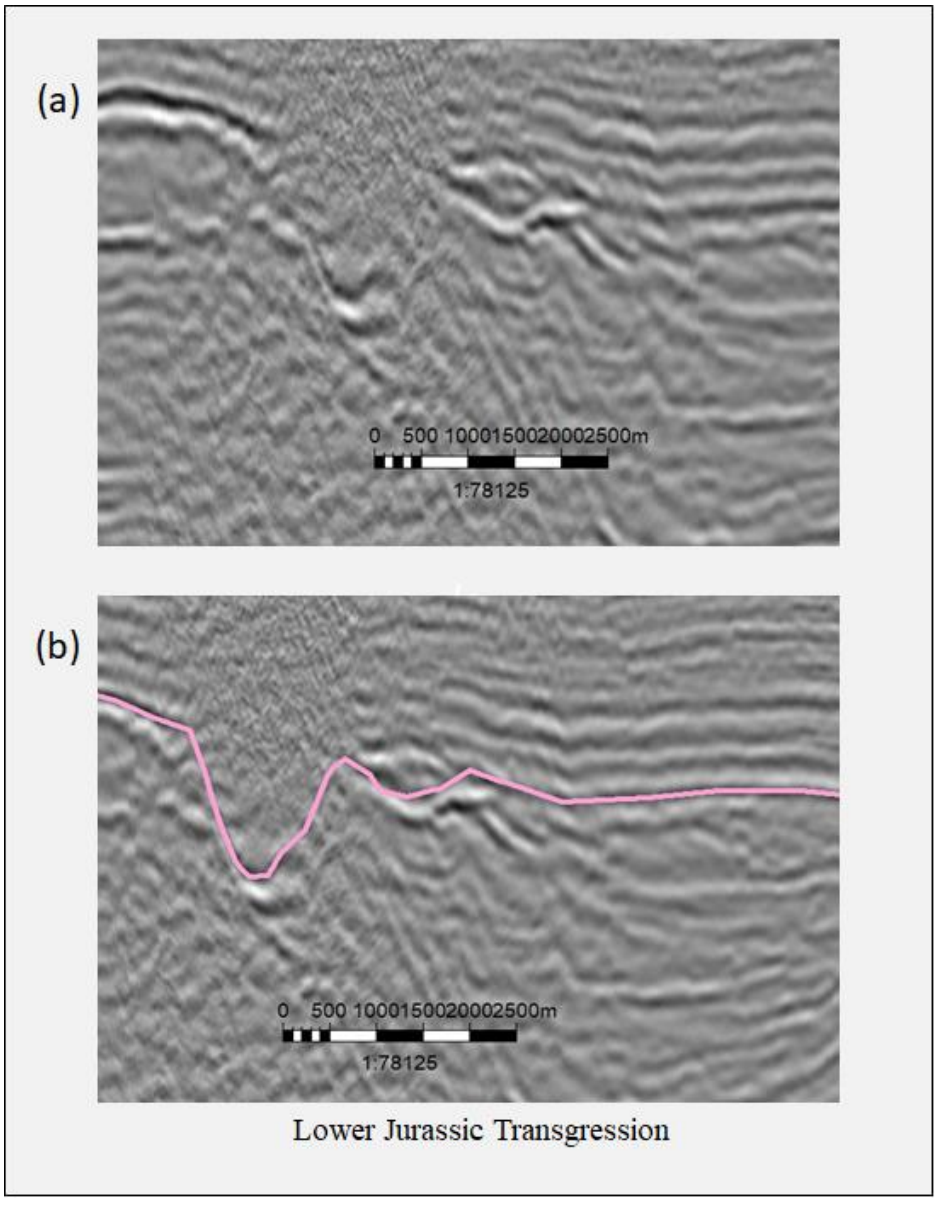

Figure 5.9 - Seismic profile in the Mandawa Basin highlighting stratigraphic sequences: Lower Jurassic Transgression in (a) the seismic transect unmapped and in (b) the pink reflector interpreted as the high amplitude sandstones.

5.4.3 Lower Jurassic Transgressive Surface

This event was interpreted as a marine transgressive characterised by the Horizon D – Mihambia Formation event of Lower Jurassic age (Figure 5.9). The event terminated all evaporite deposition in the Mandawa area wells and was marked by the onset of open marine conditions.

5.4.4 Middle Jurassic Sequence Boundary

This is a major unconformity noted within the Middle Jurassic that exhibits a gradual upward decrease in gamma response trend from clastic to carbonate dominated facies.

5.4.5 Middle – Upper Jurassic Transgression

This sequence is a regional transgression extending across the top of Middle Jurassic mapped low amplitude carbonate facies of Horizon E – Mtumbei Limestone Formation reflectors.

5.4.6 Upper Jurassic – Lower Cretaceous Sequence Boundary

This is marked sequence boundary by a gradual upward increase in gamma response reflected by an upward fining trend of Horizon F – Zone F at the Upper Jurassic.

5.4.7 Lower Cretaceous Unconformity

This unconformity surface equates to the Lower Cretaceous age but is poorly-constrained biostratigraphically (Hudson, 2011). The Lower Cretaceous Unconformity may be a continuation of the unconformity that was mapped along the Lukuledi-1 well (Horizon G – Zone G) in Ruvuma Basin detailed in Chapter 4, where claystones, shales, and siltstones interbedded were mapped from the Lower Cretaceous, however it is currently difficult to establish the extension. Also possibly associated to the Kilwa Group (Hudson, 2011; Hudson and Nicholas, 2014).

5.4.8 Lower Cretaceous Transgressive Surface

Characterised by a rapid deepening of proximal to shallow marine environments mapped by parallel reflectors of the Horizon G – Zone G. It is potentially diachronous, possibly extending into Lower Cretaceous, but would appear to be widespread and may be linked to a tectonic phase with increased subsidence.

CHAPTER 6

SALT TECTONICS

6.1 CONCEPTS

6.1.1 Salt composition and properties

Salt is an effective conductor of heat, elevating the thermal maturity of rocks above salt structures and cooling rocks lie below or adjacent to salt bodies (Warren, 1999). The word “salt” is typically used to include all rock bodies composed primarily of halite but that contain varying amounts of other evaporites such as anhydrite and gypsum.

Sedimentary rocks lose effective porosity within the first 100-200 meters of burial, after which they will become less compressible. With salt, density will remain more or less constant, for example, 2160 kg/m3 in pure halite (Talbot and Jackson, 1987a, Talbot and Jackson, 1987b). This property differs from that of siliciclastic sediments, which progressively lose their porosity and permeability as a result of compaction (Hudec and Jackson, 2007).

The ability of salt to flow like a fluid makes it unique compared to the brittle behaviour of siliciclastic and carbonate rocks, under similar geological strain rates. Its ability to flow depends on the strength of the overburden and the boundary friction within the salt layer (Hudec and Jackson, 2007).

Evaporites are precipitated from a saturated surface or near-surface brines by hydrologies driven by solar evaporation (Warren, 1999), buried in restricted basins where the outflow of water by evaporation exceeds inflow. Salt layers in sedimentary basins often include other (evaporite) minerals such as hydrate, anhydrite and carnallite, and interbedded carbonate and siliciclastic sediments (Warren, 2006). The evaporite facies typically vary laterally, controlled partly by the crystallization sequence from increasingly concentrated hypersaline waters (Hudec and Jackson, 2007).

Evaporites such as salt (halite) or anhydrite have thermal conductivities that are generally higher than the maximum values for other sedimentary rocks. For example, the thermal conductivity of anhydrite ranges from 4.8 to 5.8 $W\,m^{-1}\,K^{-1}$, and that of halite ranges

from 4.8 to 6.05 W m−1 K−1 (Blackwell and Steel, 1989; Clauser and Huenges, 1995; Allen and Allen, 2005).

6.1.2. Salt Tectonics and halokinesis

The presence of a stage of halokinesis is estimated to occur in almost 120 basins around the world. Nonetheless, evaporites comprise less than 2% of the world's sediment rocks, 14 of the world's 25 largest oil fields, and 9 of the world's 25 largest gas fields are based in regions of important halokinesis (Hudec and Jackson, 2007; Yu *et al*., 2014).

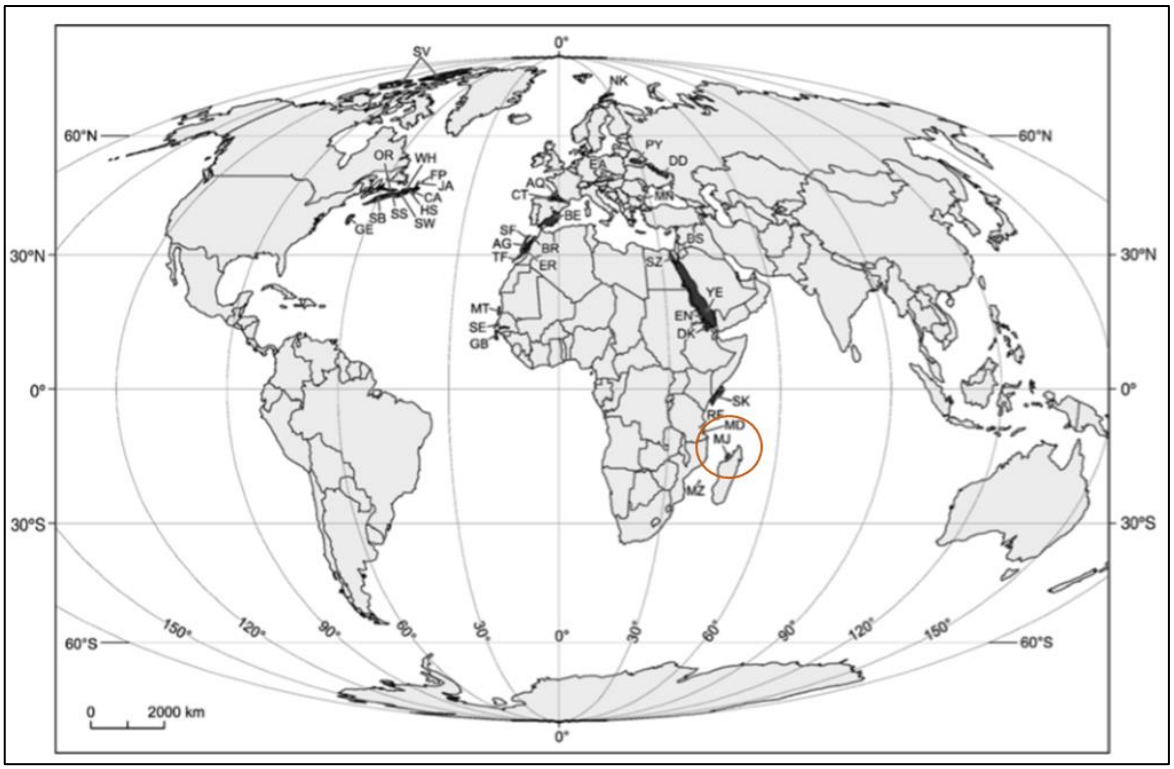

Figure 6.1 - Global distribution of sedimentary basins comprising salt structures (dark-grey areas) highlighting the major syn-rift salt basins including both mature rifts and failed rifts. The orange circle enhances the East African basins discussed in the present study area comprising evidence for salt tectonics. AG Agadir; AQ Aquitaine; BE Betic; BR Berrechid; CA Carson; CT Cantabrian–West Pyrenees; DD Dnepr–Donetz; DK Danakil; DS Dead Sea; EA East Alpine; EN Eritrean; ER Essaouira; FP Flemish Pass; GB Guinea-Bissau; GE Georges Bank; HS Horseshoe; JA Jeanne d'Arc; MD Mandawa; MJ Majunga; MN Moesian; MT Mauritania; MZ Mozambique; NK Nordkapp; OR Orpheus; PY Pripyat; RF Rufiji; SB Sable; SE Senegal; SF Safi; SK Somali–Kenya; SS Scotian Slope; SV Sverdrup; SW South Whale; SZ Suez; TF Tarfaya; WH Whale; YE Yemeni. Modified from Hudec and Jackson (2007).

Tectonism is closely tied to regional deformation according to the salt weakness. In extension or transtension, diapirs rise graben axes, taking advantage of the space created by hinning and separation of fault blocks (Hudec and Jackson, 2007).

The flux of salt under certain deposition time and P-T conditions in the subsurface, halokinesis develops above a source salt layer capable of deforming its overburden strata to a great extent (Jackson *et al.*, 1994). Active rift basins and passive margins have the main occurence of extensional salt tectonics (Jackson and Vendeville, 1994). Salt systems generally form intrinsically and kinematically linked groups of faulted intervals, diapirs, and welds connecting sub-salt and supra-salt strata (Rowan *et al*., 1999). Rifting stages as pre-rift, syn-rift, and post-rift in salt basins (Jackson and Vendeville, 1994) and within pre-rift, syn-stretching, syn-thinning, and syn-exhumation salt basins (Rowan, 2014) are recurrent in the literature regarding salt deposition and timing.

6.1.3 Geometry of salt structures

Salt structures are represented by a wide subsurface geometrical uncertainty, varying from small salt anticlines, pillows, and rollers, to large vertical salt walls, salt stocks, and horizontal salt canopies (Figure 6.2). Such structures have been defined from diverse tectonic settings although some classic regions of salt walls and diapirs are located on passive margins (Rowan *et al.* 2000; Hudec and Jackson 2004; Quirk *et al.*, 2012).

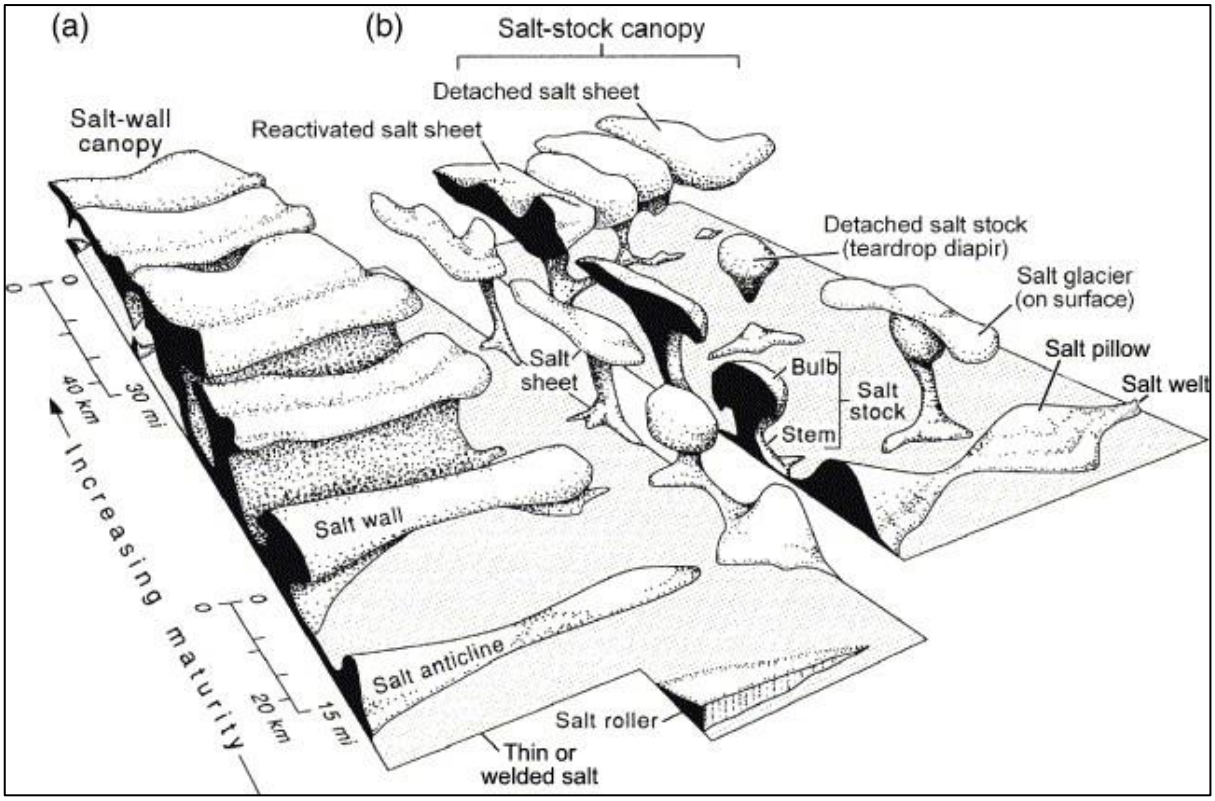

Figure 6.2 - Representation of geometries of salt structures in a block diagram. The structural maturity and size increase toward the structures shown. In (a) proposed elongated structures rising from line sources. In (b) the structures are rising from point sources. Simplified from Jackson and Talbot (1991).

In Figure 6.3, the factors as the strength of the overburden, the temperature of the salt, salt source layer thickness, tectonic regime, and sedimentation or erosion rate implies the morphology of these structures, (Fossen, 2010).

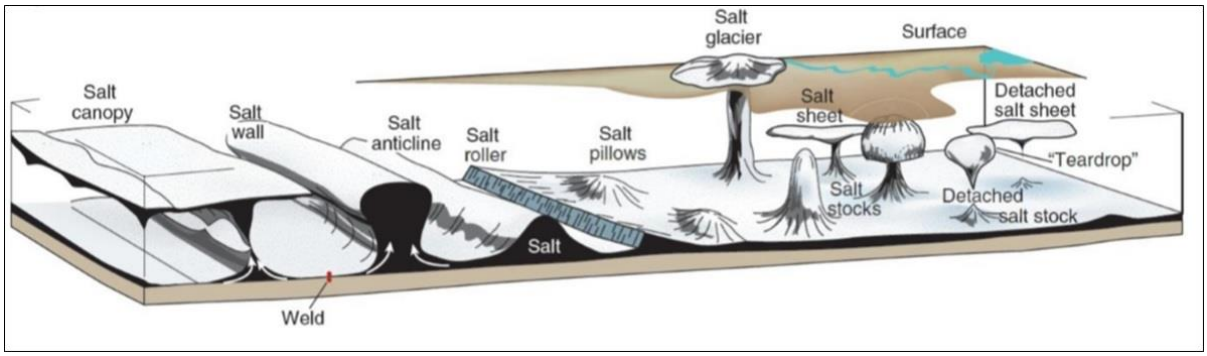

Figure 6.3 - Salt structures classification (Fossen, 2010).

According to the net sedimentation rate vs net salt supply rate relationship, there are three different scenarios of diapirism to explain the most common factor that is the foundation of the shape of salt diapirs (McGuinness and Hossack, 1993; Giles and Lawton, 2002; Hudec and Jackson, 2007).

a) Reactive diapirism

Salt structures with triangular shape as salt pillows and salt rollers contribute to be formed by high sedimentation rates vs salt supply rates (Jackson and Hudec, 2017). Generally, during this stage sediments onlap and overlap salt structures and, it is commonly observed a convergent vertical migration of depocenters towards salt structure apex. The halokinetic sequences deposited in this scenario display low-angle unconformities (Giles and Rowan, 2012) (Figure 6.4A). The first stage of diapirism is slow reactive piercement into overlying grabens or half-grabens in response to local thinning of the overburden by normal faulting during regional extension. The diapir rises in response to the movement of fault blocks to float at equilibrium levels in the pressurized source layer. Reactive diapirism ceases if regional extension ceases (McGuinness and Hossack, 1993; Giles and Lawton, 2002; Hudec and Jackson, 2007).

Regional extension, which thins the overburden above salt intervals, accounts for reactive diapirism (Jackson and Vendeville, 1994; Vendeville and Jackson, 1992a, Vendeville and Jackson, 1992b). During this process, 'room' or accommodation space is created by the thinning overburden and, more frequently, by separating faulted blocks to create space for salt to intrude. During reactive diapirism, salt diapirs will stop rising on the condition that sufficient overburden remains above the salt structures when regional extension stops, as salt diapirism is controlled by a regional extension (Jackson and Vendeville, 1994). As the breaching of the resisting forces that retard salt diapirism will result in weakened salt roofs, one possible phenomenon to take into account is that of salt diapirs intruding the overburden strata up to the surface, a process involving both active and passive diapirism (Vendeville and Jackson, 1992a, Vendeville and Jackson, 1992b, Jackson and Vendeville, 1994; Hudec and Jackson, 2007).

b) Active diapirism

In the active diapirism overburden layers are rotated upwards and eroded due to the doming caused by the salt pillow (Figure 6.4B). As salt flows towards the salt pillow, the source layer is depleted, forming small minibasins called primary rim synclines. This

process of salt depletion creating a minibasin is called down building (Fossen, 2010). The second stage of diapirism is rapid active piercement, which is virtually independent of regional extension. Fluid pressures at the crest of the diapir become sufficient for the diapir to lift and shoulder aside its thin roof (Vendeville and Jackson, 1992a, Vendeville and Jackson, 1992b, Fossen, 2010).

c) Passive diapirism

Passive diapirism was proposed by Nelson (1989) and constitutes as the third stage of diapir growth as a passive piercement, beginning when the diapir reaches the surface. Passive diapirs cannot rise but can widen if regional extension continues (Vendeville and Jackson, 1992a, Vendeville and Jackson, 1992b).

Low sedimentation rates vs net diapir growth cause diapir widening with the subsequent divergent migration of depocenters (Figure 6.4C). Due to the low sedimentation rates, this period likely develops salt glaciers or salt overhangs. Halokinetic sequences deposited in this scenario suffer large deformation, developing overturned beds (Hudec and Jackson, 2007; Fossen, 2010).

Structures as salt walls and diapirs are elongate ridges of salt formed by extension commonly found in salt basins (Jackson & Vendeville, 1994). Early concepts for salt-wall growth were largely two dimensional, simple inward flow and thickening of salt within the wall, with internal structures, prior deformed by stratigraphic layering (Dixon, 1975; Schwerdtner *et al*., 1978; Ramberg, 1981).

Most allochthonous salt is formed at very shallow levels and is a form of passive diapirism. The dip of the salt-sediment interface is dependent on the ratio between salt-supply rate and sediment-accumulation rate, with flaring or allochthonous salt resulting when the value is greater than one (McGuinness & Hossack, 1993; Talbot, 1995).

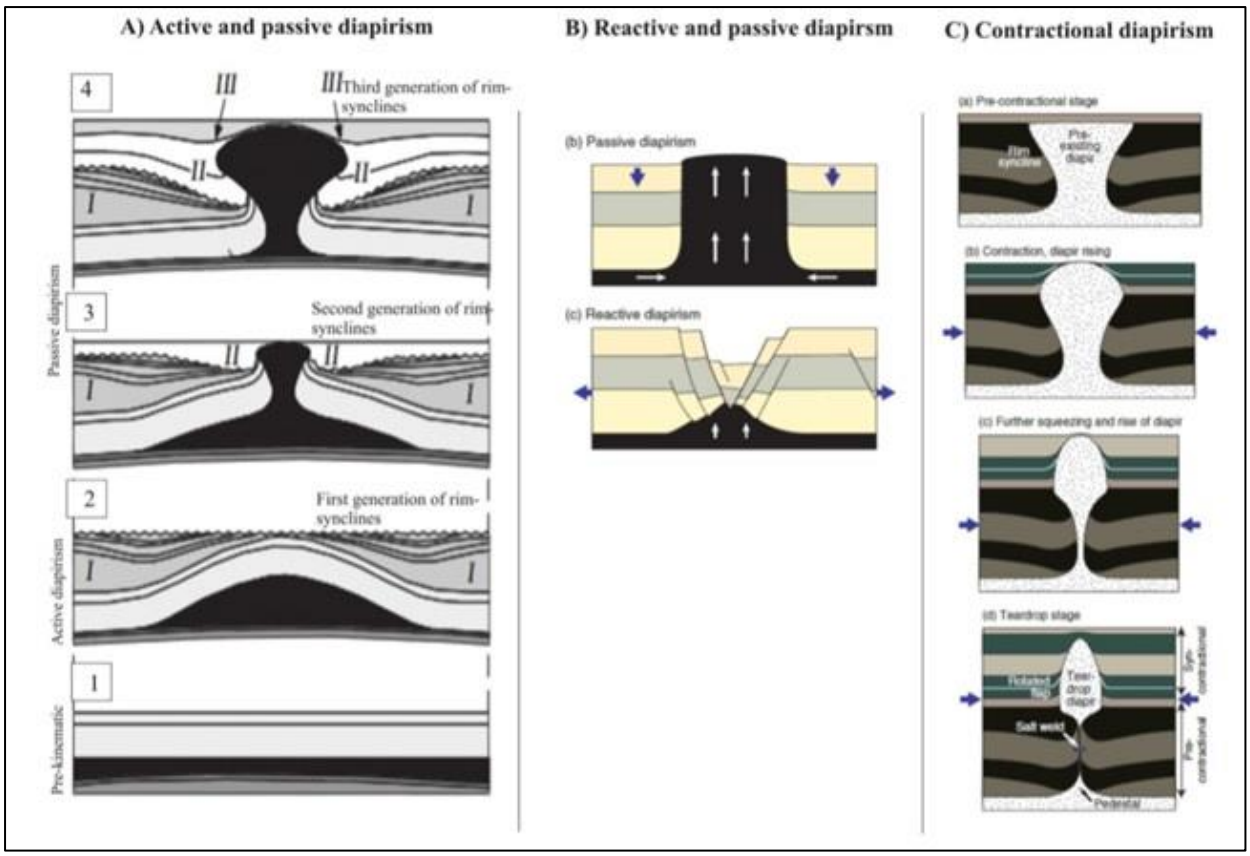

Figure 6.4 - The stages of Active and Passive diapirism (A), Reactive and passive diapirism (B), and Contractional diapirism (C) (Trusheim, 1960, Fossen, 2010, Hudec and Jackson, 2007; Fossen, 2010).

Structurally oriented semblance highlights structural elements. Attributes as bedform enhance the continuity of reflectors in minibasins and improve the resolution of strata terminations such as downlap, onlap, and truncations (Ferguson *et al.*, 2010).

6.2 TYPES OF SALT IN MANDAWA BASIN ACCORDING TO GEOPHYSICAL WELL LOGS

The identification of different evaporative minerals in a sedimentary basin is generally made based on the description of cores, however, in the absence of coring in salt intervals, an interpretation based on the analysis of electrical geophysical well logs can be performed (Taylor, 1985). The physical properties of different salts (such as density, radioactivity from gamma ray, and transit-time from the sonic log) are used in the interpretation of profiles. Intrasalt carbonates and siliciclastic rocks relate in GR values in terms of evaporites (Schoenherr *et al*., 2009), although siliciclastics present an increase in Neutron values (+/- 0.3) than carbonates (+/-0.1) or compared to evaporites (approximately 0.15). The density of evaporites (mainly from halite), is effectively invariant with depth, in terms of whether effects of compaction with increasing depth of burial (Jenyon, 1986). Furthermore, evaporites may lack in seismic reflections due to mobility and destruction of beddings. Evaporites are also less dense than clastic rocks and limestone rocks, a property that contributes to strong reflections for incident waves at the interface with the underlying sediments (Hudson, 2011).

A total of six wells present in Mandawa Basin in this study have the occurrence of salt types. It is evidenced by well log responses of velocities across different rock types in the manner of the acoustic impedance seen from the sonic log in the majority of wells, followed by neutron log NPHI. These well logs tend to indicate constant values for the minerals and if analysed with a secondary log, in the study here the density log RHOB, the identification of which type of salt is sufficient.

Sequences of halite were interpreted in most of the wells, such as Mbuo-1, Mihambia-1, East Lika-1, Mita Gamma-1, Mbate-1, and Mandawa-7 evidenced by the values of the sonic log responses varying from 66.7 to 67.0 μs/ft and density log value of 2.03 gm/cc.

Anhydrite is found interbedded with claystone and sandstone in Milhambia-1 and East-Lika-1 wells and hypothetical traces of gypsum were interpreted in Kizimbani-1 well according to the low delta transit time response from the sonic log of 52 μs/ft.

6.3 SALT STRUCTURES IN MANDAWA BASIN BASED ON SEISMIC ATTRIBUTES

The regional tectonic salt domains are shown in a transect crossing the central-south part of the basin. Whereas the 2D reflection seismic data available revealed that the major aspects of salt tectonics along the tectonic domains of the Mandawa Basin, the salt diapirs increased in the W-E direction from observations of the Mihambia-1, Mbuo-1 and Mandawa-7 wells.

The interpretation of the salt structures has suggested that the gypsum is restricted to NNW-SSE trending, fault-bounded domes areas. Seismic 2D accuracy, in the range of low data quality, also suggested salt/gypsum diapirs are controlled by the normal faults and are present with similar geometry.

The 2D seismic line DOM-06-MIH-04 suggests that Upper Jurassic limestones are directly overlying salt diapirs (Figure 6.5), wherein subsurface these diapirs may have been eroded and infilled with sandstone before capping with limestones.

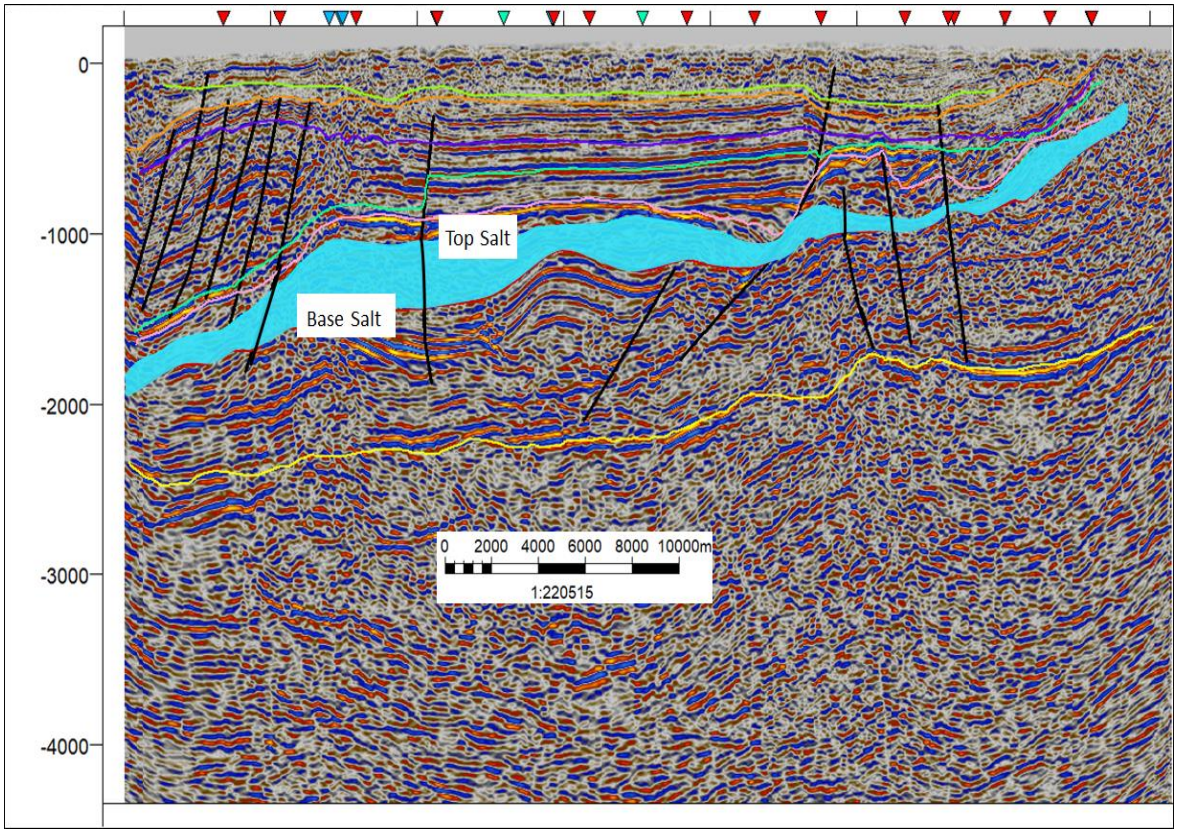

Figure 6.5 - Seismic interpretation proposing extensional tectonism producing listric faults overbalanced by a residual salt dome, the reference in 2D seismic line DOM-06-MIH-4 in TWT. The interpreted subsalt is shown in semi-transparent light blue colour. Note that although the base of the salt is reasonably well defined, the top salt pick is unclear.

Mbate-1 and East Lika-1 wells indicate a condensated pre-salt section along the western basin margin.

Salt-withdrawal mini-basins are rooted in autochthonous salts at depth 1,500 ms to 1,800 ms showing in Figure 6.6 a continuous subsidence in a seaward-migrant belt of sediment loaded between the Lower to Middle Jurassic onward.

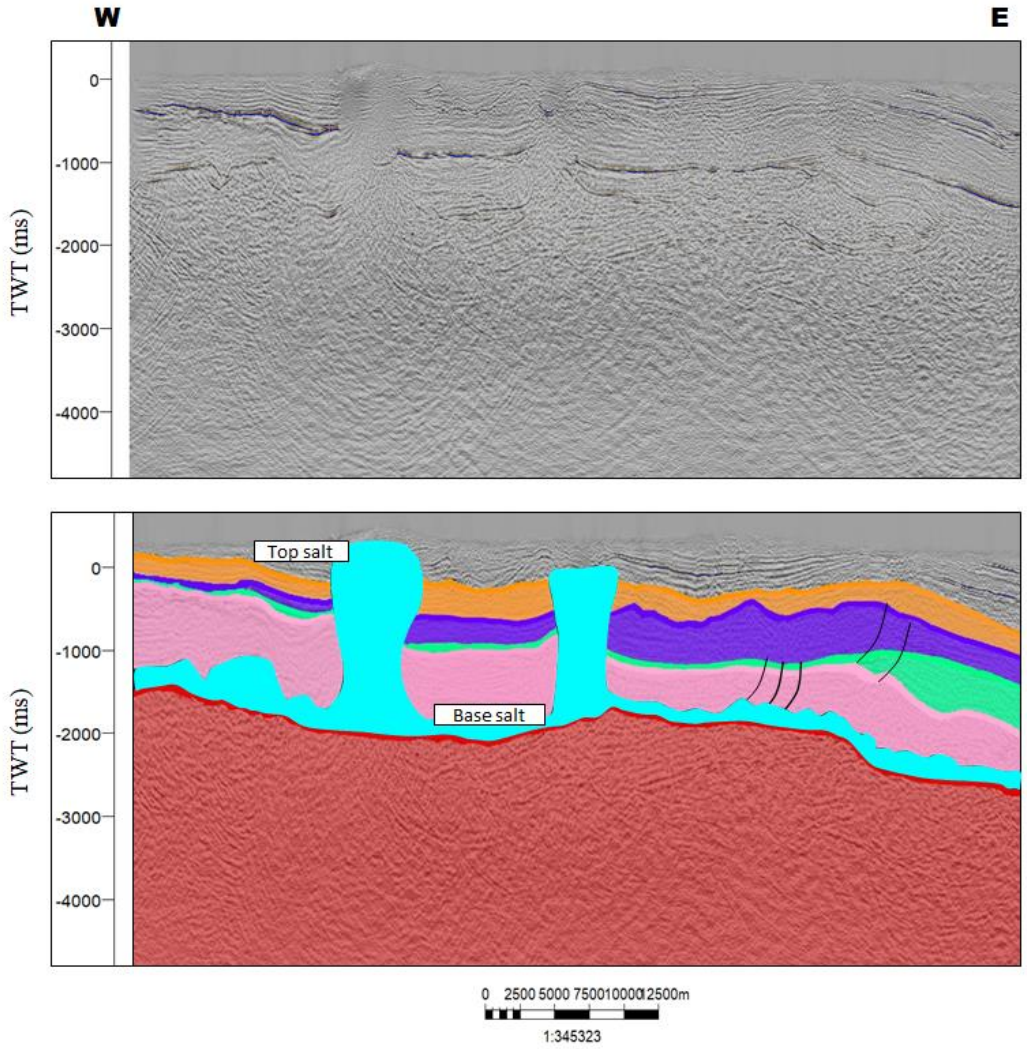

Figure 6.6 - A 2D seismic line MW-87-236 not interpreted and its regional west-east transect interpreted (in TWT) illustrating the influence of faults to identify autochthonous salt canopy domain in the Mandawa Basin. The interpreted salt is shown in light blue colour.

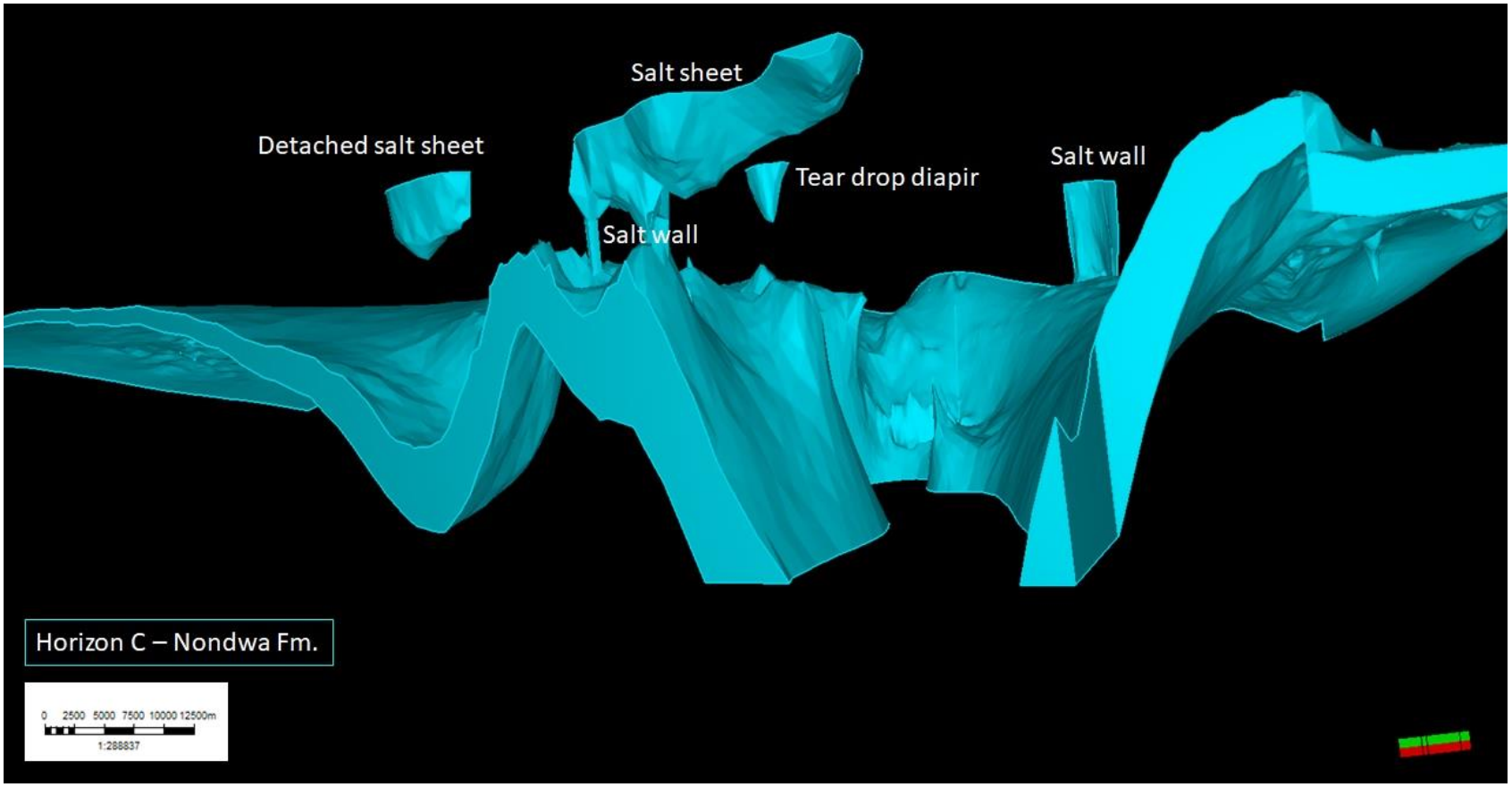

Figure 6.7 - Potential salt structures interpreted in the Horizon C – Nondwa Fm. in Mandawa Basin from left to right: detached salt sheet, salt sheet, salt wall, tear drop diapir and salt wall.

:

The salt in Mandawa Basin has been interpreted as mostly autochthonous building up from the Lower Jurassic below the present-day shelf. The appearance of an allochthonous detached salt sheet structure extending into the Lower Cretaceous strata.

As in this thesis, the data available consisted with 2D seismic reflection in terms of seismic data, the interpretation of salt structures in the Mandawa Basin suggested a variety of salt structures including both autochthonous and allochthonous structures which include salt dome, salt walls, detached salt sheet, salt sheet, teardrop diapir, salt diapir and withdrawal minibasin where the Lower Jurassic syn-rift salt ramped up through Lower Cretaceous strata forming a broad allochthonous detached salt sheet (Figure 6.7). However, it would be potentially relevant to address in a further work the reconnaissance timing and sediment loading compared to regional tilting of the basin in the initiation of allochthonous salt tectonics.

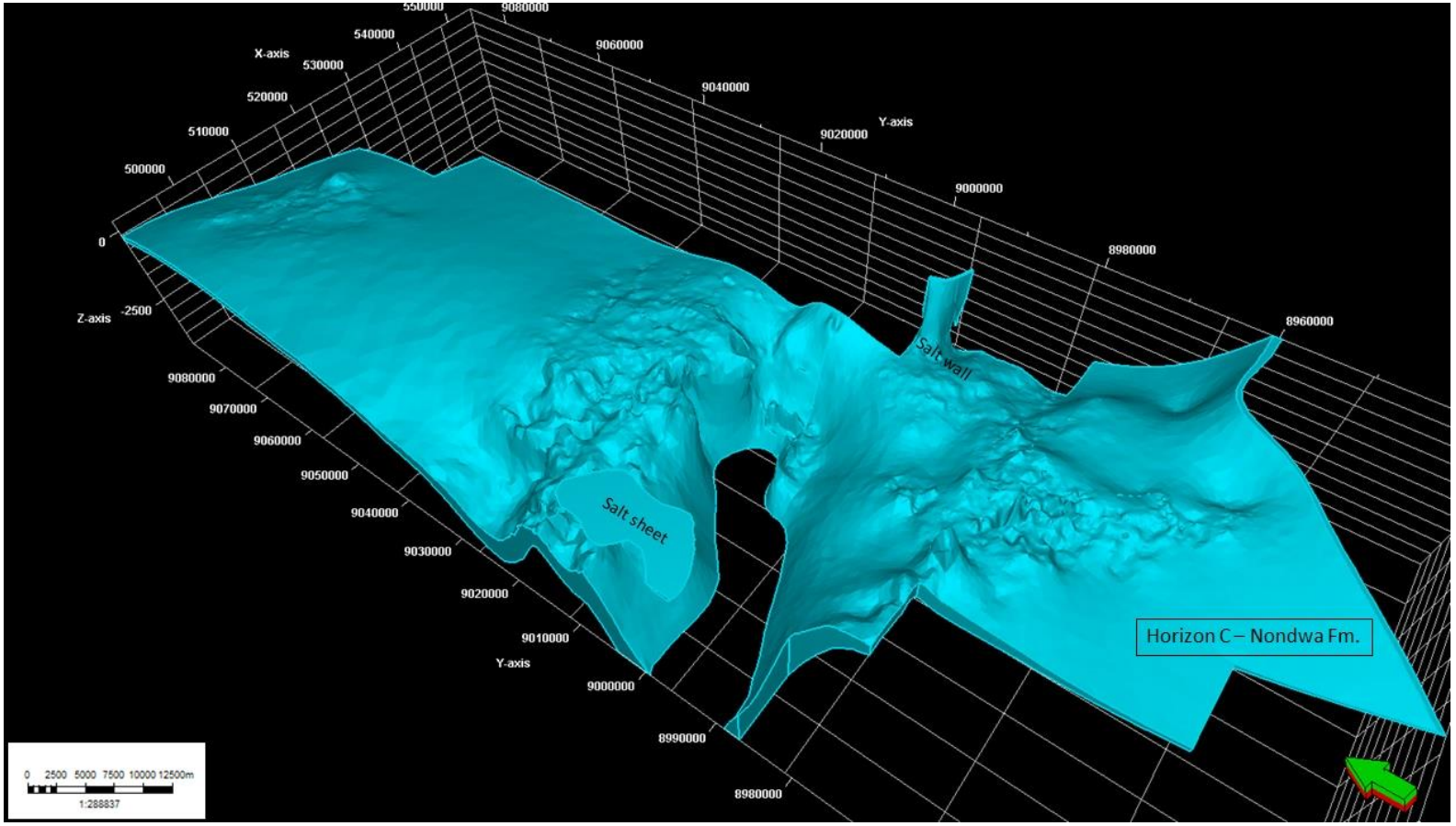

Figure 6.8 - Salt structures seen in the Horizon C - Nondwa Formation – salt sheet and salt wall – viewed from above.

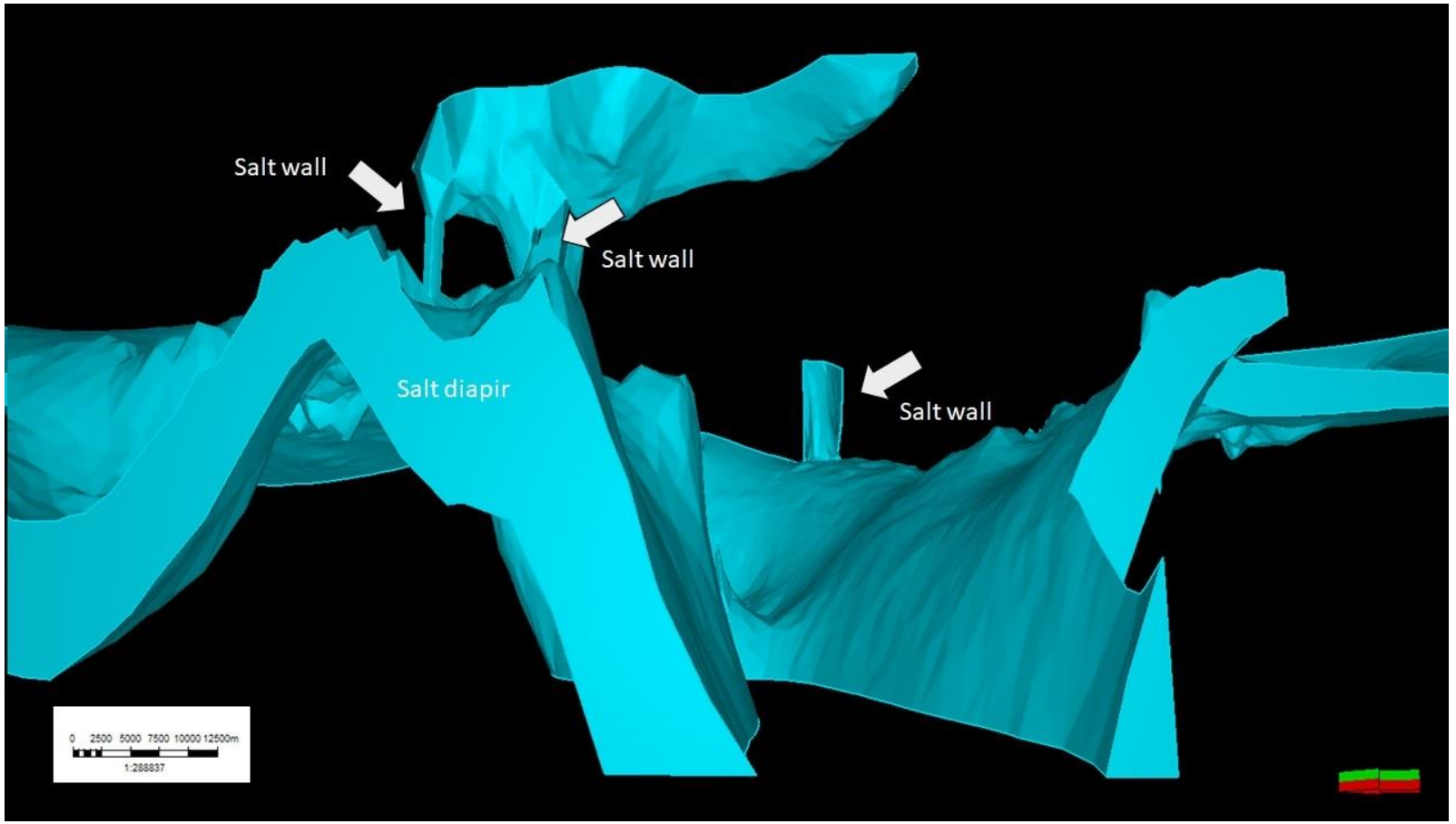

Figure 6.9 - Movement of Lower Jurassic salt diapir with salt walls in detail.

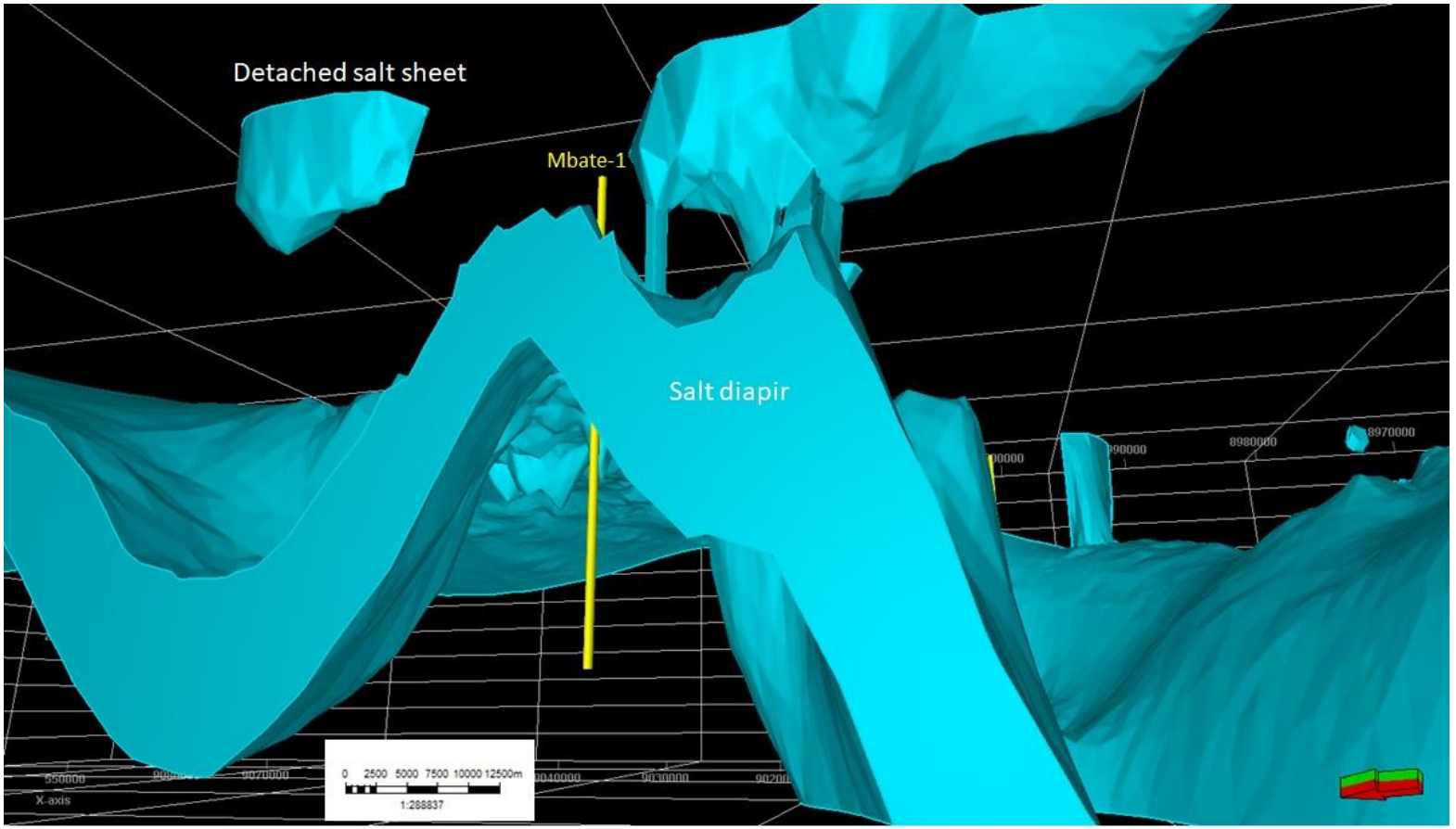

Figure 6.10 - Detached salt sheet or reactivated salt sheet.

The rim synclines across the frontal part of the faulted domain do not reflect the base of the salt geometry fairly to show its inferred rim synclines/flat geometry. However, some of the inlines and crosslines on the west-east dip revealed the autochthonous nature of the salt (Figures 6.8, 6.9, and 6.10). The lateral ramp of the salt nappe built up through the Lower Jurassic and into Lower Cretaceous age strata potentially observed several pulses of basinward salt flow.

An evaporitic sequence had developed in a more rapidly subsiding part of the basin allowing a restricted marine deposition as Sabkha environment (Mpanda, 1997).

The major zones of inversion played an important part in the creation of a minibasin infilling evaporites sequences across the Mandawa Basin.

The lateral facies change associated with differential tectonic subsidence potentially occurred across a basement-involved normal fault in between Horizon C – Nondwa Formation and Horizon D – Mihambia Formation, where shoreface sandstone deposits slowly subsiding progressed into deposits in the more rapidly subsiding southern Mandawa Basin. This lateral change indicates that accommodation generation locally outpaced sediment supply in the normal faults.

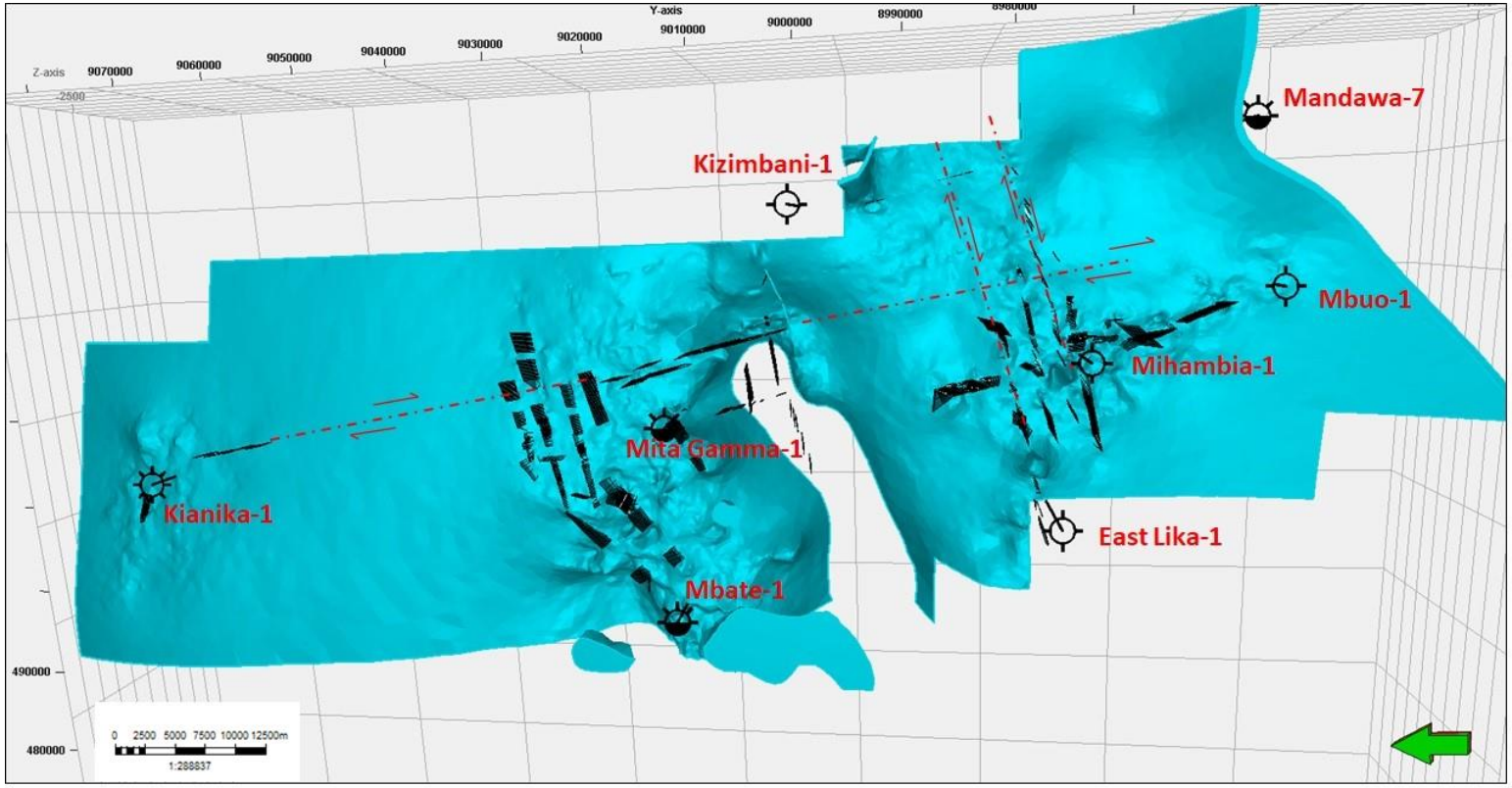

Figure 6.11 - Inferred faults (dashed in red) according to the faults modelled as fault pillars in Petrel.

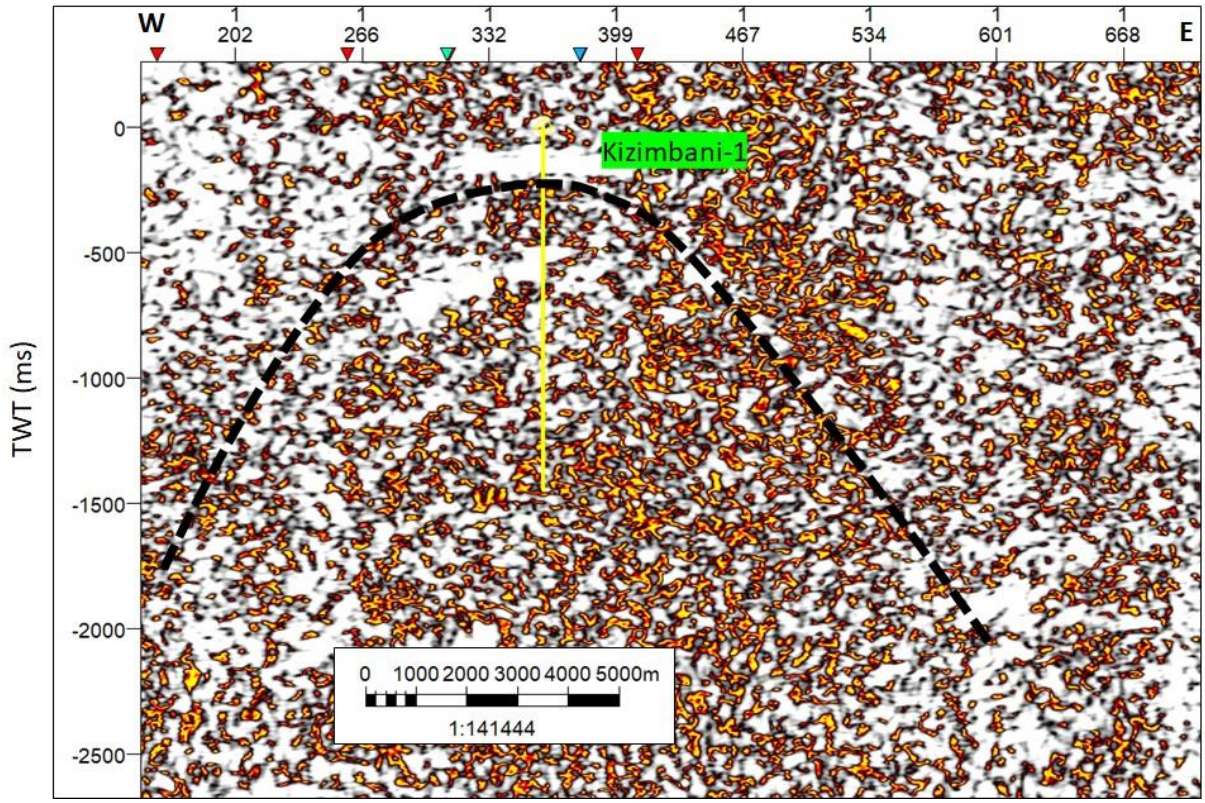

Figure 6.12 - In the 2D seismic line TL-116_d (TWT) suggests being a salt dome interpretation in Kizimbani-1 well where low amplitude (white) contrasted with yellow and red colours (high amplitudes) extracted from seismic attribute Chaos.

Low amplitudes at -174.50 ms contrasting with high amplitudes at -629.56 ms suggested that a paleo gradient, possibly a salt dome, emerged west-east Tanzania and northern Mozambique, changing facies distribution laterally and depositional environments, formed by an evaporitic sequence and silty shales in the Mandawa Basin. The autochthonous Lower Jurassic salt structure likely delineated with the use of the volume attribute chaos as observed in the 2D seismic line TL-116_d in TWT in the surrounding of the Kizimbani-1 well (Figure 6.12) and in the seismic line DOM-06-KID-01 (Figure 6.13), approximately 4,3 km from the well were appeared to be conformable.

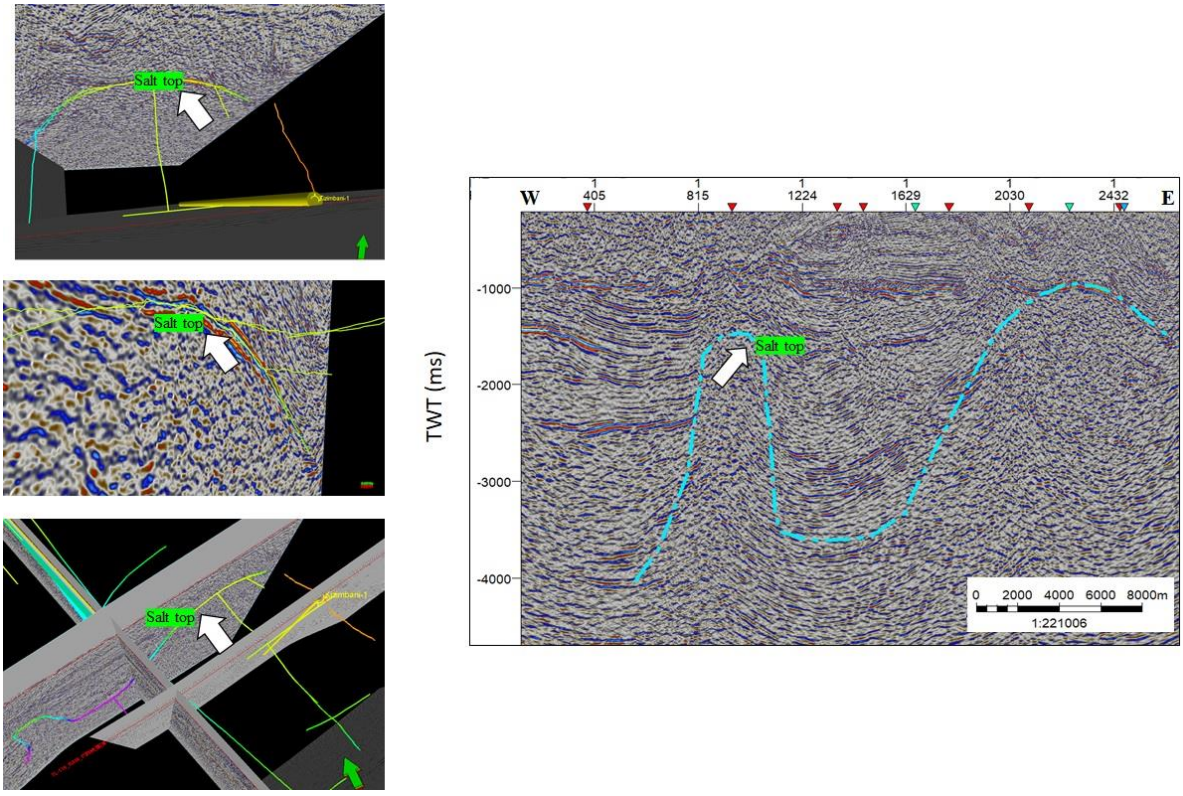

Figure 6.13 - Salt top delineation seen in the 2D seismic line DOM-06-KID-01 approximately 4,3 km away from Kizimbani-1 well. This configuration suggests the continuity of the salt towards Kizimbani where it is supposed to be the region where the Kizimbani is structurally high.

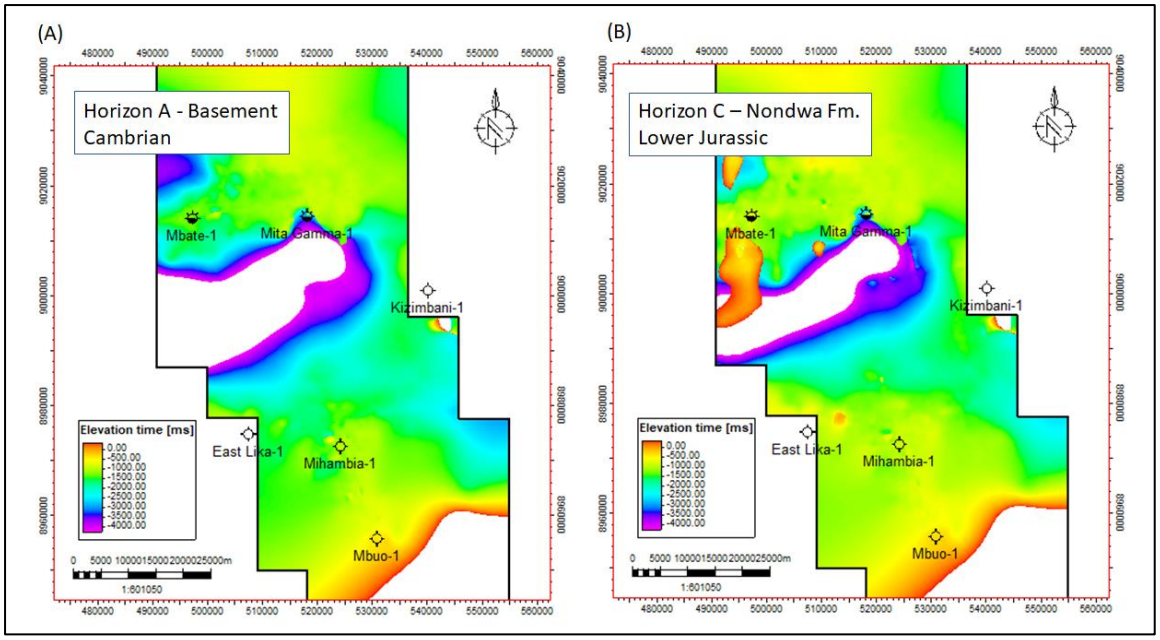

Figure 6.14 - Isochron maps between (a) basement (Cambrian) and (b) base salt (Lower Jurassic) indicating the thickness of the syn-rift.

The mechanism of salt diapirs formation in the Mandawa Basin is related to extentional regime in a salt basin, with faults affecting the sedimentary strata overload. These diapirs were noticed through seismic sections analysis where structures of the internal reflectors are conditioning the geometry and where the salt domes, salt walls occur. These rigid blocks, formed by the Zone E - Mtumbei Limestone Fm. and Zone F beddings, are superimposed on a ductile layer of evaporites that during flow conditioned chaotic seismic facies shifted by normal listric faults and occasionally by reverse faults. These faults broke rigid strata and controlled the growth of a sedimentary section deposited with the salt movement.

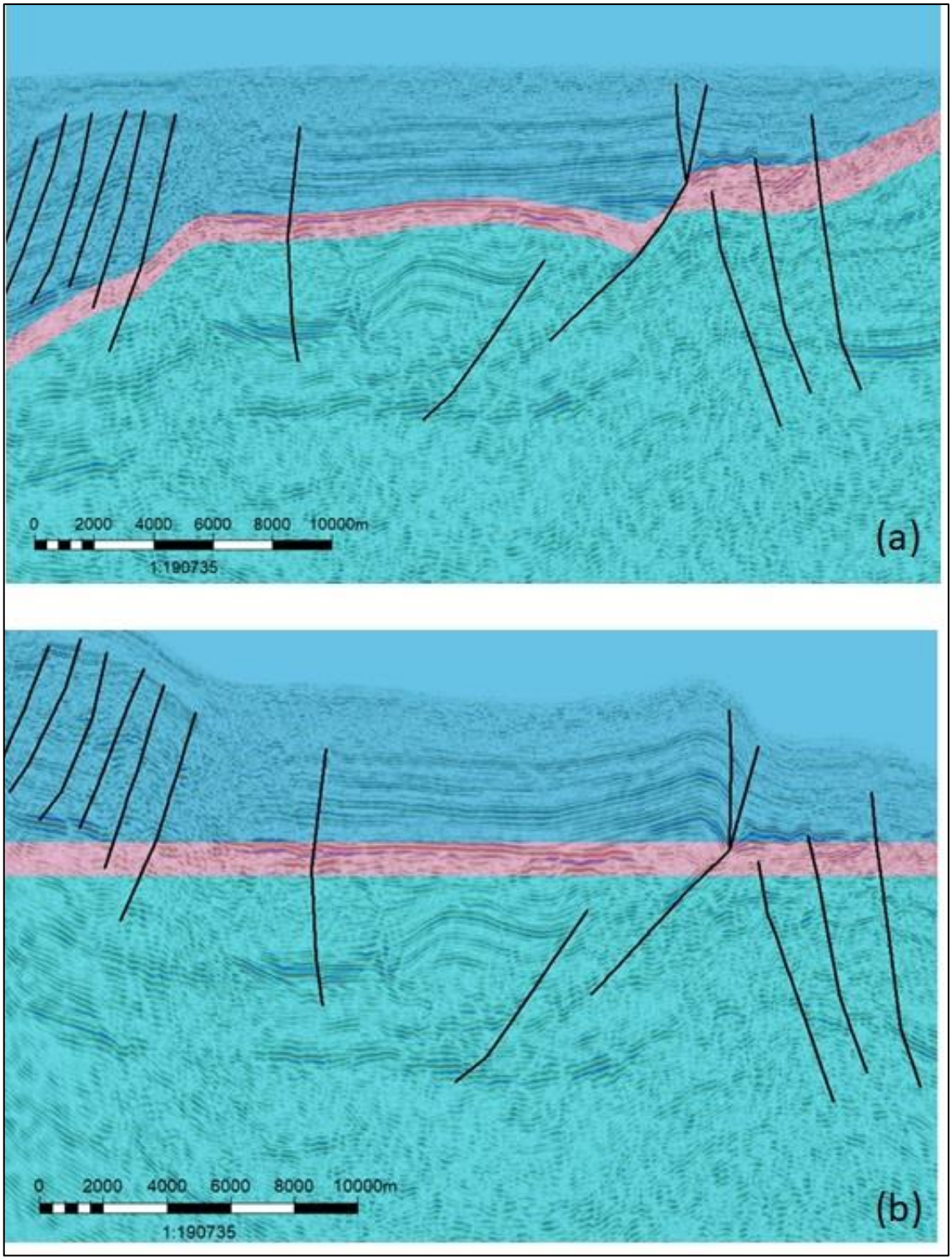

Figure 6.15 - Structural reconstruction of the Lower Jurassic sequence represented by horizon D (pink) showing parallel seismic reflectors within conformable sequences.

In the Oil & Gas industry, the restoration technique is used to investigate the hydrocarbon and mineral prospective of deformed sedimentary basins. In the oil and gas industry, this technique is particularly used to test the position of source rock, the validity of migration routes, and the timing of generation, expulsion, and migration of hydrocarbons; to analyze the geometry and formation of structural traps; and determine the timing of trap formation and/or destruction (Buchanan,1996). Paleoenvironmental reconstructions are important for several reasons, both inside and outside the scope of sequence stratigraphy. From a sequence stratigraphic perspective, the spatial and temporal relationships of depositional systems, including their shift directions through time, are essential criteria to validate the interpretation of sequence stratigraphic surfaces and systems tracts. Within this framework, the genesis, distribution and geometry of petroleum reservoirs, coal seams, or mineral placers may be assessed in relation to the process sedimentation principles that are relevant to each depositional environment. The identification of specific depositional elements is also critical at this stage, as their morphology has a direct bearing on the economic evaluation of the stratigraphic units of interest. (Catuneanu, 2002).

The movement of the Lower Jurassic salt is marked by the toplap/downlap terminations above and below the main zones (seismic sequences) classified in this study. The rise of a diapir by reactive bearing to the formation of a graben (a) associated with the extension of sedimentary overload, as a function of differential extension. The restoration of the structure (b) suggests that the salt layer and the overlapping layers had tabular geometry prior to extension. The picture 6.14 described the seismic interpretation proposing extensional tectonism producing listric faults overbalanced by a residual salt dome, as referenced in 2D seismic line DOM-06-MIH-4 in TWT.

6.4 MINIBASIN OR BASIN WITHDRAWAL

The term minibasin was introduced by Worall and Snelson (1989), following an early description of sedimentary basins controlled by salt withdrawal (Trusheim, 1960; Lehner, 1969). Such sedimentary accumulation related to salt escape was defined as “a syn-kinematic basin subsiding into relatively thick, allochthonous or autochthonous salt” independently from the basement absolute subsidence (Jackson and Talbot, 1991), a definition which is mostly descriptive and should not bear any a priori mechanical assumption The stratigraphical analysis of salt minibasins provides valuable information about the timing of salt movement and also describes the morphology of the structural and stratigraphic traps located adjacent to salt structures. Periods of salt diapirism are characterised by successions of growth strata bounded by unconformities at top and base. The analysis of the different strata terminations such as onlaps, downlaps, and truncations, provides evidence of periods of diapirism well known as halokinetic sequences (Giles and Lawton, 2002; Giles and Rowan, 2012).

Minibasins constitute a distinct type of sedimentary basin constituting a smaller in size if compared to sedimentary basins (typically only a few kilometers in diameter at maximum) but even though their size, they do subside several orders of magnitude faster than most crustal basins (up to 10 km/m.y. (6 Mi/m.y) over short periods; Worrall and Snelson, 1989; Prather, 2000).

The rim of salt structures, welds, and walls, which surround minibasins distinguishes them from other types of salt-withdrawal structures, which feed less-continuous networks of diapirs and walls. The network of salt-related topographical highs relief in turns exert a strong influence on sediment distribution both in a continental and deep marine settings forcing fluvial channels as well as turbidity currents to deviate and pond in bathymetric low corresponding to already subsiding older basins. As the pounded minibasins are filled to their rim, they allow for sediments to spill toward downslope minibasins (Winker and Booth, 2000).

In Mandawa Basin, estimating the original depositional thickness of the salt has been challenging due to poor seismic imaging that could allow delineating the lateral migration and its properties of losing volume occasionally by dissolution.

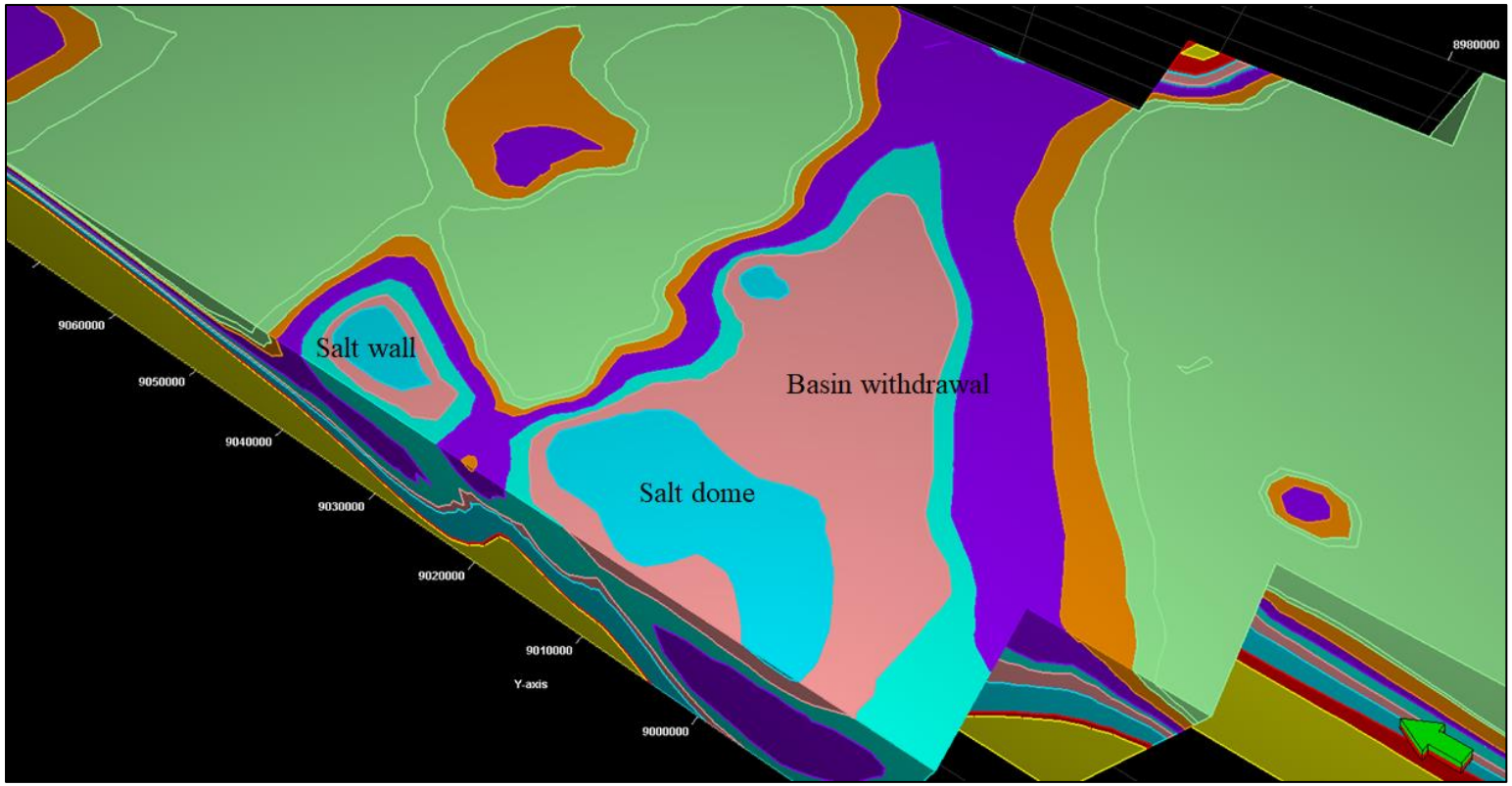

Figure 6.16 - Minibasin with salt dome and salt wall structures were interpreted and modelled in Mandawa Basin.

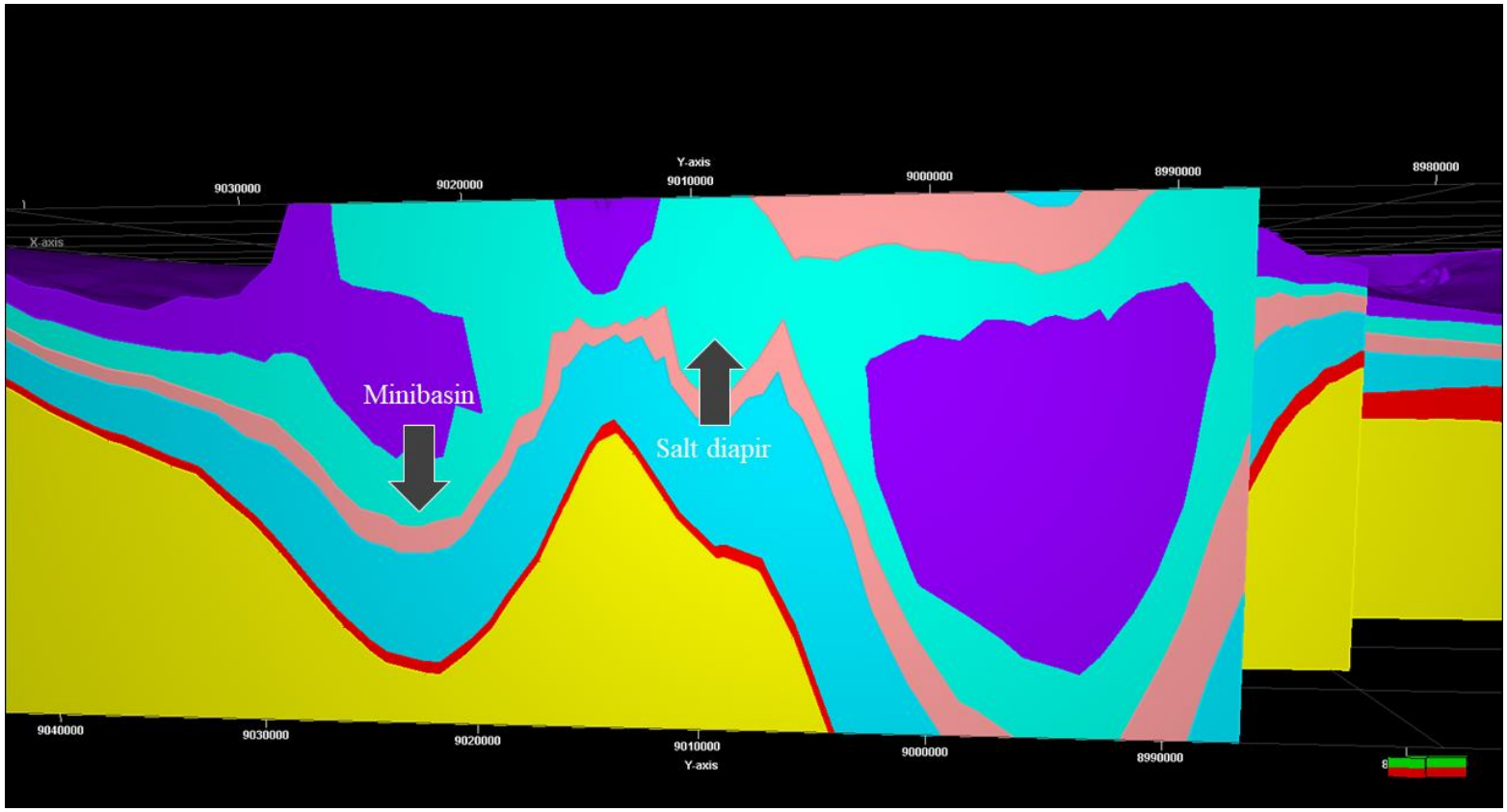

Figure 6.17 - Minibasin scheme for Mandawa Basin showing regions of subsidence, thinning the Middle Jurassic, accommodation by movement of salt into and adjacent region.

The thick sedimentary sequences around the salt structures may indicate the presence of the early salt movement in the basin before the deposition of those sequences during the Middle Jurassic (Bajocian and Bathonian). The salt pillow was a product of movement controlled by Upper Jurassic and Cretaceous deposition in southern Tanzania (Mbede and Dualeh, 1997).

As the depositional accommodation space was created, at some point controlled by normal faults, the Lower Jurassic succession was highly influenced by salt movement described as the Horizon C – Nondwa Formation in Chapter 4. The thickness of the Jurassic succession has been characterised as thin over the Jurassic salt structures and thickens in the minibasin adjacent to the salt structures (Figure 6.15). The Middle Jurassic succession slight thins above the Lower Jurassic to a basin withdrawal (Figure 6.16). The Upper Jurassic succession showed a thickening above salt minibasin with faults displacement affecting the continuity of the salt as allochthonous potentially extending as the tectonic setting of a transform margin movement.

The Upper Jurassic to Lower Cretaceous left lateral movement that split the Kizimbani and Pande highs are thought to have also cause salt flow which resulted in the formation of the N-S trending Mandawa anticline. These movements are thought to have been related to the southward drift of Madagascar (Mbende and Dualeh, 1997). Lower Cretaceous succession is characterised by thin thickness into tabular geometry where the accommodation suggested to be controlled by the salt discharge underneath the minibasins. The subtle thickness variation of the Cretaceous sedimentary package might indicate that the salt welded in several locations around salt structures.

CHAPTER 7

3D GEOCELLULAR MODEL

This thesis covered the application of a workflow suitable with the available dataset in order to produce a structural 3D geocellular model of the subsurface of the onshore Mandawa Basin. The workflow in Petrel software of Schlumberger Company is composed by two different models: the structural framework performed honoring the geological features with faults integrating the steps of seismic attributes, horizon interpretation, fault framework modelling, structural reconstruction to validate the interpretation, structural framework model construction, and refinement and an alternate model without faults, simple grid, less detailed for the purposes in this study (Figure 7.1). The structural framework resulted in to visualize the extension of the diapirism, investigate structural and stratigraphic features on seismic sections, trap geometries associated with the salt movement in the basin.

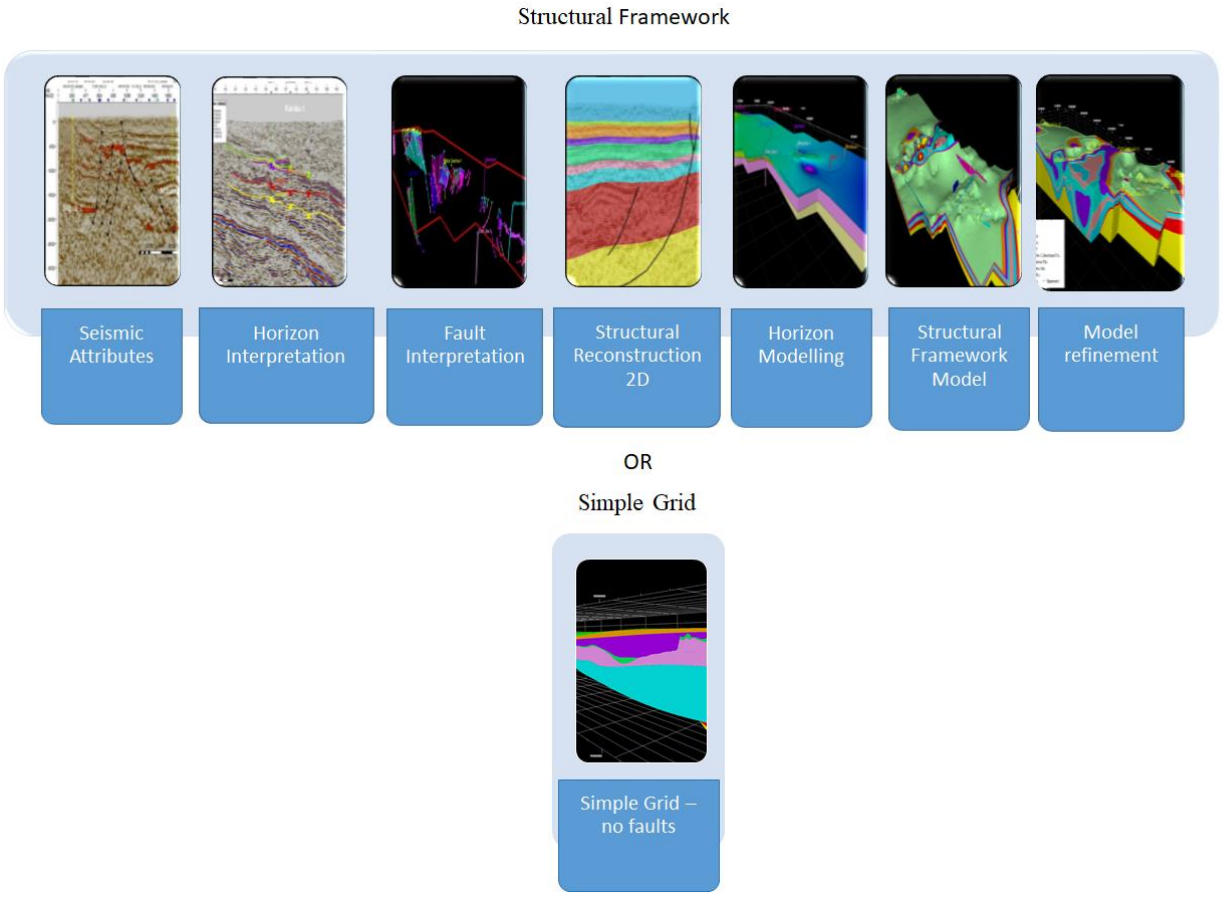

Figure 7.1 - The detailed workflow for the 3D geocellular model of the Mandawa Basin.

7.1 SEISMIC ATTRIBUTES IN THIS THESIS

Widely used in petroleum exploration since the 1970s, seismic attributes have been under development into many types in order to indicate lithology, facies, or fluid content and correlate with rock properties (Chopra and Marfurt, 2005). Seismic attributes used on seismic data originate from three seismic properties - waves, amplitude, phase and frequency - and are used to indicate where a certain geological feature is preconditioning to occur revealing its characteristics relating to the amplitude, shape, and position of the seismic waveform; enhance structural and stratigraphic features on maps, get information on lithology, facies or fluid content for reservoir characterisation, correlate with rock properties (Sheriff, 1994; Chopra and Marfurt, 2005; Cosentino, 2011; Koson, 2014). The information extracted using the volume attribute analysis in this thesis was used to identify the occurrence of salt diapirism, focusing in the central and south Mandawa Basin and essentially to investigate geometries of geological lineaments.

In Petrel, two types of seismic attributes are applicable and contain a library of different attribute classes - volume attributes and surface attributes. Volume attributes are based on several properties of the analytical signal. The resulted attribute is produced a virtual or physical volume of the input seismic (Schlumberger, 2018); it includes a comprehensive package of seismic attributes used in hydrocarbon reservoir modeling in order to decrease the uncertainty and also to substitute the lack of the available seismic data (Sheline, 2005; Azevedo and Pereira, 2009).

7.1.1 Chaos

Chaos attribute is characterised as a measure of the "lack of organization" in the dip and azimuth estimation method (Koson *et al.*, 2014). Particularly, as explained in Pigot *et al*. (2013) and Schlumberger (2018), chaos attribute can highlight features as faults and discontinuities within seismic data. Consequently, chaos attribute can be used to distinguish different sediment facies in lithology variation environments as it will be affected by gas migration paths, salt body intrusions, reef textures, channel infill, and seismic classification of chaotic texture. Chaos in the signal can be used to illuminate faults and discontinuities and for seismic classification of chaotic texture. Chaos can be related to local geologic features as it will be affected by gas migration paths, salt body intrusions, reef textures, channel infill, etc. (Pigott *et al*., 2013; Schlumberger, 2018).

Zones of maximum chaoticness indicate zones of reflector discontinuities such as fault zones, angular unconformities, channel sand bodies probably composed by anhydrite, halite, gypsum intercalated with carbonates, and possible zones of fractures (Pigott *et al*., 2013).

The Chaos attribute (Ferguson *et al*., 2010) is scaled from 0 to 1, showing the following seismic textures:

a) Amplitudes > 0,60: These values are revealed by red colors and are overall caused by strapping variation in dip and azimuth. These variations are primarily produced by salt structures or highly faulted areas (Figure 7.2).

b) Amplitudes from 0,30 to 0,60: Grey/red colors indicate small variations of dip and azimuth mainly caused by salt-related radial faults or faulted areas.

c) Amplitudes from 0,30 to 0: This range of values is represented by white colors and corresponds to areas with no evidence of strong variation of estimated dip and azimuth,

which are usually located away from salt diapirs where there are not structural elements originating amplitudes diverse within the seismic horizons.

Seismic multi-trace structural attributes like Chaos tend to be applicable for defining salt-related structural elements as radial faults (Figure 7.3). The Chaos volume attribute highlights areas where the 2D seismic lines show large variation in the locally estimated dip and azimuth, in this case, high amplitude > 0.60.

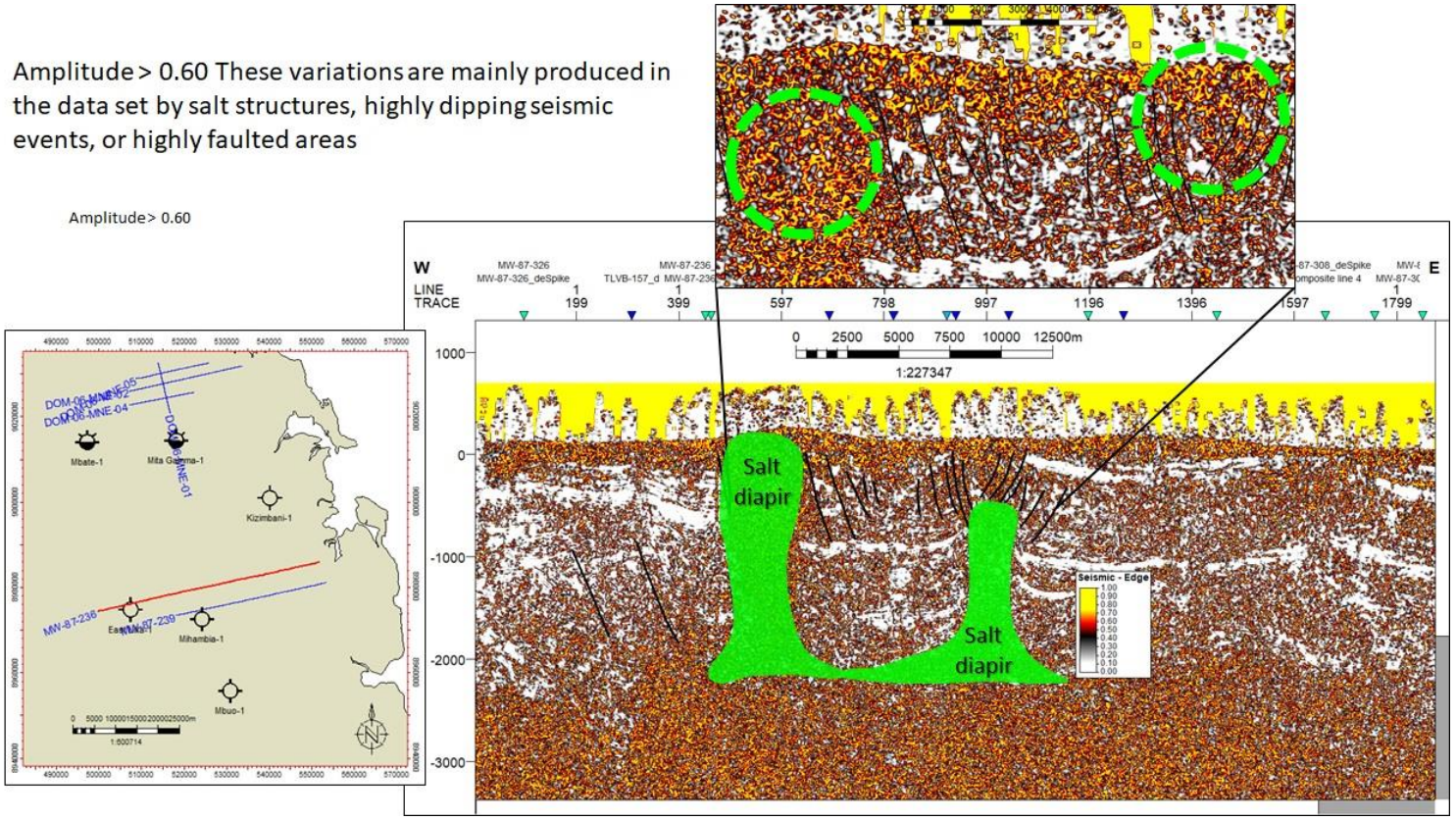

Figure 7.2 - The use of chaos attribute in certain parts of the 2D seismic line MW-87-236 highlighted the amplitude > 0.60 (green dots) where the salt structure (salt diapirs in green) was interpreted in Chapter 6.

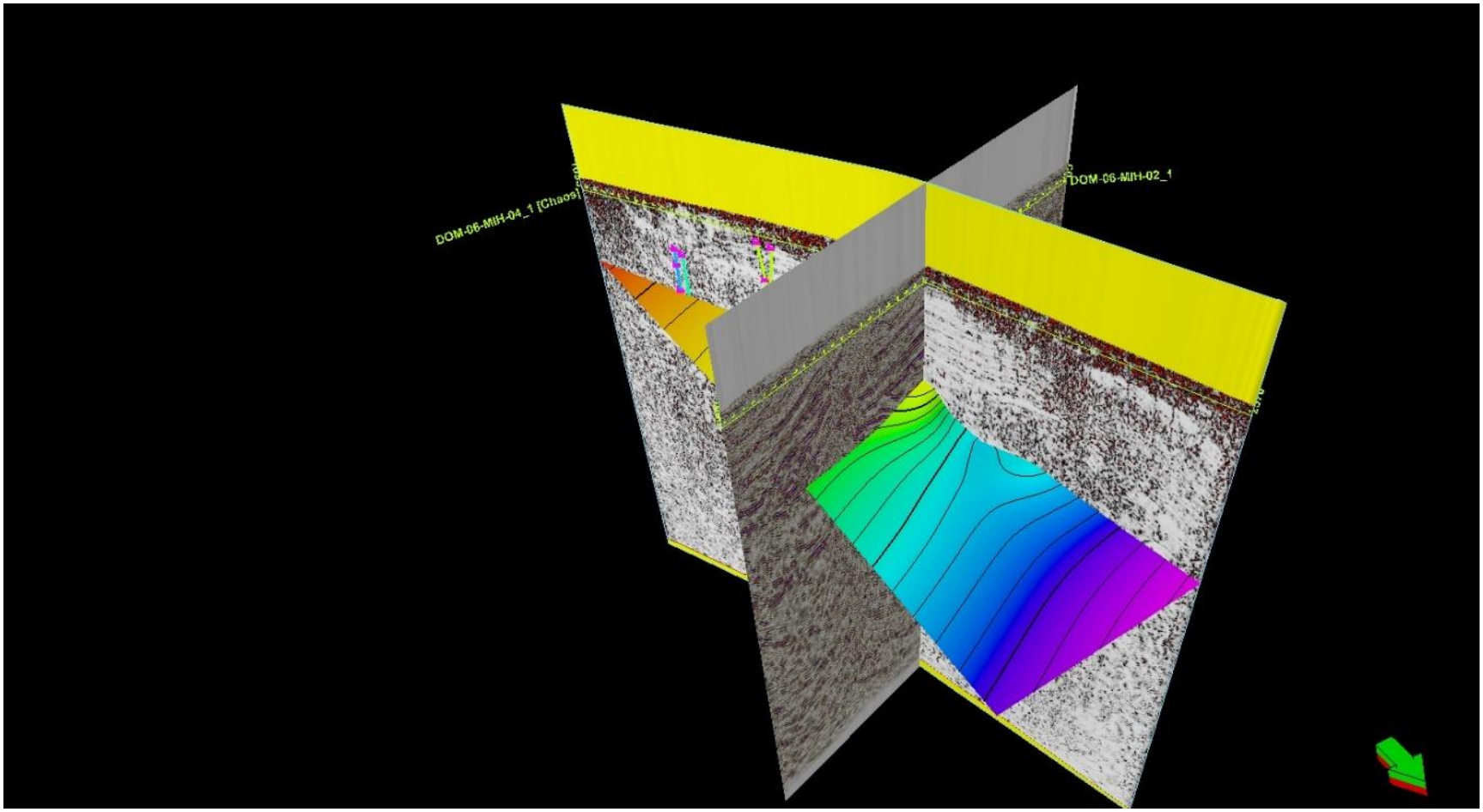

Figure 7.3 - Horizon interpreted according to the DOM-06-MIH-04_1 [Chaos] inline and crossline DOM-06-MIH-02_1 with the Chaos attribute emplaced.

7.1.3 Cosine of Phase

The Cosine of phase is commonly used for guiding interpretation in areas poorly resolved on the amplitude or to enhance the definition of structural delineation. Used together with the Instantaneous phase for comparison (Schlumberger, 2018).

This attribute is also known as Normalized Amplitude because as is unresponsive to amplitude variations. Hence, this attribute enhances the definition of structural delineations in these poorly solved areas of uncertainty located in the vicinity of salt structures where it may provide evidence of drape folding of growth strata away from salt structures. In addition, the Cosine of Phase is an excellent indicator of seismic facies changes and strata terminations (Giles and Rowan, 2012; Schlumberger, 2018).

Cosine of Phase is an excellent indicator of seismic facies changes sand strata terminations. Generally, three types of seismic facies have been encountered within the data set:

1) Chaotic. This type is characterised by chaotic seismic events without any kind of continuity. Thus, it might be related to chaotic deposits without layering as salt, marine debris flows, or alluvial fans.

2) Semi-continuous or faulted. The continuity of the seismic events is continuously interrupted by probably small faults.

3) Continuous. The seismic events do not show any disturbance and can be easily followed.

In Mandawa Basin (Figure 7.4) the seismic attribute was applicable to interpret the salt dome.

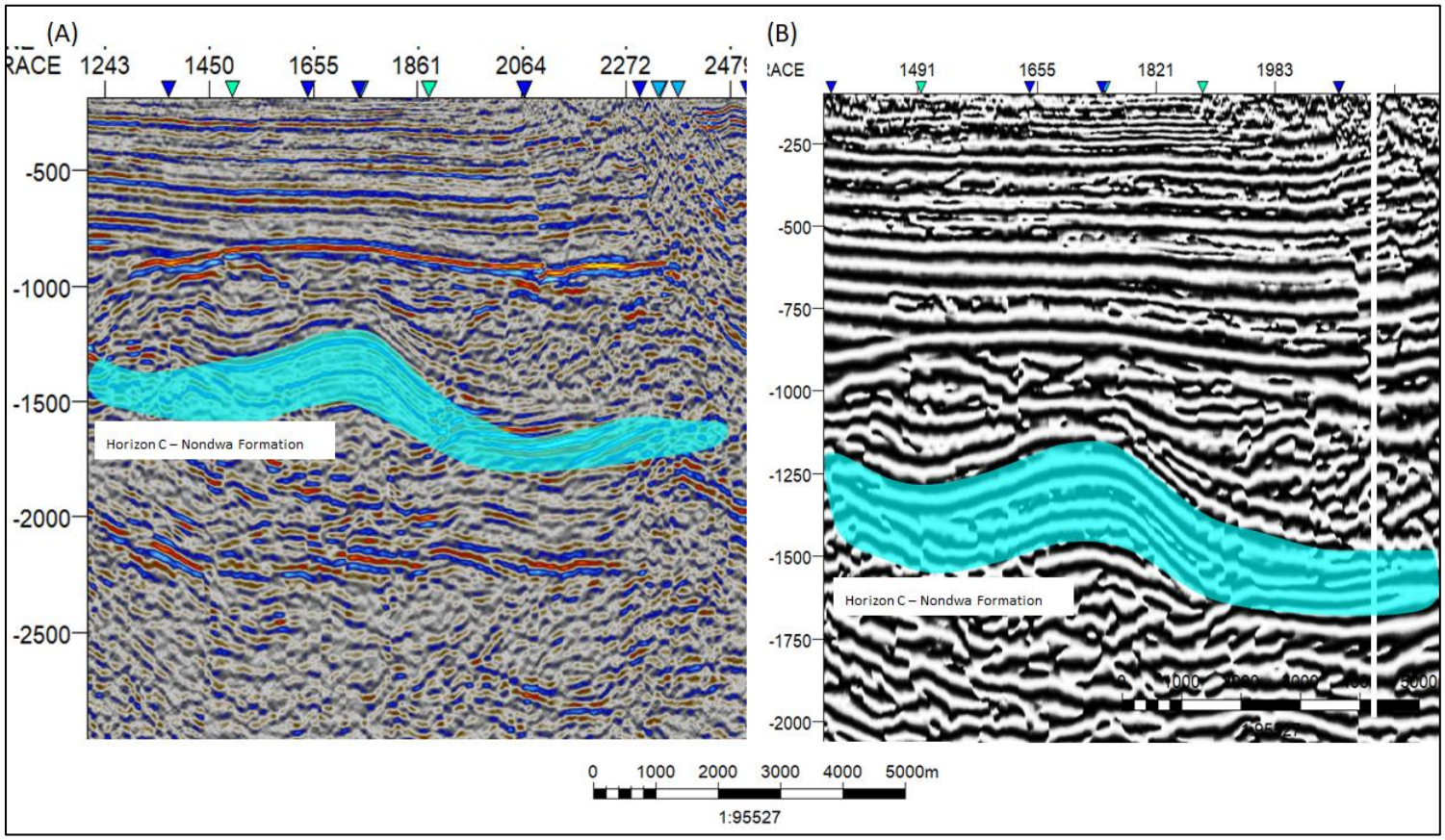

Figure 7.4 - The Cosine of Phase attribute highlights the continuity of the reflectors as the resolution to interpret a salt dome in Mandawa Basin. (A) Showing the original seismic line and (B) is the extracted attribute.

7.1.4 Envelope

The envelope attribute is of importance detecting bright spots, on both negative and positive events, caused by gas accumulations, detecting major lithological changes that are caused by a strong energy, reflections, and sequence boundaries (Figure 7.5). The attribute clearly shows subtle lithological changes that may not be apparent on the seismic data (Koson, 2014; Schlumberger, 2018). The Envelope can be used to help recognize phase differences between seismic versions; useful in highlighting discontinuities, changes in lithology, faults The peak energy should align independent of the phase of the data (Schlumberger, 2018) (Figure 7.6).

Envelope stands as the total instantaneous energy of the analytic signal (the complex trace), independent of phase (Schlumberger, 2018).

$$Env = \sqrt{f^2 + g^2}$$

Where:

$\boldsymbol{f}$ and $\boldsymbol{g}$ are the "real" and "imaginary" components of the seismic trace. So, if f is the real part, which is just the original seismic trace samples, $\boldsymbol{g}$ will be the samples from the Hilbert transform (also called quadrature amplitude) of the seismic trace (Schlumberger, 2018).

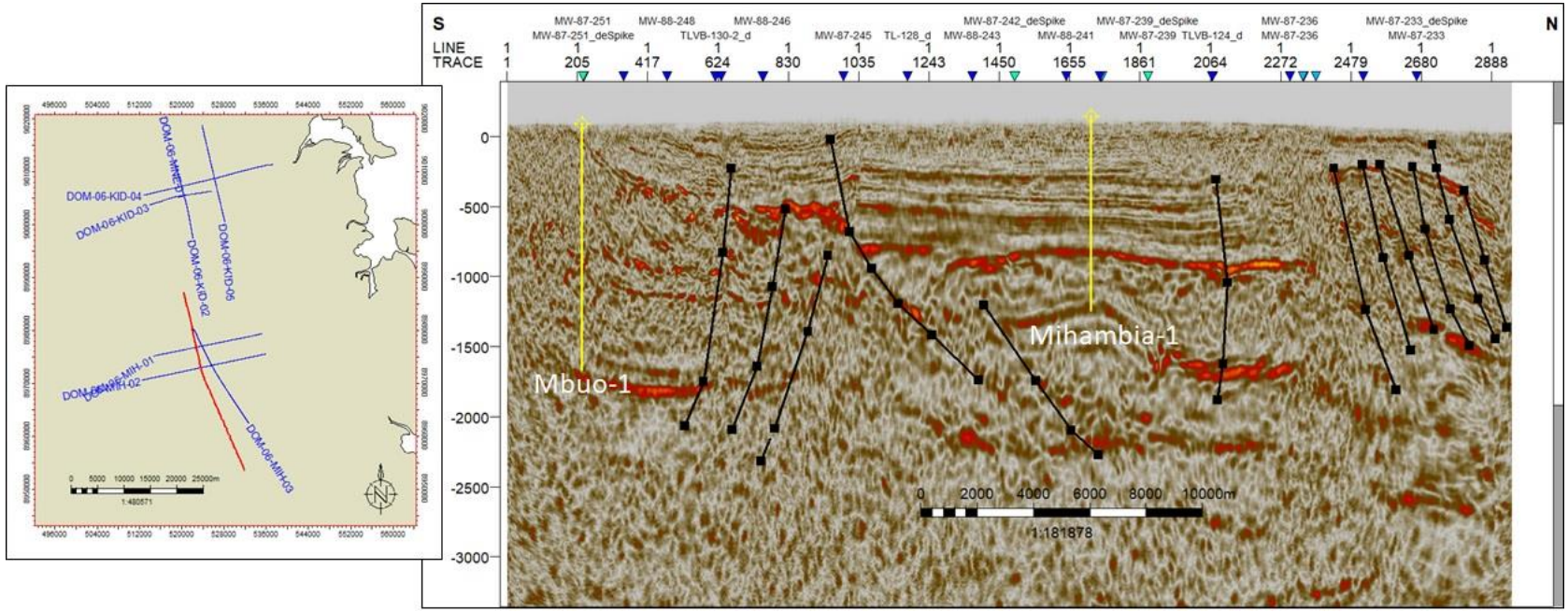

Figure 7.5 - Example of Envelope attribute along the N-S DOM-06-MIH-04 2D seismic line. Representative normal faults are shown.

7.1.5 Root mean square (RMS)

This seismic attribute calculates the RMS ratio between of squared amplitudes divided by the number of samples within the specified window used. The two data sets would typically be a base survey and a monitor survey for Time Lapse Analysis (Schlumberger, 2018).

This attribute is commonly used map hydrocarbon indicator in a zone of interest to analyze the difference between two seismic traces ***f*** and ***g*** inside a specific window *t1-t2*, by quantifying the rms ratio. Computes the square root of the sum of squared amplitudes divided by the number of samples within the specified window (Koson, 2014; Schlumberger, 2018).

$$RMS\ ratio = \frac{RMS(f_t)}{RMS(g_t)}$$

where:

$$RMS(x_t) = \sqrt{\frac{\sum_{t_1}^{t_2}(x_t)^2}{N}}$$

N is the number of samples in the window t_1-t_2.

Longer windows produce a smoother amplitude estimation highlight coarse-grained facies, marl in limestone, and unconformities (Koson, 2014).

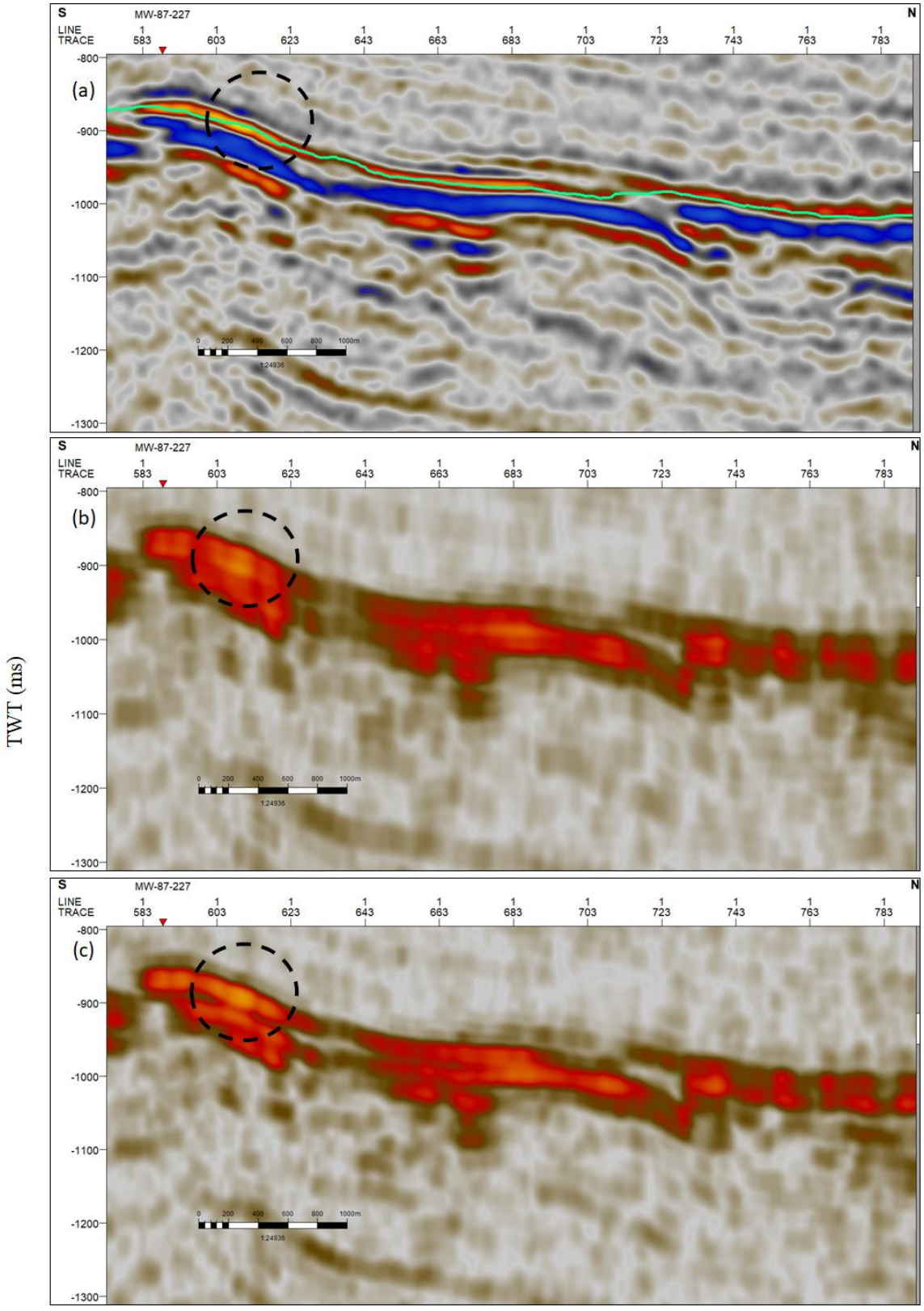

Figure 7.6 - The seismic line showing the Horizon E - Mtumbei Limestone Formation in original at -900 ms (a); dashed circle shows seismic with 9 lengths of window and amplitude of 6,121.47 at -900 ms (B) and seismic with 6 lengths of window (dashed circle) and amplitude of 6,624.24 at -900 ms.

7.1.6 Structural Smoothing

Smoothing of the input signal guided by the local structure to increase the continuity of the seismic reflectors (Randen, 2002). The Structural smoothing attribute can also be used to illuminate flat spots within the seismic volume (Figure 7.7). By running the smoothing operation without Dip guiding, horizontal features such as fluid contacts can be emphasized.

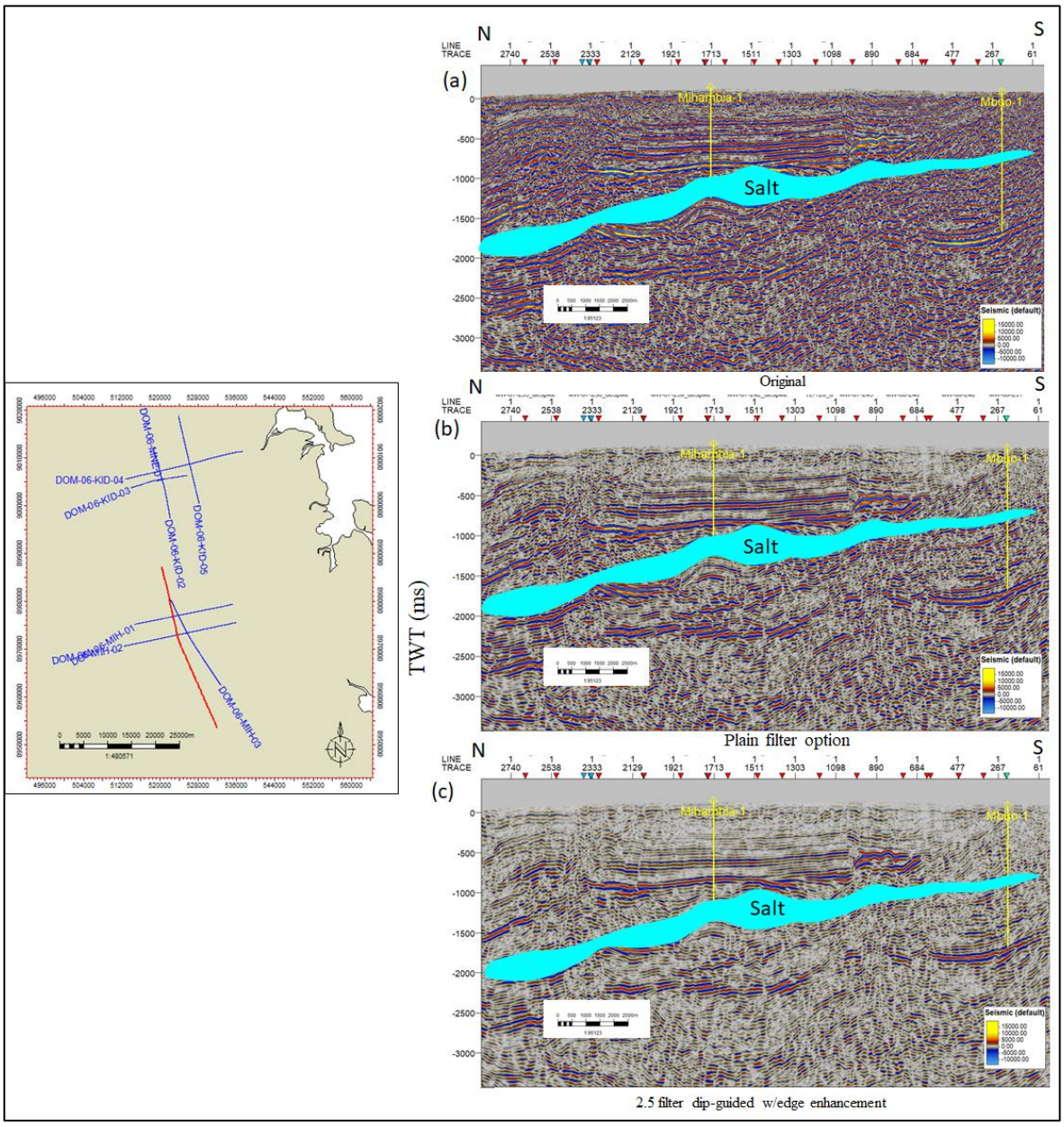

Figure 7.7 - North-south trending interpreted composite line crossing the wells Mbuo-1 and Mihambia-1 as original (a) and where the volume attribute Structural Smooth has been applied (b and c) showing the high and subsiding structure of an evaporite (in light blue colour).

7.1.7 Sweetness

Structural smoothing is an extremely valuable operation to run before auto-tracking as it can stabilize the results. The results could be snapped back to the original data, or used as a smooth interpretation of regional surfaces.

Sweetness is the implementation of two combined attributes (Envelope and Instantaneous Frequency) and is used for the identification of features where the overall energy signatures change in the seismic data (Schlumberger, 2018).

Sweetness is defined by the formula (Radovich and Oliveros, 1998):

$$\text{Sweetness} = \frac{Envelope}{SQRT(Instant\ Frequency)}$$

In sequence is an example of sweetness to highlight a progressing channel sequence bounded by reverse faults crossing Kianika-1 well (Figure 7.8).

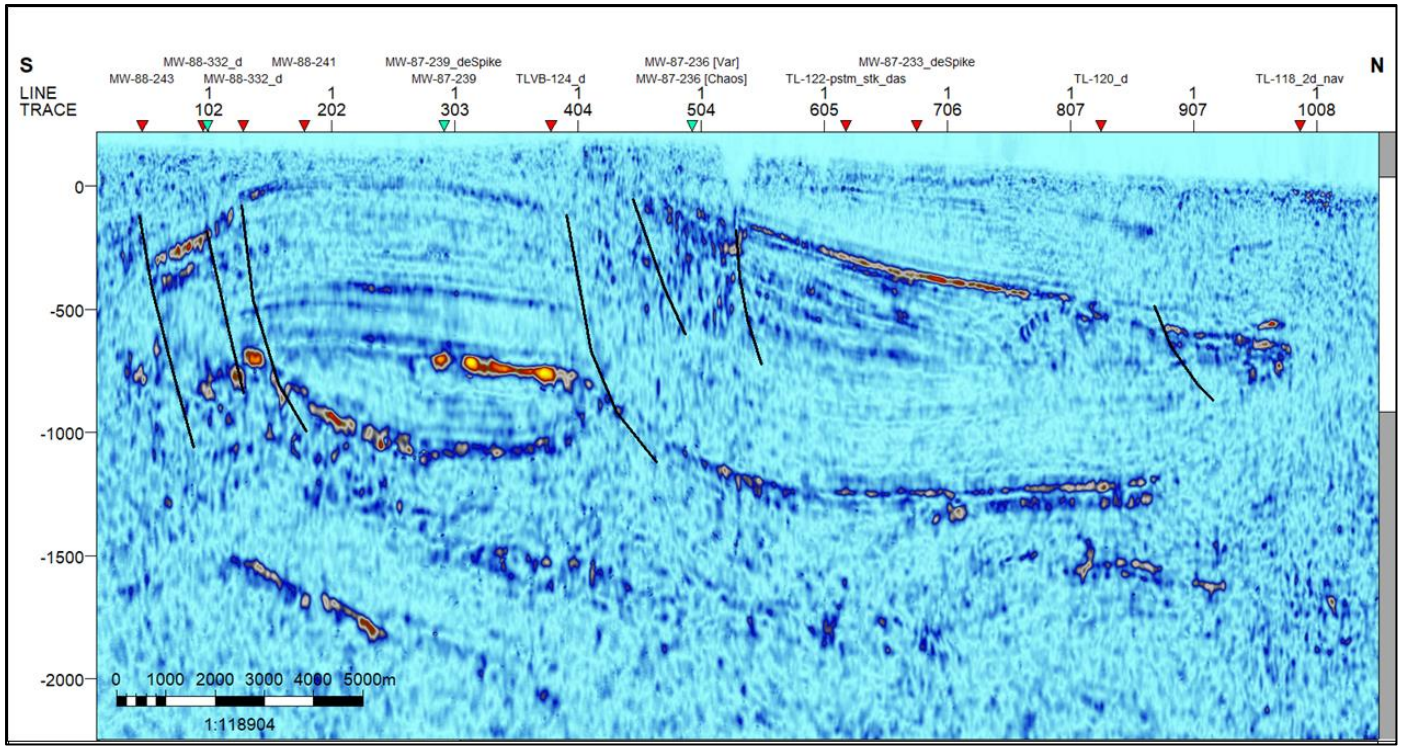

Figure 7.8 - The sweetness attribute with edited opacity in the 2D seismic line MW-88-311 crossing Kianika-1 well indicating reverse faults.

7.2 SEISMIC INTERPRETATION WORKFLOW

7.2.1 Horizons Interpreted

Seismic interpretation today involves a delicate balance between geophysics, geology, and computer science (Brown, 2005).

The horizon interpretation outlined in this thesis was done in Petrel software in the seismic interpretation process. After importing the seismic and well data in the software, a synthetic seismogram was performed for each well by convolving an extracted wavelet from the seismic data afterward generated a good correlation between the seismic and well data as a previous step to tie in the geological horizons along with consistent reflections of the same zero-phase seismic data. Troughs that correspond to the reflectors were traced along the seismic transects and interpretations were carried out separately (see Chapter 3).

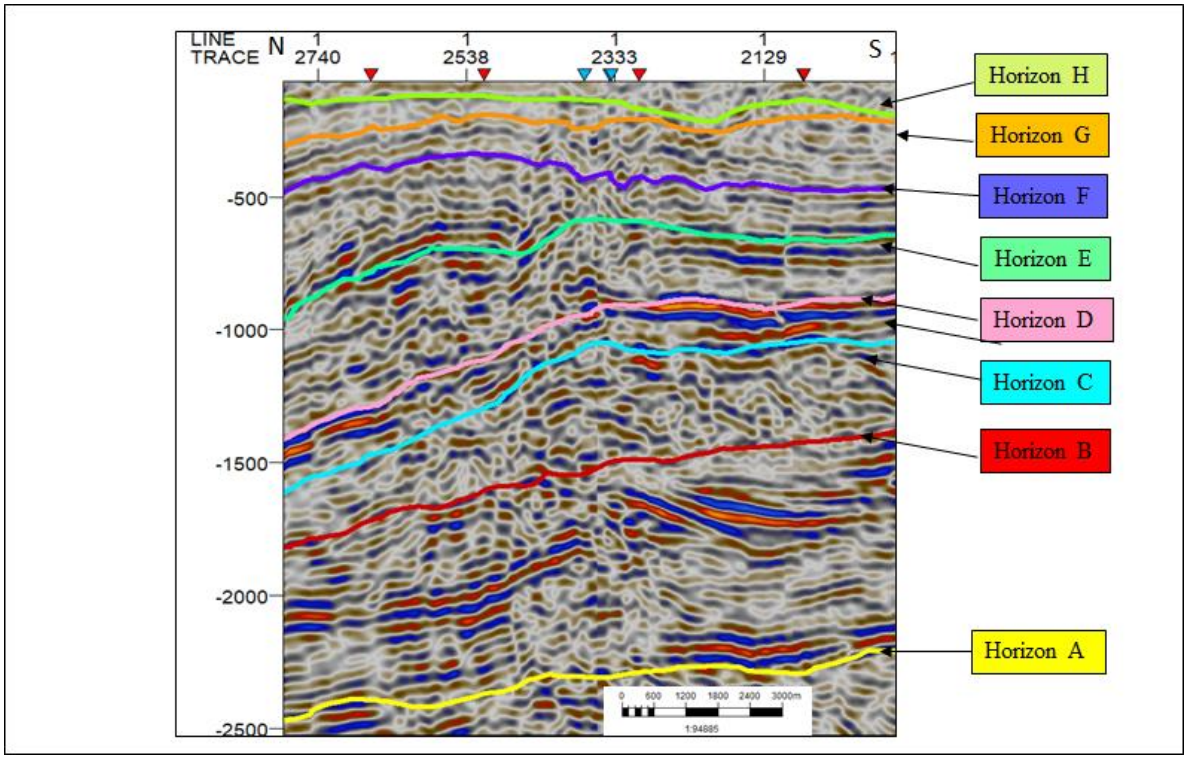

Figure 7.9 - Horizons A, B, C, D, E, F, G, and H picked in DOM-06-MIH-04 inline.

Horizons were interpreted manually (manual picking in Petrel) following their significant seismic reflections due to poor quality data (Figure 7.9). The major stratigraphic packages according to the lithostratigraphy of Mandawa Basin were mapped and reported in Chapter 4; unconformities, sequence stratigraphy boundaries were analysed in Chapter

5. As part of the seismic interpretation workflow of inlines and crosslines of the Mandawa Block, eight horizons were identified: Horizon A, Horizon B, Horizon C, Horizon D, Horizon E, Horizon F, Horizon G and Horizon H (Figure 7.9). Based on the geometry of seismic reflectors, the mentioned horizons have been associated with four stratigraphic units (from the base to top) and also, in addition, strike and dip measured: Precambrian/Cambrian, Lower Jurassic, Middle Jurassic, Upper Jurassic, and Lower Cretaceous.

The seismic horizon that defines the basis of the lithospheric breakup surface was the first element to be identified, as it is a clear reflector that, besides being identifiable, was well characterised and mapped in this study area.

7.2.2 Surfaces

Surfaces were created in Petrel software using the convergent interpolation algorithm which honors the data building the model into stages. Surfaces derivate at each iteration are interpolated and fed into the next iteration (Schlumberger, 2018). For each horizon mapped a surface was generated to visualize how the stratigraphic features in 2D structural grids differ from structural features vertically along the 2D seismic lines. Time structural maps for each surface are presented below.

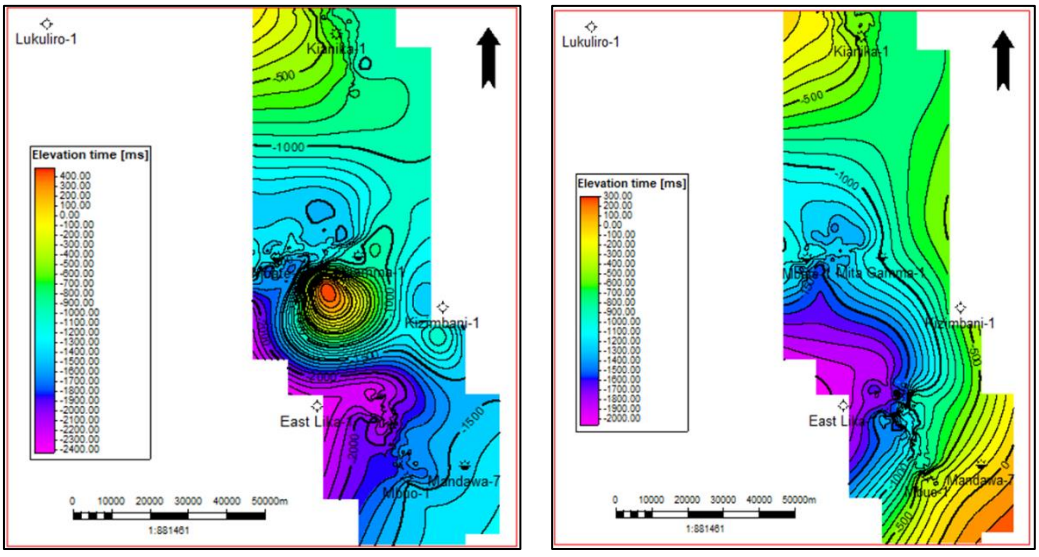

Figure 7.10 - Surfaces of Horizon A (left) and Horizon B (right)

Surface Horizon A

The basement surface Horizon A located at the base of the sedimentary strata in Mandawa Basin was configured by chaotic to wavy reflections, discontinuous, moderate to high amplitude patterns. This surface is associated with a relevant geodynamic event in understanding the evolution of the basin at the regional level, and thus constituted an important starting point for the establishment of the remaining seismic horizons (Figure 7.10).

Surface Horizon B

The overlying surface Horizon B was mapped corresponding to a negative reflector of low to medium amplitude at the depth of 1,000 m in Mbuo-1 well coinciding with the top of Mbuo Formation. Some reflectors were interpreted as stratified, bounded by sharp erosion depression by negative reflection (Figure 7.10).

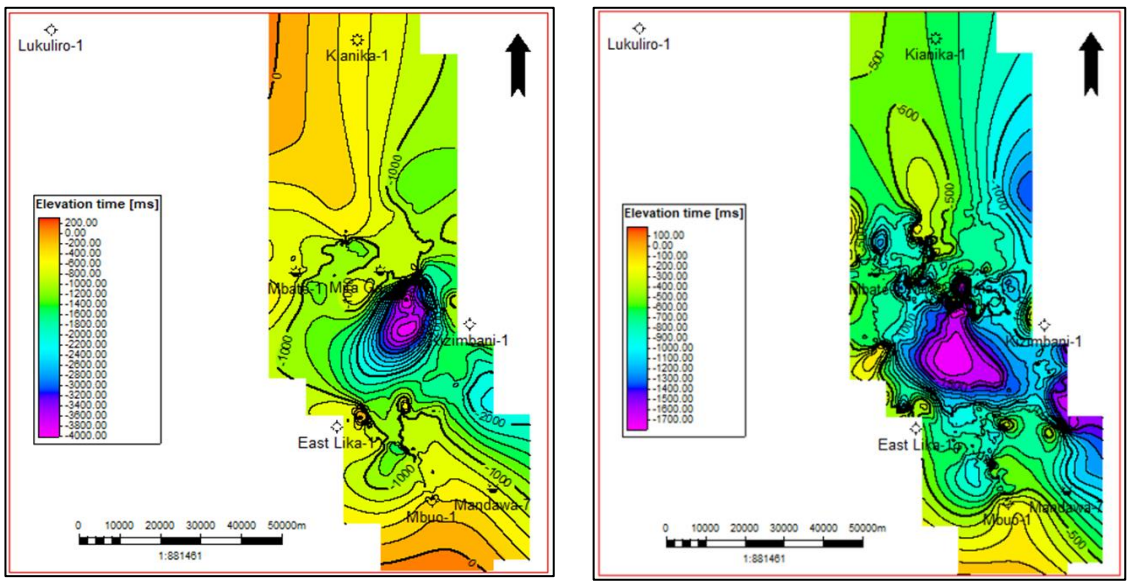

Figure 7.11 - Surfaces of Horizon C (left) and Horizon D (right).

Surface Horizon C

The base of surface Horizon C (Figure 7.11) was defined by chaotic reflectors, medium amplitudes with loss of reflection continuity originally of non-continuous evaporite, wherein some areas data quality degraded to provide better visualization, beneath salt walls for example, leading to a high level of uncertainty compromising the identification of the base of the evaporite. The top of the surface Horizon C was interpreted by regional

high amplitude in seismic reflectors representing the top or near the top of the Nondwa Formation, marked in the well by the first appearance of anhydrite and halite.

Wells to the north of Mandawa, Lukuliro-1 and Kianika-1, do not contain the surface Horizon C that is associated with the Nondwa Formation, therefore there is a northern limit to this section to the east and south of these wells. The location of this northern limit is not at present known due to the general lack of well penetrations in the north Mandawa – east Kisangire area.

Surface Horizon D

The fourth surface interpreted was identified by high amplitude reflectors according to Mihambia-1 well with a depth of 1,609 m. This surface marked the Middle Jurassic. The internal configuration of the surface Horizon D (Figure 7.11) was mapped as semi-continuous to continuous with loss of reflection continuity where the salt dome and salt walls were noticed forming intrusions.

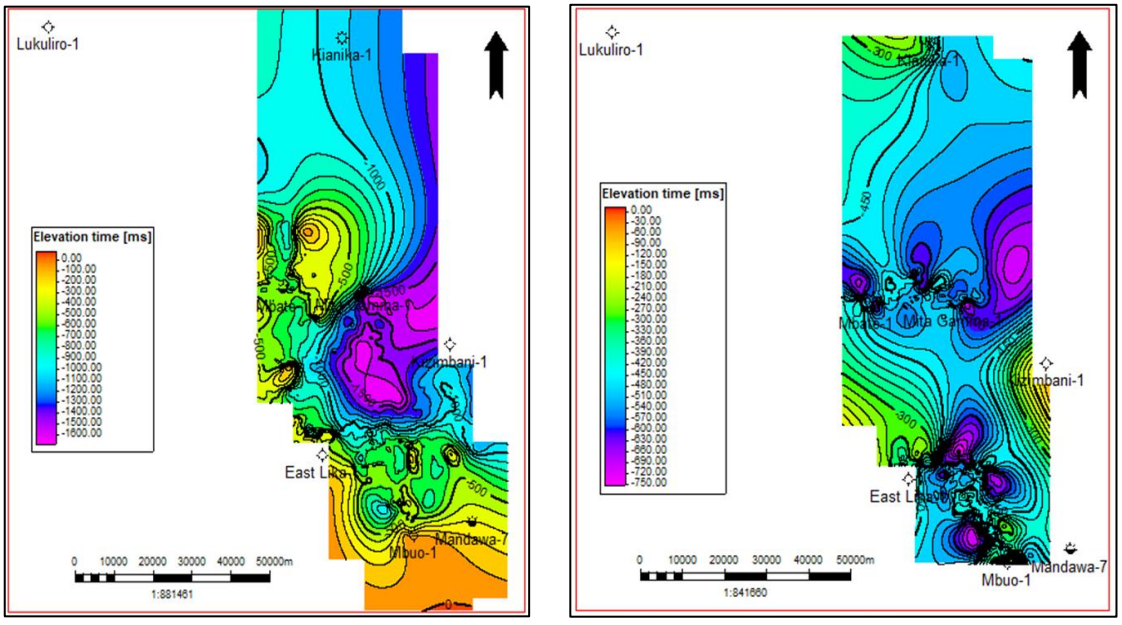

Figure 7.12 - Surfaces of Horizon E (left) and Horizon F (right).

Surface Horizon E

The surface Horizon E corresponded to a high amplitude of reflections characterised by the limestone facies of the Mtumbei Limestone Formation. Reflectors were interpreted as sub-horizontal to horizontal parallel continuous as characteristic of carbonate platform

of Upper Jurassic age in the onshore Mandawa Basin. The depth of this surface ranged from 1,629 m to 743 m in the southeast part of the basin (Figure 7.12).

Surface Horizon F

The surface Horizon F was configured as representing the boundary between the Upper Jurassic and Lower Cretaceous strata (Figure 7.12). The pattern of reflectors was distinguished by parallel of medium to high amplitude, sub-continuous, truncation below the boundary.

Surface Horizon G

The surface Horizon G marked the Lower Cretaceous unconformity (Chapter 6), containing one of the highest degrees of erosion in comparison to the previous horizons identified (Figure 7.13), as the seismic structure within the presence of a major depocentre on the northwest flank of the Mita Gamma-1 well upwards Kianika-1 well, possibly representing the southern part of the Rufiji Trough.

Surface Horizon H

The top surface Horizon H marked was described as the top of the Lower Cretaceous where features of furrows as plough marks and lineations composed the surface (Figure 7.13).

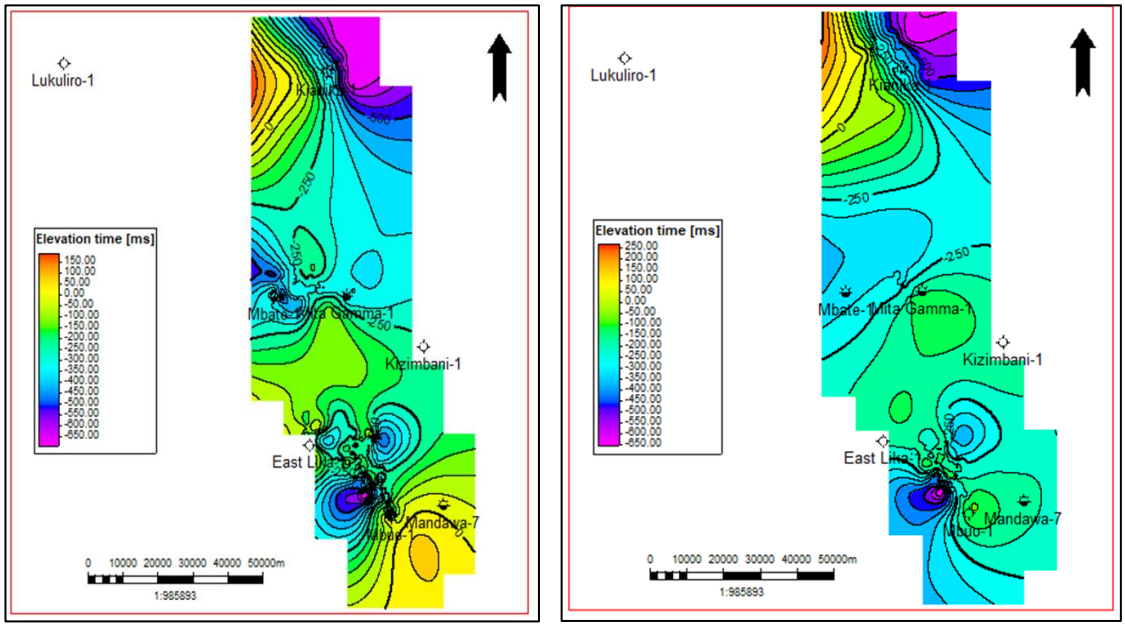

Figure 7.13 - Surfaces of Horizon G – Zone G (left) and Horizon H – Zone H (right).

The horizons interpreted with the well tops (markers) associated were used further for the model construction in the Structural Framework process in Petrel. The eight surfaces stacked (Figures 7.14 and 7.15) were used as input in preparation to create a simple grid with faults as a quality check model for visualization of the stratigraphy thickness in Mandawa Basin.

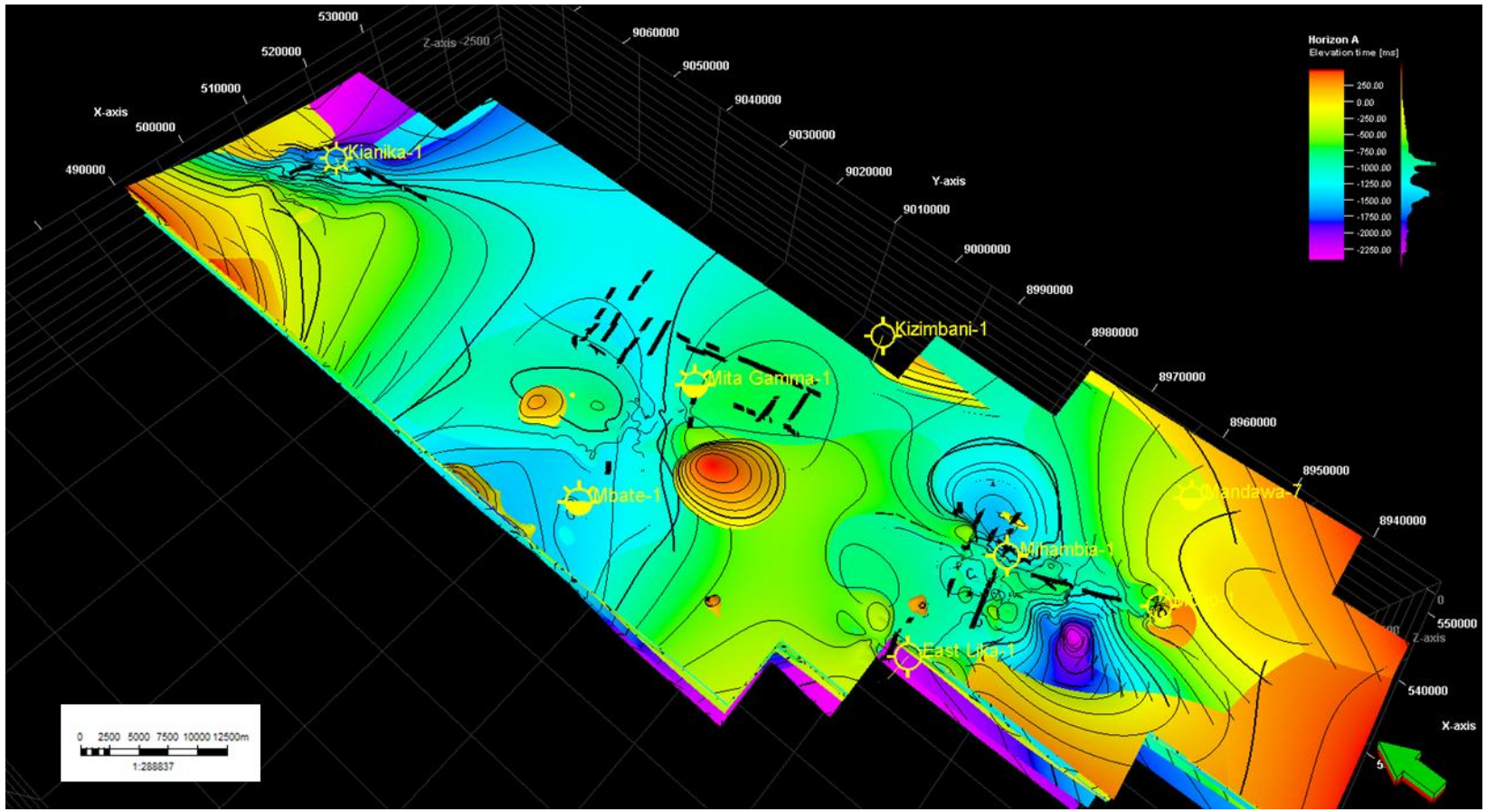

Figure 7.14 - The stacked surfaces - from the upper to the bottom horizon - created (in time domain) by the interpreted horizons in Petrel; the interpreted faults are highlighted in black colour; wells are indicated in yellow colour.

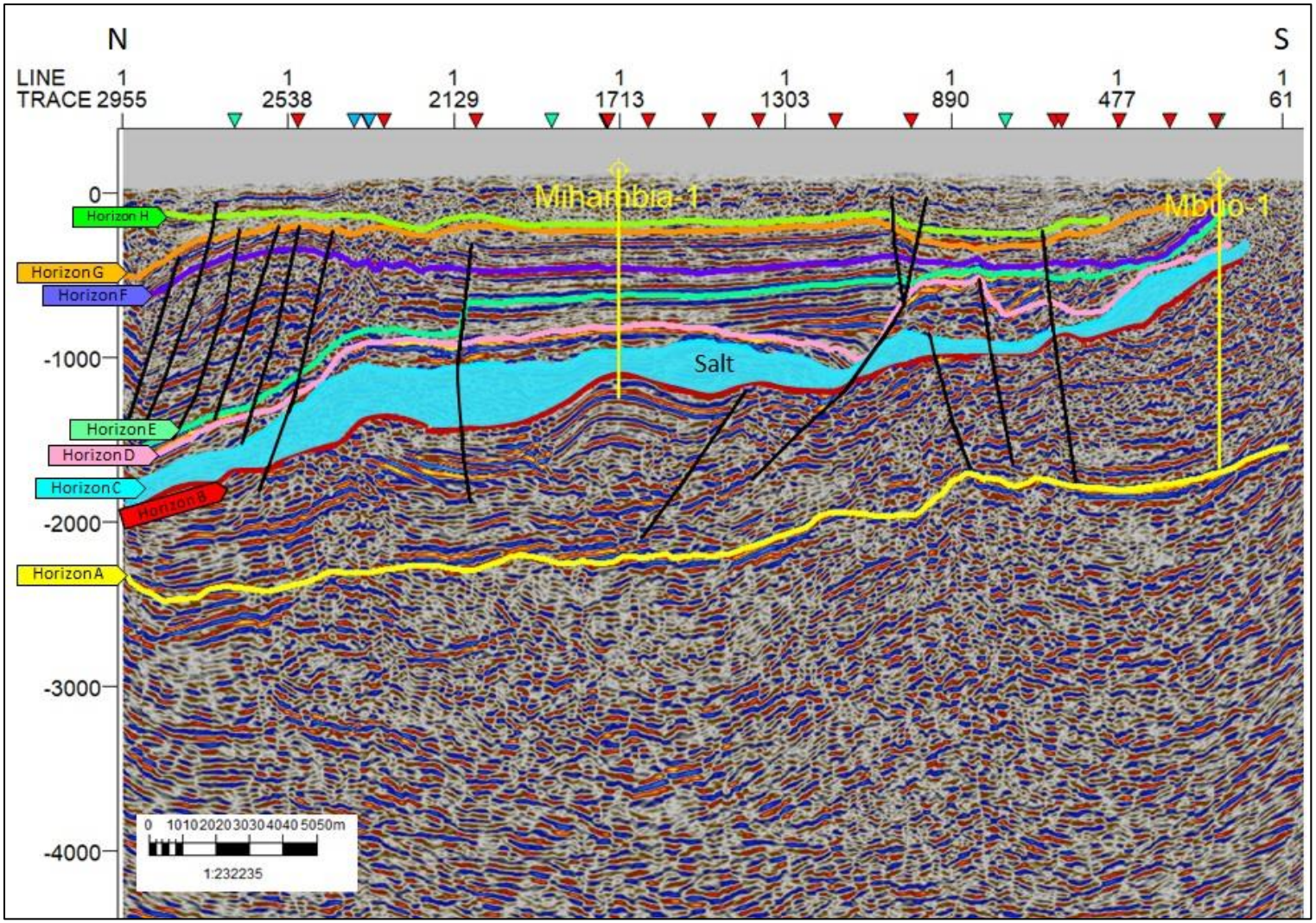

Figure 7.15 - Interpreted seismic line viewed in north-south trending dip lines, showing the salt extensional geometry with structures reaching the Lower Jurassic.

7.2.2 Faults Interpreted

Faults were described as Fault segments (also referred to as fault sticks) interpreted by simply digitizing directly on a seismic intersection in Petrel Platform software (Schlumberger, 2018). Reflection disruption and offset are the most apparent characters used to identify faults in seismic data (Brewer, 1987; Dorn *et al*., 2010). Abrupt vertical displacement of several reflectors along a distinct line (fault plane) is the best indicator for the presence of faults (Marillier *et al*., 2006).

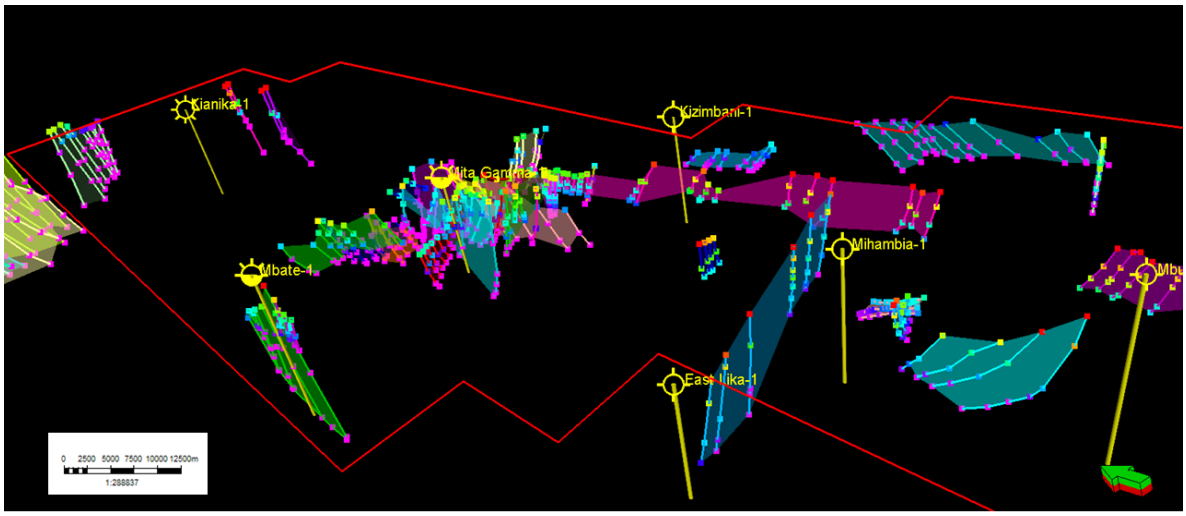

Figure 7.16 - Fault segments interpreted in Mandawa Block and around Lukoliro-1 well outside the block.

Fault interpretation was performed similarly to the horizon interpretation process by identifying and defining the major fault patterns observed on the 2D seismic lines around Mihambia-1 well and expanding to the closest wells and seismic lines respectively (Figure 7.16). In this thesis, it was necessary to create one or more than one fault by digitalizing a set of points on a single vertical seismic display for a given seismic line which comprised a fault segment, automatically triangulated as a fault surfaces in the software process. Faults were assigned as normal or reverse for major faults and the minor faults were addressed as unassigned faults (see Appendix 7.2.2).

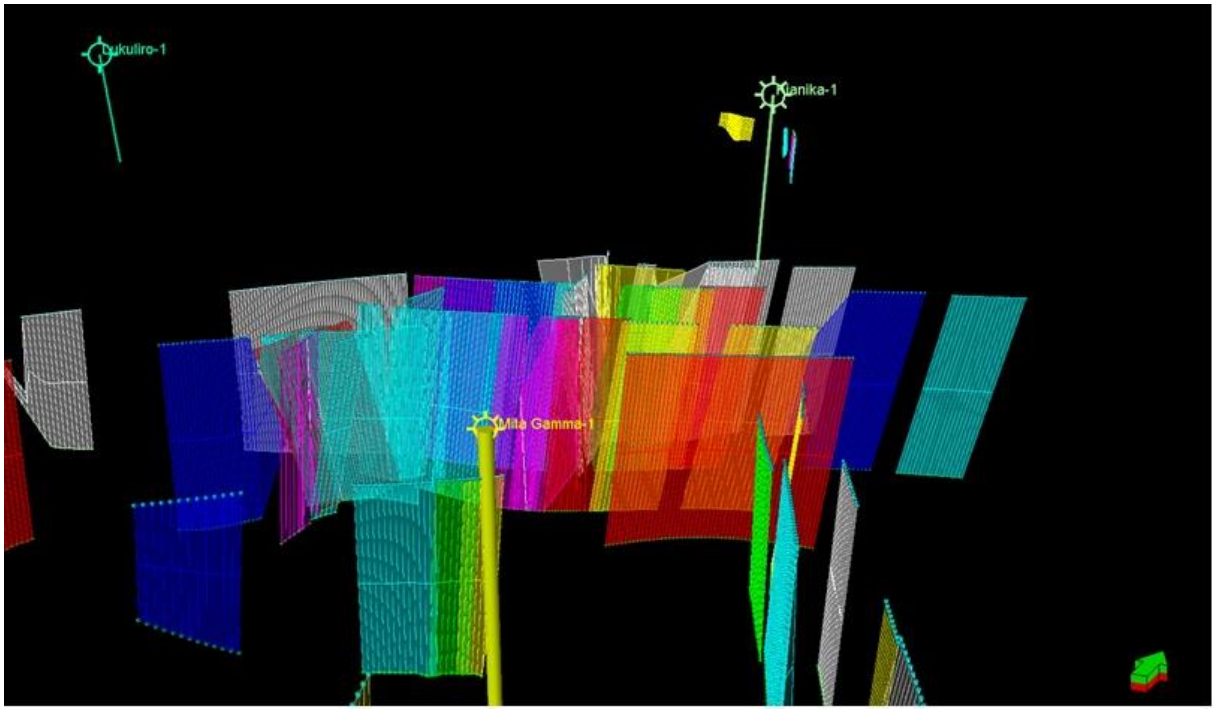

Figure 7.17 - Fault segments interpreted in central and south Mandawa Basin.

Three main trends have been addressed in the Mandawa area: NW-SE, NE-SW, and WNW-ESE (Hudson, 2011). On the 2D seismic lines, faults may have developed as distributed zones of discontinuous horizon reflectors. According to Mandawa Basin's history, the area presented significant structural challenges for fault interpretation (Figure 7.17). A number of faults in the central (Figure 7.18) and north Mandawa appeared to have extensional dominant structures in the Lower Jurassic that have had reactivated and inverted due to compression later during Pliocene (Nicholas *et al.*, 2007). The longest normal fault of sub-parallel, elongated geometry, north-south strike penetrated through the Jurassic strata and formed half-grabens and horst structures.

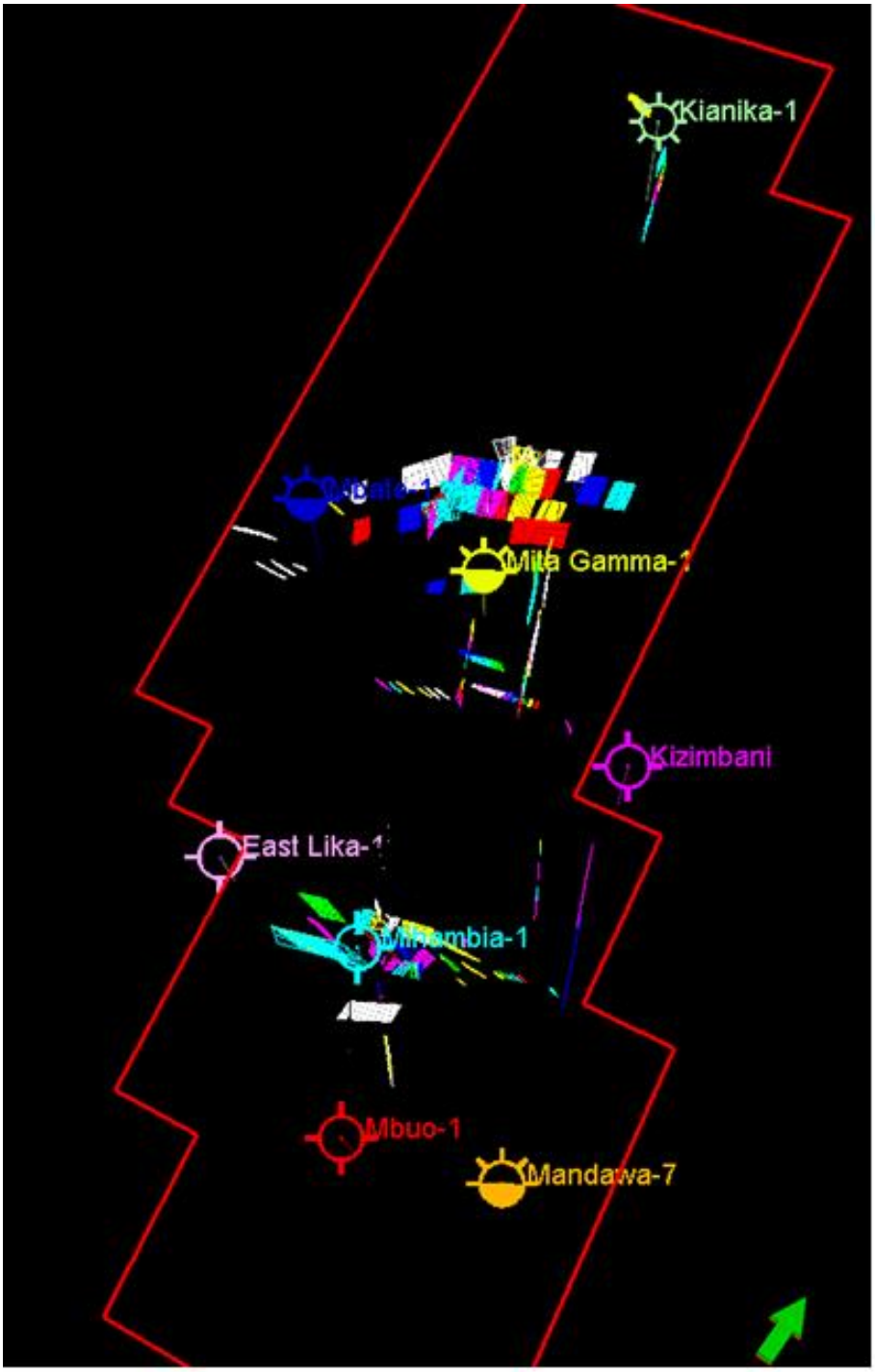

Figure 7.18 - The presence of major faults interpreted around Mihambia-1 well, Mita Gamma-1 and Mbate-1 wells.

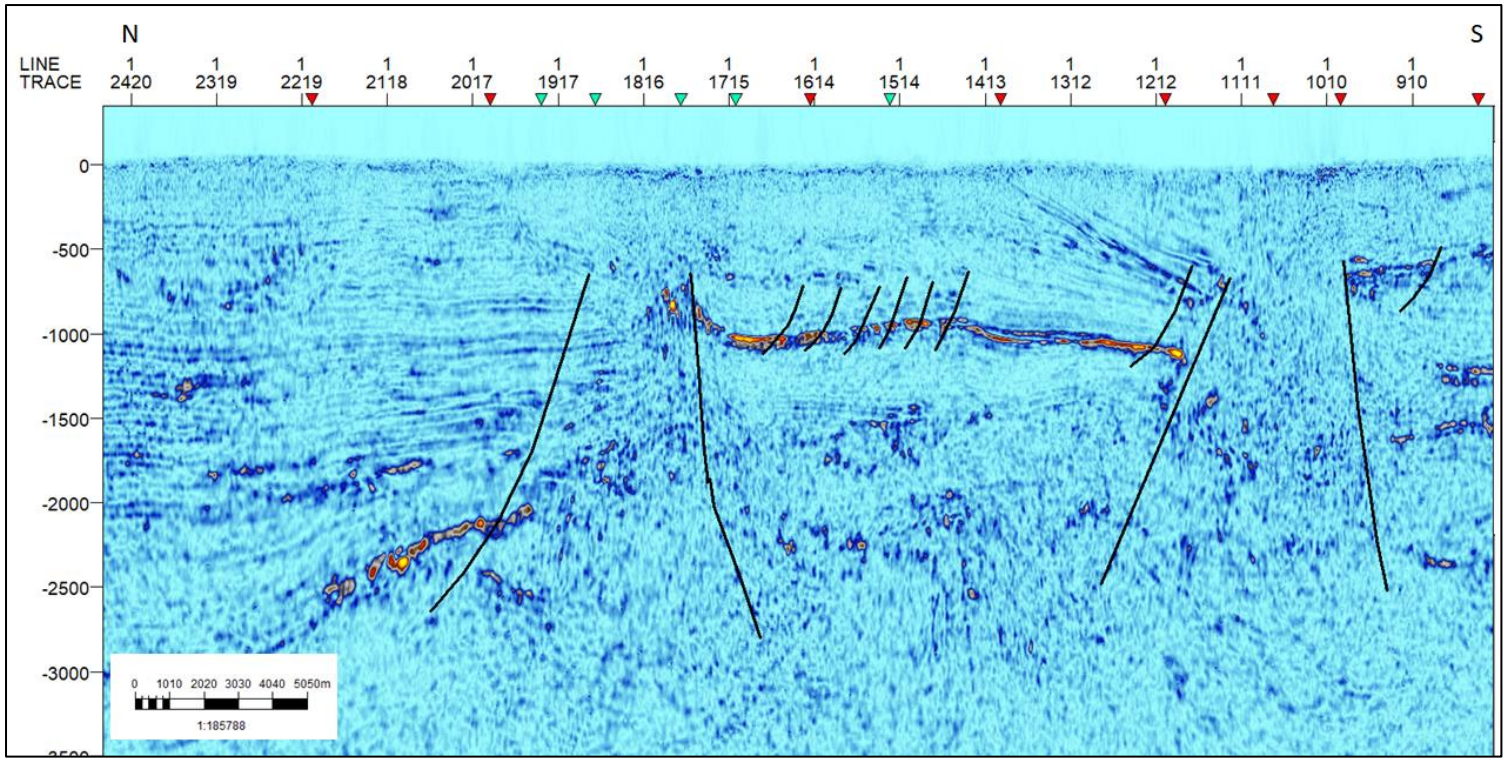

Figure 7.19 - Seismic attribute Sweetness in a composite line used to identify normal and reverse faults.

Compression that could have caused inversion can be seen in a number of places on the seismic lines (Figure 7.19), especially where the seismic horizons have buckled between faults. The surface topography has been interpreted as reflecting where inversion (reverse faulting) has taken place. Field relationships indicate that the magnitude of inversion displacement varies from around 60 m to 150 m. It is believed that the inversion most probably occurred during post Base Pliocene time. Similar pop-up structures have been described from further south on the Kilwa Peninsula (Nicholas *et al.*, 2007).

In addition, to reverse movement on faults, a number of open anticlinal structures have been identified in the seismic area of north Mandawa. They are indicated on the geological map by their fold axes and imply an NW-SE directed compression.

7.2.3 The Structural Framework Model Workflow

The initial step in building a computer model is the seismic interpretation-based structural modelling. The fundamental features of a structural model are the interpreted horizons and fault surfaces (Cosentino, 2001; Avseth *et al.*, 2005). In Petrel, the structural framework is a workflow that models and derived structural grids contain faults, horizons, and zones, which are structurally and stratigraphically consistently using the volume-based modeling (VBM) algorithm, which has an underlying tetrahedral mesh (Schlumberger, 2018).

A structural framework has been developed considering the processes in Petrel: Model Boundary, Fault Framework, Model Construction, Quality Check, and Model Refinement. The model boundary encompassed the lateral and vertical boundary of the model. A validated fault framework reinforces that the interpreted horizons are structurally and stratigraphically consistent in terms of geological principles.

The structural modeling starts building the horizon surfaces as a skeleton or frame for the model. The final product is a 3D structural grid surface. This interpretation contained basic geological information that has been in use to evaluate the model.

7.2.4 Model Boundary

The Model Boundary used was Mandawa's block area shapefile as a lateral boundary of the structural model volume of interest (VOI) and the fault framework as the vertical extent boundary (Figure 7.20).

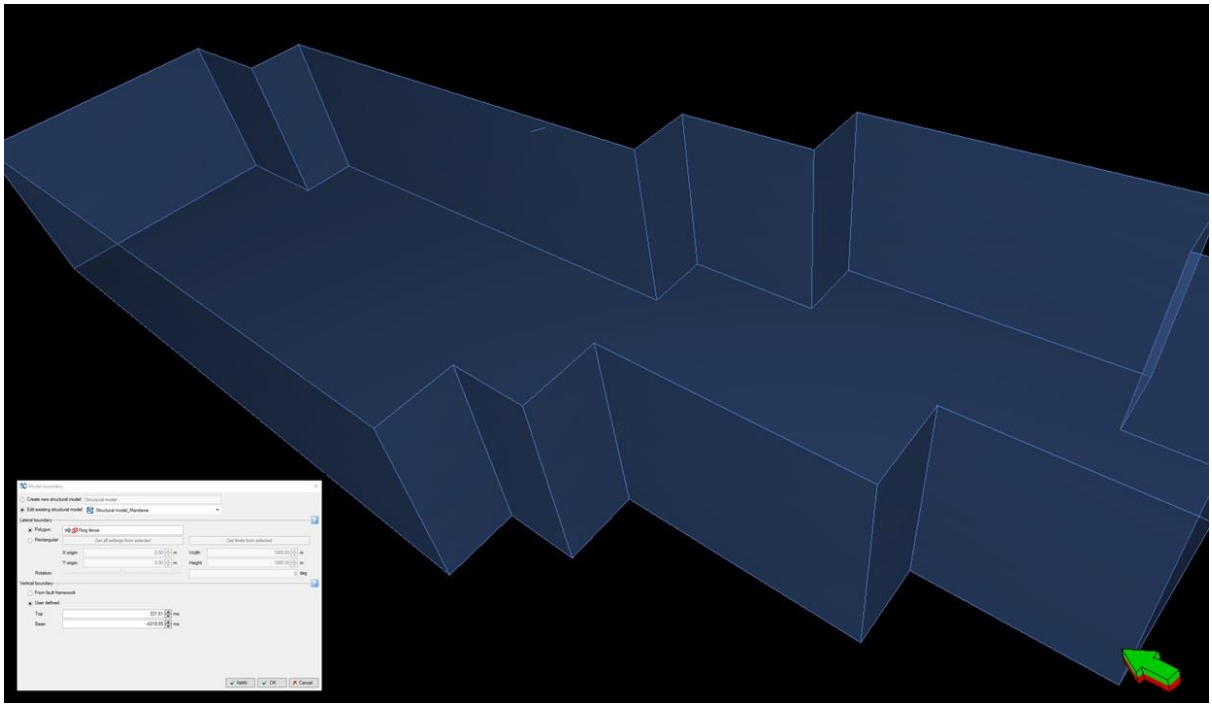

Figure 7.20 - Model boundary creation.

7.2.5 Fault Framework

The fault segments with the general striking NW-SE, NE-SW, and WNW-ESE are large enough with the throw enabling fault displacement served as the input in the Fault Framework. Seven fault relationships within major-minor fault truncation were established after the fault pairs have been verified in the quality check analysis.

The volume-based modeling algorithm has a specific fault displacement rule that only enables a large horizon displacement if the fault used is large enough to be consistent with the throw (Schlumberger, 2018). The overview of the process is shown in Figure 7.21. The dominance of salt diapirs in the southern part of the basin led faults to be dipping eastwards which is inferred to be the direction of basin extension.

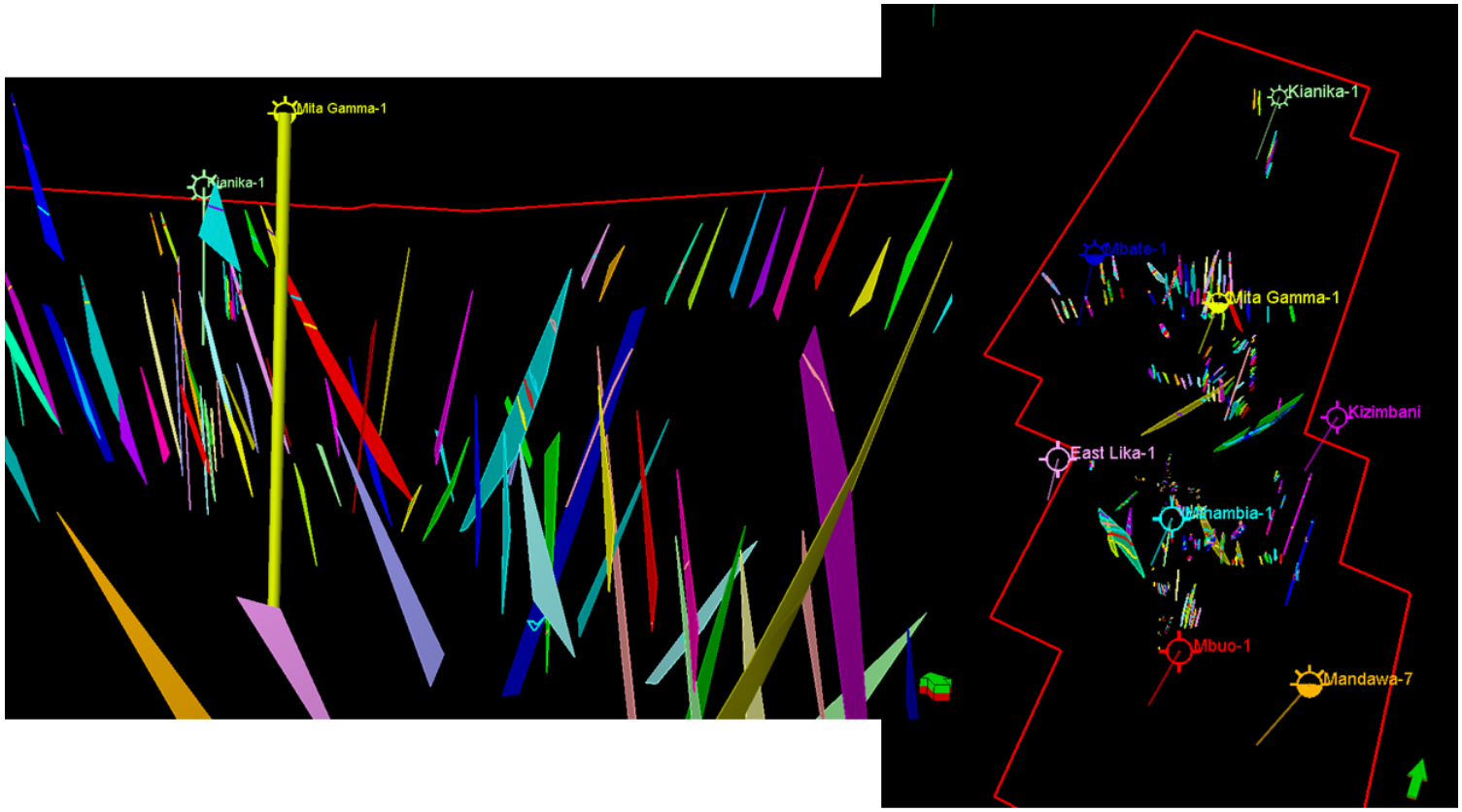

Figure 7.21 - Faults modelled using the Fault Framework process in Mandawa PSA.

7.2.6 Model Construction

The Model Construction is based on an unrefined structural modelled using the Volume-Base Modelling (VBM) algorithm (Schlumberger, 2018). The VBM is used to calculate the stratigraphic function adding well tops and thickness maps in TWT. Along with the model construction, a quality check of fault relationships and horizons was performed as the dataset provided had widely spaced 2D seismic lines.

The thickness maps (Figures 7.22, 7.23, 7.24, 7.25) as isochores have been created during this study and presented in this thesis to provide information on the vertical and lateral thickness of Mandawa Basin's sedimentary units, and their regional understanding and local tectonic setting. The isochores have been treated as an input to guide the modelling of the zones. This division separates zones of common heterogeneity interpreted if it is applied to a region/zone with similar geological patterns (Caers, 2005). Salt movement is characterised by an increase of thickness along the central part to the southern of the onshore basin.

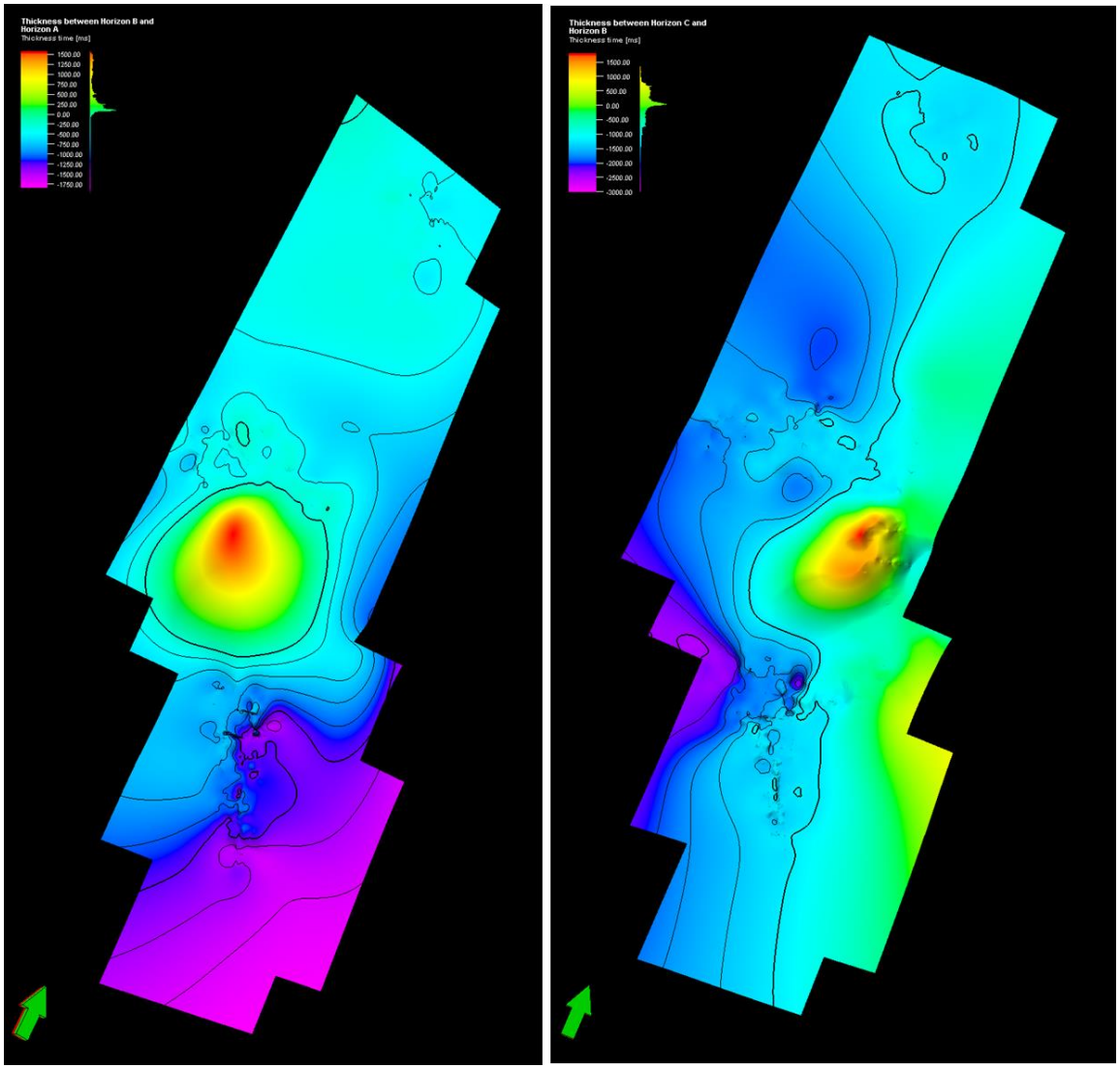

Figure 7.22 - Thickness maps between Horizon A and B (left) and Horizon B and C (right).

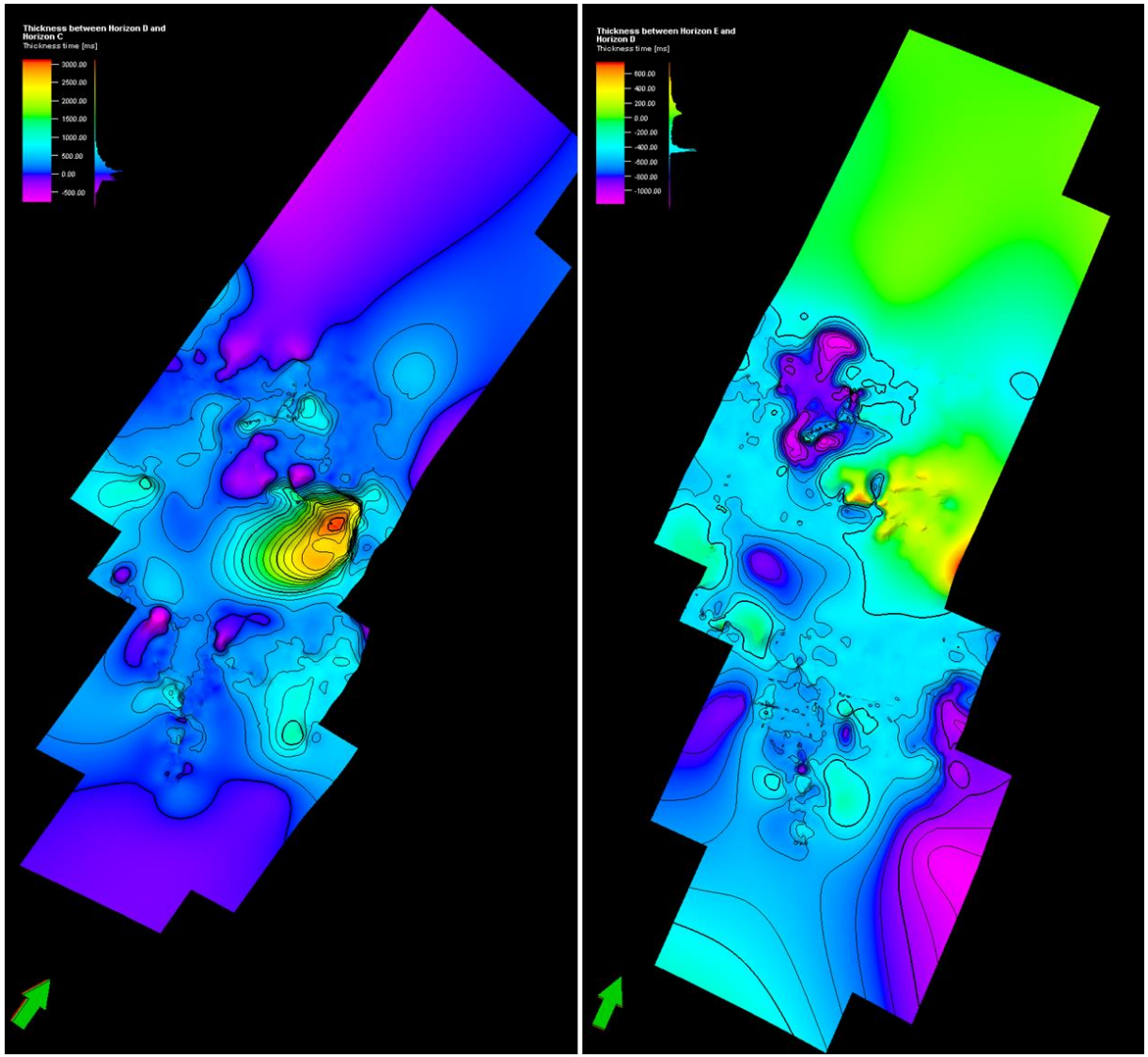

Figure 7.23 - Thickness maps between Horizon C and D (left) and Horizon D and E (right).

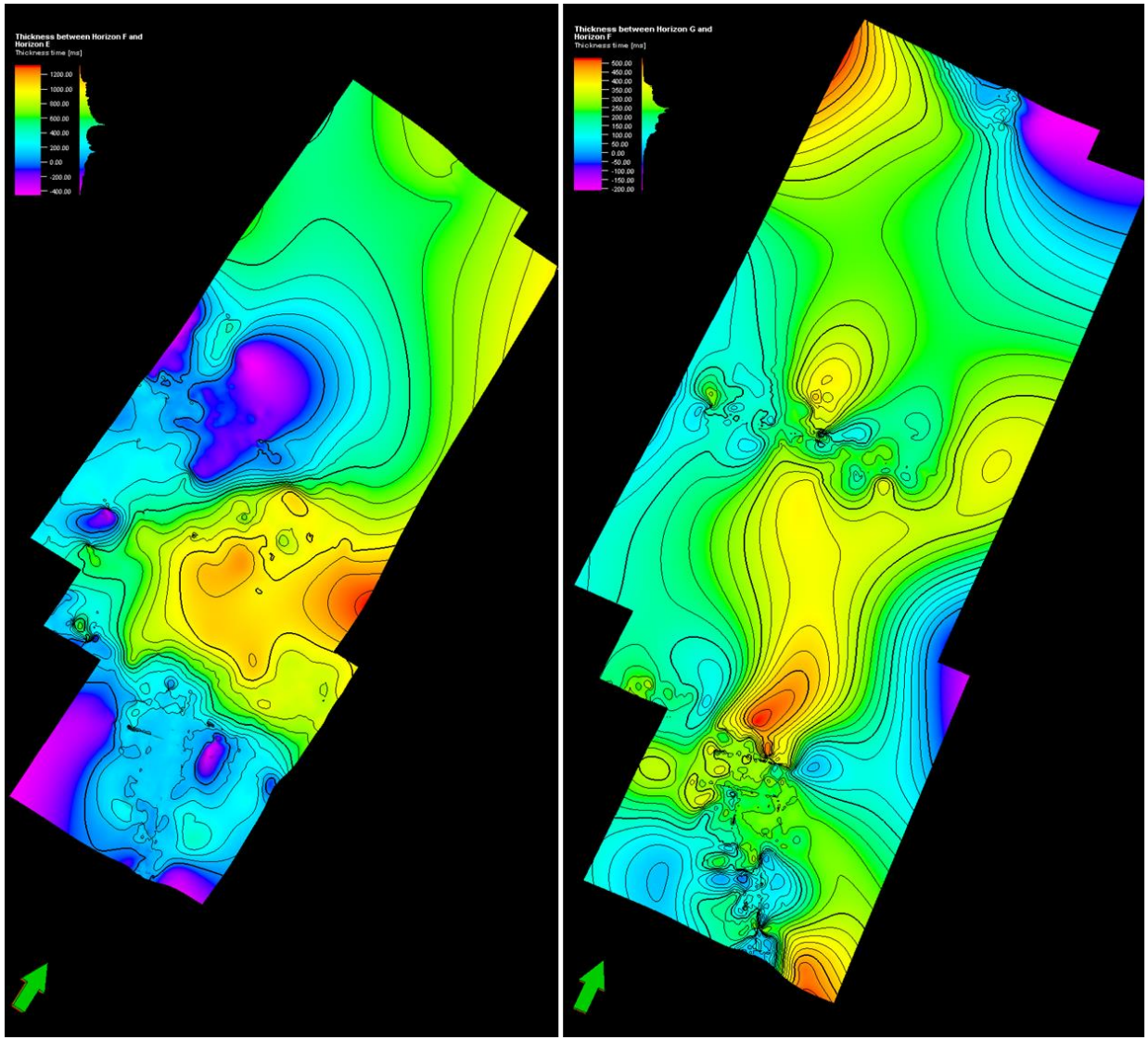

Figure 7.24 - Thickness maps between Horizon E and F (left) and Horizon F and G (right

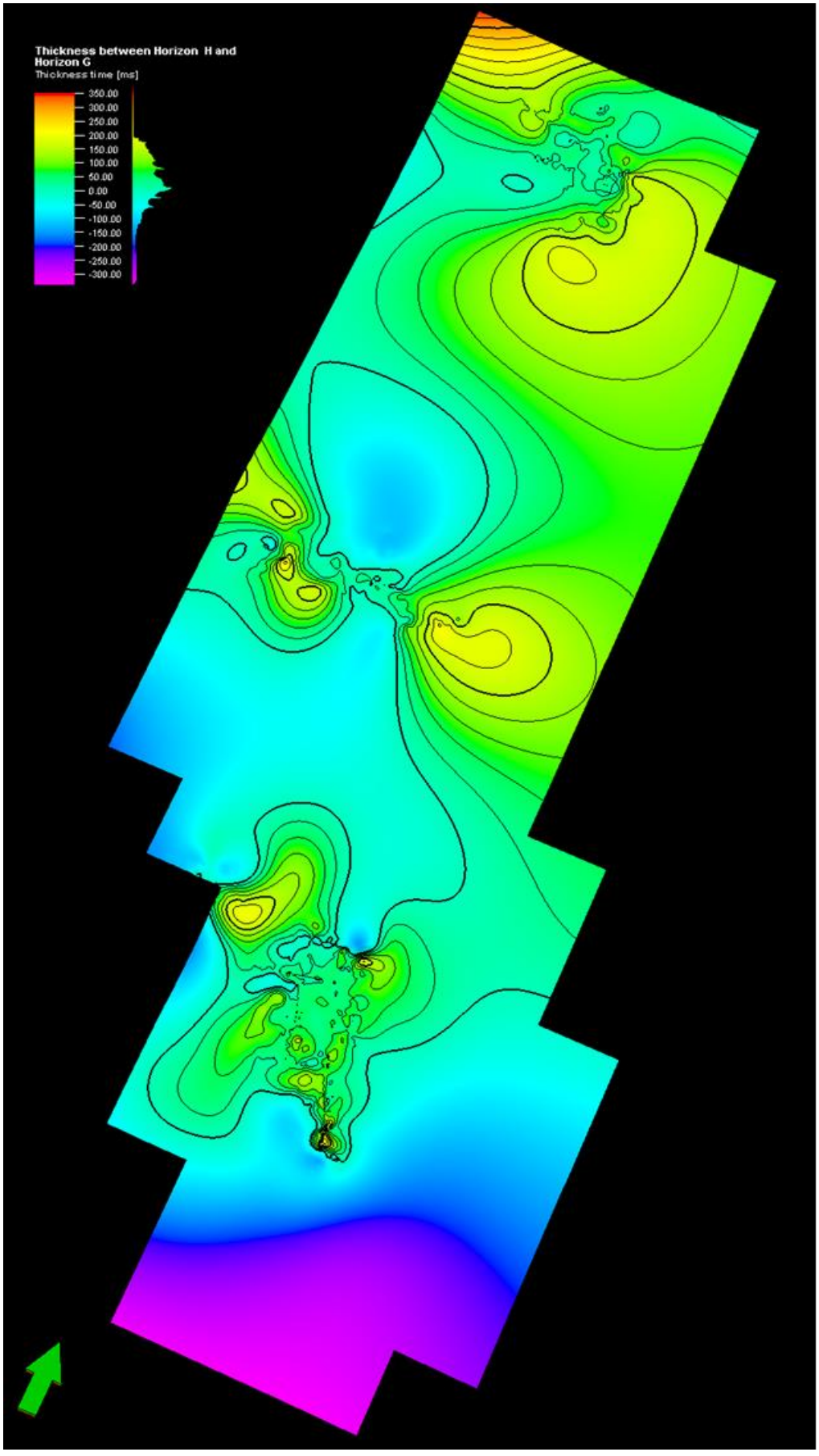

Figure 7.25 - Thickness map between Horizon G and H.

A number of modelled horizons were also constructed to view in detail the evolution of the sedimentary basin from the Precambrian/Cambrian basement to Lower Cretaceous. They were inserted into the 3D model, and the layer surfaces were projected and realized by block, used to show the fault displacement. The eight horizons were selected according to the stratigraphy section and imported into the Model Construction process, considering the fault modeling and quality check in the input data. The output of the process mentioned is shown below in the Figure 7.26 as a view from above; Figure 7.27 as a view southeast to northwest; Figure 7.28 view from west and Figure 7.29 view from the north.

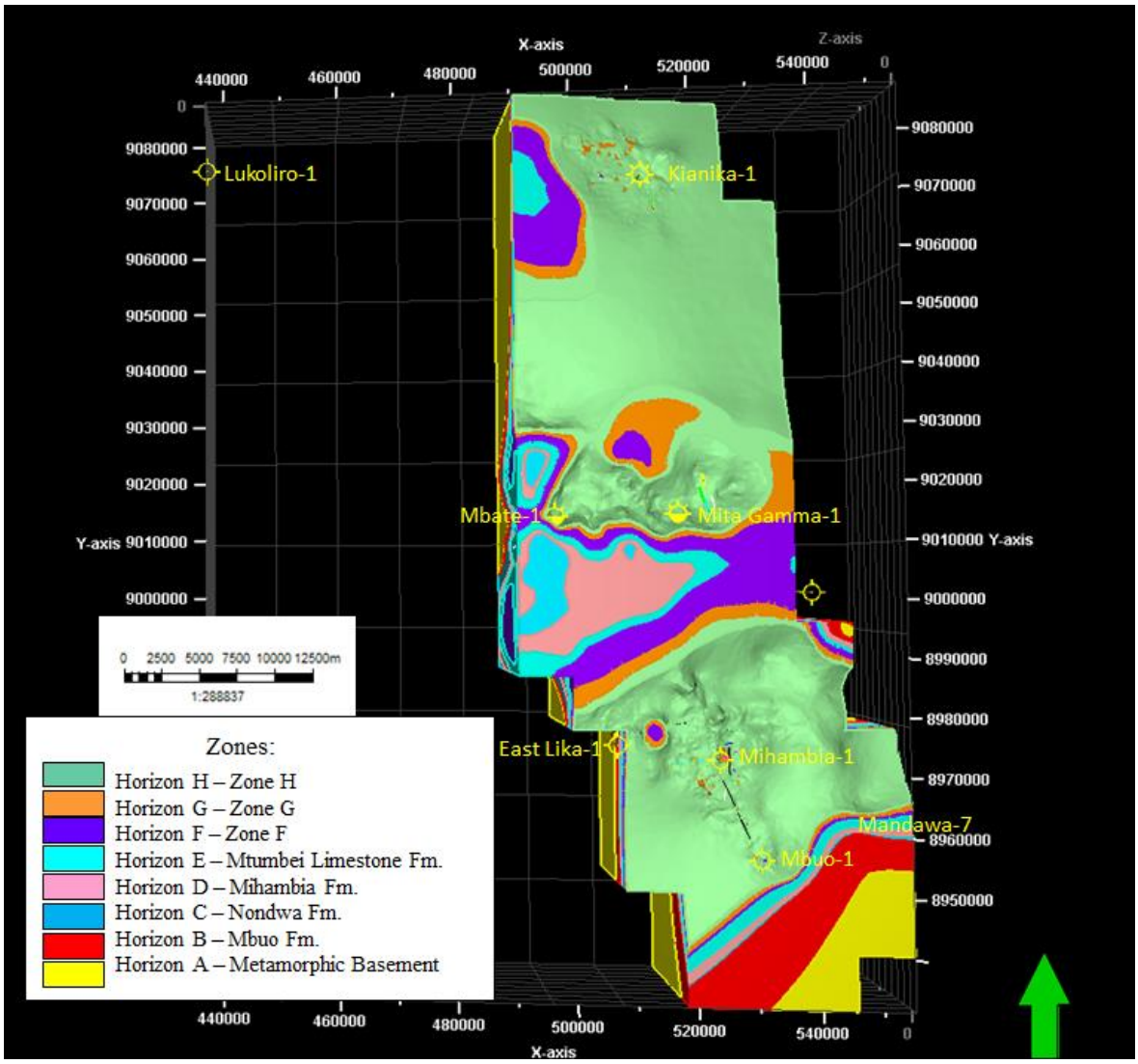

Figure 7.26 - Mandawa Basin model as a view from above according to the lithostratigraphic zones (identified in the Chapter 4) and drilled wells.

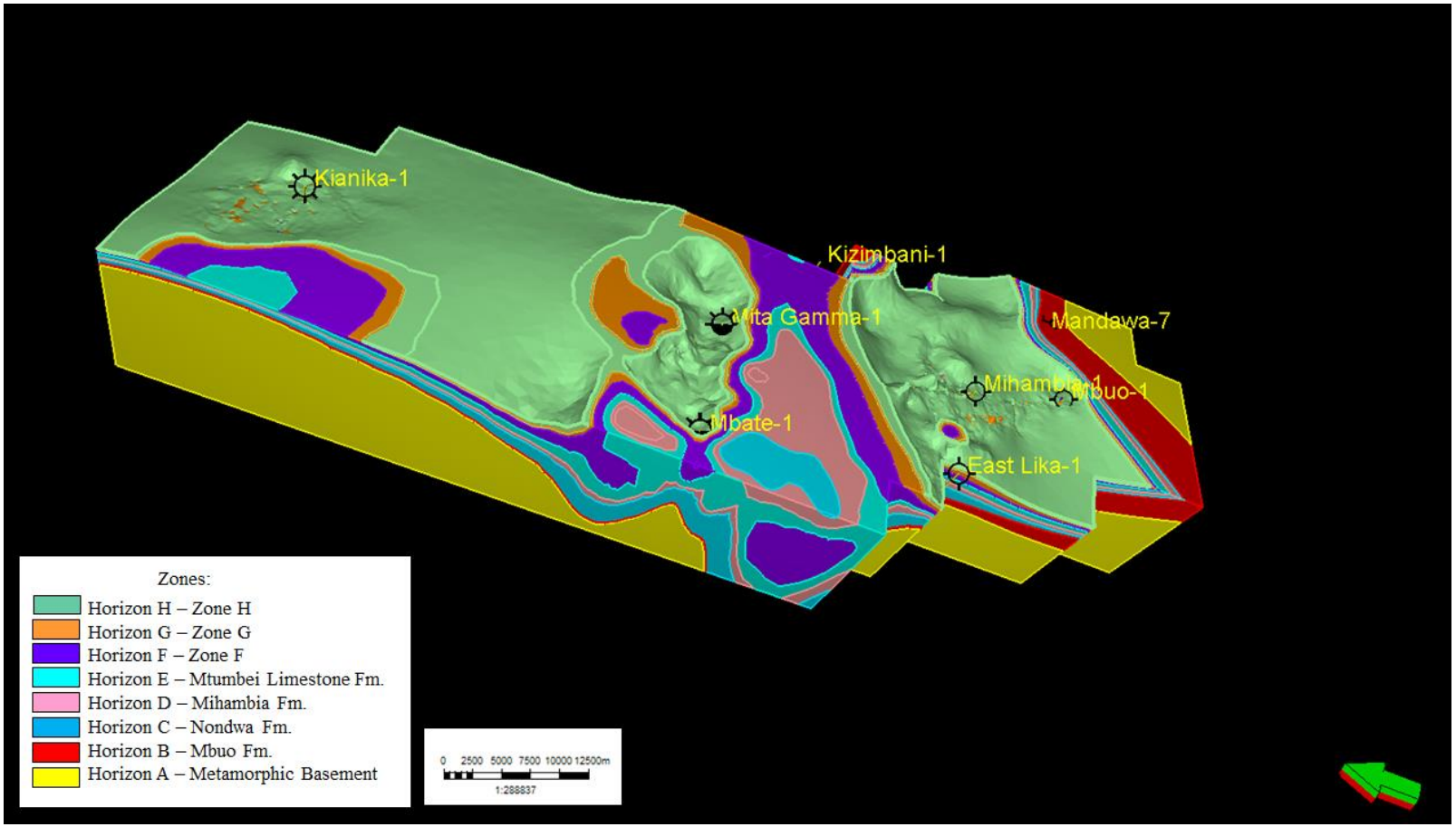

Figure 7.27 - Geological model of Mandawa Basinrefined in a south-north view.

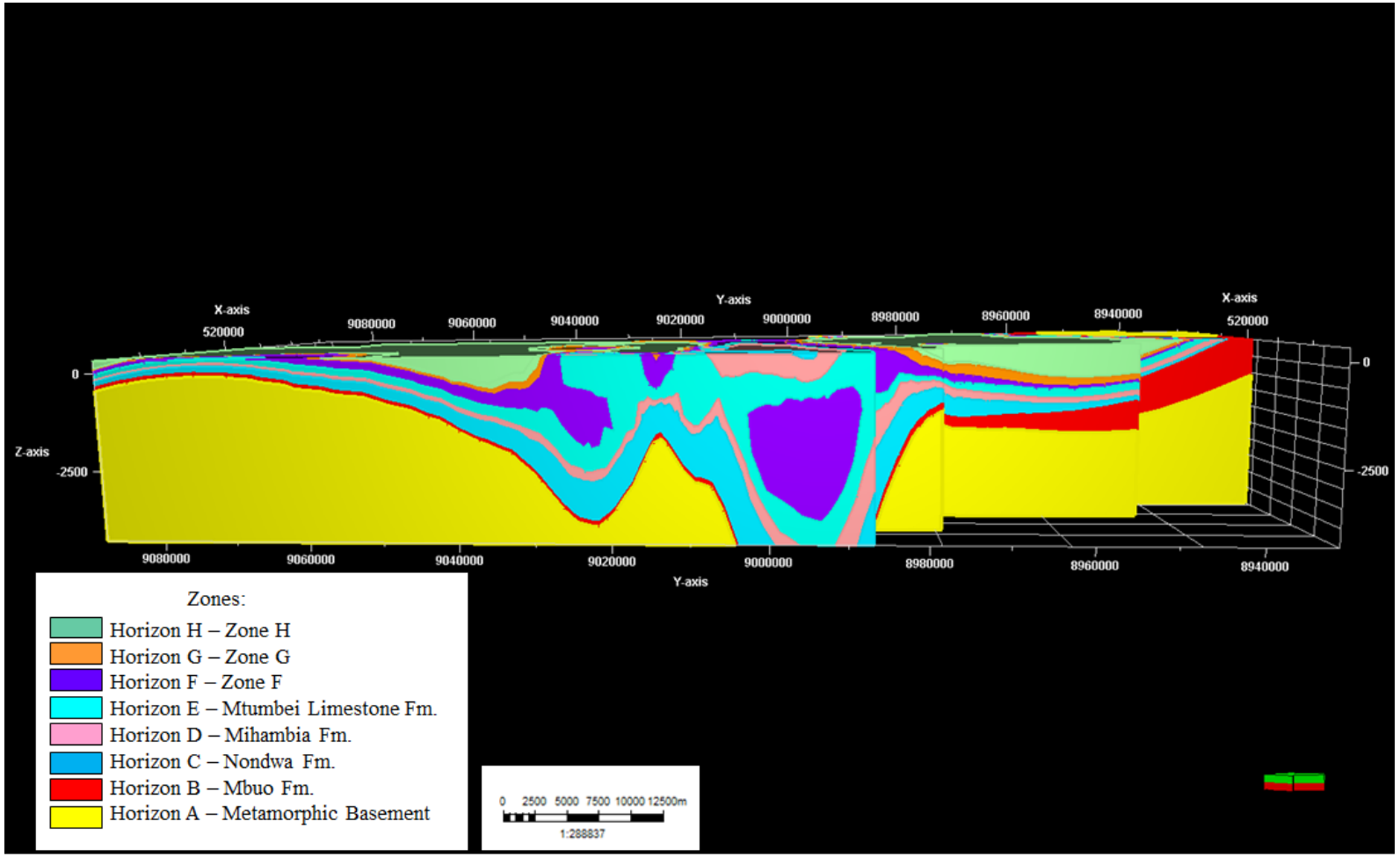

Figure 7.28 - Geological model of Mandawa Basin refined viewed from west.

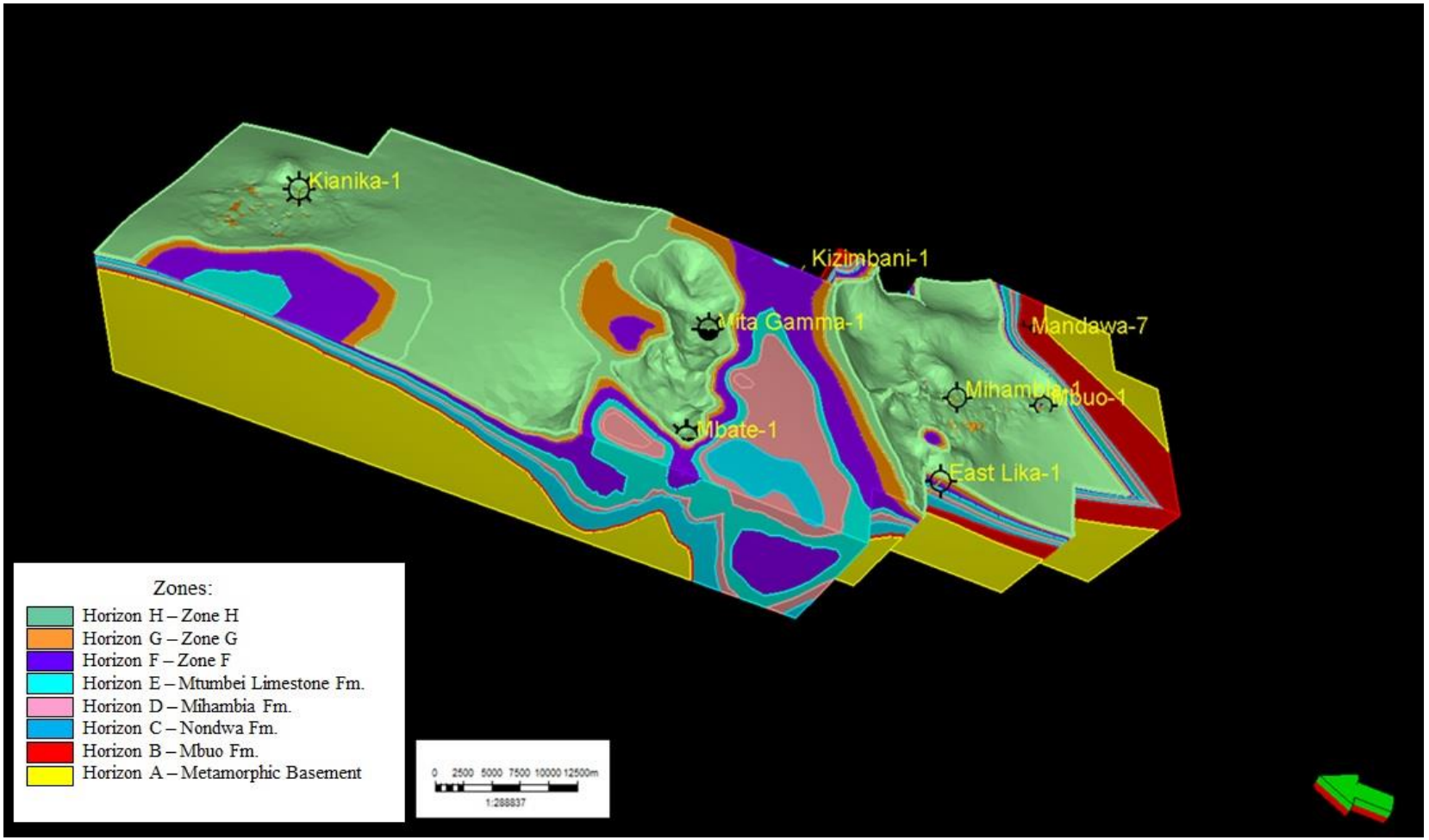

Figure 7.29 - Geological model of Mandawa Basin refined viewed from north.

Each modelled horizon was analysed separately to delineate the detailed structural and stratigraphical setting of the Mandawa Basin. Extensional block faulting – horst and graben formation – during the Cambrian - Lower Jurassic (Figure 7.30, Horizon A – Metamorphic Basement and Horizon B – Mbuo Formation). A stratigraphic pinch-out setting formed during restricted conditions triggered by the evolution of the mini-basin occurred approximately in the Middle Jurassic followed by a major Upper Jurassic transgression (Figure 7.31, Horizon C – Nondwa Formation and Horizon D – Mihambia Formation), corroborating with Hankel (1987), Veeken and Titov (1996) and Peel (2014) regarding restricted conditions, deposition of anoxic marine shale and locally evaporites of the mini-basin. The carbonate platform was extinguished by the progradation of marine siliciclastic sediments from the Upper Jurassic - Lower Cretaceous sequence boundary (Figure 7.32, Horizon E – Mtumbei Limestone Formation and Horizon F – Zone F). Rifts and inversion were active during the Lower Cretaceous (Macgregor, 2017) as the depositional environment suggested a deltaic – fluvio-marine clastic progradation followed by successions of shallow marine clastic sediments and inverse faults (Figure 7.33, Horizon G – Zone G and Horizon H – Zone H).

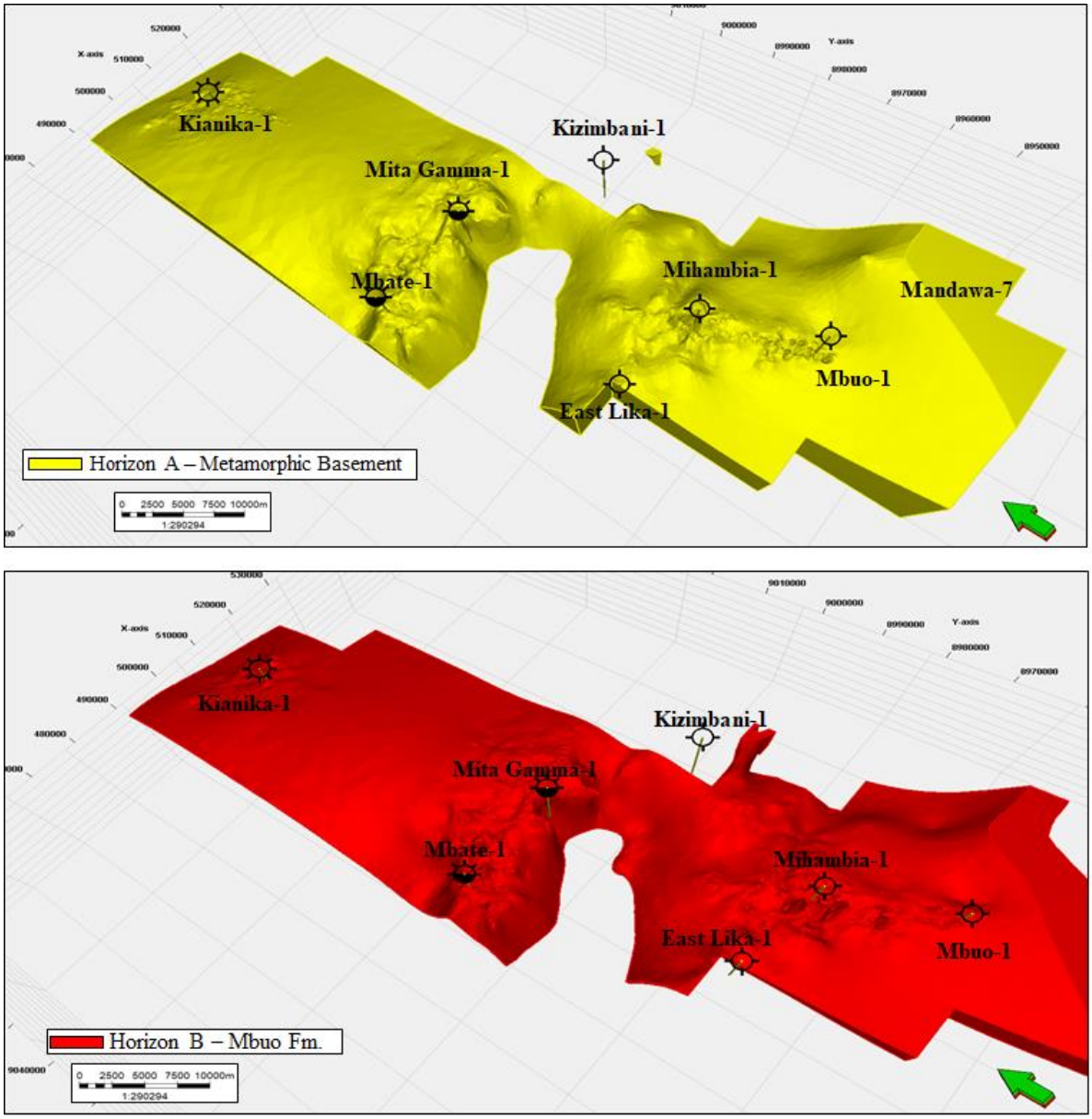

Figure 7.30 - Modelled Horizon A – Metamorphic Basement in yellow (top) and Horizon B – Mbuo Formation in red (base).

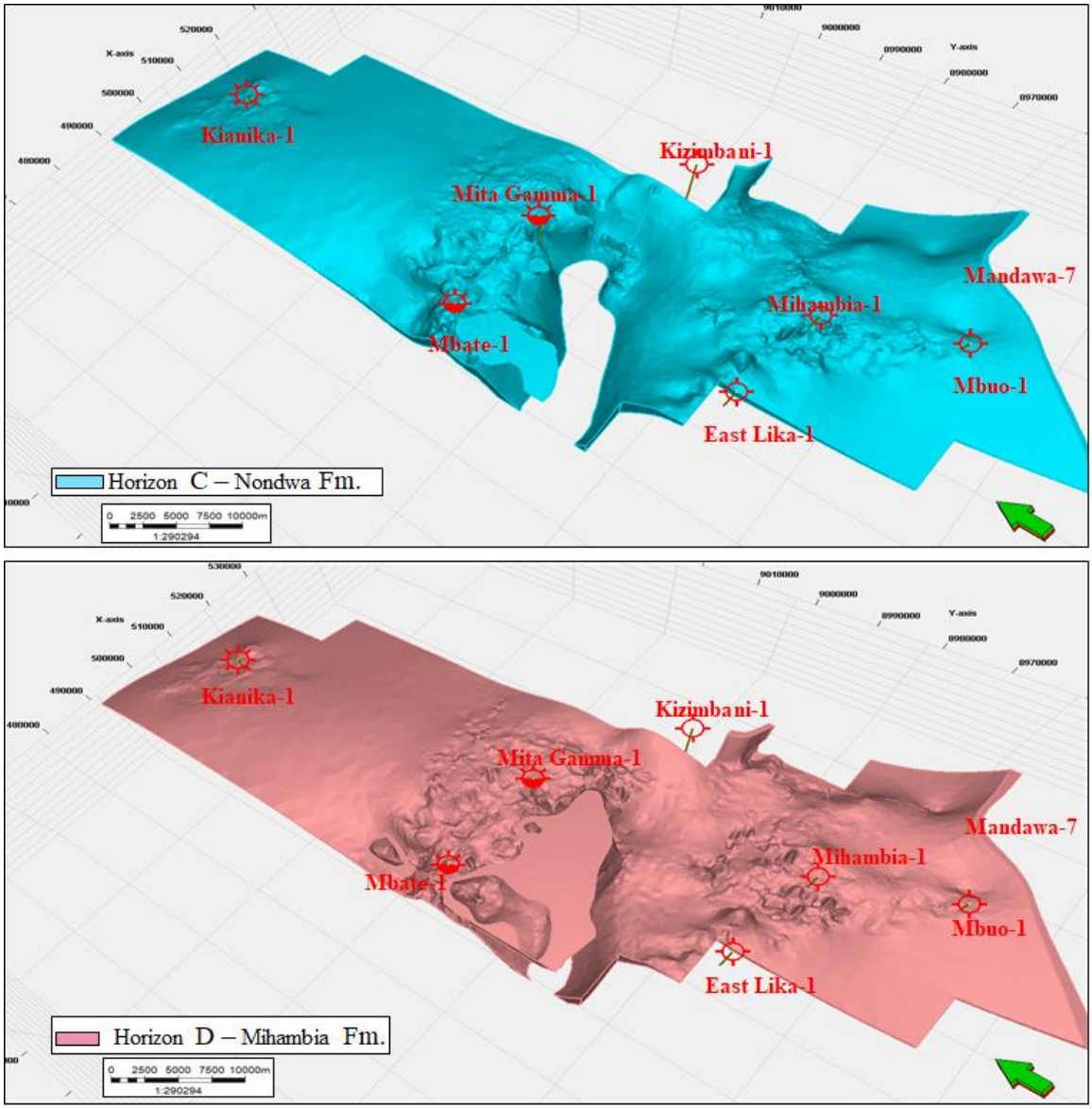

Figure 7.31 - Modelled Horizon C – Nondwa Formation in blue (top) and Horizon D – Mihambia Formation in pink (base).

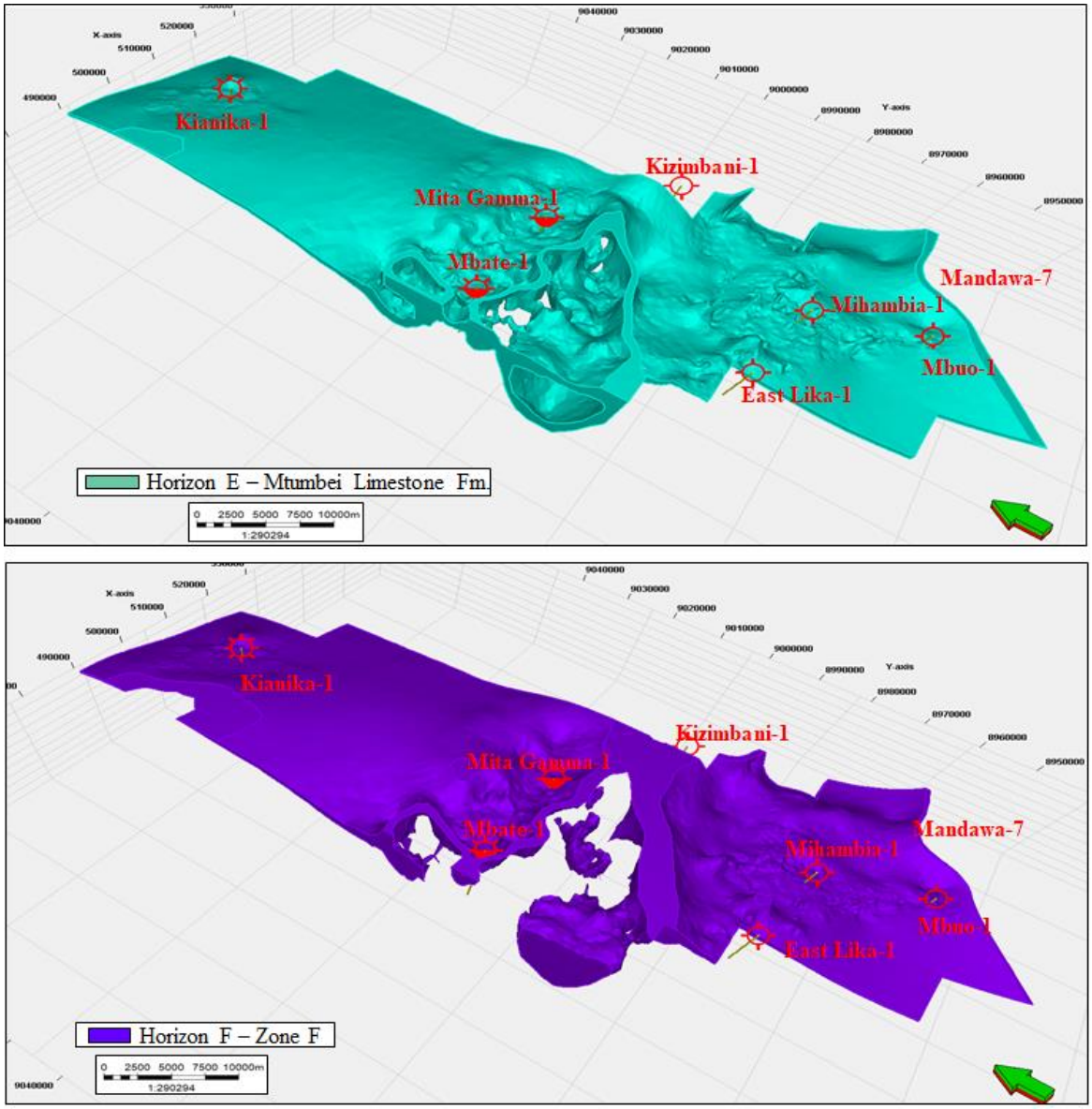

Figure 7.32 - Modelled Horizon E – Mtumbei Limestone in green (top) and Horizon F – Zone F in purple (base).

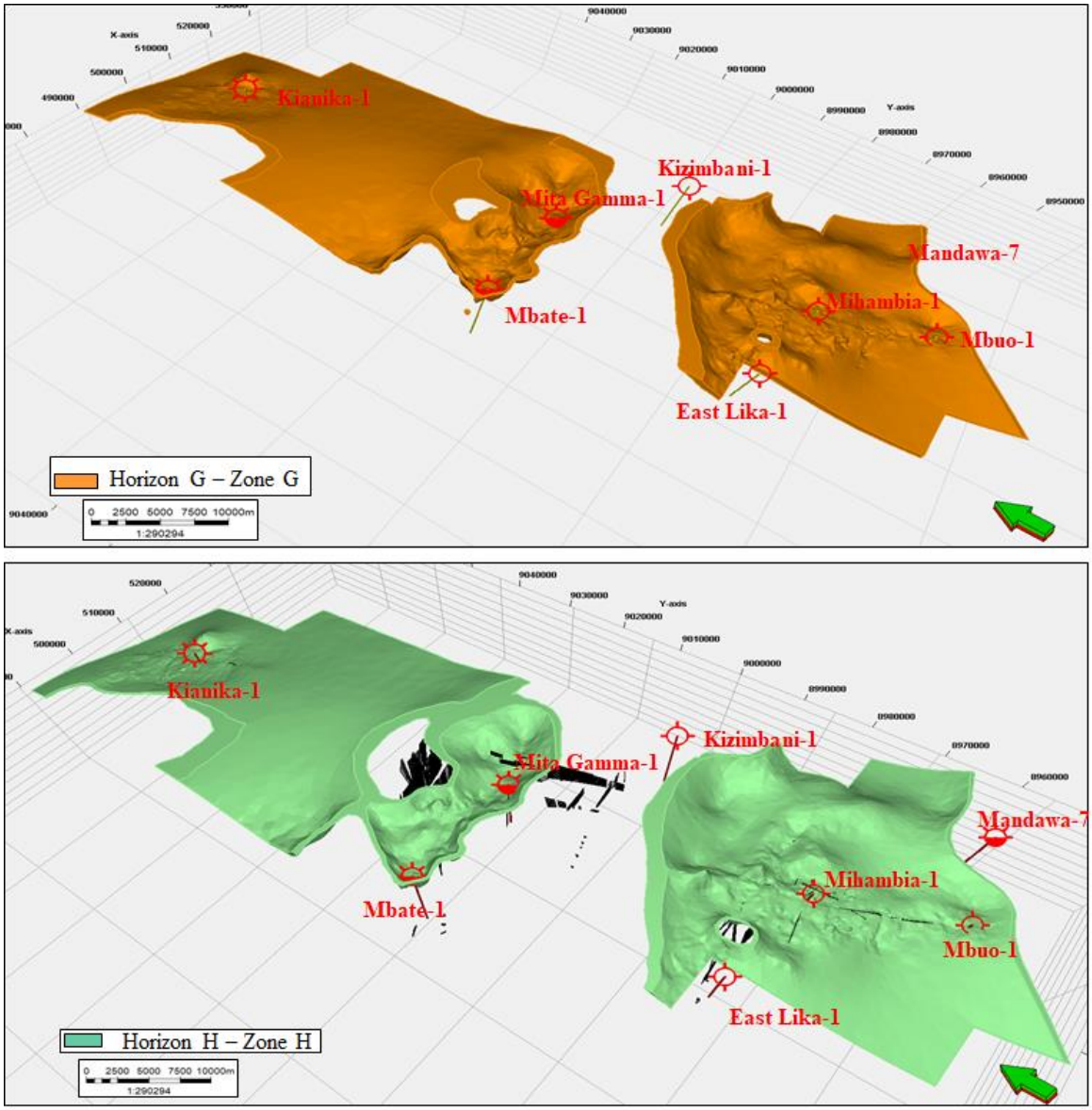

Figure 7.33 - Modelled Horizon G – Zone G in orange (top) and Horizon H – Zone H in green (base).

7.2.7 Model refinement

The model refinement gathered post-processing the model horizons produced by the volume-based modelling algorithm. The stratigraphic function created using volume-based modelling (VBM) presents smooth trends that approximate the horizon input data. Therefore, the unrefined model horizons extracted from the stratigraphic function might not fit the horizon input data points. The lacking fit is recovered in the subsequent Model refinement process (Schlumberger, 2018). The refinement of the model horizons involves a re-meshing step, a data fitting step, and a smoothing operation.

The final result was a 3D structural model constructed with 1281 m in i x 313 m in j x 8 m in k grid cells, separated into eight horizons and seven zones where 100 fault surfaces, horizons have been modelled and displayed. The model is configured with approximately 3 million cells with 50 m x 50 m grid increments with conformable horizon rule where horizons were truncated as erosional, discontinuous, or base. The horizontal extent of the 3D model is limited in 15,6 km x 5 km from - 3000 milliseconds to - 420 milliseconds. The main orientation of the axis was defined as the NE - SW trend. The faults that delimit the compartments of the Lower Jurassic extension are described as normal faults that formed horsts, grabens, and half-grabens whilst the faults from Lower Cretaceous were interpreted as reverse faults.

7.3 SIMPLE MODEL WITHOUT FAULTS

An alternative model of the Mandawa Basin has been created in time (milliseconds) using the Make simple grid process in Petrel with no faults (Figure 7.34). The aim of the model was to have a preview of how surfaces would correspond accordingly to stratigraphic rules for horizons as conformable, erosional, discontinuous, and base. As a simple forward-modelling grid, the absence of honoring simple stratigraphical and structural mechanism, this model was limited to indicate salt movement in Mandawa Basin compared to the structural 3D model workflow suggested in this thesis (Figure 7.35).

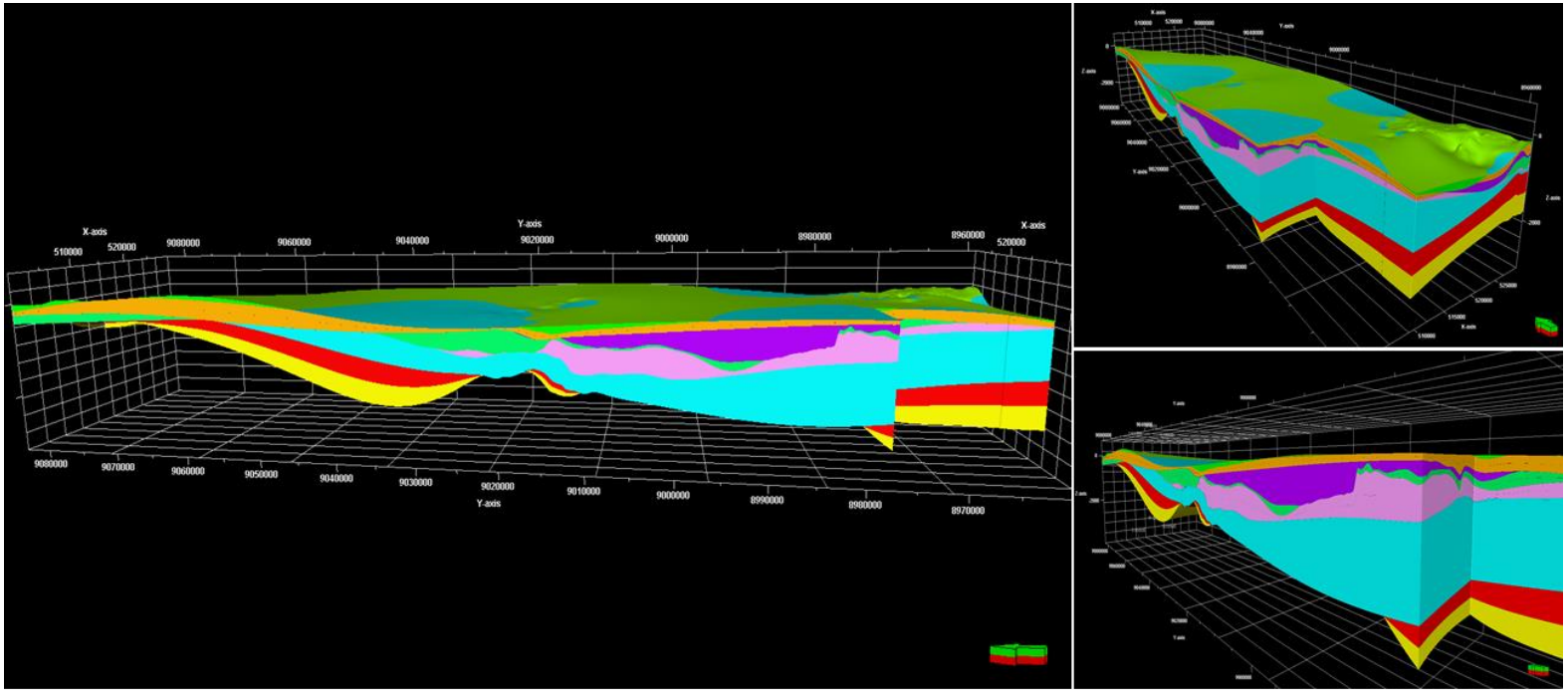

Figure 7.34 - Model constructed without faults visualization with the horizons tended not to follow stratigraphical rules.

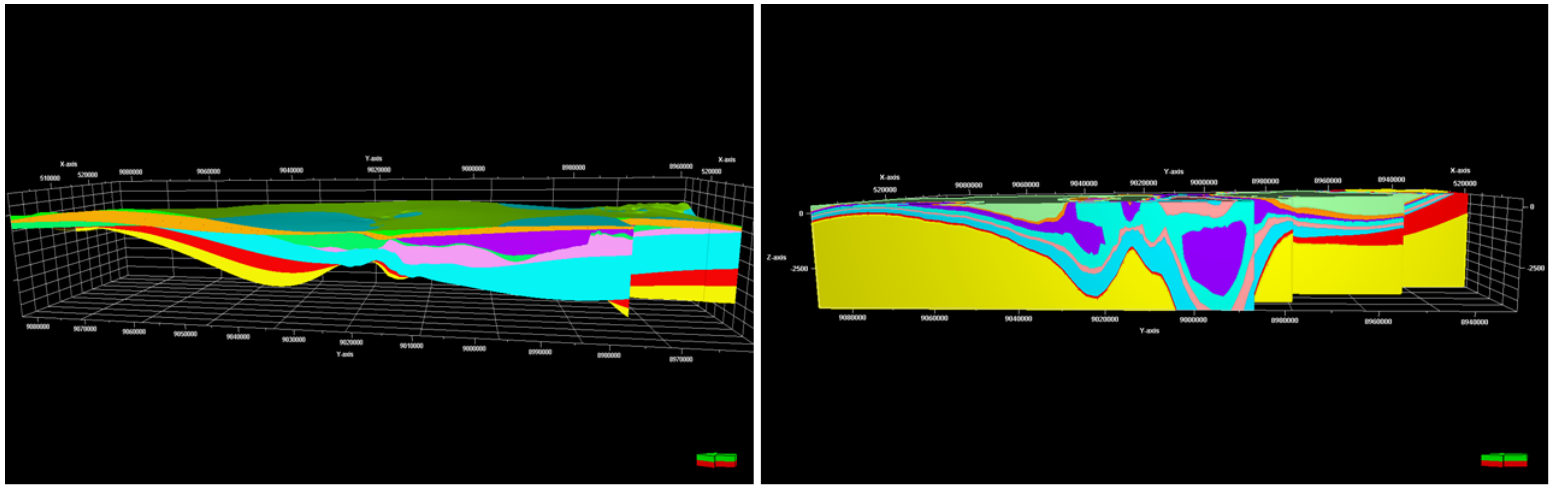

Figure 7.35 - A comparison of the model without faults (left) and the model created using the structural framework (right) displaying structural mechanisms of extension in the basin.

7.5 VELOCITY MODEL AND DEPTH CONVERSION

Different approaches can be used in the generation of different velocity models such as stacking, RMS, migration, and well velocity (Gadallah, 1994). A seismic velocity model encompasses of mapping the depth and thickness of subsurface layers originally interpreted from seismic reflectors. Admitting that velocity varies within the subsurface and sediment compaction increases with depth, the uncertainty for depth conversion process can be complex taking into account fault analysis, salt tectonics, dip, and azimuth of sediment layers and burial history of the basin. The workflow (figure 7.36) used to prepare the seismic velocity model consists of quality check the interval velocity versus depth, display wells with interval velocity in a cross-section for comparison, a velocity map and the velocity model, and depth conversion.

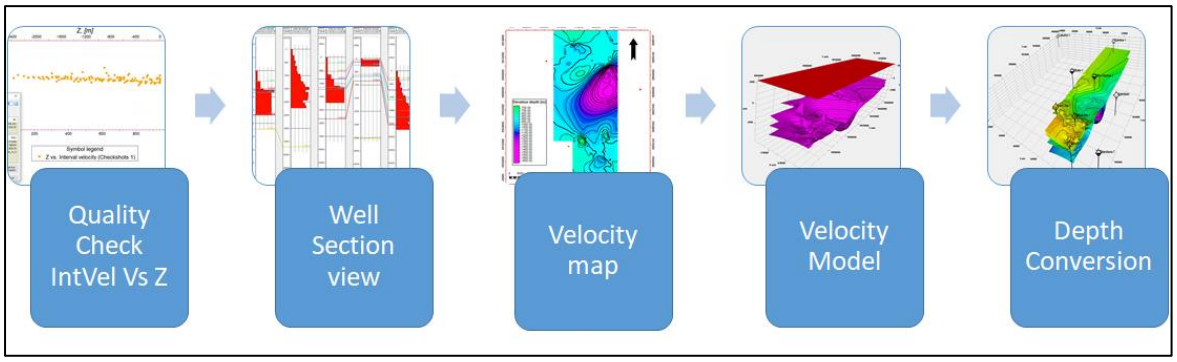

Figure 7.36 - Workflow for the seismic velocity model created in Petrel software.

In this research, the information about the interval velocity is limited to the Jurassic - Cretaceous sequence in the Mandawa Basin due to the limited frequency content and the data resolution of the interpreted horizons, in particular, the top and base of salt whether is susceptible in areas where a combination of resolution and distortions due to the structural framework of the minibasin.

The regional velocity model was developed based on the 2D seismic line DOM-06-MIH-04 (Figure 7.37). Figure 7.38 has shown the checkshot information as interval velocities versus depth for Mihambia-1 well. The interpretation consisting of the Metamorphic Basement (Horizon A), Mbuo Fm. (Horizon B), Nondwa Fm. (Horizon C), Mihambia Fm. (Horizon D), Mtumbei Limestone Fm. (Horizon E), Horizon F, Horizon G, and Horizon H have been tied to wells Mihambia-1, East Lika-1, Mita Gamma-1, Kianika-1 and Lukoliro-1 with previous checkshot calibration of sonic logs (Δt) (Appendix 7.5) via the 2D seismic lines DOM-06-MIH-04, TLVB-157_d, 99MW-4_d and 83-SE-46

respectively. The velocity analysis took potential lateral velocity variations where the interval velocity for Zone B - Mbuo Fm. is relatively high (+/- 4,000 ms), while speeds in Zone C - Mihambia Fm. overlapping speeds are even higher (+/- 4,900 ms). Slower velocities were noted in the reflectors at the top of Zone C - Nondwa Formation however the IntVel x Depth in Mandawa Basin function is suggested of no correlation as evaporites do not compact. Assuming the stacking velocities to be true root-mean-square in the surroundings of Mihambia-1 well, they were then converted to internal velocities using Dix equation (Dix, 1955):

$$Vint = [(t2\ VRMS22 - t1\ VRMS12) / (t2 - t1)]1/2$$

Where:

Vint = interval velocity

t1 = travel time to the first reflector

t2 = travel lime to the second reflector

VRMS1 = root-mean-square velocity to the first reflector

VRMS2 = root-mean-square velocity to the second reflector.

The time-depth conversion process was limited to a layer cake model vertical made based on seismic velocity data and calibrated to the well data available and using the upscaling the internal velocities from wells Mihambia-1, Mita Gamma-1, Lukoliro-1 and Kianika-1 were analyzed, interpolated the upscaled data in order to evaluate the sensitivity of the structures (zones) according to the checkshot, calibrated sonic profile, for scoping analysis of a 2D seismic line used in the synthetic seismogram, speed contrasts in order to convert the time grid zones of the main velocity horizons to depth giving continuity to structural modelling. Due to lack of well data with checkshot across the block in Mandawa, the depth conversion uncertainty is considerable suggesting that layers resulted in a constant interval velocity (Figure 7.39) apart from the salt structures where high velocities are encountered and estimated salt velocity of 2500 ms was assigned. Figures 7.40 and 7.41 are shown as the final 3D structural map in depth (m), where most of the siliciclastic layers preserved the thickness in time and depth domains.

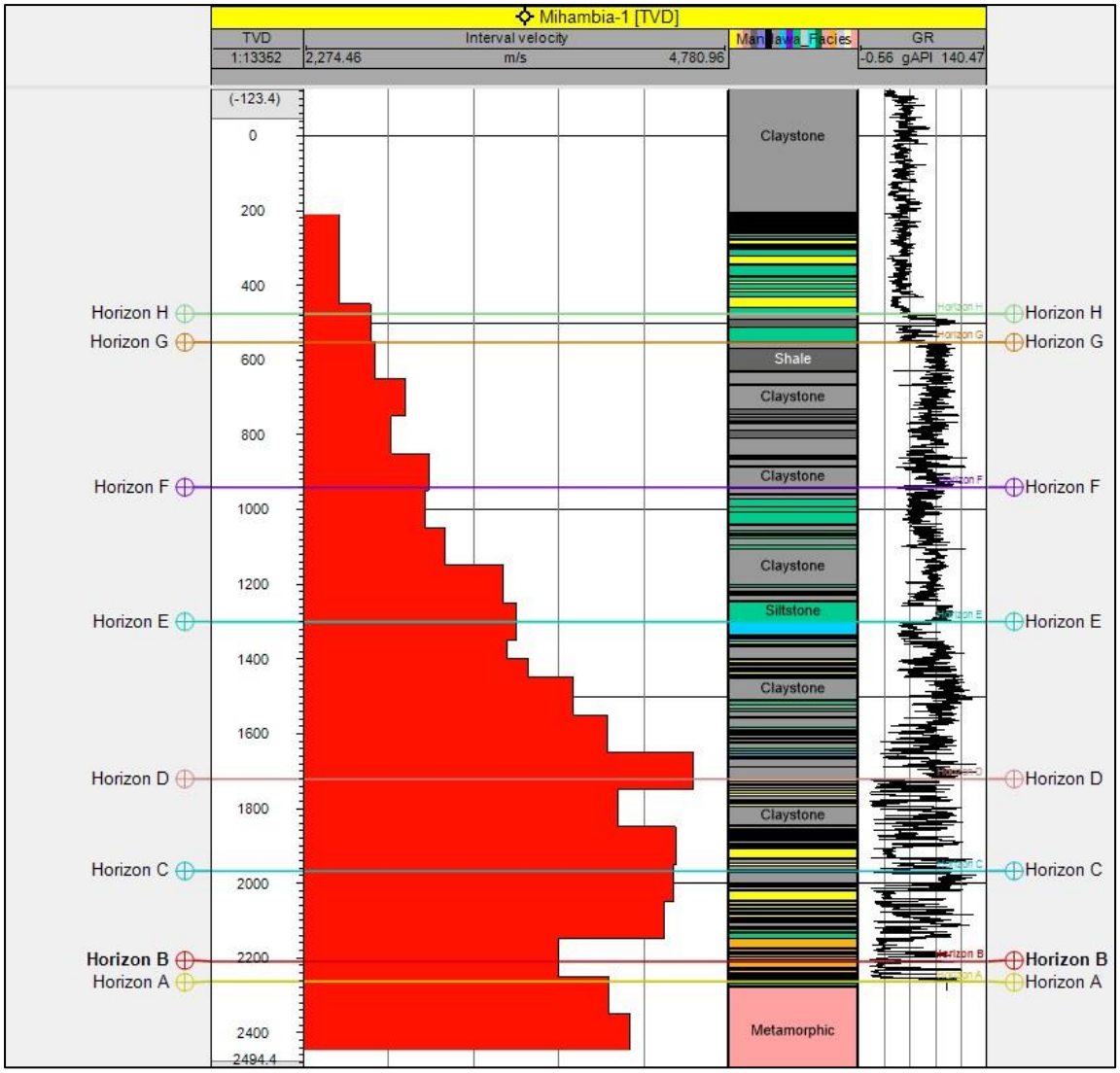

Figure 7.37 - Internal Velocity (in red rectangles) of Mihambia-1 well in a cross-section with the associated facies, geological markers, and GR well log.

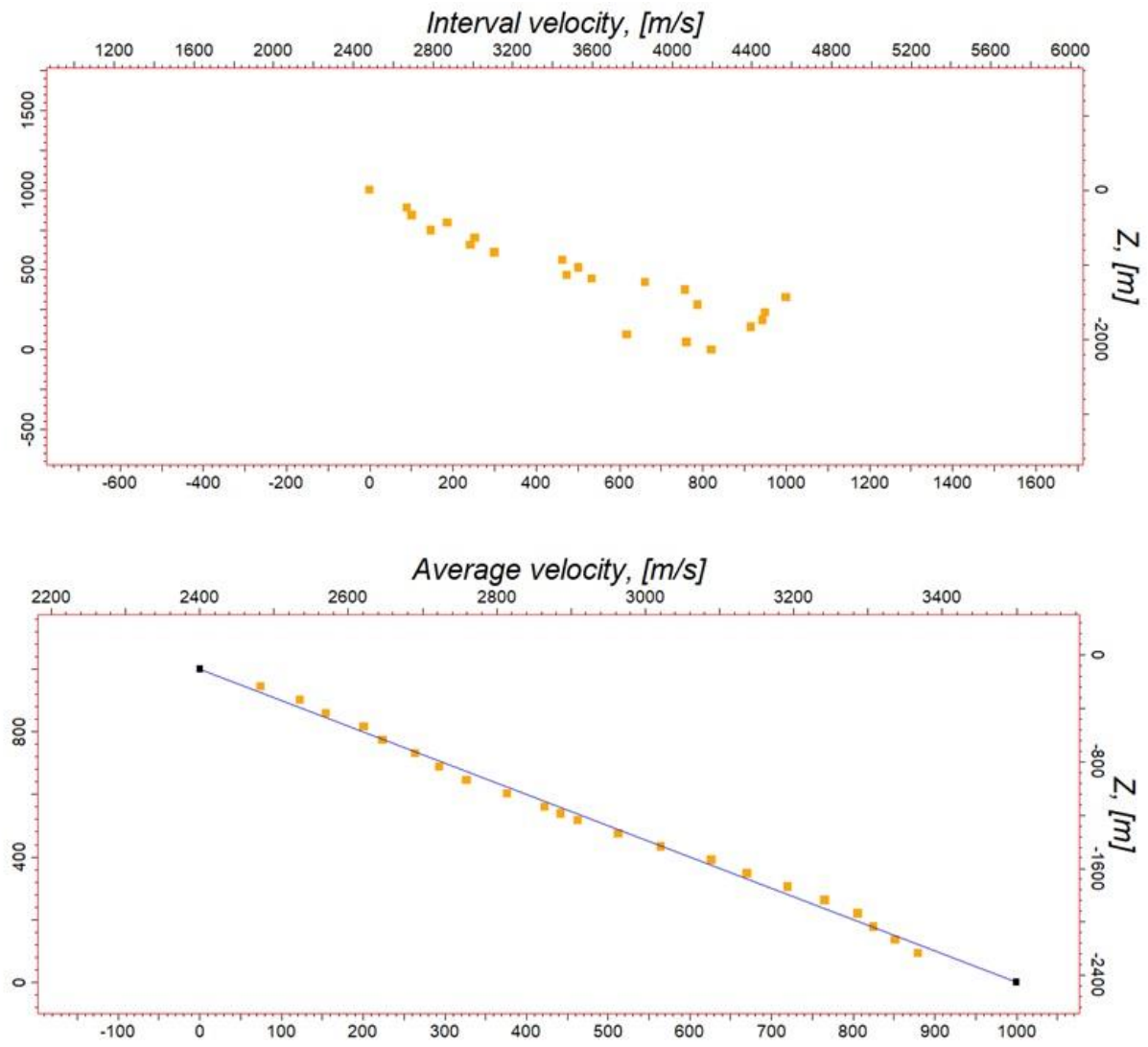

Figure 7.38 - Crossplot of interval velocities vs. depth (Z) from Mihambia-1 showing scattered interval velocities (left). Average velocities vs. depth from Mihambia-1 well (right). Both crossplots present an inverse correlation.

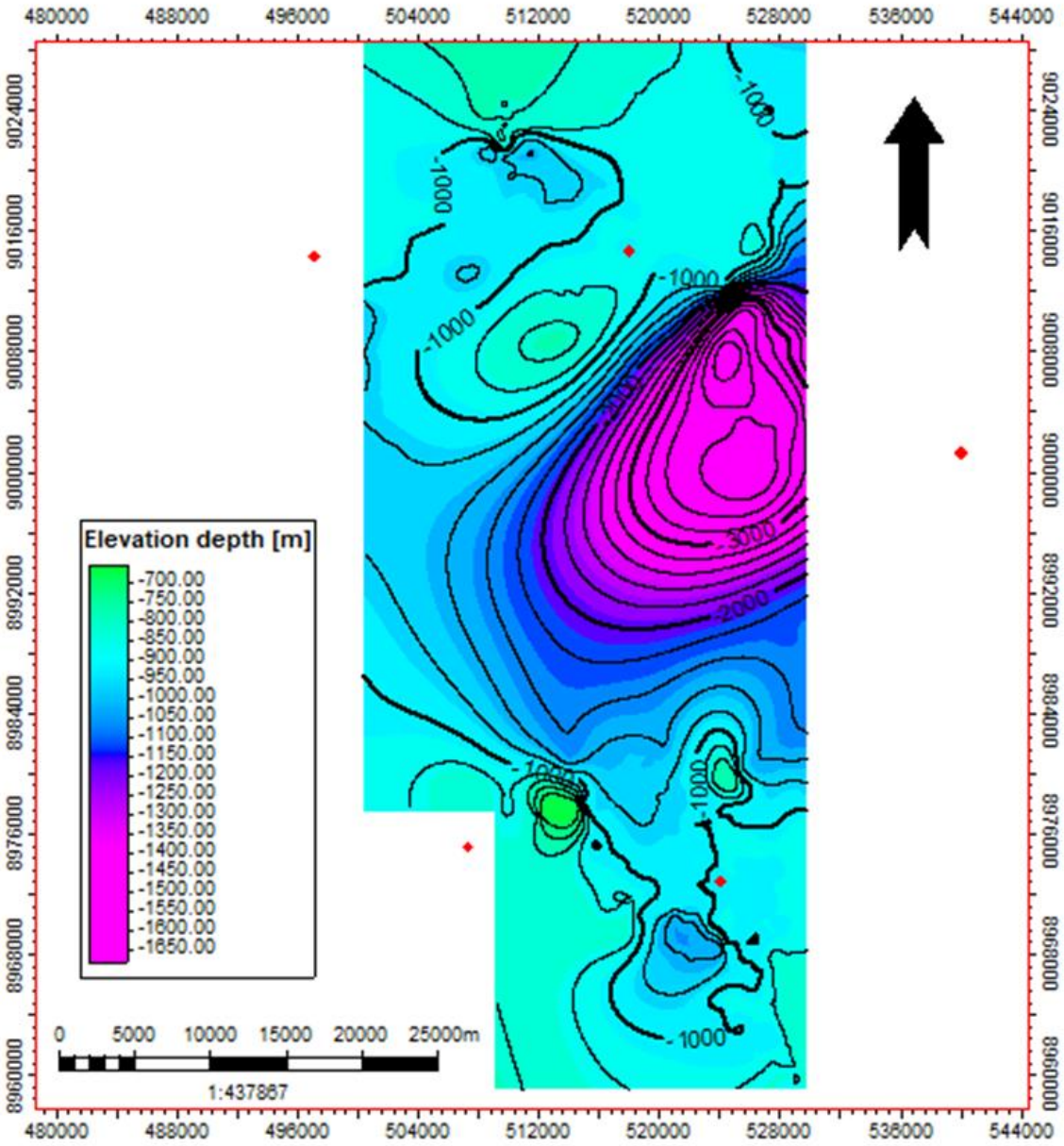

Figure 7.39 - Velocity map used for time-depth conversion. The red dots are the interval velocity corresponding to the well with checkshot data.

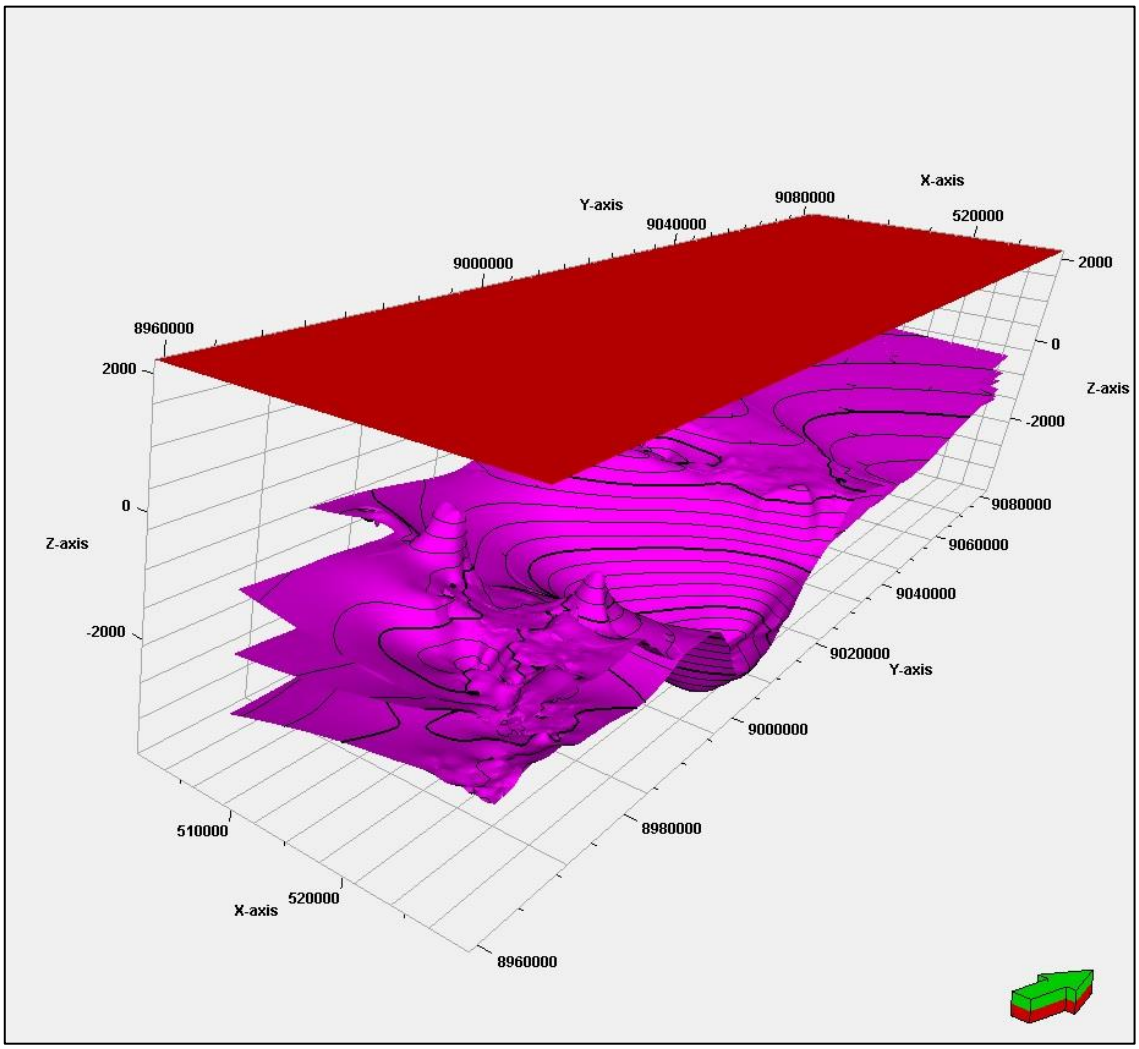

Figure 7.40 - Horizons depth converted to meters from the seismic velocity model.

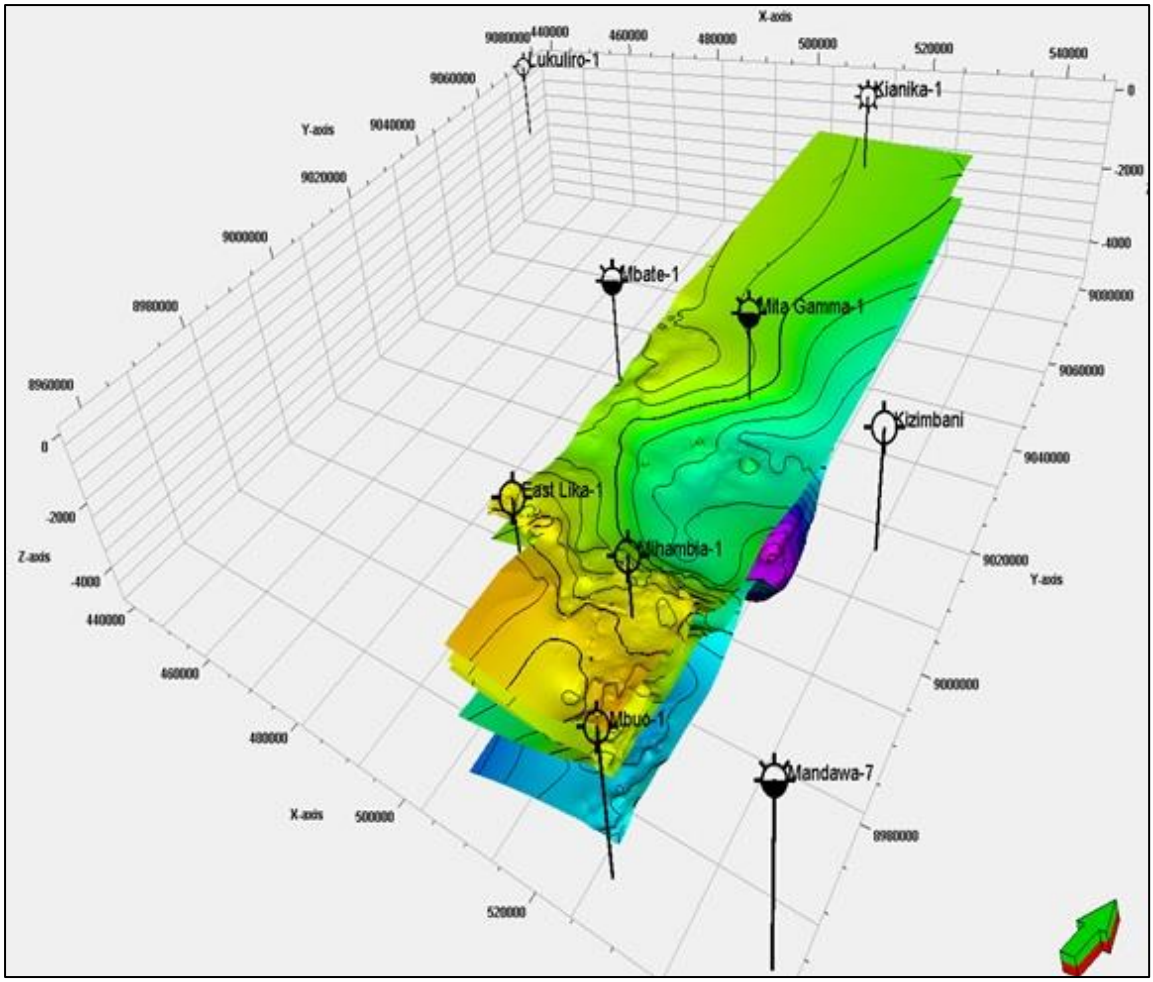

Figure 7.41 - Depth Conversion of the 3D geocellular model from time (ms) to depth (m).

The horizons modelled shown in Figure 7.42 were interpreted to be composed of mixed clastic sediments and salt pinch-out. Horizons modelled (depth) shows a high of the Horizon C – Nondwa Formation. The salt layer pinch-out and progressively extends southern the updip and downdip ends of the salt basin as a function of depth of burial.

.

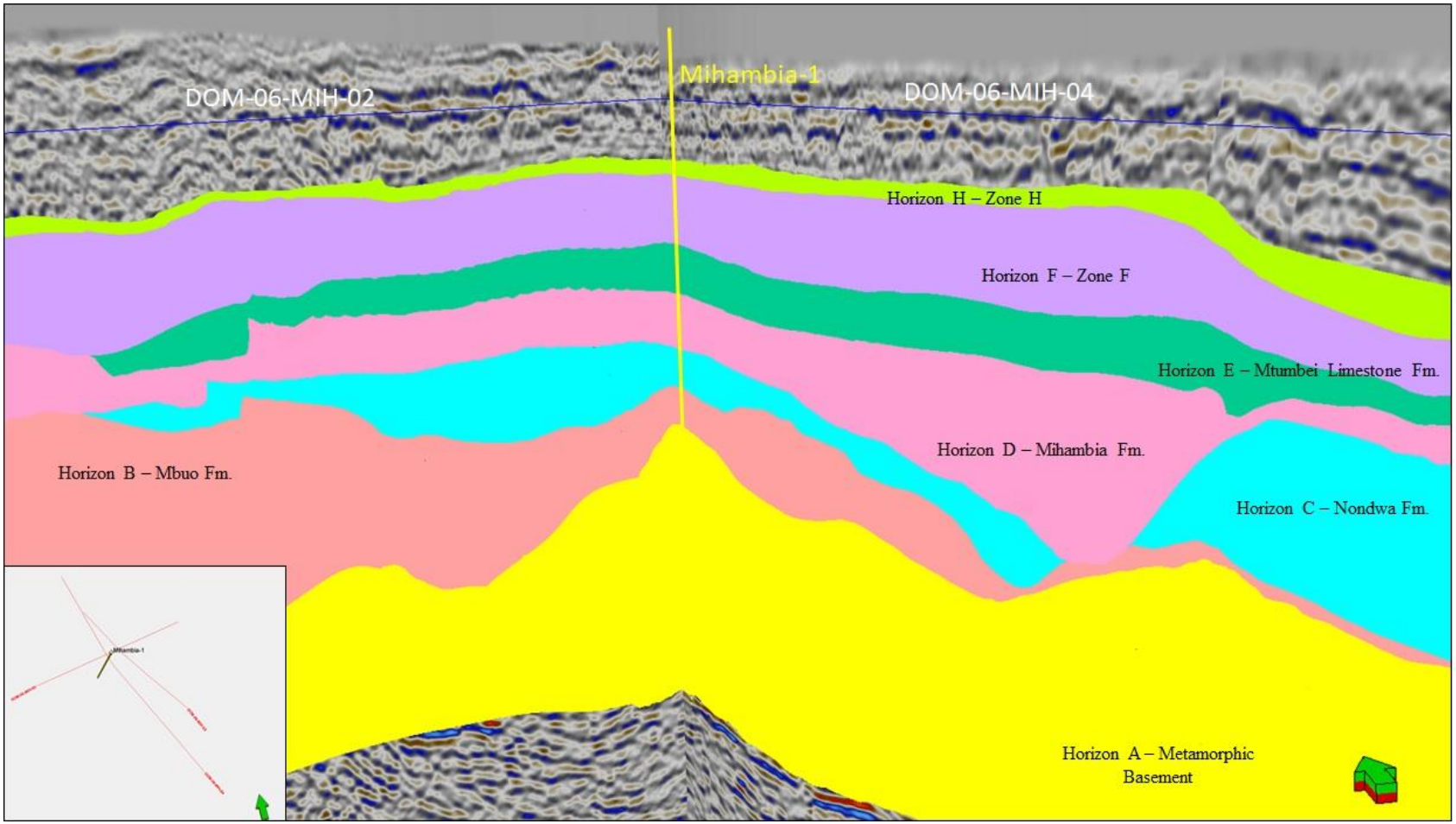

Figure 7.42 - View of 2D seismic lines DOM-06-MIH-02 (N-S) transecting DOM-06-MIH-04 (W-E) where Mihambia-1 well is located.

CHAPTER 8

DISCUSSION

The results presented in this study provide a general overview of the extent of evaporite deposition and its diapirism in the subsurface in southern Tanzanian basins. The main observation points about the different types of salt present in the Mandawa Basin indicate they are halite, anhydrite, and gypsum, as described in Chapters 4, 5, 6, and 7. These findings were based on geophysical well logs analysis according to Carmichael (1982) and Glover (2012). Through the accessed data in this study, it may be suggested that sequences of halite are present in most of the wells, such as Mbuo-1, Mihambia-1, East Lika-1, Mita Gamma-1, Mbate-1, and Mandawa-7. The values of sonic log responses varied from 66.7 to 67.0 μs/ft in most of the wells analysed and for the density log value of roughly 2.03 gm/cc. These results reflect those of Hudec and Jackson (2007) built on existing evidence of the salt tectonic basins related in the literature use the term "salt" to aggregate the rocks composed mostly of halite. Another evaporite type as anhydrite salt has been identified interbedded with claystones and sandstones sediments in Milhambia-1 and East-Lika-1 wells.

From the data available and approach taken during the 1990s, for example as Balduzzi *et al*. (1992) suggested, the evaporites from the Upper Jurassic age, Pindiro Evaporites, had no indication of diapirism or faulting. However, according to the resulting outputs from this study using the analysis of geophysical well logs methodology as described in Chapter 3, it seems that hypothetical traces of gypsum salt wall exist in evaporitic strata in Kizimbani-1 well. This assumption is linked to the lower delta time (Δt) response from sonic geophysical log identified as Horizon C – Nondwa Formation since salt bodies are roughly two times faster than the surrounding siliciclastic sediments. One interesting finding is that the salt in Mandawa Basin has been interpreted in this work as mostly autochthonous building up from the Lower Jurassic, below the present-day shelf. In addition to these findings, the appearance of an allochthonous detached salt sheet structure extending into the Lower Cretaceous strata in central Mandawa Basin suggests that the salt pillow originates from Upper Jurassic and with deposition during the Cretaceous. These results further support the idea of Mbede and Dualeh (1997).

The approach of investigating the timing of marine evaporite diapirism has been accessed in this research by stratigraphic seismic interpretation based on Chopra and Marfurt (2016). In Mandawa Basin, the separation from Africa suggested that variations through time in stratigraphy (source rocks) and structural movements (salt diapirs) occurred in the Lower Jurassic. The analysis here suggests that toplap/downlap terminations above and below the main zones (seismic sequences), contributes to a clearer understanding of restricted conditions in the Lower Jurassic according to the accessed 2D seismic lines available. These findings indicate that the rise to the deposition and sedimentation of anoxic marine shale and locally evaporites have been triggered by the evolution of the salt minibasin, approximately in the Middle Jurassic, marked by extensional tectonism producing listric faults overbalanced by a residual salt dome. It is important to mention that the use of restoration technique in the 2D seismic line DOM-06-MIH-4 in time (TWT) was used and has been proposed in this work where the salt layer and the overlapping layers had tabular geometry prior to extension. It has been followed by a rise of a diapir by reactive bearing to the formation of a graben associated with the extension of sedimentary overload.

An initial objective of the project was to evaluate the lithostratigraphy of the Mandawa Basin. This study proposed a new insight of the lithostratigraphy in the Mandawa Basin according to geophysical well logs analysis. Despite the common sense of a stratigraphic nomenclature based on Shell (1990) among authors and oil companies, the terminology here refrains from the previous published stratigraphic nomenclature adopted due to misreading upon decades of petroleum exploration. The well correlation compassed here allowed to observe the ten wells in a well section, produce well tops (markers), formation zones and their boundaries calculated by the stratigraphic interval between each delimiting horizon.

The results of this study indicate eight geological markers bounded in stratigraphic order marked by stratal thickness changes across salt structures and most normal and reverse faults, according to the geophysical well logs responses: Horizon A, Horizon B, Horizon C, Horizon D, Horizon E, Horizon F, Horizon G, and Horizon H. Seven zones have been defined in between the markers (well tops) where four of them specifically may correlate to previous stratigraphic units proposed firstly by Shell (1990). Those zones for the onshore Mandawa Basin are named: Mbuo Formation, Nondwa Formation, and Mtumbei Limestone Formation. In terms of age, the formation zones comprehending as Zone B -

Mbuo Formation (Fm.), Zone C - Nondwa Formation (Fm.), Zone D - Mihambia Formation (Fm.) are similar to the formations Basement (Precambrian/Cambrian), Mbuo Formation (Lower Jurassic), Nondwa Formation (Lower Jurassic), Mihambia Formation (Middle Jurassic), respectively, described by Hudson (2011). The current study detected the Horizon E - Mtumbei Limestone Formation in two of the wells investigated, Lukuliro-1 and Mita Gamma-1, as a formation from the Upper Jurassic compared to the findings of Kent *et al.* (1971), Balduzzi *et al.* (1992) and Hudson (2011) that suggested the marine carbonates characterised as from Middle Jurassic age divided in two members: Mtumbei Limestone and Mtumbei Formation. Regarding the Zones F, G, and H in this study, they have been mainly described as packages of siltstones and claystones interbedded with shale which were not linked to any previous nomenclature.

One of the key issues for petroleum exploration along the Tanzanian margin is to summarize the extension of the evaporite and its diapirism. In respect of trap geometries, the arguments addressed primarily the proposed diapirism has affected the Cambrian/ Lower Jurassic normal faults. These normal faults were interpreted as first (an old) event followed by the Upper – Lower Cretaceous, where a number of open anticlinal structures have been identified in the seismic lines. The most interesting finding was that the interpretation of the salt structures in this thesis has suggested that the gypsum is restricted to NNW-SSE trending, fault-bounded domes areas. Yet, seismic 2D accuracy, in the range of poor data quality, also indicated that salt-gypsum diapirs are controlled by the normal faults and are present with similar geometry, as salt bodies velocities are around two times faster than the surrounding siliciclastic sediments. Additionally, the implications of salt bodies have been a crucial element for the modelling process in this study. These results considered that regional tectonic salt domains are shown in a transect crossing the central-south part of the Mandawa Basin. The most obvious finding to emerge from the analysis is that whereas the 2D reflection seismic data were available revealed that the major aspects of salt tectonics along with the tectonic domains of the Mandawa Basin, the salt diapirs slightly increased in the W-E direction from observations of the Mihambia-1, Mbuo-1, and Mandawa-7 wells.

One interesting finding in this research is that the normal faults along Tanzania and Ruvuma basins likely follow N-S to NNW-SSE trend. These results corroborate to the findings of a previous work in Wu *et al.* (2019) and possibly contribute to explain the evolution of trap geometries during the strike-slip rifting stage that followed the

separation of Madagascar from Africa. The Toarcian rifts followed by the drift of Madagascar to the south from the coast of Somalia to its present location controlled the Jurassic deposits to the Neocomian, leading to the formation of traps in Majunga and Morondava basins in Madagascar. The original normal faults of the offshore Morondava Basin and other rift basins to the north along trend have been re-activated by dextral strike-slip faulting. Major faults should have large throws with thick sediment piles developed in transtensional basins (Rusk & Bretagne, 2003). Towards the north Mandawa, main reverse faults interpreted were possibly the Davie Fracture Zone shear region played the main cause for inversion. It could be concluded with the existing three major zones of inversion in the Mandawa basin in Hudson (2011) and Reeves (2017). They are indicated on the geological map (Hudson, 2011) by their fold axes and imply an NW-SE directed compression.

As mentioned in Chapter 1, the present study was not designed to review the petroleum systems such as the main elements and processes related as suggested by several researchers and oil companies since it implies the study of geochemical analysis, basin modelling that had not been under the suggested workflow. It can thus propose an improved sequence stratigraphy analysis for Mandawa Basin, and it may be considered similar to Sansom (2016) on the basis of the sequence stratigraphy guidelines of Posamentier *et al.* (1988), Van Wagoner *et al.* (1988) and on Brown and Fisher's classification modified from Vail *et al*. (1977). The system tracts interpreted were based on the lowstand system tract (LST) as an overall regressive stratigraphic unit of the metamorphic basement. A claystone package interbedded evaporite filling into the basin to transgressive (TST) which showed low gamma ray and the sharp boundary was recognized as a retrogradational parasequence set bounded. Upward sandstones marked the high system tract (HST) was recognized as prograding unit bounded and associated overlying limestone indicates a gradual change from clastic to carbonate establishing the composite sequence scale. The stacking pattern of several siltstone and sandstone established the composite sequence set. The dataset followed the workflow used in the oil industry to perform the structural model suggested that the autochthonous salt movement took place in central to southern Mandawa. A crucial point in interpreting the seismic image was to identify reliable reflectors in conjunction with the well tops (markers) in the wells although poor quality in some areas was visible.

It is unfortunate that the study did not include a high-resolution 3D seismic volume and more well data within the salt minibasin, as it is essential to have more data available in particular more onshore well and seismic data in Ruvuma Basin and Selous Basin to construct subsurface geocellullar models. As mentioned by Peel (2004) a simple forward-modelling approach, in the absence of any mechanism, can model a minibasin as the consequence of the salt movement. Since there was only one well interpreted in each basin, investigations of salt movement are yet considered open for further analysis and interpretations in order to estimate the total amount of basinal sediments and extension from diapirism by possibly performing petrophysical modelling that would represent the volume for the zones analysed, a 3D grid cellular model that aggregates the extension within the three basins.

As presented in Chapter 4, the absence of any salt type was notorious in the Selous Basin by analysis of geophysical well logs according to Carminchel (1982) and Glover (2012). The facies distribution described for the Liwale-1 well-marked the presence of Karoo sediments in the deep basement section followed by a Jurassic siltstone and claystone interbedded package similar to the descriptions of Hankel (1987), Kreuser *et al.* (1990) and Catuneanu *et al.* (2005). The three horizons and two respective markers mapped in Lukuledi-1 well from Lower Jurassic and Lower Cretaceous, respectively and two Cretaceous zones in a tentative equivalence of lithology and nomenclature from the Mandawa Basin with the Ruvuma Basin recognized siliciclastic sediments from Jurassic to Lower Jurassic age. This study supports evidence from previous observations of Smelror *et al*. (2008) and Key *at al.* (2008).

This study set out within respect of the evaporitic strata in Kizimbani-1 well with the results expressed to be linked to the Horizon C - Nondwa Formation from Lower Jurassic age. The suggestion is based on the well log correlation and the seismic attribute analysis and horizon surface interpretation with the result has been explained in Chapter 7. However, the salt, according to results from this work, possibly be a form of passive diapirism and has been interpreted here as allochthonous salt due to thickening above salt minibasin during the tectonic setting of a transform margin movement that influenced the salt expansion. However, in this study, it could not be possible to estimate the salt supply rate in shallow levels. This means that the salt sheet was modelled in the 2D seismic lines but nothing more significant could be interpreted from than.

The Upper Jurassic to Lower Cretaceous left lateral movement that divided the Kizimbani and Pande highs that are concerned to have also caused salt flow which resulted in the formation of N-S trending in Mandawa anticline, which movements are thought to be related to the southward drift of Madagascar (Mbede and Dualeh, 1997).

The present study has indicated a correlation between lateral migration of allochthonous salt in the form of gypsum has occurred onwards to offshore Majunga Basin.

The establishment of the salt basin of Majunga took place just before the drift towards the southwest of Madagascar (Wu *et al*., 2019). The Lower Jurassic salt became mobile soon after deposition and resulted in allochthonous detached salt sheets in Mandawa and confirmed in Majunga Basin, Madagascar (Tari *et al*., 2014). A possible explanation for these results may be the non-presence of salt in the Selous Basin, through the interpretation of Liwale-1 well may be explained due to its position in the Selous Rift by the Neogene Faulting and the Lindi Fault Area. Triassic sediments probably have been removed or reworked by Jurassic erosion, disconformities (Mbede and Dualeh, 1997). A possible explanation for this might be that the early salt movement and rim syncline development has finished prior to the Base Dogger unconformity (Clark, 2002). Another possible interpretation could be based on Tari *et al*. (2014) and described in Jeans and Van Meerbeke (1995) naming gypsum the salt from the Upper Isalo (Isalo II) Formation.

Importantly, the seismic attributes technique in addition to standard seismic stratigraphic practices contributed to the identification and interpretation of the occurrence of salt diapirism. The concentration of 2D seismic lines in the central and south Mandawa Basin permitted essentially to investigate geometries of geological lineaments.

It is interesting to note that in this thesis, the seismic attributes such as chaos and cosine of phase were mainly used to highlight the continuity of reflectors from the seismic line DOM-06-MIH-04 across the Mihambia-1 well. According to Pigott *et al*. (2013). A possible explanation for zones of maximum chaoticness were observed whether reflector discontinuities such as fault zones, angular unconformities, channel sand bodies probably were composed by anhydrite, halite, gypsum intercalated with carbonates, and possible zones of fractures. The use of chaos in certain parts of the 2D seismic line highlighted the amplitude higher than 0.60 where the salt structure was interpreted in Chapter 6. The cosine of phase attribute detected evidence for the continuity of the reflectors as the resolution to interpret a salt dome in central Mandawa.

The legacy data from the onshore wells was particularly useful in an providing indication of the tectonic evolution and trend of Karoo structures preserved along the main transform margin (McAfee, 2012).

The evidence of Karoo deposits in Selous and Mandawa Basin through the geophysical well logs responses indicated as basinal for both onshore basins similar to Catuneanu *et al*. (2005). Tilted fault blocks potentially containing the Karoo and Jurassic syn-rift sandstones with possible overlying shallow marine carbonates.

In the interest of this research, the extensional margins neighbour could address the Karoo trend in the southern Tanzanian basins, through the Mandawa Basin, tectonic events, reactivation of faults during the subsequent Jurassic rifting of East and West Gondwana.

Since the study was limited in terms of well data within the southern Tanzanian basins, the petrophysical and facies distributions were conceptually based on the geophysical well logs, well data, personal seismic interpretation of the 2D seismic lines and well correlation, accordingly, that created a 3D geocellular model for the Mandawa Basin.

The absence of a 3D volume of the study area resulted in not being able to perform a volume visualization in 3D and further restricting the use of certain processes in Petrel. The first restriction was regarding the use of volume seismic attributes, such as ant-tracking, the algorithm that automatically extracts fault surfaces from fault attributes, and dip illumination, both attributes are effective indicators of salt domes in timeslices views, in respect of noisy areas.

The scope of this study was limited in terms of using the technique of picking seismic horizons using autotracking was also not possible as it is necessary the use of good quality lines of the reprocessed 2D seismic lines. Instead, the horizon interpretation has been performed by manual picking and refining their relationships and checking the consistency of the horizon interpretation across faults in such a challenging dataset.

Another implication in this study was the fault interpretation process in respect to the distance between faults and the continuation of faults interpreted across the lines. In Mandawa Basin the distance between the lines turned out in the fault interpretation very critical as distance varied in kilometers, affecting the calculation of the variation of displacement across the fault surface. These results therefore need to be interpreted with

caution. The effects of systematic errors become second-order relative to those inherent in the interpreter's model (Boult *et al*., 2008).

The cons of using a 3D volume would allow the interpretation into modelling using the most advanced and constantly updated processes in Petrel. After the interpretation of horizons and faults, the whole structural modelling step would be subjected to the Pillar Gridding, the process of using faults in the fault model as a basis for generating a 3D grid. Due to limitations in interpreting faults as they would be the boundary in creating pillars along the Mandawa block, this process could not be in use for fault interpretation. However, it brought to the attention the necessity to reduce the spare set of faults in Mandawa Block. It was necessary to create a set of structural models restricting to the Mandawa PSA. The main 3D geocellular model of this thesis, more precisely around the Mihambia-1 well, where the set of 2D seismic lines covered a larger area and a model without faults have been performed providing surfaces correlating to the horizons interpreted. However, this model falls to be accurate as it does not create a reliable prognosis of the basins without faults. Next would be the Make Zones and Layering processes, scale up the well logs as is the interpolation or simulation of continuous data (for example, porosity or permeability) throughout the model grid (Schlumberger, 2018).

Furthermore, it would even integrate the data using geostatistical property modeling processes. Geometrical property modeling would be carried out generating properties from the geometry and structure of the grid, reservoir, and wells for use in quality control, volumetrics, and property calculation (Schlumberger, 2018). A facies model of Mandawa Basin would distribute the discrete data (e.g. facies customized for this thesis) throughout the 3D model whether using stochastic and deterministic methods. Also, a petrophysical model would be addressed interpolating the continuous data throughout the model grid using deterministic and stochastic methods (Schlumberger, 2018).

The results of this study did not 3D geocellular models for Ruvuma and Selous basins that would be gathered with the Mandawa Basin model. If this was possible to do it would partially enable us to access new information and, perhaps, reveal if there is a pre-Karoo section present in the Mandawa Basin area which is frequently debated within the scientific community.

This research presented used a suite of datasets as input for the preparation of a standard 3D geologic framework model. The workflow included seismic and well data acquisition,

well correlation for lithostratigraphy analysis, the salt distribution in the minibasin, seismic attribute analysis, 2D regional seismic interpretation in two-way time, structural framework model in time domain of surfaces and faults, sequential 2D reconstruction, and finally time-to-depth conversion. All the above were investigated with the aim to reappraise the Mandawa and Ruvuma basin evaporites and determine their effects along the Tanzanian continental margin and understanding the basin's structural evolution area affected by different tectonic events.

Seismic interpretation played an important part in this thesis characterizing a whole workflow of interpreting horizons, faults, the types of salts according to reflectors distinguished by changes in amplitudes, continuous, low frequency, medium-high amplitude facies units, in seismic lines that all combined performed a 3D geocellular model. Define a salt basin is challenging due to the region, the data available being characterised by the presence of salt diapirs that resulted in closed systems of pressure distribution. Modelled horizons were analysed and interpreted separately to delineate the detailed structural and stratigraphical setting of the Mandawa Basin. Due to several variations regard fault lengths and in a sparse seismic dataset available for this study, strike-slip faults were difficult to connect.

The 3D geocellular model suggested the extensional block faulting – horst and graben formation – during the Cambrian - Lower Jurassic. The most obvious finding to emerge from the analysis is that a stratigraphic pinch out setting formed during restricted conditions triggered by the evolution of the mini-basin occurred approximately in the Middle Jurassic followed by a major Upper Jurassic transgression corroborating with Hankel (1987), Veeken and Titov (1996) and Peel (2014) regarding restricted conditions, deposition of anoxic marine shale and locally evaporites of the mini-basin. The carbonate platform was extinguished by the progradation of marine siliciclastic sediments from the Upper Jurassic - Lower Cretaceous sequence boundary. Rifts and inversion were active during the Lower Cretaceous (Macgregor, 2017; Macgregor *et al.*, 2017) as the depositional environment suggested a deltaic - fluviomarine clastic progradation followed by successions of shallow marine clastic sediments and inverse faults.

CHAPTER 9

CONCLUSIONS

This study set out to review the Mandawa and Ruvuma basin evaporites along the Tanzanian continental margin and to likely associate the evaporite extention to analogue basins in Madagascar. The main conclusions from this thesis are the following:

- This research identified seven zones defined in between the markers where four of them specifically may correlate to previous stratigraphic units proposed firstly by Shell in 1990 for the onshore Mandawa Basin, Mbuo Formation, Nondwa Formation, and Mtumbei Limestone Formation. From the lowermost to the uppermost, the zones are comprehending as Zone B - Mbuo Formation (Fm.), Zone C - Nondwa Formation (Fm.), Zone D - Mihambia Formation (Fm.), Zone E - Mtumbei Limestone Formation (Fm.), Zone F, Zone G, and Zone H.

- The results of this investigation show that the seismic sequences analysis in this thesis has been carried out as a simplified Mandawa Basin area sequence stratigraphy potentially divided the strata into eight seismic sequences following the pattern of stacked seismic units based on high amplitude reflections and its geometry. The profiles selected for regional seismic-stratigraphic analysis are oriented in NE-SW, running from shelf to deep offshore area. Sequence boundaries were identified by truncation, onlap, toplap and, downlap stratal terminations based on the seismic resolution dataset and area of extension.

- This thesis has provided a deeper insight into the sequences of halite that were interpreted in most of the wells, such as Mbuo-1, Mihambia-1, East Lika-1, Mita Gamma-1, Mbate-1, and Mandawa-7 evidenced by the values of sonic log responses varying from 66.7 to 67.0 μs/ft and density log value of 2.03 gm/cc.

- The research has also shown that anhydrite has been detected interbedded with claystones and sandstones in Milhambia-1 and East-Lika-1 wells with

hypothetical traces of gypsum were interpreted in Kizimbani-1 well according to the low delta transit time response from the sonic log of 52 μs/ft.

- This study has raised important questions about the nature of the regional tectonic of Mandawa Basin. Salt domains are indicating to be crossing the central-south part of the basin. The salt diapirs suggest an increase in the W-E direction from observations of the Mihambia-1, Mbuo-1, and Mandawa-7 wells.

- The current data highlight the importance of interpreting the salt structures has suggested that the gypsum is restricted to NNW-SSE trending, fault-bounded domes areas and are controlled by the normal faults and are present with similar geometry.

- The investigation of the geophysical well logs available for this study has shown, through produced thickness maps, that the lateral deposition of salt in a form of halite and anhydrite in most of the wells in the Mandawa Basin. Velocities vary laterally and horizontally due to compaction, lithological contrast, tectonic setting, and burial depth.

- The insights gained from this study may be of assistance to recognize a variety of salt structures that include both autochthonous and allochthonous structures such as salt dome, salt walls, detached salt sheet, salt sheet, teardrop diapir, salt diapir in Mandawa Basin. The Mandawa withdrawal minibasin suggested evolving from the Lower Jurassic syn-rift salt ramping up through Lower Cretaceous strata forming a broad allochthonous detached salt sheet.

- Synthetic Seismogram has been suitable to define the marker reflectors, which proposed the lithostratigraphy interpretations in this study from older to younger strata.

- This is the first study to proposes a comprehensive 3D geocellular model for the salt distribution in the Mandawa Basin. The extensional block faulting – horst and graben formation – during the Cambrian - Lower Jurassic. A stratigraphic pinch out setting formed during restricted conditions triggered by the evolution of the

minibasin occurred approximately in the Middle Jurassic followed by a major Upper Jurassic transgression.

- The present study lays the groundwork for future research into salt tectonics using seismic reflection analysis in Mandawa Basin. A time-depth velocity model has been performed for the onshore basin in Tanzania according to the upscaling of the internal velocities. A constant interval velocity has been addressed to convert apart from the salt structures where high velocities were encountered. Modelled surfaces and faults have been upscaled to evaluate the sensitivity of the structures (zones) to convert the zones in the time domain to depth domain giving continuity to structural modelling.

- Prior to this study it was difficult to associate and gather given stratigraphy units for central Mandawa formations. Unpublished or outdated terminologies from several studies lithostratigraphy analysis was carried out making possible the characterisation of three horizons and two respective markers in a tentative equivalence of lithology and nomenclature from the Mandawa Basin with the Ruvuma Basin. Faults played a major control on sedimentation causing lateral changes. Continental clastic sandstones, marine shale siltstones interbedded with successions of non-deposition sandstones suggested transitional conditions during the Jurassic that widespread to three unconformity periods in the Lower Cretaceous.

- This work proposes a well correlation based on well logs from one well in the Selous Basin. Five markers and respective seismic horizons have been named as the geological ages respectively with other studies.

Promising approaches and key recommendations for future work:

- Further research may provide comprehension of the salt movement within the tectonic setting. A reasonable approach to tackle this issue could be to acquire more seismic sections, 3D volume, well data, well logs data from both Ruvuma and Selous basins so as the conjugate basins in Madagascar, Majunga, and Morondava, respectively.

REFERENCES

Adcock, S. (1993). In search of the well tie: what if we don't have a sonic log? *The Leading Edge.* 1161-1164.

Alberty, M. W. (1994). Standard interpretation; part 4—wireline methods, in D. Morton-Thompson and A. M. Woods, eds., Development Geology Reference Manual: *AAPG Methods in Exploration Series* 10, p. 180–185.

Alconsult. (1997). The hydrocarbon potential of Tanzania. Regional non-exclusive report.

Allen, P. A. and Allen, J. R. (2005). Basin Analysis: Principles and Applications, 2nd ed., 549 pp., *Blackwell Publishing, Malden, Mass.*

Asquith, G.B. and Gibson, C.R. (1982). Basic Well Log Analysis for Geologists. *The American Association of Petroleum Geologists (AAPG)*. Tulsa.

Atlas, D. (1982). Well Logging and Interpretation Techniques: The Course for Home Study. *Dresser Atlas.*

Avseth, P., Mukerji, T. and Mavkro, G. (2005). Quantitative Seismic Interpretation: Applying Rock Physics to Reduce Interpretation Risk. *Cambridge University Press, Cambridge*.

Azevedo, L. and Pereira, G.R. (2009). Seismic Attributes in Hydrocarbon Reservoir Characterization. *Universidade de Aveiro,* Departamento de Geociências.

Balduzzi, A., Msaky, E., Trincianti, E., Manum, S. B. (1992). Mesozoic Karoo and post-Karoo Formations in the Kilwa area, southeastern Tanzania – a stratigraphic study based on palynology, micropalaeontology and well log data from the Kizimbani Well. *Journal of African Earth Sciences.* 15, 405–427.

Banks, N., Cooper, B., Jenkins, S. & Razafindrakoto, E. (2008). Evidence for the onshore extension of the deep water Jurassic salt basin in the Majunga Basin, northwest Madagascar. *Abstract, AAPG Annual Convention & Exhibition, San Antonio, Texas*.

Bartucz, D. (2009). Exploration of Geothermal Systems with Petrel Modeling Software. *School for Renewable Energy*. p.69.

Bassias, Y. (1992). Petrological and geochemical investigation of rocks from the Davie fracture zone (Mozambique Channel) and some tectonic implications. *Journal of African Earth* Sciences. 15, 321 – 339.

Bassias, Y., Christoffersen, T., Roberts, G. (2015). The crustal nature of the Southern Mozambique Channel between Madagascar and Mozambique (i.e. the Central Mozambique Channel Basin) and observations concerning its petroleum potential. *PESGB/HGS 2015 Africa Conference*, Poster session and extended abstract, London, September 2015.

Besairie, H. (1972). Géologie de Madagascar: 1, Les terrains sédimentaires. *Annales Géologiques de Madagascar*. 35: 1-463.

Bingen, B., Jacobs, J., Viola, G., Henderson, I., Skår, Ø., Boyd, R., Thomas, B., Solli, A., Key, R., Daudi, E.X.F. (2009). Geochronology of the Precambrian crust in the Mozambique belt in NE Mozambique, and implications for Gondwana assembly. *Precambrian Research*. 170. 231-255. 10.1016/j.precamres.2009.01.005.

Blackwell, D.D. and Steel, J.L. (1989). Thermal conductivity of sedimentary rocks: Measurement and significance, *in* Thermal History of Sedimentary Basins, edited by N. D. Naeser, and T. H. McCulloh, pp. 13–36, *Springer-Verlag*, London.

Boger, S. & Miller, J. (2004). Terminal suturing of Gondwana and the onset of the Ross-Delamerian Orogeny: The cause and effect of an Early Cambrian reconfiguration of plate motions. *Earth and Planetary Science Letters – Earth Planet Sci Lett*. 219. 35-48. 10.1016/S0012-821X (03)00692-7.

Bornhardt, W. (1900). Zur Oberflächengestaltung und Geologie Deutsch Ost-Afrikas. *Bd. VIII. Dietrich-Reimer, Berlin.*

Boult, P., Freeman, B. and Yielding, G. (2008). Reducing the Structural Uncertainty in Poor 2-D Seismic Data, Gambier Embayment, Otway Basin, Australia - a Minimum Strain Approach. *Search and Discovery*. Article #40371.

Bown, P.R. (2005). Palaeogene calcareous nannofossils from the Kilwa and Lindi areas of coastal Tanzania (Tanzania drilling project 2003–2004). *Journal of Nannoplankton Research*. 27, 21–95.

Bown, P.R., Dunkley, J.T. (2006). New Palaeogene calcareous nannofossil taxa from coastal Tanzania: Tanzania Drilling Project Sites 11 to 14. *Journal of Nannoplankton Research* 28, 17–34.

Bown, P.R., Dunkley, J.T., Lees, T.J.A., Pearson, P.N., Randell, R., Coxall, H.K., Mizzi, J., Nicholas, C., Karega, A., Singano, J., Wade, B.S. (2008). A calcareous microfossil Konservat-Lagerstätte from the Paleogene Kilwa Group of coastal Tanzania. *GSA Bulletin*. 120, 3–12.

Bown, P.R., Pearson, P.N. (2009). Calcareous plankton evolution and the Paleocene/Eocene thermal maximum event: New evidence from Tanzania. *Mar. Micropaleontol*. 71, 60–70.

Brewer J. (1987). Seismic reflection studies of major crustal faults. *Structural Geology and Tectonics. Encyclopaedia of Earth Science. Springer.* Berlin, Heidelberg.

Brown, A.R. (2005). Interpretation of Three-Dimension Seismic Data – Sixth Edition. *AAPG Memoir 42, SEG Investigations in Geophysics 9*. AAPG-SEG, Tulsa, USA. ISBN 0-89181-364-0. Hard cover.

Brown, A.R. and Abriel, W.L. (2014). The polarity of zero-phase wavelets. *Interpretation*. 2 (1), 19F-19F.

Buchanan, J. G. (1996). The application of cross-section construction and validation within exploration and production: a discussion. Geological Society, London. *Special Publications*. 99, 41-50, 1 January 1996, https://doi.org/10.1144/GSL.SP.1996.099.01.05

Caers, J. (2005). Petroleum Geostatistics. *Society of Petroleum Engineers*.

Cant, D.J. (1992). Subsurface facies analysis. In: Walker RG, James NP, editors. Facies models, response to sea level changes. *Geol. Assoc. Canada*. 1992. p. 27-45.

Carmichael, R.S. (1982). Handbook of Physical Properties of Rocks. *CRC Press Inc*. Vol. 2, 1-228. Boca Raton, Florida.

Catuneanu, O. (2002). Sequence stratigraphy of clastic systems: Concepts, merits, and pitfalls. Journal of African Earth Sciences. 35. 1-43. 10.1016/S0899-5362(02)00004-0.

Catuneanu, O., Wopfner, H., Eriksson, P.G., Cairncross, B., Rubidge, B.S., Smith, R.M.H. and Hancox, P.J. (2005). The Karoo basins of south-central Africa. *Journal of African Earth Sciences.* 43(1-3), pp.211-253.

Catuneanu, O. (2006). Principles of Sequence Stratigraphy. *Elsevier*. Amsterdam, 375 p.

Catuneanu, O., Abreu, V., Bhattacharya, J., Blum, M.D., Dalrymple, R., Eriksson, P.G., Fielding, C., Fisher, W.L., Galloway, W., Gibling, M., Giles, K., Holbrook, J., Jordan, R., Kendall, C., Martinsen, O., Miall, A.D., Neal, J., Nummedal, D., Winker, C.. (2009). Towards the Standardization of Sequence Stratigraphy. *Earth-Science Reviews*. 92. 1-33. 10.1016/j.earscirev.2008.10.003.

Cedeño, A., Rojo, L.A., Cardozo, N., Centeno, L., Escalona, A. (2019). The Impact of Salt Tectonics on the Thermal Evolution and the Petroleum System of Confined Rift Basins: Insights from Basin Modeling of the Nordkapp Basin, Norwegian Barents Sea. *Geosciences*. 9. 316. 10.3390/geosciences9070316.

Chopra, S. and Marfurt, K.J. (2005). Seismic attributes for prospect identification and reservoir characterization. *SEG Geophysical Development Series* No. 11, 464 p.

Chopra, S. and Marfurt, K. (2016). Understanding the seismic disorder attribute and its applications. *Society of Exploration Geophysicists.*

Chorowicz, J. (2005). The East African rift system. *Journal of African Earth Sciences*. 43 (1-3), 379-10.

Clark, D.N. (1998). Review of the exploration potential of Madagascar. Houston Geol. Soc. Bull., Houston Geological Society, Vol.40, pp. 23–29, 1998.

Clark, D.N., and Ramanampisoa, L. (2002). Review of the occurrence and distribution of potential source rocks in Madagascar; in Tracts, plays and fairways along the Tethyan margin: *Abstracts and Programme*, Kingston University, unpaged. Kingston.

Clauser, C. and Huenges, E. (1995), Thermal conductivity of rocks and minerals, in Rock Physics and Phase Relations—A Handbook of Physical Constants, edited by T. J. Ahrens, AGU Reference Shelf, vol. 3, 105–126, *American Geophysical Union*, Washington, D. C.

Coffin, M.F. and Rabinowicz, P.D. (1987). Reconstruction of Madagascar and Africa: evidence from the Davie fracture zone and western Somali basin. *Journal of Geophysical Research*, 92 (B), 9385-9406.

Commission for the Geological Map of the World (1990). International geological map of Africa 6: 6 of 6.

Cosentino, L. (2001). Integrated reservoir studies. *Technip*. Paris, 310.

Cotton, L., Pearson, P.N. (2009). Larger benthic foraminifiera from the Middle Eocene to Oligocene of Tanzania. *Austrian Journal of Earth Sciences.* Volume 105/1, 189-199, Vienna, Austria.

Core Lab/GHG (2009). Hydrocarbon source rocks in Tanzania. Initial interim review. East Africa Reservoirs & Seals. *Regional CoreLab Study*.

Core Lab/TPDC (2009). Core Laboratories Sales N.V. and Tanzania Petroleum Development Corporation. East African Reservoirs and Seals, Phase 1 - Tanzania, 188 pp *Report*.

Cooper, B.A. (2006). Review of geochemical data from the Dominion Petroleum Mandawa and Kisangire Blocks & adjacent areas, onshore Tanzania. *Horus Petroleum Report for Dominion Petroleum.*

Copestake, P. (2008). Tanzania, Mandawa & Coastal Area – Review of Upper Jurassic, Lower Cretaceous and younger stratigraphy. Dominion internal technical meeting.

Cubizolle, F., Valding, T., Lacaze, S. and Pauget, F. (2015). Global method for seismic-well tie based on real time synthetic model. *SEG Technical Program Expanded Abstracts*. 2015: pp. 1776-1781, doi: 10.1190/segam2015-5862834.1.

Davidson, I. and Steel, I. (2017). Geology and hydrocarbon potential of the East African continental margin: a review. *Petroleum Geoscience.* 24 (1): 57–91.

Delvaux, D. (1991). The Karoo to recent rifting in the western branch of the East-African Rift System: A Bibliographical synthesis. *Mus. roy. Afr. centr., Tervuren (Belg.).* Dept. Geol. Min, Rapp. ann. 1989-1990, 63-83.

De Wit, M.J., Guillocheau, F., and de Wit, M.C. J. (Eds.) (2015). Geology and Resource Potential of the Congo Basin. *Springer*. doi:10.1007/978-3-642-29482-2.

Dirkx, R. (2016). Observations on tectonic evolution and Prospectivity of Madagascar offshore basins based on interpretation of new seismic data. *TGS-NOPEC Geophysical Company ASA*.

Dix, C.H. (1955). Seismic Velocities from Surface Measurements. *Geophysics*. 20, 1, 68–86.

Dixon, J.M. (1975). Finite strain and progressive deformation in models of diapiric structures. *Tectonophysics*, 28 (1975), pp. 89-124.

Dominion, P.L. (2006). Confidential report. Tanzania.

Dorn, C., Green, A.G., Jongens, R., Carpentier, S., Kaiser, A.E., Campbell, F., Horstmeyer, H., Campbell, J., Finnemore, M., and Pettinga, J. (2010). High-resolution seismic images of potentially seismogenic structures beneath the northwest Canterbury Plains. *Journal of Geophysical Research.* New Zealand. 115, B11303, doi:10.1029/2010JB007459.

Duncan, R.A., Richards, M.A. (1991). Hotspots, mantle plumes, flood basalts and true polar wander. *Reviews of Geophysics*, 29, pp. 31-50

Duncan, R.A., Hooper, P. R., Rehacek, J., Marsh, J. G., Duncan, A.R. (1997). The timing and duration of the Karoo igneous event, southern Gondwana, *Journal of Geophysical Research*, 102, 18,127–18,138.

Ebinger, C. J. and Sleep, N.H. (1998). Cenozoic magmatism throughout east Africa resulting from impact of a single plume: *Nature*, v. 395, p. 788-791, doi: 10.1038/27417.

Edgar, J. and Van der Baan, M. (2011). How reliable is statistical wavelet estimation? *Geophysics*, 76, V59V68.

Emery, D. and Myers, K. J. (1996). Sequence Stratigraphy. 297 pp. *Oxford: Blackwell Science*. ISBN 0 632 03706 7.

Emmel, B., Jacobs, J. and Razakamanana, T. (2004b). Titanite and apatite fission track analyses on basement rocks of central-southern Madagascar: constraints on exhumation and denudation rates along the eastern rift shoulder of the Morondava basin. *Journal of African Earth Sciences*, 38: 343-361.

Emmel, B., Kumar, R., Ueda, K., Jacobs, J., Daszinnies, M.C., Thomas, R.J. and Matola, R. (2011). Thermochronological history of an orogen-passive margin system: An example from northern Mozambique. *Tectonics.* Vol. 30, TC2002, doi:10.1029/2010TC002714.

Engvik, A.K., Tveten, E., Bingen, B., Viola, G., Erambert, M., Feito, P. and De Azavedo, S. (2007). P-T-t- evolution and textural evidence for decompression of Pan-African high-pressure granulites, Lurio Belt, northeastern Mozambique. *Journal of Metamorphic Geology,* 25, 1-18.

Ferguson, C.J., Avu, A., Schofield, N. and Paton, G.S. (2010). Seismic analysis workflow for reservoir characterization in the vicinity of salt. *First Break,* 28 (10), 107–113.

Filippova, K., Kozhenkov, A. and Alabushin, A. (2011). Seismic inversion techniques: choice and benefits. *First Break*, 29, 103-114.

Flores, G. and Noseda, C. (1961). The geology of the Rovuma area. *Unpublished Report, Mozambique Gulf Oil Company*. Instituto Nacional de Geologia, Maputo.

Fossen, H., (2010). Structural Geology: Published in the United States of America. *Cambridge University Press*. New York.

Gadallah, M.R. (1994). Reservoir seismology, geophysics in nontechnical language. *PennWell Books*, Tulsa, p 384.

Gaina, C., Torsvik, T.H., Van Hinsbergen, D.J.J., Medvedev, S., Werner, S.C. and Labails, C. (2013). The African Plate: A history of oceanic crust accretion and subduction since the Jurassic. *Tectonophysics*, 604, 4-25.

Galloway, W. E. (1989). Genetic stratigraphic sequences in basin analysis, I. Architecture and genesis of flooding-surface bounded depositional units. *American Association of Petroleum Geologists Bulletin.* Vol. 73, pp. 125–142.

Geiger, M. (2004). Sedimentary and stratal patterns in Jurassic successions of western Madagascar: Facies, stratigraphy, and architecture of Gondwana breakup and drift sequences. *PhD Thesis, Department of Geosciences, University of Bremen, Germany*. http://elib.suub.uni-bremen.de/diss/docs/E-Diss1245_Geiger_2004.pdf.

Geiger, M., Clark, D.N. and Mette, W. (2004). Reappraisal of the timing of the break-up of Gondwana based on sedimentological and seismic evidence from the Morondava

Basin, Madagascar. *Journal of African Earth Sciences*, 38, 3 6 3 – 3 8 1, doi:10.1016/ j.jafrearsci.2004. 02.003.

GeoMark Research Ltd. (2004). *Reservoir Fluid Database*.

Georepository. (2016). Datum: Not specified (based on Clarke 1880 (Arc) ellipsoid. URL:https://georepository.com/datum_6013/Not-specified-based-on-Clarke-1880-Arc-ellipsoid.html [accessed on 16. July 2016].

Giles, K. A., and Lawton, T. F. (2002). Halokinetic sequence stratigraphy adjacent to the El Papalote Diapir, northeastern Mexico. *AAPG Bulletin*. v. 86, p. 823-840.

Giles, K. & Rowan, M. (2012). Concepts in halokinetic-sequence deformation and stratigraphy. *Geological Society of London Special Publications*. 363. 7-31. 10.1144/SP363.2.

Glover, P.W.J. (2012). Petrophysics. *University of Aberdeen Press*. Aberdeen: Department of Geology and Petroleum Geology. UK.

Hancox, P.J., Brandt, B. and Edwards, H. (2002). Sequence stratigraphic analysis of the Early Cretaceous Maconde Formation (Rovuma basin), northern Mozambique. *Journal of African Earth Sciences*, 34, 291-297.

Handley, L., Pearson P.N., McMillan, I. K., Pancost, R.D. (2008). Large terrestrial and marine carbon and hydrogen isotope excursion in a new Paleocene/Eocene boundary section from Tanzania. *Earth and Planetary Science Letters*. 275, 17– 25.

Handley, L., O'Halloran, A., Pearson, P.N., Hawkins, E., Nicholas, C.J., Schouten, S., McMillan, I.K., Pancost, R.D. (2012). Changes in the hydrological cycle in tropical East Africa during the Paleocene-Eocene Thermal Maximum. *Palaeogeography, Palaeoclimatology, Palaeoecology*. 329–330, 10–21.

Handerson Petrophysics. (2011). Some Causes for Bad Sonic Logs and Some Editing Options. from http://www.hendersonpetrophysics.com/sonic_w_frames.htm

Hankel, O. (1987). Lithostratigraphic subdivision of the Karoo rocks of the Luwegu Basin (Tanzania) and their biostratigraphic classification based on microfloras, macrofloras. fossil woods and vertebrates. *Geologische Rundschau*. 76 (2). 539-565. Stuttgart.

Hankel, O. (1994). Early Permian to Middle Jurassic rifting and sedimentation in East Africa and Madagascar. *Geologische Rundschau*. 83, 703–710.

Haq, B., Hardenbol, J., Vail, P. (1988). Mesozoic and Cenozoic Chronostratigraphy and Cycles of Sea-Level Change. *Society of Economic Paleontologists and Mineralogists*, v. 42, p. 71-108 10.2110/pec.88.01.0071.

Hedberg, D. (1976). International Subcommission on Stratigraphic Classification (ISSC). *International Stratigraphic Guide*, John Wiley and Sons, New York (1976), p. 200.

Heirtzler, J.R. and Burroughs, R.H. (1971). Madagascar's Paleoposition: New Data from the Mozambique Channel. *Science*, 174, 488-490.

Higgins, R and Sofield, M. (2011). East Africa Transform Margin – The view from Tanzania and Madagascar. *10th PESGB/HGS Conference on African E & P*, London, September 7-8, 2011.

Hudec, M.R., Jackson, M.P.A. (2004). Regional restoration across the Kwanza Basin, Angola: Salt tectonics triggered by repeated uplift of a metastable passive margin: American *Association of Petroleum Geologists Bulletin*, v. 88, p. 971– 990, doi:10.1306/02050403061.

Hudec, M.R. and Jackson, M.P.A. (2007). Terra Infirma: Understanding salt tectonics. *Earth Science Reviews.* v. 82, p. 1-28.

Hudson, W.E. (2011). The Geological Evolution of the Petroleum Prospective Mandawa Basin Southern Coastal Tanzania. *Unpublished PhD Thesis*. Trinity College, University of Dublin, Ireland.

Hudson, W.E. and Nicholas, C.J. (2014). The Pindiro Group Triassic to Early Jurassic Mandawa Basin, southern coastal Tanzania): Definition, palaeoenvironment, and stratigraphy. *Journal of African Earth Sciences*. 92 (2014) 55–67.

ICS. (2019). International Commission on Stratigraphy: International Chronostratigraphic Chart, v2019/05.

Jackson, M.P.A. and Talbot, C. J. (1991). A Glossary of Salt Tectonics. The University of Texas at Austin, *Bureau of Economic Geology, Geological Circular*. 91-4, 44 p. doi.org/10.23867/gc9104D.

Jackson, M.P.A. and Vendeville, B. C. (1994). Regional extension as a geological trigger for diapirism. *Geological Society of America Bulletin*. 106, 57–73

Jackson, M.P.A., Vendeville, B.C., Schultz-Ela, D.D. (1994). Structural dynamics of salt systems. *Annual Review of Earth and Planetary Sciences*. 22,93–117.

Jackson, M., and Hudec, M. (2017). Salt Stocks and Salt Walls. In Salt Tectonics: Principles and Practice (pp.76-118). *Cambridge: Cambridge University Press*. Doi:10.1017/9781139003988.008.

Jacobs, J., Thomas., R.J. (2004). Oblique collision at about 1.1Ga along the southern margin of the Kaapvaal Craton continent, south east Africa. *Geologische Rundschau*, 83 (1994), pp. 322-333.

Jacobs, J., Bingen, B., Thomas, R.J., Bauer, W., Wingate, M. T. D., Feitio, P. (2008). Early Palaeozoic orogenic collapse and voluminous late-tectonic magmatism in Dronning Maud Land and Mozambique: Insights into the partially delaminated orogenic root of the East African–Antarctic Orogen? in Geodynamic Evolution of East Antarctica: A Key to the East-West Gondwana Connection, edited by M. Satish-Kumar et al., *Geological Society Special Publications*, 308, 69–90, doi:10.1144/SP308.3.

Jarvis, K. (2006). Integrating Well and Seismic Data for Reservoir Characterisation: Risks and Rewards. *ASEG Extended Abstracts*. 2006:1, 1-4, DOI: 10.1071/ASEG2006ab074.

Jeans, P.J.F. and Van Meerbeke, G.L.E. (1995). Geological Evolution and Hydrocarbon Habitat of the Majunga Basin and Karroo Corridor, Madagascar. *Cent. Geocongr*. 1995, Johannesburg, p. 1027-1032.

Jenyon, M.K. (1986). Salt Tectonics. *Elsevier Applied Science*, London.

Jiménez Berrocoso, Á., MacLeod, K.G., Huber, B.T., Lees, J.A., Wendler, I., Bown, P.R., Mweneinda, A.K., Isaza Londoño, C., Singano, J. (2010). Lithostratigraphy, biostratigraphy and chemostratigraphy of Upper Cretaceous sediments from southern Tanzania: Tanzania drilling project sites 21–26. *Journal of African Earth Sciences*. 57, 47–69.

Jiménez Berrocoso, Á., Huber, B.T., MacLeod, K.G., Petrizzo, M.R., Lees, J.A., Wendler, I., Coxall, H., Mweneinda, A.K., Falzoni, F., Birch, H., Singano, J.M., Haynes,

S., Cotton, L., Wendler, J., Bown, P.R., Robinson, S.A., Gould, J. (2012). Lithostratigraphy, biostratigraphy and chemostratigraphy of Upper Cretaceous and Paleogene sediments from southern Tanzania: Tanzania Drilling Project Sites 27–35. *Journal of African Earth Sciences*. 70, 36–57.

Jiménez Berrocoso, Á., Huber, B.T., MacLeod, K.G., Petrizzo, M.R., Lees, J.A., Wendler, I., Coxall, H. et al. (2015). The Lindi Formation (upper Albian–Coniacian) and Tanzania Drilling Project Sites 36–40 (Lower Cretaceous to Paleogene): Lithostratigraphy, biostratigraphy and chemostratigraphy. *Journal of African Earth Sciences*. Volume 101, January 2015, Pages 282-308.

Johnson, M.R., Van Vuuren, C.J., Hegenberger, W.F., Key, R., Shoko, U. (1996). Stratigraphy of the Karoo Supergroup in southern Africa: an overview. *Journal of African Earth Sciences*. 23 (1), 3-15.

Kapilima S., (2002). Tectonic and sedimentary evolution of the coastal basin of Tanzania during the Mesozoic times. *Tanz. J. Sci.* Vol. 29 (1).

Kagya, M.L.N. (1996). Geochemical characterization of Triassic petroleum source rock in the Mandawa basin, Tanzania. *Journal of African Earth Sciences*. vol 23/1, 73-88.

Kearey, P., Brooks, M., Hill, I. (2002). An Introduction to Geophysical Exploration, 3e - 2192. *Malden, MA: Blackwell Science*.

Krabbendam, M. and Barr, T.T. (2000). Proterozoic orogens and the break-up of Gondwana: why did some orogens not rift? *Journal of African Earth Sciences*, 31: 35-49.

Kent, P.E., Hunt, J.A. and Johnstone, D.W. (1971). The geology and geophysics of coastal

Tanzania. Institute of Geological Sciences, *Geophysical Paper*, London, Vol. 6, 1-101.

Key, R.M., Smith, R.A., Smelor, M., Sæther, O.M, Thorsnes, T., Powell, J.H., Njange, F., Zandamela, E.B. (2008). Revised lithostratigraphy of the Mesozoic-Cenozoic succession of the onshore Rovuma Basin, northern coastal Mozambique. *South African Journal of Geology*. 111, 89–108.

Key, R.M., and Reeves, C.V. (2012). The post-Gondwana development of East Africa's coastline with emphasis on the development of the Rovuma Basin. Extended abstract. *Geological Society meeting*, London, October 24-26.

Killingley, J. S. (1983). Effects of diagenetic recrystallization of 18O/16O values of deep-sea sediments. *Nature.* London, 301:594-597.

Klimke, J. and Franke, D. (2016). Gondwana breakup: No evidence for a Davie Fracture Zone offshore northern Mozambique, Tanzania and Kenya. *Terra Nova*. 28. n/a-n/a. 10.1111/ter.12214.

König, M. and Jokat, W. (2010). Advanced insights into magmatism and volcanism of the Mozambique Ridge and Mozambique Basin in the view of new potential field data. *Geophysical Journal International*, 180, 158–180.

Koson, S. (2014). Enhancing Geological Interpretation with Seismic Attributes in Gulf of Thailand. *B.Sc. report*, Chulalongkorn Uni., Thailand, 42 p.

Koson, S., Chenrai, P., Choowong, M. (2014). Seismic Attributes and Their Applications in Seismic Geomorphology. *Bulletin of Earth Sciences of Thailand*. 6. pp. 1-9.

Lalaharisaina, J.V. and Ferrand, N.J. (1994). Cretaceous may hold promise in Majunga Basin, Madagascar. *Oil and Gas Journal*, p. 54-58.

Langer, M.C., da Rosa Á.A.S., Montefeltro, F.C. (2017). Supradapedon revisited: geological explorations in the Triassic of southern Tanzania. *Peer J5*: e4038; DOI 10.7717/peerj.4038.

Lehner, P. (1969). Salt tectonics and Pleistocene stratigraphy on continental slope of northern Gulf of Mexico. *American Association of Petroleum Geologists Bulletin*. v. 53, p. 2431–2479, doi: 10.1306/5D25C945-16C1-11D7-8645000102C1865D.

Lindseth, R.O. (1979). Synthetic sonic logs – A process for stratigraphic interpretation. *Geophysics*. 44, 3-26.

Lonropet SARL. (2000). Rovuma Basin, Mozambique. Fieldwork Interpretation and Analyses Report. The Petroleum Geology and Hydrocarbon Prospectivity of Mozambique '2000'. *Confidential Report.* ING, Maputo, Mozambique.

Maende, A. and Mpanju, F. (2003). Geochemistry and Source Rock Potential of East African Passive Margin. *East African Petroleum Conference*, Nairobi, 5 March 2003.

Maende, A. et al. (2008). Geochemical evaluation of source rocks and oil seeps from Tanzania's sedimentary basins. *AAPG International Convention*, Cape Town, December 2008, poster and abstract.

Macgregor, D. (2017). History of the development of Permian–Cretaceous rifts in East Africa: A series of interpreted maps through time. *Petroleum Geoscience*. 24. Petgeo 2016-155. 10.1144/petgeo2016-155.

Macgregor, D., Argent, J. and Sansom, P. (2017). Introduction to the thematic set: Tectonics and petroleum systems of East Africa. *Petroleum Geoscience,* 24, 3-7, 8 December 2017, https://doi.org/10.1144/petgeo2017-105.

Mahanjane, E.S. (2012). A geotectonic history of the northern Mozambique Basin including the Beira High–a contribution for the understanding of its development. *Marine and Petroleum Geology,* 36,1–12.

Marillier, F., Eichenberger, U., Sommaruga, A. (2006). Seismic synthesis of the Swiss Molasse Basin. *Schweizerische Geophysilaische Kommission SGPK*. Annual Report., pp.1–16.

Mbede, E.I. (1991). The sedimentary basins of Tanzania – reviewed. *Journal of African Earth Sciences (and the Middle East)*, Volume 13, Issues 3–4, 1991, Pages 291-297, ISSN 0899-5362. https://doi.org/10.1016/0899-5362(91)90092-D.

Mbede, E.I. and Dualeh, A. (1997). Chapter 10 The coastal basins of Somalia, Kenya and Tanzania. African Basins. Sedimentary Basins of the World, 3 edited by R.C. Selley (ed) African Basins, Sedimentary Basins of the World 3, *Elsevier Science*, p. 211-233.

McAfee, A. (2012). Transverse Troughs and a Transform Margin: Controls on Sandstone Deposition and Reservoir Development in the Kenyan and Tanzanian Coastal Basins. East Africa: Petroleum Province of the 21st Century. *Conference.*

McGuinness, D. and J. Hossack, (1993). The development of allochthonous salt sheets as controlled by the rates of extension, sedimentation, and salt supply: Rates of geological processes. *Gulf Coast Section SEPM 14th Annual Research Conference*. p. 127-139.

Meert, J. G. (2002). A synopsis of events related to the assembly of eastern Gondwana, *Tectonophysics*, 362, 1–40, doi:10.1016/S0040-1951(02)00629-7.

Miall, A.D. (1991). Stratigraphic sequences and their chronostratigraphic correlation. *Journal of. Sedimentary Research*, 61 (1991), pp. 497-505.

Mitchum, R.M. Jr. (1977). Seismic stratigraphy and global changes of sea level, part 11: glossary of terms used in seismic stratigraphy.

Mitchum, R.M. Jr., Vail, P.R. (1977). Seismic stratigraphy and global changes of sea-level, part 1: stratigraphic interpretation of seismic reflection patterns in depositional sequences.

Mitchum, R.M., Jr., Vail, P.R., and Thompson, S., III, (1977). Seismic stratigraphy and global changes of sea-level, Part 2: The depositional sequence as a basic unit for stratigraphic analysis, in Payton, C.E., ed., Seismic Stratigraphy—Applications to Hydrocarbon Exploration: *American Association of Petroleum Geologists Memoir* 26, p. 53–62.

Mitchum, R.M. and Van Wagoner, J.C. (1991). High frequency sequences and their stacking patterns: sequence-stratigraphic evidence of high-frequency eustatic cycles *Sediment. Geol*., 70 (1991), pp. 131-160.

Mpanda. (1997). Geological development of the East African coastal basin of Tanzania. *Stockholm Contributions in Geology*. 45, 1-212, University of Stockholm, Sweden.

Mpanju F., Ntomola, S., Kagya, M. (1991). The source rock potential of the Karroo coals of the south western Rift Basin of Tanzania. *Journal of Southeast Asian Earth Sciences*, Vol. 5, Nos 1 4, pp. 291 303, 1991.

Mpanju, F. and Philp. R.P. (1994). Organic geochemical characterization of bitumen, seeps, rock extracts and condensates from Tanzania. *Organic Geochemistry*. vol.21/3-4, 359-371.

Nairn, A., Lerche, E.M., Lliffe, E.I.J. (1991). Geology, basin analysis and hydrocarbon potential of Mozambique and the Mozambique Channel. *Earth-Science Reviews*. 30, 81e124.

Nelson, T.H. (1989). Style of salt diapirs as a function of the stage of evolution and the nature of encasing sediments. In: *Gulf Coast Section of the Society for Economic*

Palaeontologists and Mineralogists Annual Research Conference Program and Abstracts. Houston, Texas, pp. 109-110.

Nicholas, C.J., Pearson, P.N., Bown, P.R., Dunkley Jones, T., Huber, B.T., Karega, A., Lees, J.A., McMillan, I.K., O'Halloran, A., Singano, J., Wade, B.S. (2006). Stratigraphy and sedimentology of the upper Cretaceous to Paleogene Kilwa Group, southern coastal Tanzania. *Journal of African Earth Sciences*. 45, 431– 466.

Nicholas, C.J., Pearson, P.N., McMillan, I.K., Ditchfield, P.W., Singano, J.S. (2007). Structural evolution of coastal Tanzania since the Jurassic. *Journal of African Earth Sciences*. 48, 273–297.

Norris, R. D. and P. A. Wilson. (1998). Low-latitude sea-surface temperatures for the mid-Cretaceous and the evolution of planktic foraminifera. *Geology*, 26, 823–826, 1998.

Nuñez, C. (2015). Structural modeling workflow applied to a case study: Petrel 2014.4. TI G&G Exploration & Development, Repsol, Petrel support.

Nyambe, I.A. (1999). Tectonic and climatic controls on sedimentation during deposition of the Sinakumbe Group and Karoo Supergroup, in the mid-Zambezi Valley Basin, southern Zambia. *Journal of African Earth Sciences*. 28(2), 443-463.

Omar, V., Torres-Verdin, C. And Lake, L. (2006). On the value of 3D amplitude data to reduce uncertainty in the forecast of reservoir production. *Journal of Petroleum Science and Engineering*. 20, 269-284.

Payton, C.E. (1977). Seismic Stratigraphy — Applications to Hydrocarbon Exploration, Memoir, vol. 26, *American Association of Petroleum Geologists.* pp. 53-62.

Payton, C.E. (1977). Seismic Stratigraphy — Applications to Hydrocarbon Exploration, Memoir, vol. 26, *American Association of Petroleum Geologists*. pp. 135-144.

Payton, C.E. (1977). Seismic Stratigraphy — Applications to Hydrocarbon Exploration, Memoir, vol. 26, *American Association of Petroleum Geologists*. pp. 205-212.

Pearson, P., Ditchfield, P., Singano, J., Harcourt-Brown, K., Nicholas, C., Olsson, R., Shackleton, N. and Hall, M. (2001). Erratum: Warm tropical sea surface temperatures in the Late Cretaceous and Eocene epochs. *Nature*. 413. 481-487. 10.1038/35097000.

Pearson, P.N., Nicholas, C.J, Singano, J.M., Bown, P.R., Coxall, H.K., van Dongen, B.E., Huber, B.T., Karega, A., Lees, J.A., MacLeod, K., McMillan, I.K., Pancost, R.D., Pearson, M., Roberts, A.P. (2004). Paleogene and Cretaceous sediment cores from the Kilwa and Lindi areas of coastal Tanzania: Tanzania drilling project sites 1–5. *Journal of African Earth Sciences*. 39, 25–62.

Pearson, P.N., Nicholas, C.J., Singano, J.M., Bown, P.R., Coxall, H.K., van Dongen, B.E., Huber, B.T., Karega, A., Lees, J.A., MacLeod, K., McMillan, I.K., Pancost, R.D., Pearson, M., Msaky, E. (2006). Further Paleogene and Cretaceous sediment cores from the Kilwa area of coastal Tanzania: Tanzania drilling project sites 6–10. *Journal of African Earth Sciences*. 45, 279–317.

Pearson, P.N., Van Dongen, B.E., Nicholas, C.J., Pancost, R.D., Schouten, S., Singano, J.M., Wade, B.S. (2007). Stable warm tropical climate through the Eocene Epoch. *Geology*. 35 (3): 211–214. doi: https://doi.org/10.1130/G23175A.1.

Pearson P.N., McMillan, I.K., Singano, J.M., Wade, B.S., Jones, T.D., Coxall, H.K., Bown, P.R., Lear, C.H. (2008). Extinction and environmental change across the Eocene–Oligocene boundary in Tanzania. *Geology*. 36, 179–182.

Peel, F.J. (2014). How do salt withdrawal minibasins form? Insights from forward modelling, and implications for hydrocarbon migration. *Tectonophysics*. Volume 630, 2014, Pages 222-235, ISSN 0040-1951.

Pereira-Rego, M.C., Carr, A.D.,Cameron, N.R. (2013). Gas success along the margin of East Africa, but where is all the generated oil? *Search and Discovery*. Adapted from presentation at East Africa Petroleum Conference, October 24-26, 2012.

Peters, K., Walters, C., & Moldowan, J. (2004). The Biomarker Guide. *Cambridge: Cambridge University Press*. doi:10.1017/CBO9780511524868

Petrowiki. (2006). Acoustic logging tool.

Pigott, J.D., Kang, M.H., and Han, H.C. (2013). First order seismic attributes for clastic seismic facies interpretation: Examples from the East China Sea. *Journal of Asian Earth Sciences*. v.66, 34-54.

Pili, E., Ricard, Y., Lardeaux, J.M. and Sheppard, S.M.F. (1997). Lithospheric shear zones and mantle-crust connections. *Tectonophysics*, 280: 15-29.

Pinna, P., Jourde, G., Calvez, J. Y., Mroz, J. P., Marques, J. M. (1993). The Mozambique belt in northern Mozambique: Neoproterozoic (1100–850 Ma) crustal growth and tectogenesis, and superimposed Pan-African (800–550 Ma) tectonism, *Precambrian Res*., 62, 1–59, doi:10.1016/0301-9268(93)90093-H.

Piqué, A., Laville, E., Bignot, G., Rabarimanana, M., Thouin, C. (1999). The initiation and development of the Morondava Basin (Madagascar) from the Late Carboniferous to the Middle Jurassic: sedimentary, palaeontological and structural data. *Journal of African Earth Sciences.* 28, 931– 948.

Posamentier, H.W. and Vail, P. (1988). Eustatic controls on clastic deposition II – Sequence and Systems Tract Models. In: C. K. Wilgus, B. S. Hastings, C. G. St. C. Kendall, H. W. Posamentier, C. A. Ross and J. C. Van Wagoner, Editors, Sea Level Changes — An Integrated Approach, Special Publication vol. 42, *Society of Economic Paleontologists and Mineralogists* (SEPM) (1988), pp. 125–154. 10.2110/pec.88.01.0125.

Posamentier, H.W., Jervey, M.T. and Vail, P. R. (1988). Eustatic controls on clastic deposition I — conceptual framework. In: C. K. Wilgus, B. S. Hastings, C. G. St. C. Kendall, H. W. Posamentier, C. A. Ross and J. C. Van Wagoner, Editors, Sea Level Changes — An Integrated Approach, Special Publication vol. 42, *Society of Economic Paleontologists and Mineralogists* (SEPM) (1988), pp. 110–124.

Posamentier, H.W., Allen, P.G., James, D.P.; Tesson, M. (1992). Forced regression in a seismic stratigraphic framework: concepts, examples and exploration. *AAPG Bulletins*, v. 76, p. 1687-1709. 1992.

Posamentier, H.W., Allen, P.G. (1993). Variability of the sequence stratigraphic model: effects of local basin factors, *Sedimentary Geology*, Volume 86, Issues 1–2, 1993, Pages 91-109, ISSN 0037-0738, https://doi.org/10.1016/0037-0738(93)90135-R.

Prather, B.E., (2000). Calibration and visualization of depositional process models for above-grade slopes: a case study from the Gulf of Mexico. *Marine and Petroleum Geology*, v.17, p. 619638.

Quirk, D.G., Schodt, N., Lassen, B., Ings, S.J., Hsu, D., Hirsch, K.K., Von Nicolai, C. (2012). Salt tectonics on passive margins: examples from Santos, Campos and Kwanza basins

G.I. Alsop, S.G. Archer, A.J. Hartley, N.T. Grant, R. Hodgkinson (Eds.), Salt Tectonics, Sediments and Prospectivity, *Geological Society of London Special Publications*, vol. 363, pp. 207-244.

Rabinowitz, P., Coffin, M., & Falvey, D. (1982). Salt Diapirs Bordering the Continental Margin of Northern Kenya and Southern Somalia. *Science*, 215(4533), 663-665. Retrieved from www.jstor.org/stable/1688205.

Rabinowitz, D.P., Coffin, M. and Falvey, D. (1983). The Separation of Madagascar and Africa. *Science*. 220. 67-69. 10.1126/science.220.4592.67.

Radovich, B.J., and Oliveros, R.B. (1998). 3-D sequence interpretation of seismic instantaneous attributes from the Gorgon field: *The Leading Edge*, v. 17, p. 1286–1293.

Ramberg, H. (1981). Gravity, Deformation and the Earth's Crust in Theory, Experiments and Geological Applications, *Academic Press*, (2nd edn), London.

Rapolla, A., Cella, F., & Dorre, A. S. (1995). Gravity study of the crustal structures of Somalia along International Lithosphere Program geotransects. *Journal of African Earth Sciences*, 20(3–4), 263–274. https://doi.org/10.1016/0899-5362(95)00053-V.

Red, C. (1982). Handbook of Physical Properties of Rocks. *CRC Press Inc*. Vol. 2, 1-228. Boca Raton, Florida.

Reeves, C.V., Sahu, B.K., de Wit, M.J., (2002). A re-examination of the palaeo-position of Africa's eastern neighbours in Gondwana. *Journal of African Earth Sciences*. 34, 101–108.

Reeves, C.V. (2009). Re-examining the evidence from plate-tectonics for the initiation of Africa's passive margins. Extended abstract, *Geological Society of Houston/Petroleum Exploration Society of Great Britain,* London, 2009 September 9-10.

Reeves, C.V., Teasdale, J.P. and Mahanjane, E.S. (2016). Insight into the Eastern Margin of Africa from a new tectonic model of the Indian Ocean. In: Nemcok, M., Rybár, S., Sinha, S.T., Hermeston, S.A. & Ledvényiová, L. (eds) Transform Margins: Development, Controls and Petroleum Systems. Geological Society, London, *Special Publications*, 431, 299 –322, https://doi.org/10.1144/SP431.12.

Reeves, C.V. (2017). The development of the East African margin during Jurassic and Lower Cretaceous times: A perspective from global tectonics. *Petroleum Geoscience*. 24. petgeo2017-021. 10.1144/petgeo2017-021.

Rider, M.H. (1986). The geological interpretation of well logs. *United States: John Wiley and Sons, Inc.*

Rider, M.H. (1996). Rider, M., 1996. The geological interpretation of well-logs, second edition. *Whittles Publishing, Caithness*, 268 pp.

Rider, M.H. (2002). The Geological Interpretation of Well Logs. *Rider-French Consulting.*

Roberts, G.F., Christoffersen, T., Spec Partners Ltd., Jingwei, X., BGP Multi Client. (2018). Offshore Madagascar Part I: Hydrocarbon Potential. What is the hydrocarbon potential of the Mozambique Channel, and what has the 'Golden Zone' theory got to do with it? *GeoExpro. Exploration Africa.*

Robertson and TPDC. (1986). TPDC internal report by Robertson Research Limited. The Source Rock Potential of Tanzania. *Report and Geochemical Data*, (unpublished), 650 pp.

Rowan, M.G., Jackson, M.P.A. and Trudgill, B.D. (1999). Salt-related fault families and fault welds in the northern Gulf of Mexico. *AAPG Bulletin*. 83, 1454 - 1484.

Rowan, M.G. (2014). Passive-margin salt basins: hyperextension, evaporite deposition, and salt tectonics. *Basin Research*. 26, 154-182.

Rusk, Bertagne & Associates. (2003). Petroleum Geology and Geophysics of the Mozambique Channel. *Multi-Client Report* 2003.

Said, A., Moder, C., Clark, S., Abdelmalak, M.M. (2015). Sedimentary budgets of the Tanzanian coastal basin and implications for uplift history of the East African rift system. *Journal of African Earth Sciences*. 111, 288-295.

Salman, G. and Abdula, I. (1995). Development of the Mozambique and Ruvuma sedimentary basins, offshore Mozambique. *Sedimentary Geology*. 96, 7–41.

Sandwell, D.T. and Smith, W. H. F. (2009). Global marine gravity from retracked Geosat and ERS-1 altimetry: Ridge segmentation versus spreading rate. *Journal of Geophysical Research*, 114, B01411, doi:10.1029/2008JB006008.

Sandwell, D.T., Müller, D.R., Smith, W.H.F., Garcia, E. and Francis, R. (2014). New global marine gravity model from CryoSat-2 and Jason-1 reveals buried tectonic structure. *Science*, 346,65–67.

Sansom, P. (2016). Sequence Stratigraphic scheme for the Jurassic-Neogene of coastal and offshore Tanzania. East Africa from research to reserves. *Geological Society*, London, UK.

Sarg, J.F. (1988). Carbonate sequence stratigraphy, in C.K. Wilgus, B.S. Hastings, and C.G. Kendall, (eds.), Sea level changes — an integrated approach: *SEPM Special Publication*, v. 42, p. 155-181.

Schettino, A., & Scotese, C. R. (2005). Apparent polar wander paths for the major continents (200 Ma to the present day): A palaeomagnetic reference frame for global plate tectonic reconstructions. *Geophysical Journal International*, 163(2), 727–759. https://doi.org/10.1111/j.1365-246X. 2005.02638.x

Schlager, W. (1992). Sedimentology and sequence stratigraphy of reefs and carbonate platforms. *American Association for Petroleum Geologists Continuing Educational Course Note Series* 34, pp 71.

Schlumberger. (2017). Oilfield Glossary.

Schlumberger Limited. (1974). Log Interpretation: Applications. 1974 ed.

Schlumberger Well Services Inc. (1989). Log Interpretation Principles/Applications, vol. I. Houston, *Schlumberger Well Services, Inc.*

Schlumberger Well Services. (1991). Log Interpretation Charts.

Schlumberger User Guide. (2018). Petrel version 2018.1.

Schlüter, T. (1997). Geology of East Africa. *Borntraeger*, Stuttgart, 512 pp.

Schoenherr, J., Reuning, L., Kukla, P. Littke, R., Urai, J., Siemann, M. and Rawahi, Z. (2009). Halite cementation and carbonate diagenesis of intra-salt reservoirs from the Late

Neoproterozoic to Early Cambrian Ara Group (South Oman Salt Basin). *Sedimentology*. 56. 567 - 589. 10.1111/j.1365-3091.2008.00986.x.

Schrag, D. P. (1999). Effects of diagenesis on the isotopic record of late Paleogene tropical sea surface temperatures. *Chemical Geology*,161, 215–224.

Schwerdtner, W.M., Sutcliff, R.H., Troeng, B. (1978). Patterns of total strain within the crestal region of immature diapirs. *Canandian Journal of Earth Sciences*, 15 (1978), pp. 1437-1447.

Scrutton, R.A. (1978). Davie fracture zone and the movement of Madagascar. *Earth and Planetary Science Letters*, 39, 84-88.

Serra, O. (1988). Fundamentals of well-log interpretation. 3rd ed. *New York: Elselvier science publishers*. B.V.: 261-262.

Seward D, Grujic, D., Schreurs, G. (2004). An insight into the breakup of Gondwana: identifying events through low-temperature thermochronology from the basement rocks of Madagascar. *Tectonics*. 23, 1– 20.

Sheline, H.E. (2005). The use and abuse of seismic attributes. *Search and discovery*. Article #40143.

Shell. (1990). Map, stratigraphy and geological history of the Mandawa Basin, (Enclosures in Veeken, P.C.H.). *Shell Petroleum Development Tanzania/TPDC Geofile* 296.90 EB. Unpublished (90/1).

Sheriff, R.E. (1994). Encyclopaedia of exploration geophysics. Society of Exploration *Geophysics*. 1994.

Sheriff, R.E. and Geldart, L.P. (1995). Exploration Seismology, 2nd Edition. *Cambridge University Press*, Cambridge. 1995. doi:10.1017/CBO9781139168359.

Shuey, R. T. (1985). A simplification of the Zoeppritz equations. *Geophysics*. 50: 609-614.

Sinha, S. T., Saha, S., Longacre, M., Basu, S., Jha, R., & Mondal, T. (2019). Crustal architecture and nature of continental breakup along a transform margin: New insights from Tanzania-Mozambique margin. *Tectonics*, 38, 1273– 1291.

Smelror, M., Key, R.M., Daudi, E., Njange, F. (2006). Frontier with high expectations. *GeoExpro*. 3(2):14–18.

Smelror, M., Key, R.M., Smith, R.A., Thorsnes, T., Saether, O.M., Zandamela, E.B., Powell, J.H. (2008). Revised lithostratigraphy of the onshore Rovuma Basin, northern Mozambique *South African Journal of Geology*; Mar 2008, Vol. 111 Issue 1, p89.

Smith, M. (1994). Stratigraphic and structural constraints on mechanisms of active rifting in the Gregory Rift, Kenya: *Tectonophysics*, v. 236, p.3-22 doi: 10.1016/0040-1951(94)90166-x.

Smith, W.H.F. and Sandwell, D.T. (1997). Global sea floor topography from satellite altimetry and ship depth soundings. *Science,* 277, 1956– 1962.

Spence, J. (1957). The geology of part of the Eastern Province of Tanganyika. Bull. No. 28, *Geological Survey Tanganyika*. 62 pp.

Spence, J. (1959). Geological completion report of Mandawa well no.7.

Stern, R.J. (1994). Arc assembly and continental collision in the Neoproterozoic East-African Orogen — implications for the consolidation of Gondwanaland. *Annual Reviews of Earth and Planetary Sciences,* 22 (1994), pp. 319-351.

Stewart, D.R.M., Pearson, P.N., Ditchfield, P.W., Singano, J.M. (2004). Miocene tropical Indian Ocean temperatures: evidence from three exceptionally preserved foraminiferal assemblages in Tanzania. *Journal of African Earth Sciences*. 40, 173–190.

Talbot, C. J. and Jackson, M. P. (1987). Salt tectonics. *Scientific American*, 257, 7079.

Talbot, C. (1995). Molding of salt diapirs by stiff overburden. *AAPG Memoir*. 65.

Tamannai, M.S. (2008). An Evaluation of the Petroleum System Offshore Morondava Basin, Madagascar. *Proceedings 70th EAGE Conference and Exhibition*. Rome, 4 p.

Tamannai, M.S., Winstone, D., Deighton, I., Conn, P. (2010). Geological and Geophysical Evaluation of Offshore Morondava Frontier Basin Based on Satellite Gravity, Well and Regional 2D Seismic Data Interpretation. *AAPG Search & Discovery*. Article #10229.

Tanzanian Petroleum Development Corporation - TPDC (2005). *Promotion Brochure*. Dar es Salaam, Tanzania.

Tanzania Petroleum Development Corporation *Promotion Brochure*. (2009). Tanzania Petroleum Development Corporation, 1-50.

Taylor, J.C.M. *et al.* (1985). The Role of Evaporites in Hydrocarbon Exploration. Joint Association of Petroleum Explorationists (UK). Course notes No. 39 *Geological Society*, London.

Tari, G., Coterill, K., Molnar, J., Valasek, D., Walters, G. and Alvarez, Y. (2004). Salt Tectonics and Sedimentation in the Offshore Majunga Basin, Madagascar. *Transactions GCSSEPM Foundation*. 24. 614-628. 10.5724/gcs.04.24.0614.

Tari, G. and Rock, G. (2016). Exploration analogy between the offshore Morondava Basin, Madagascar, and the transform margin of West Africa. PESGB/HGS Africa Conference, Houston, September 2016.

Thigpen, B.B, Dalby, A. E. and Landrum, R. (1975). Report on Subcommittee on Polarity Standards: *Geophysics*, 40, no. 04, 694-699. (* Discussion in GEO-41-02-0324-0324; Reply in GEO-41-02-0324-0324).

Thomas, R. J., Jacobs, J., Horstwood, M.S.A., Ueda, K., Bingen, B., Matola, R. (2010). The Mecubúri and Alto Benfica groups, NE Mozambique: Aids to unravelling ca. 1 Ga and 0.5 Ga events in the East African Orogen, *Precambrian Res*., 178, 72–90.

Tittman, J. and Wahl, J.S. (1965). The physical foundations of formation density logging (Gamma-Gamma). *Geophysics.* v, 30, p. 284-294.

Tranter, N. (2017). Offshore Madagascar: hydrocarbon potential in frontier basins. TGS – Africa and Middle East. *TGS-NOPEC Geophysical Company* ASA.

Trusheim, F. (1960). Mechanism of salt migration in northern Germany. *AAPG Bulletin*. 44, 1519-1540.

Tucker, M.E. (1991). Sequence stratigraphy of carbonate-evaporite basins: models and application to the Upper Permian (Zechstein) of northeast England and adjoining North Sea. *Journal of the Geological Society;* 148 (6): 1019–1036.

Vail, P.R., Mitchum, R.M. Jr. and Thompson III, S. (1977). Seismic stratigraphy and global changes of sea level, part four: global cycles of relative changes of sea level. American *Association of Petroleum Geologists Memoir* 26, pp. 83–98.

Vail, P.R., Audemard, F., Bowman, S.A., Eisner, P. N. and Perez-Cruz, C. (1991). The stratigraphic signatures of tectonics, eustasy and sedimentology - an overview. In: Einsele, G., Ricken, W. & Seilacher, A. (eds) *Cycles and Events in Stratigraphy*. Springer-Verlag, Berlin, 617-659.

Van Dongen, B.E., Talbot, H.M., Schouten, S., Pearson, P.N., Pancost, R.D. (2006). Well preserved Palaeogene and Cretaceous biomarkers from the Kilwa area, Tanzania. *Organic Geochemistry*. 37, 539–557.

Van Wagoner, J.C., Posamentier H.W., Mitchum R.M., Vail P.R., Sarg J.F., Loutit T.S., Hardenbol, J. (1988). An Overview of the Fundamentals of Sequence Stratigraphy and Key Definitions, Sea-Level Changes: An Integrated Approach. Cheryl K. Wilgus, Bruce S. Hastings, Henry Posamentier, John Van Wagoner, Charles A. Ross, Christopher G. St. C. Kendall.

Veeken, P. and Titov, K. (1996). Gravity modelling along a seismic line across the Mandawa basin, southeastern Tanzania. *Journal of African Earth Sciences*. 22. 207-217. 10.1016/0899-5362(96)00001-2.

Verniers, J., Jourdan, P.P., Paulis, R.V., Frasca-Spada, L. and De Bock, F. R. (1989). The Karroo Graben of Metangula, Northern Mozambique. *Journal African Earth Sciences*. 9 (1), 137–158; Oxford.

Viola, G., Henderson, I. H. C., Bingen, B., Thomas, R.J., Smethurst, M.A., de Azavedo, S. (2008). Growth and collapse of a deeply eroded orogen: Insights from structural and geochronological constraints on the Pan-African evolution of NE Mozambique, *Tectonics*, 27, TC5009, doi:10.1029/2008TC002284.

Wade, B.S., Pearson, P.N., (2008). Planktonic foraminiferal turnover, diversity fluctuations and geochemical signals across the Eocene/Oligocene boundary in Tanzania. Mar. *Micropaleontology*. 68, 244–255.

Walden, A.T. and White, R.E. (1984). On errors of fit and accuracy in matching synthetic seismograms and seismic traces. *Geophysical Prospecting*. 32,871–891.

Warren, J. (1999). Evaporites. Their Evolution and Economics. *Oxford: Blackwell Science*. ISBN 0 632 05301 1. 438 pp.

Warren, J.K. (2006). Evaporites: Sediments, Resources and Hydrocarbons: Sediments, Resources, and Hydrocarbons, *Springer*.

Warren, J.K. (2018). Well (wireline) log interpretation of evaporites: An overview. Salty Matters. *Saltworks Consultants*.

Wescott, W.A. and Diggins, J.N. (1997). Depositional history and stratigraphical evolution of the Sakoa Group (Lower Karoo Supergroup) in the southern Morondava Basin, Madagascar. *Journal of African Earth Sciences* 24(4): 585-601.

Wescott, W.A. and Diggins, J.N. (1998). Depositional history and stratigraphical evolution of the Sakamena Group (Middle Karoo Supergroup) in the Morondava basin, Madagascar. *Journal of African Earth Sciences* 27, 461 – 479.

White, R.E. (1997). The accuracy of well ties: practical procedures and examples. Expanded Abstract. RC1.5, 67th SEG Meeting, Dallas.

White, R. E. and Hu, T. (1998). How accurate can a well tie be? *The Leading Edge*. 18 (8), 1065-1071.

White, R., and Simm, R. (2002). Tutorial: Phase, polarity and the interpreter's wavelet. *First Break*. 20 (5), p 277–281.

White, R., and Simm, R. (2003). Tutorial: Good practice in well ties. *EAGE first break*, 21,75 – 83.

Wichura, H., Bousquet, R., Oberhänsli, R., Strecker, M., Trauth, M. (2010). Evidence for middle Miocene uplift of the East African Plateau. *Geology*. 38. 543-546. 10.1130/G31022.1.

Wilson, P. A., and R. D. Norris. (2001). Warm tropical ocean surface and global anoxia during the mid- Cretaceous period. *Nature*, 412, 425–429, 2001.

Wilson, P. A., R. D. Norris, M. J. Cooper. (2002). Testing the Cretaceous greenhouse hypothesis using glassy foraminiferal calcite from the core of the Turonian tropics on Demerara Rise. *Geology*, 30, 607–610, 2002.

Winker, C.D and Booth, J.R. (2000). Sedimentary dynamics of the salt-dominated continental slope, Gulf of Mexico: Integration of observations from the seafloor, near-surface, and deep subsurface, in P. Weimer, R. M. Slatt, J. Coleman, N. C. Rosen, H.

Nelson, A. H. Bouma, M. J. Styzen, and D. T. Lawrence, eds., Deep-water Reservoirs of the World. *SEPM Gulf Coast Section 20th Annual Research Conference*. p. 1059-1086.

Wopfner, H. (1994). The Malagasy Rift, a chasm in the Tethyan margin of Gondwana: Gondwana dispersion and Asian accretion. *Journal of Southeast Asian Earth Sciences*. 9, 451–461.

Wopfner, H. (2002). Tectonic and climatic events controlling deposition in Tanzanian Karoo basins. *Journal of African Earth Sciences*. 34, 167-177.

Worrall, D.W. and Snelson, S. (1989). Evolution of the northern Gulf of Mexico, with emphasis on Cenozoic growth faulting and the role of salt. A.W. Bally, A.R. Palmer (Eds.), The Geology of North America — An Overview, Vol. A, *Geological Society of America*. Boulder, CO (1989), pp. 97-138.

Wu D., Ramaniraka, J.I., Xu, F., Shao, J., Zhou, Y., Zhao, Y., Ralison, B. (2019). Characteristics and potential analysis of Madagascar hydrocarbon-bearing basins, China *Geology*, Volume 2, Issue 1, 2019, Pages 56-66, ISSN 2096-5192.

Yu, Y., Tang L., Yang, W., Huang, T., Qiu, N. & LI, W. (2014). Salt structures and hydrocarbon accumulations in the Tarim Basin, northwest China. *AAPG Bulletin*. 98, 135-159.

Zongying, Z., Ye, T., Shujun, L., Wenlong., D. (2013). Hydrocarbon potential in the key basins in the East Coast of Africa. *Petroleum Exploration and Development*, Volume 40, Issue 5, 2013, Pages 582-591, ISSN 1876-3804.

APPENDICES

APPENDICES

Appendix 2.2.1 – Summary of the LAS files used in this thesis. The data were manually imported for each well. GR – Gamma Ray, PHIE – Effective Porosity, RHOB – Density, SGR – Gamma Ray, SP – Spontaneous Potential, CALI- Caliper, ILD – Resistivity, DT – Sonic, AI – Acoustic Impedance – DT-E – P-Sonic, DT-E-corrected – Sonic corrected.

Well	GR	PHIE	RHOB	SGR	SP	CALI	ILD	DT	AI	RC	ΔT-E	ΔT-E-corrected
East Lika-1	Yes	No	Yes	No	Yes	Yes	Yes	Yes	No	No	No	No
Kizimbani-1	Yes	No	No	No	Yes	No	No	Yes	No	No	Yes	No
Lukuliro-1	Yes	No	Yes	No	Yes	Yes	Yes	Yes	No	No	No	No
Mbate-1	Yes	Yes	Yes	No	Yes	Yes	No	Yes	No	No	No	No
Mbuo-1	Yes	No	Yes	No	Yes	Yes	No	Yes	No	No	No	No
Mihambia-1	Yes	No	Yes	No	No	Yes	No	Yes	Yes	Yes	Yes	Yes
Mita Gamma-1	Yes	Yes	Yes	Yes	Yes	No	No	Yes	No	No	No	No
Kianika-1	Yes	No	Yes	No	Yes	Yes	No	Yes	No	No	No	No
Lukuledi-1	Yes	No	Yes	No	Yes	Yes	Yes	Yes	No	No	No	No
Mandawa-7	Yes	No	Yes	No	Yes	Yes	No	No	No	No	No	No
Liwale-1	Yes	No	No	No	No	No	No	Yes	No	No	No	No

Appendix 2.2.2 – Summary of Well heads. Well (well name), Surface X – UTM E, Surface Y – UTM N, Latitude, Longitude, Well datum – Kelly Bushing.

Well	Surface X	Surface Y	Latitude	Longitude	Well datum
East Lika-1	507431	8974961	9°16'22.9228"S	39°04'3.5720"E	KB =7
Kizimbani-1	540110	9001125	9°02'10.3390"S	39°21'53.8405"E	KB = 7
Lukuliro-1	437042	9076079	8°21'28.7896"S	38°25'41.4779"E	KB = 128.5
Mbate-1	497250	9014200	8°55'5.2364"S	38°58'29.9497"E	KB = 100
Mbuo-1	530829	8955956	9°26'41.3769"S	39°16'51.0001"E	KB = 148.8
Mihambia-1	524183	8972728	9°17'35.4120"S	39°13'12.7097"E	KB = 211.6
Mita Gamma-1	518126	9014547	8°54'53.8086"S	39°09'53.5400"E	KB =7
Kianika-1	512437.06	9073565.96	8°22'52.0516"S	39°06'46.6817"E	KB =140.4
Lukuledi-1	572953	8876193	.0°09'56.4942"S	39°39'57.5383"E	KB = 47
Mandawa-7	545857	8959104	9°24'58.3863"S	39°25'3.6945"E	KB = 170
Liwale-1	337629.4	8957110.66	9°25'53.0000"S	37°31'16.0000"E	KB = 503.5

Appendix 2.2.2 – Summary of Well heads. Well (well name), Well symbol – defined custom symbol previously, TVDSS - True Vertical Depth measured from Mean Sea Level, MD – Measure Depth, Bottom hole X – Bottom hole coordinate in Y, Bottom hole Y – Bottom hole coordinate in Y.

Well	Well symbol	TVDSS	MD	Bottom hole X	Bottom hole Y
East Lika-1	Dry	1995	2002	507431	8974961
Kizimbani-1	Dry	2690	2697	540110	9001125
Lukuliro-1	Dry	2238.5	2367	437042	9076079
Mbate-1	Abandoned	3217	3317	497250	9014200
Mbuo-1	Dry	3164.2	3313	530829	8955956
Mihambia-1	Dry	2296.4	2508	524183	8972728
Mita Gamma-1	Abandoned	2383	2390	518126	9014547
Kianika-1	Gas	2781.6	2922	512437.06	9073565.96
Lukuledi-1	Undefined	1894	1941	572953	8876193
Mandawa-7	Abandoned	3895	4065	545857	8959104
Liwale-1	Dry	1258.5	1762	337629.4	8957110.66

Appendix 2.2.2 – Summary of Well heads. Well (well name), Weathering velocity in ms, ground elevation from mean sea level in ms, bottom of weathering elevation from mean sea level in m.

Well	Weathering velocity [m/s]	Ground elevation (from MSL) [m]	Velocity below weathering[m/s]	Bottom of weathering elevation (from MSL) [m]
East Lika-1	2400	7	2400	7
Kizimbani-1	1524	18	2400	25
Lukuliro-1	1880	128.5	2400	128.5
Mbate-1	2400	100	2400	100
Mbuo-1	2400	148.8	2400	148.8
Mihambia-1	2400	205	1875.6	205
Mita Gamma-1	1564	92.65	2400	92.65
Kianika-1	2400	140.4	2400	140.4
Lukuledi-1	2400	47	2400	47
Mandawa-7				
Liwale-1	2400	504	2400	504

Appendix 2.2.3 – Summary of the wells that have checkshots used in this study. Well (well name, MD – Measure Depth, TWT – Two -way - time, Average velocity, Interval velocity, Sonic time, Sonic Interval Velocity, Drift – Residual drift.

Well	MD	TWT	Average velocity	Interval velocity	Sonic time	Sonic Int. Velocity	Drift
Mita Gamma-1	223	142.36	3034.56	2621.48	71.18		0
Mita Gamma-1	305	204.92	2908.45	2767.16	98.51	3000.01	-3.95
Mita Gamma-1	381	259.85	2878.58	3005.32	123.88	2995.63	-6.04
Mita Gamma-1	457.2	310.56	2899.28	2947.21	147.52	3223.19	-7.76
Mita Gamma-1	533.4	362.27	2906.12	3075.91	171.9	3126.37	-9.24
Mita Gamma-1	580	392.57	2919.22	2232.34	187.28	3030.18	-9.01
Mita Gamma-1	656	460.66	2817.7	4339.82	211.84	3094.15	-18.49
Mita Gamma-1	762	509.51	2963.63	3143.09	247.04	3011.41	-7.72
Mita Gamma-1	838	557.87	2979.19	3258.69	270.79	3199.35	-8.14
Mita Gamma-1	914.4	604.76	3000.86	3459.7	294.36	3242.45	-8.02
Mita Gamma-1	990.6	648.81	3032.01	3346.56	315.36	3627.07	-9.04
Mita Gamma-1	1045.4	681.56	3047.13	3708.21	332.35	3225.47	-8.43
Mita Gamma-1	1143	734.2	3094.52	3598.62	356.28	4079.24	-10.82
Mita Gamma-1	1195	763.1	3113.62	3500.09	369.73	3864.95	-11.82
Mita Gamma-1	1295.4	820.47	3140.64	3706.23	395.71	3864.7	-14.52
Mita Gamma-1	1371.6	861.59	3167.63	3496.57	416.79	3615.3	-14
Mita Gamma-1	1448	905.29	3183.51	3626.14	438.35	3543.15	-14.29
Mita Gamma-1	1499.6	933.75	3197	3789.08	452.71	3594.95	-14.17
Mita Gamma-1	1600.2	986.85	3228.86	3674.95	477.69	4025.97	-15.73
Mita Gamma-1	1676.4	1028.32	3246.85	4067.25	497.61	3826.39	-16.55
Mita Gamma-1	1752.6	1065.79	3275.69	4273.7	516.45	4043.54	-16.44
Mita Gamma-1	1828.8	1101.45	3308	4226.29	534.53	4215.39	-16.19

Mita Gamma-1	1905	1137.51	3337.11	4460.72	552.1	4337.81	-16.66
Mita Gamma-1	1972	1167.55	3366.02	4243.48	567.17	4443.9	-16.6
Mita Gamma-1	2057.4	1207.8	3395.26	4425.09	584.58	4906.73	-19.32
Mita Gamma-1	2133.6	1242.24	3423.82	4182.22	600.63	4748.15	-20.49
Mita Gamma-1	2209.8	1278.68	3445.43	4766.71	618.41	4283.8	-20.93
Mita Gamma-1	2304.3	1318.33	3485.17	5153.19	640.33	4312.94	-18.84
Mita Gamma-1	2388.4	1350.97	3525.47				
Kizimbani-1	25	22	1636.36	2282.35	11		0
Kizimbani-1	219	192	2208.33	4446.43	90.16	2450.75	-5.84
Kizimbani-1	966	528	3632.58	3207.32	266.07	4246.52	2.07
Kizimbani-1	1755	1020	3427.45	5777.78	504.75	3305.72	-5.25
Kizimbani-1	1807	1038	3468.21	3695.65	516.77	4323.08	-2.23
Kizimbani-1	1892	1084	3477.86	3651.52	537.62	4077.97	-4.38
Kizimbani-1	2374	1348	3511.87	3944.44	669.72	3648.62	-4.28
Kizimbani-1	2587	1456	3543.96	3943.87	726.1	3778.31	-1.9
Kizimbani-1	2635.9	1480.8	3550.65		737.17	4418.04	-3.23
Mihambia-1	211.5	0		2483.33	0		0
Mihambia-1	449.9	192	2482.29	2670.23	89.45	2665.23	-6.55
Mihambia-1	549.9	266.9	2535.03	2695.42	124.13	2883.3	-9.32
Mihambia-1	649.9	341.1	2569.92	2873.56	159.89	2796.36	-10.66
Mihambia-1	749.9	410.7	2621.38	2790.5	192.74	3044.26	-12.61
Mihambia-1	849.8	482.3	2646.49	3010.56	226.7	2941.47	-14.45
Mihambia-1	949.6	548.6	2690.48	2989.54	258.06	3182.47	-16.24
Mihambia-1	1049.6	615.5	2722.99	3110.42	286.83	3476.25	-20.92
Mihambia-1	1149.6	679.8	2759.64	3451.72	315.29	3513.82	-24.61
Mihambia-1	1249.7	737.8	2814.04	3530.04	343.5	3547.78	-25.4
Mihambia-1	1349.6	794.4	2865.06	3472.22	368.54	3990.19	-28.66
Mihambia-1	1399.6	823.2	2886.3	3597.12	380.75	4094.44	-30.85

Mihambia-1	1449.6	851	2909.52	3864.6	392.49	4257.57	-33.01
Mihambia-1	1549.5	902.7	2964.22	4065.04	417.17	4048.12	-34.18
Mihambia-1	1649.5	951.9	3021.12	4572.08	440.16	4350.94	-35.79
Mihambia-1	1749.4	995.6	3089.19	4128.1	462.01	4571.51	-35.79
Mihambia-1	1849.3	1044	3137.36	4468.75	483.42	4666.49	-38.58
Mihambia-1	1949.4	1088.8	3192.14	4455.36	507.98	4075.69	-36.42
Mihambia-1	2049.2	1133.6	3242.06	4396.48	533.21	3955.21	-33.59
Mihambia-1	2149	1179	3286.51	3773.16	557.64	4084.29	-31.86
Mihambia-1	2248.8	1231.9	3307.41	4073.77	581.73	4142.73	-34.22
Mihambia-1	2348.2	1280.7	3336.61	4198.31			
Mihambia-1	2447.7	1328.1	3367.37				
Mandawa-7	170.1	0.1	2000	2482.54			
Mandawa-7	408.3	192	2482.29	2670.23			
Mandawa-7	508.3	266.9	2535.03	2695.42			
Mandawa-7	608.3	341.1	2569.92	2873.56			
Mandawa-7	708.3	410.7	2621.38	2790.5			
Mandawa-7	808.2	482.3	2646.49	3010.56			
Mandawa-7	908	548.6	2690.48	2989.54			
Mandawa-7	1008	615.5	2722.99	3110.42			
Mandawa-7	1108	679.8	2759.64	3451.72			
Mandawa-7	1208.1	737.8	2814.04	3530.04			
Mandawa-7	1308	794.4	2865.06	3472.22			
Mandawa-7	1358	823.2	2886.3	3597.12			
Mandawa-7	1408	851	2909.52	3864.6			
Mandawa-7	1507.9	902.7	2964.22	4065.04			
Mandawa-7	1607.9	951.9	3021.12	4572.08			
Mandawa-7	1707.8	995.6	3089.19	4128.1			
Mandawa-7	1807.7	1044	3137.36	4468.75			

Mandawa-7	1907.8	1088.8	3192.14	4455.36			
Mandawa-7	2007.6	1133.6	3242.06	4396.48			
Mandawa-7	2107.4	1179	3286.51	3773.16			
Mandawa-7	2207.2	1231.9	3307.41	4073.77			
Mandawa-7	2306.6	1280.7	3336.61	4198.31			
Mandawa-7	2406.1	1328.1	3367.37				
East Lika-1	7	0		2771.19	0		0
East Lika-1	144.73	99.4	2771.19	3469.9	64.52	2134.67	14.82
East Lika-1	506.64	308	3244.41	5616.27	195.29	2767.57	41.29
East Lika-1	590.88	338	3454.93	4352.5	219.69	3452.93	50.69
East Lika-1	1117.54	580	3829.43	4607.09	312.14	5696.3	22.14
East Lika-1	1440.03	720	3980.64	3745.79	386.33	4346.82	26.33
East Lika-1	1544.91	776	3963.7	3884.3	409.06	4614.61	21.06
East Lika-1	1649.79	830	3958.53		435.47	3971.52	20.47
Mbate-1	100	0		3227.54	0		0
Mbate-1	762	410.22	3227.54	3417.23	225.36	2937.52	20.25
Mbate-1	929	507.96	3264.04	3573.86	275.67	3319.68	21.69
Mbate-1	1191	654.58	3333.44	3916.27	350.66	3493.72	23.37
Mbate-1	1249	684.2	3358.67	4143.94	366.18	3737.49	24.08
Mbate-1	1834	966.54	3588.06		511.44	4027.12	28.17
Mbuo-1	148.8	0		3379.54	0		0
Mbuo-1	200	30.3	3379.54	3988.84	10.38	4931.84	-4.77
Mbuo-1	443	152.14	3867.49		82.31	3378.48	6.24
Lukuliro-1	128	0		3749.88	0		0
Lukuliro-1	528.49	213.6	3745.2	3983.82	140.11	2858.41	33.31
Lukuliro-1	809.39	354.62	3840.09	4233.18	215.02	3749.77	37.71
Lukuliro-1	863.11	380	3866.34	5142.49	228.5	3984.09	38.5
Lukuliro-1	960.4	417.84	3981.91	4903.14	251.49	4231.71	42.57

Lukuliro-1	1802.86	761.48	4397.64	4484.28	415.31	5142.71	34.57
Lukuliro-1	1813.13	766.06	4398.16	4484.28	417.4	4913.48	34.37
Lukuliro-1	1823.4	770.64	4398.67		419.91	4091.07	34.59
Kianika-1	200.4	58.01	2068.61	2240	29.01		0
Kianika-1	235.4	89.26	2128.61	2280.13	35.32	5544.59	-9.31
Kianika-1	270.4	119.96	2167.39	2726.92	41.63	5544.59	-18.35
Kianika-1	305.4	145.63	2266.02	3486.06	47.94	5544.59	-24.87
Kianika-1	340.4	165.71	2413.86	5105.76	54.25	5544.59	-28.6
Kianika-1	375.4	179.42	2619.55	2012.65	60.57	5544.59	-29.14
Kianika-1	410.4	214.2	2521.01	4027.62	66.88	5544.59	-40.22
Kianika-1	445.4	231.58	2634.08	2366.46	73.19	5544.59	-42.6
Kianika-1	480.4	261.16	2603.77	3156.71	79.5	5544.59	-51.08
Kianika-1	550.4	305.51	2684.04	3125	92.13	5544.59	-60.63
Kianika-1	585.4	327.91	2714.16	3745.32	98.44	5544.59	-65.51
Kianika-1	620.4	346.6	2769.76	2846.69	104.75	5544.59	-68.55
Kianika-1	655.4	371.19	2774.86	5131.96	111.07	5544.59	-74.53
Kianika-1	690.4	384.83	2858.41	2736.51	117.38	5544.59	-75.04
Kianika-1	725.4	410.41	2850.81	3651.54	123.69	5544.59	-81.51
Kianika-1	760.4	429.58	2886.54	4011.46	130	5544.59	-84.79
Kianika-1	795.4	447.03	2930.45	2990.57	136.32	5544.59	-87.2
Kianika-1	830.3	470.37	2933.44	4241.69	142.61	5544.6	-92.57
Kianika-1	865.4	486.92	2977.9	3153.15	148.94	5544.58	-94.52
Kianika-1	900.4	509.12	2985.54	2923.98	155.25	5544.59	-99.31
Kianika-1	935.4	533.06	2982.78	3636.36	161.57	5544.59	-104.96
Kianika-1	970.4	552.31	3005.56	3055.43	167.89	5532.55	-108.26
Kianika-1	1005.4	575.22	3007.54	6796.12	174.29	5473.06	-113.32

Kianika-1	1075.4	595.82	3138.53	2753.45	187.38	5346.14	-110.53
Kianika-1	1110.3	621.17	3122.82	3650.55	196.82	3696.58	-113.76
Kianika-1	1145.4	640.4	3138.66	3930.38	204.91	4342.64	-115.29
Kianika-1	1180.4	658.21	3160.09	4927.84	212.75	4462.22	-116.36
Kianika-1	1250.4	686.62	3233.23	2359.29	231.01	3833.02	-112.3
Kianika-1	1285.4	716.29	3197.03	4286.59	240.01	3887.3	-118.13
Kianika-1	1355.4	748.95	3244.54	3151.73	258.58	3769.76	-115.89
Kianika-1	1390.4	771.16	3241.87	6283.66	267.98	3725.9	-117.6
Kianika-1	1425.4	782.3	3285.18	3277.15	277	3877.35	-114.15
Kianika-1	1460.4	803.66	3284.97	2568.81	285.56	4092.27	-116.27
Kianika-1	1495.4	830.91	3261.48	3428.01	293.91	4189.52	-121.54
Kianika-1	1530.4	851.33	3265.48	2794.41	301.85	4410.33	-123.82
Kianika-1	1565.4	876.38	3252.01	5656.57	310.42	4082.48	-127.77
Kianika-1	1635.4	901.13	3318.06	4461.44	327.7	4051.2	-122.87
Kianika-1	1670.4	916.82	3337.62	4691.69	335.94	4245.63	-122.47
Kianika-1	1705.4	931.74	3359.31	3828.27	343.94	4374.27	-121.93
Kianika-1	1775.4	968.31	3377.02	3323.81	360.31	4276.28	-123.84

Kianika-1	1810.3	989.31	3375.89	2708.98	369.01	4014.07	-125.65
Kianika-1	1845.3	1015.15	3358.91				
Lukuledi-1	47	0		2590.89	0		0
Lukuledi-1	93.95	36.24	2590.89	3649.15	19.5	2406.94	1.38
Lukuledi-1	678.98	356.88	3541.68	3613.85	245.28	2591.16	66.84
Lukuledi-1	1306.96	704.42	3577.29		417.36	3649.48	65.15
Liwale-1	342.19	-73.06	4415.96	4415.96	-36.53		0
Liwale-1	503.5	0		5015.14	7.52	3662.2	7.52
Liwale-1	1594.8	435.2	5015.14		247.13	4554.37	29.53

Appendix 2.3.1 – Summary of the 2D seismic lines used in this thesis. The columns represent: Name – seismic line name, Domain – Time or Depth, Type of data (2D), Direction of the seismic line, Attribute Seismic time, Original Coordinate Reference System.

Name	Domain	Type	Direction	Attribute	Original CRS
78-2-023	Time	2D	Northeast	Seismic Time	UTM84-37S
78-2-60	Time	2D	West	Seismic Time	UTM84-37S
78-2-62	Time	2D	Southeast	Seismic Time	UTM84-37S
78-2-66	Time	2D	Northwest	Seismic Time	UTM84-37S
82-SE-02	Time	2D	East	Seismic Time	UTM84-37S
82-SE-03	Time	2D	Northwest	Seismic Time	UTM84-37S
82-SE-04N	Time	2D	Northeast	Seismic Time	UTM84-37S
82-SE-05T2	Time	2D	Northeast	Seismic Time	UTM84-37S
82-SE-06	Time	2D	Northwest	Seismic Time	UTM84-37S
82-SE-07	Time	2D	Southeast	Seismic Time	UTM84-37S
82-SE-08	Time	2D	Southeast	Seismic Time	UTM84-37S
82-SE-21	Time	2D	Southeast	Seismic Time	UTM84-37S
82-SE-21T	Time	2D	Southeast	Seismic Time	UTM84-37S
82-SE-22B	Time	2D	Southeast	Seismic Time	UTM84-37S
82-SE-23	Time	2D	Southeast	Seismic Time	UTM84-37S
83-2-24	Time	2D	Southwest	Seismic Time	UTM84-37S
83-2-26	Time	2D	Northeast	Seismic Time	UTM84-37S
83-2-30	Time	2D	Southwest	Seismic Time	UTM84-37S
83-RK-04	Time	2D	Northeast	Seismic Time	UTM84-37S
83-RK-20	Time	2D	Southeast	Seismic Time	UTM84-37S

83-RK-40	Time	2D	Southeast	Seismic Time	UTM84-37S
83-RK-96	Time	2D	Northeast	Seismic Time	UTM84-37S
83-SE-46	Time	2D	Northeast	Seismic Time	UTM84-37S
83-SE-47	Time	2D	Northeast	Seismic Time	UTM84-37S
83-SE-50	Time	2D	Northwest	Seismic Time	UTM84-37S
83-SE-51	Time	2D	Southeast	Seismic Time	UTM84-37S
84-SE-52	Time	2D	Northwest	Seismic Time	UTM84-37S
84-SE-53	Time	2D	Southeast	Seismic Time	UTM84-37S
84-SE-54	Time	2D	Southeast	Seismic Time	UTM84-37S
84-SE-55	Time	2D	Southeast	Seismic Time	UTM84-37S
84-SE-56	Time	2D	Northeast	Seismic Time	UTM84-37S
84-SE-57	Time	2D	Northeast	Seismic Time	UTM84-37S
84-SE-58	Time	2D	Northeast	Seismic Time	UTM84-37S
84-SE-59	Time	2D	Southwest	Seismic Time	UTM84-37S
84-SE-60	Time	2D	Northeast	Seismic Time	UTM84-37S
84-SE-61	Time	2D	Southeast	Seismic Time	UTM84-37S
84-SE-62	Time	2D	Southeast	Seismic Time	UTM84-37S
84-SE-64	Time	2D	Southeast	Seismic Time	UTM84-37S
84-SE-66	Time	2D	Northeast	Seismic Time	UTM84-37S
84-SE-67	Time	2D	Northeast	Seismic Time	UTM84-37S
84-SE-68	Time	2D	Northeast	Seismic Time	UTM84-37S
99	Time	2D	South	Seismic Time	UTM84-37S
99MW-1_d	Time	2D	Northeast	Seismic Time	UTM84-37S
99MW-2_d	Time	2D	Northeast	Seismic Time	UTM84-37S
99MW-3_d	Time	2D	Northeast	Seismic Time	UTM84-37S

99MW-4_d	Time	2D	Northeast	Seismic Time	UTM84-37S
99MW-5_d	Time	2D	North	Seismic Time	UTM84-37S
99MW-6_d	Time	2D	Southeast	Seismic Time	UTM84-37S
99MW-7_d	Time	2D	Southeast	Seismic Time	UTM84-37S
99MW-8_d	Time	2D	South	Seismic Time	UTM84-37S
99MW-8_d_NEW	Time	2D	South	Seismic Time	UTM84-37S
99MW-9_d	Time	2D	Southeast	Seismic Time	UTM84-37S
99-MW-10_d	Time	2D	Southeast	Seismic Time	UTM84-37S
101E	Time	2D	West	Seismic Time	UTM84-37S
101sp101-1	Time	2D	South	Seismic Time	UTM84-37S
101sp20783-20890	Time	2D	South	Seismic Time	UTM84-37S
101sp20891-20980	Time	2D	South	Seismic Time	UTM84-37S
258WSP120-168	Time	2D	East	Seismic Time	UTM84-37S
267 B	Time	2D	North	Seismic Time	UTM84-37S
267	Time	2D	North	Seismic Time	UTM84-37S
270W	Time	2D	Southeast	Seismic Time	UTM84-37S
310	Time	2D	East	Seismic Time	UTM84-37S
310Wsp36-1	Time	2D	East	Seismic Time	UTM84-37S
310Wsp85-37	Time	2D	East	Seismic Time	UTM84-37S
9455-87	Time	2D	Southeast	Seismic Time	UTM84-37S
781084	Time	2D	Northwest	Seismic Time	UTM84-37S
781084N	Time	2D	Northwest	Seismic Time	UTM84-37S
781102	Time	2D	Northeast	Seismic Time	UTM84-37S
781105	Time	2D	West	Seismic Time	UTM84-37S
BIG97-1	Time	2D	Southwest	Seismic Time	UTM84-37S

BIG97-2	Time	2D	Southwest	Seismic Time	UTM84-37S
BIG97-3	Time	2D	South	Seismic Time	UTM84-37S
BIG97-4	Time	2D	South	Seismic Time	UTM84-37S
BIG97-7	Time	2D	Southwest	Seismic Time	UTM84-37S
DOM-06-KID-01	Time	2D	East	Seismic Time	UTM84-37S
DOM-06-KID-02	Time	2D	North	Seismic Time	UTM84-37S
DOM-06-KID-03	Time	2D	East	Seismic Time	UTM84-37S
DOM-06-KID-04	Time	2D	East	Seismic Time	UTM84-37S
DOM-06-KID-05	Time	2D	North	Seismic Time	UTM84-37S
DOM-06-MIH-01	Time	2D	East	Seismic Time	UTM84-37S
DOM-06-MIH-02	Time	2D	East	Seismic Time	UTM84-37S
DOM-06-MIH-03	Time	2D	Northwest	Seismic Time	UTM84-37S
DOM-06-MIH-04	Time	2D	North	Seismic Time	UTM84-37S
DOM-06-MKREG	Time	2D	Northwest	Seismic Time	UTM84-37S
DOM-06-MNE-01	Time	2D	North	Seismic Time	UTM84-37S
DOM-06-MNE-02	Time	2D	East	Seismic Time	UTM84-37S
DOM-06-MNE-04	Time	2D	East	Seismic Time	UTM84-37S
DOM-06-MNE-05	Time	2D	East	Seismic Time	UTM84-37S
KIM 08-106-1 MP07-06	Time	2D	South	Seismic Time	UTM84-37S
KIM 08-107-1	Time	2D	Southeast	Seismic Time	UTM84-37S
KIMB 08-101-1	Time	2D	East	Seismic Time	UTM84-37S
KIMB 08-102-1	Time	2D	North	Seismic Time	UTM84-37S
KIMB 08-103-1	Time	2D	East	Seismic Time	UTM84-37S
KIMB 08-105-1	Time	2D	East	Seismic Time	UTM84-37S
KIMB 08-108-1	Time	2D	North	Seismic Time	UTM84-37S

KIS-08-101	Time	2D	Southeast	Seismic Time	UTM84-37S
KIS-98-01_RAW_PSTM_STK	Time	2D	South	Seismic Time	UTM84-37S
MC-89-236ABCD	Time	2D	Southeast	Seismic Time	UTM84-37S
MDW07-01	Time	2D	Northeast	Seismic Time	UTM84-37S
MDW07-02	Time	2D	Southeast	Seismic Time	UTM84-37S
MDW07-03	Time	2D	Northeast	Seismic Time	UTM84-37S
MDW07-04	Time	2D	Southeast	Seismic Time	UTM84-37S
MDW07-05	Time	2D	Northeast	Seismic Time	UTM84-37S
MDW07-07	Time	2D	Northeast	Seismic Time	UTM84-37S
MDW07-09	Time	2D	Northeast	Seismic Time	UTM84-37S
MDW07-11	Time	2D	East	Seismic Time	UTM84-37S
MDW07-13	Time	2D	East	Seismic Time	UTM84-37S
MW-87-215	Time	2D	East	Seismic Time	UTM84-37S
MW-87-218	Time	2D	East	Seismic Time	UTM84-37S
MW-87-221	Time	2D	East	Seismic Time	UTM84-37S
MW-87-227	Time	2D	East	Seismic Time	UTM84-37S
MW-87-227-E	Time	2D	East	Seismic Time	UTM84-37S
MW-87-233	Time	2D	East	Seismic Time	UTM84-37S
MW-87-236	Time	2D	East	Seismic Time	UTM84-37S
MW-87-239	Time	2D	East	Seismic Time	UTM84-37S
MW-87-242	Time	2D	East	Seismic Time	UTM84-37S
MW-87-245	Time	2D	East	Seismic Time	UTM84-37S
MW-87-248	Time	2D	East	Seismic Time	UTM84-37S
MW-87-251	Time	2D	East	Seismic Time	UTM84-37S
MW-87-253	Time	2D	East	Seismic Time	UTM84-37S

MW-87-256	Time	2D	East	Seismic Time	UTM84-37S
MW-87-305	Time	2D	North	Seismic Time	UTM84-37S
MW-87-308	Time	2D	North	Seismic Time	UTM84-37S
MW-87-314	Time	2D	North	Seismic Time	UTM84-37S
MW-87-315	Time	2D	North	Seismic Time	UTM84-37S
MW-87-317	Time	2D	North	Seismic Time	UTM84-37S
MW-87-318	Time	2D	Northwest	Seismic Time	UTM84-37S
MW-87-326	Time	2D	North	Seismic Time	UTM84-37S
MW-88-205	Time	2D	East	Seismic Time	UTM84-37S
MW-88-208	Time	2D	East	Seismic Time	UTM84-37S
MW-88-210	Time	2D	East	Seismic Time	UTM84-37S
MW-88-213	Time	2D	East	Seismic Time	UTM84-37S
MW-88-214	Time	2D	East	Seismic Time	UTM84-37S
MW-88-241	Time	2D	East	Seismic Time	UTM84-37S
MW-88-243	Time	2D	East	Seismic Time	UTM84-37S
MW-88-246	Time	2D	East	Seismic Time	UTM84-37S
MW-88-248	Time	2D	East	Seismic Time	UTM84-37S
MW-88-251	Time	2D	East	Seismic Time	UTM84-37S
MW-88-253nav	Time	2D	East	Seismic Time	UTM84-37S
MW-88-258	Time	2D	East	Seismic Time	UTM84-37S
MW-88-258_d	Time	2D	East	Seismic Time	UTM84-37S
MW-88-262_d	Time	2D	East	Seismic Time	UTM84-37S
MW-88-268_d	Time	2D	East	Seismic Time	UTM84-37S
MW-88-311	Time	2D	North	Seismic Time	UTM84-37S
MW-88-312_d	Time	2D	North	Seismic Time	UTM84-37S

MW-88-313_d	Time	2D	North	Seismic Time	UTM84-37S
MW-88-315_d	Time	2D	North	Seismic Time	UTM84-37S
MW-88-316	Time	2D	North	Seismic Time	UTM84-37S
MW-88-317	Time	2D	North	Seismic Time	UTM84-37S
MW-88-320	Time	2D	North	Seismic Time	UTM84-37S
MW-88-323	Time	2D	North	Seismic Time	UTM84-37S
MW-88-332_d	Time	2D	North	Seismic Time	UTM84-37S
MW-88-334	Time	2D	North	Seismic Time	UTM84-37S
TL101B	Time	2D	South	Seismic Time	UTM84-37S
TL-105_d	Time	2D	North	Seismic Time	UTM84-37S
TL-105_RAW_PSTM_STK	Time	2D	North	Seismic Time	UTM84-37S
TL-109_d	Time	2D	North	Seismic Time	UTM84-37S
TL-109_RAW_PSTM_STK	Time	2D	North	Seismic Time	UTM84-37S
TL-110_d	Time	2D	East	Seismic Time	UTM84-37S
TL-111_d	Time	2D	North	Seismic Time	UTM84-37S
TL-113	Time	2D	North	Seismic Time	UTM84-37S
TL-116_d	Time	2D	East	Seismic Time	UTM84-37S
TL-116_RAW_PSTM_STK	Time	2D	East	Seismic Time	UTM84-37S
TL-117_d	Time	2D	North	Seismic Time	UTM84-37S
TL-118_2d_nav	Time	2D	East	Seismic Time	UTM84-37S
TL-120_d	Time	2D	East	Seismic Time	UTM84-37S
TL-122-2_RAW_PSTM_STK	Time	2D	East	Seismic Time	UTM84-37S
TL-122-PSTM_STK_DAS	Time	2D	East	Seismic Time	UTM84-37S
TL-124-A	Time	2D	East	Seismic Time	UTM84-37S
TL-128_d	Time	2D	East	Seismic Time	UTM84-37S

TL-138_d	Time	2D	East	Seismic Time	UTM84-37S
TL-140_d	Time	2D	East	Seismic Time	UTM84-37S
TLVB-105_PSTM_STK_DAS	Time	2D	North	Seismic Time	UTM84-37S
TLVB-110_d	Time	2D	East	Seismic Time	UTM84-37S
TLVB-110_PSTM_STK_DAS	Time	2D	East	Seismic Time	UTM84-37S
TLVB-115_d	Time	2D	Northwest	Seismic Time	UTM84-37S
TLVB-122_d	Time	2D	East	Seismic Time	UTM84-37S
TLVB-124_d	Time	2D	East	Seismic Time	UTM84-37S
TLVB-126_d	Time	2D	East	Seismic Time	UTM84-37S
TLVB-130-2_d	Time	2D	Northeast	Seismic Time	UTM84-37S
TLVB-130-3_d	Time	2D	East	Seismic Time	UTM84-37S
TLVB-148_d	Time	2D	East	Seismic Time	UTM84-37S
TLVB-149_d	Time	2D	North	Seismic Time	UTM84-37S
TLVB-149-3_d	Time	2D	North	Seismic Time	UTM84-37S
TLVB-151_d	Time	2D	North	Seismic Time	UTM84-37S
TLVB-154_d	Time	2D	East	Seismic Time	UTM84-37S
TLVB-155_d	Time	2D	North	Seismic Time	UTM84-37S
TLVB-155-2_d	Time	2D	Northwest	Seismic Time	UTM84-37S
TLVB-155-3_d	Time	2D	North	Seismic Time	UTM84-37S
TLVB-157_d	Time	2D	North	Seismic Time	UTM84-37S
TLVB-159_d	Time	2D	North	Seismic Time	UTM84-37S
TNZ81-110	Time	2D	East	Seismic Time	UTM84-37S
TNZ81-114	Time	2D	East	Seismic Time	UTM84-37S
TNZ81-115	Time	2D	East	Seismic Time	UTM84-37S
TNZ81-116	Time	2D	North	Seismic Time	UTM84-37S

TNZ81-117	Time	2D	North	Seismic Time	UTM84-37S
TNZ81-118	Time	2D	North	Seismic Time	UTM84-37S
TNZ81-119	Time	2D	Southwest	Seismic Time	UTM84-37S
TNZ81-119EXT	Time	2D	Southwest	Seismic Time	UTM84-37S
TNZ83-101T	Time	2D	North	Seismic Time	UTM84-37S
TNZ83-102	Time	2D	Northeast	Seismic Time	UTM84-37S
TNZ83-103	Time	2D	Northeast	Seismic Time	UTM84-37S
TNZ83-104-A	Time	2D	North	Seismic Time	UTM84-37S
TNZ83-104-B	Time	2D	North	Seismic Time	UTM84-37S
TNZ83-104-C	Time	2D	North	Seismic Time	UTM84-37S
TNZ83-108-A	Time	2D	East	Seismic Time	UTM84-37S
TNZ83-108-B	Time	2D	East	Seismic Time	UTM84-37S
TNZ83-108-C	Time	2D	East	Seismic Time	UTM84-37S
TNZ83-109-A	Time	2D	East	Seismic Time	UTM84-37S
TNZ83-109-B	Time	2D	East	Seismic Time	UTM84-37S
TNZ83-109-C	Time	2D	East	Seismic Time	UTM84-37S
TNZ83-109-D	Time	2D	East	Seismic Time	UTM84-37S
TL-101-A_RAW_PSTM_STK	Time	2D	North	Seismic Time	UTM84-37S
TL-101A_d - 1	Time	2D	North	Seismic Time	UTM84-37S
TL-101A_d - 2	Time	2D	Southwest	Seismic Time	UTM84-37S
TL-101A_d - 3	Time	2D	Northwest	Seismic Time	UTM84-37S
TL-101A_d - 4	Time	2D	Southwest	Seismic Time	UTM84-37S
TL-101A_d - 5	Time	2D	North	Seismic Time	UTM84-37S
MW-88-330_d	Time	2D	North	Seismic Time	UTM84-37S

Appendix 2.4 – Summary of the Shapefile for Mandawa Block imported in the study. Polyline, Vert, UTM coordinate X, UTM coordinate Y, Z value.

Poly	Vert	X	Y	Z
1	1	490845	8986813	0
1	2	500000	8986814	0
1	3	500000	8977601	0
1	4	509153	8977600	0
1	5	509147	8949963	0
1	6	518294	8949959	0
1	7	518285	8931534	0
1	8	545712	8931511	0
1	9	545723	8940724	0
1	10	554868	8940711	0
1	11	554920	8977563	0
1	12	545767	8977575	0
1	13	545788	8996000	0
1	14	536630	8996009	0
1	15	536696	9069708	0
1	16	527522	9069715	0
1	17	527533	9088139	0
1	18	490822	9088146	0
1	19	490845	8986813	0

Appendix 4.5 – Summary of Well tops from Selous Basin. Well name, well top (marker), respective sequence stratigraphy surface, coordinate X, coordinate Y, MD – Measure Depth, automatic Two-way-time corresponding.

Well	Surface	X	Y	Z	MD	TWT auto
Liwale-1	Jurassic Breakup	337629.4	8957111	33.23	470.27	-15.05
Liwale-1	Karoo Upper Triassic	337629.4	8957111	-260.13	763.63	105.55
Liwale-1	Karoo Middle Triassic	337629.4	8957111	-766.56	1270.06	311.04
Liwale-1	Karoo Lower Triassic	337629.4	8957111	-923.03	1426.53	374.53
Liwale-1	Precambrian Basement	337629.4	8957111	-1192.9	1696.43	484.04

Appendix 4.6 – Summary of Well tops from Mandawa Basin. Well name, well top (marker), respective sequence stratigraphy surface, coordinate X, coordinate Y, MD – Measure Depth, automatic Two-way-time corresponding.

Well	Well top	Sequence stratigraphy surface	X	Y	Z	MD	TWT auto
East Lika-1	Horizon G	Lower Cretaceous Unconformity	507431	8974961	-142.51	149.51	102.68
East Lika-1	Horizon F	Upper Jurassic - Lower Cretaceous SB	507431	8974961	-499.64	506.64	335.18
East Lika-1	Horizon E	Middle - Upper Jurassic Transgression	507431	8974961	-583.88	590.88	374.37
East Lika-1	Horizon D	Lower Jurassic Transgression	507431	8974961	-1026.8	1033.75	553.99
East Lika-1	Horizon C	Triassic - Lower Jurassic Base Evaporite	507431	8974961	-1433	1440.03	732.05
East Lika-1	Horizon B	Precambrian - Cambrian Basement	507431	8974961	-1537.9	1544.91	782.52
Kianika-1	Horizon H	Lower Cretaceous TS	512437.1	9073566	-870.09	1010.49	318.67
Kianika-1	Horizon G	Lower Cretaceous Unconformity	512437.1	9073566	-918.54	1058.94	339.17
Kianika-1	Horizon F	Upper Jurassic - Lower Cretaceous SB	512437.1	9073566	-960.79	1101.19	360
Kianika-1	Horizon B	Precambrian - Cambrian Basement	512437.1	9073566	-1357.7	1498.07	554.38
Kizimbani-1	Horizon F	Upper Jurassic - Lower Cretaceous SB	540110	9001125	-246.88	253.88	113.06
Kizimbani-1	Horizon D	Lower Jurassic Transgression	540110	9001125	-337.52	344.52	154.97
Kizimbani-1	Horizon C	Triassic - Lower Jurassic Base Evaporite	540110	9001125	-448.05	455.05	206.49
Kizimbani-1	Horizon B	Precambrian - Cambrian Basement	540110	9001125	-1000.4	1007.41	490.34
Lukuledi-1	Horizon H	Lower Cretaceous TS	572953	8876193	-349.93	396.93	236.25
Lukuledi-1	Horizon G	Lower Cretaceous Unconformity	572953	8876193	-631.98	678.98	422.42
Lukuledi-1	Horizon B	Precambrian - Cambrian Basement	572953	8876193	-1260	1306.96	768.28
Lukuliro-1	Horizon H	Lower Cretaceous TS	437042	9076079	-399.99	528.49	213.34
Lukuliro-1	Horizon G	Lower Cretaceous Unconformity	437042	9076079	-680.89	809.39	358.76
Lukuliro-1	Horizon F	Upper Jurassic - Lower Cretaceous SB	437042	9076079	-734.6	863.1	384.93
Lukuliro-1	Horizon E	Middle - Upper Jurassic Transgression	437042	9076079	-831.9	960.4	426.83
Lukuliro-1	Horizon D	Lower Jurassic Transgression	437042	9076079	-1666.9	1795.37	759.47
Lukuliro-1	Horizon B	Precambrian - Cambrian Basement	437042	9076079	-1682.4	1810.88	765.88

Mandawa-7	Horizon C	Triassic - Lower Jurassic Base Evaporite	545857	8959104	-79.47	249.47	0
Mbate-1	Horizon H	Lower Cretaceous TS	497250	9014200	-219.42	319.42	144.31
Mbate-1	Horizon G	Lower Cretaceous Unconformity	497250	9014200	-539.26	639.26	349.62
Mbate-1	Horizon F	Upper Jurassic - Lower Cretaceous SB	497250	9014200	-826.85	926.85	516.41
Mbate-1	Horizon D	Lower Jurassic Transgression	497250	9014200	-1144.1	1244.07	680.48
Mbate-1	Horizon C	Triassic - Lower Jurassic Base Evaporite	497250	9014200	-1220.3	1320.27	719.9
Mbate-1	Horizon B	Precambrian - Cambrian Basement	497250	9014200	-2336.7	2436.71	1297.38
Mbuo-1	Horizon G	Lower Cretaceous Unconformity	530829	8955956	-47.55	196.35	30.2
Mbuo-1	Horizon F	Upper Jurassic - Lower Cretaceous SB	530829	8955956	-126	274.8	79
Mbuo-1	Horizon E	Middle - Upper Jurassic Transgression	530829	8955956	-243.76	392.56	144.49
Mbuo-1	Horizon D	Lower Jurassic Transgression	530829	8955956	-603.26	752.06	339.15
Mbuo-1	Horizon C	Triassic - Lower Jurassic Base Evaporite	530829	8955956	-675.66	824.46	377.24
Mbuo-1	Horizon B	Precambrian - Cambrian Basement	530829	8955956	-849.97	998.77	468.07
Mihambia-1	Horizon H	Lower Cretaceous TS	524183	8972728	-266.18	477.78	186.29
Mihambia-1	Horizon G	Lower Cretaceous Unconformity	524183	8972728	-342.94	554.54	239.31
Mihambia-1	Horizon F	Upper Jurassic - Lower Cretaceous SB	524183	8972728	-728.53	940.13	469.89
Mihambia-1	Horizon E	Middle - Upper Jurassic Transgression	524183	8972728	-1154.5	1366.12	690.71
Mihambia-1	Horizon D	Lower Jurassic Transgression	524183	8972728	-1509.4	1720.95	859.66
Mihambia-1	Horizon C	Triassic - Lower Jurassic Base Evaporite	524183	8972728	-1762.4	1973.97	981.64
Mihambia-1	Horizon B	Precambrian - Cambrian Basement	524183	8972728	-1987.4	2199.03	1091.09
Mita Gamma-1	Horizon G	Lower Cretaceous Unconformity	518126	9014547	-548.68	555.68	347.78
Mita Gamma-1	Horizon F	Upper Jurassic - Lower Cretaceous SB	518126	9014547	-942.04	949.04	572.02
Mita Gamma-1	Horizon E	Middle - Upper Jurassic Transgression	518126	9014547	-2048.4	2055.43	1057.75
Mita Gamma-1	Horizon C	Triassic - Lower Jurassic Base Evaporite	518126	9014547	-2072.2	2079.18	1067.49
Mita Gamma-1	Horizon B	Precambrian - Cambrian Basement	518126	9014547	-2117.7	2124.74	1088.03

Appendix 4.7 – Summary of Zones in Mandawa Basin. Well (well name), Start Measure Depth (MD), Zone log, DT – Sonic log.

Well	Start MD	Zone log	DT
East Lika-1	149.51	Zone G	110.2
East Lika-1	506.64	Zone F	88.3
East Lika-1	590.88	Zone E - Mtumbei Limestone Fm.	53.5
East Lika-1	1033.75	Zone D - Mihambia Fm.	70.1
East Lika-1	1440.03	Zone C - Nondwa Fm.	66
East Lika-1	1544.91	Zone B - Mbuo Fm.	80.6
East Lika-1	1942.02	Zone A	
Kianika-1	1010.49	Zone H	55.8
Kianika-1	1058.94	Zone G	73.2
Kianika-1	1101.19	Zone F	77
Kianika-1	1498.07	Zone B - Mbuo Fm.	72.3
Kianika-1	1771.47	Zone A	
Kizimbani-1	253.88	Zone F	69.8
Kizimbani-1	344.52	Zone D - Mihambia Fm.	71.1
Kizimbani-1	455.05	Zone C - Nondwa Fm.	70.9
Kizimbani-1	1007.41	Zone B - Mbuo Fm.	86.5
Kizimbani-1	2615.02	Zone A	
Lukuledi-1	396.93	Zone H	117.7
Lukuledi-1	678.98	Zone C - Nondwa Fm.	83.5
Lukuledi-1	1306.96	Zone B - Mbuo Fm.	84.3
Lukuliro-1	528.49	Zone H	81.3
Lukuliro-1	809.39	Zone G	76.5
Lukuliro-1	863.1	Zone F	72
Lukuliro-1	960.4	Zone E - Mtumbei Limestone Fm.	59.3
Lukuliro-1	1795.37	Zone D - Mihambia Fm.	62.2
Lukuliro-1	1810.88	Zone B - Mbuo Fm.	68
Lukuliro-1	2347.14	Zone A	
Mandawa-7	249.47	Zone C - Nondwa Fm.	
Mandawa-7	3866.96	Zone A	
Mbate-1	319.42	Zone H	100.2
Mbate-1	639.26	Zone G	95.4
Mbate-1	926.85	Zone F	84.1
Mbate-1	1244.07	Zone D - Mihambia Fm.	
Mbate-1	1320.27	Zone C - Nondwa Fm.	73.6
Mbate-1	2436.71	Zone B - Mbuo Fm.	
Mbate-1	2601.49	Zone A	
Mbuo-1	196.35	Zone G	96.8
Mbuo-1	274.8	Zone F	92.8
Mbuo-1	392.56	Zone E - Mtumbei Limestone Fm.	76.7

Mbuo-1	752.06	Zone D - Mihambia Fm.	88.4
Mbuo-1	824.46	Zone C - Nondwa Fm.	72
Mbuo-1	998.77	Zone B - Mbuo Fm.	86.3
Mbuo-1	3175.55	Zone A	
Mihambia-1	477.78	Zone H	106.7
Mihambia-1	554.54	Zone G	104
Mihambia-1	940.13	Zone F	89.7
Mihambia-1	1366.12	Zone E - Mtumbei Limestone Fm.	
Mihambia-1	1720.95	Zone D - Mihambia Fm.	70.2
Mihambia-1	1973.97	Zone C - Nondwa Fm.	73.3
Mihambia-1	2199.03	Zone B - Mbuo Fm.	
Mihambia-1	2262.57	Zone A	
Mita Gamma-1	555.68	Zone G	96.6
Mita Gamma-1	949.04	Zone F	77.2
Mita Gamma-1	2055.43	Zone E - Mtumbei Limestone Fm.	56.7
Mita Gamma-1	2079.18	Zone C - Nondwa Fm.	66.8
Mita Gamma-1	2124.74	Zone B - Mbuo Fm.	70.6
Mita Gamma-1	2305.37	Zone A	

Appendix 7.2.2 – Summary of faults interpreted in Mandawa Basin. Fault name, Resolution - Type the average triangle edge length in horizontal distance project units, form of the tip loop and Extrapolation - Type an extension of the tip loop in horizontal distance project units.

Fault name	Resolution	Tip loop	Extrapolation
Main_Normal_Fault_DOM-06-MIH-04	200.00	Convex hull	50.00
Fault 1 Normal_DOM-06-MIH-04	200.00	Convex hull	50.00
Fault_DOM-06-KID-01_Normal	200.00	Convex hull	50.00
Fault in MW-87-236	200.00	Convex hull	50.00
Fault in MW-87-239	200.00	Convex hull	50.00
Fault in DOM_06-KID-05_Normal	200.00	Convex hull	50.00
Fault in DOM_06-KID-03_Normal	200.00	Convex hull	50.00
Fault in DOM_06-KID-02_Normal	200.00	Convex hull	50.00
Fault in DOM_06-KID-01_Normal	200.00	Convex hull	50.00
Fault in DOM-06-MKREG_Normal	200.00	Convex hull	50.00
Fault Normal_DOM-06-MIH-02	200.00	Convex hull	50.00
Fault Normal_DOM-06-MIH-03	200.00	Convex hull	50.00
Fault DOM-06-MNE-01	200.00	Convex hull	50.00
Fault DOM-06-MNE-02	200.00	Convex hull	50.00
Fault DOM-06-MNE-04	200.00	Convex hull	50.00
Fault DOM-06-MNE-05	200.00	Convex hull	50.00

Fault in 99MW-4_d MITA	200.00	Convex hull	50.00
Fault TLVB-148_d	200.00	Convex hull	50.00
Fault TLVB-149_3_d	200.00	Convex hull	50.00
Fault 99MW-1_d	200.00	Convex hull	50.00
Fault 99 MW-2_d	200.00	Convex hull	50.00
Fault TL101B	200.00	Convex hull	50.00
Fault TL-117_d	200.00	Convex hull	50.00

Appendix 7.5 – Summary of wells that checkshots were used to produce the velocity model. From two-way-time (ms) to Z (depth) in (m); coordinates XY in (m). Horizon name, X-value, Y-value, Z-value, Horizon after, Difference after.

Velocity model						
From:	**TWT [ms]**					
To:	**Z [m]**					
XY:	**[m]**					
Horizon G	Well	X-value	Y-value	Z-value	Horizon after	Diff after
	Mita Gamma-1	518126	9014547	-548.68	-896.64	347.96
	Lukuliro-1	437042	9076079	-680.89	Outside	
	Mihambia-1	524183	8972728	-340.78	-896.87	556.09
	Kianika-1	512437.1	9073566	-918.54	-751.92	-166.62
Horizon F	Well	X-value	Y-value	Z-value	Horizon after	Diff after
	Mita Gamma-1	518126	9014547	-942.04	-896.64	-45.41
	Lukuliro-1	437042	9076079	-734.6	Outside	
	Mihambia-1	524183	8972728	-728.53	-896.87	168.33
	Kianika-1	512437.1	9073566	-960.79	-751.92	-208.87
Horizon E	Well	X-value	Y-value	Z-value	Horizon after	Diff after
	Mita Gamma-1	518126	9014547	2048.43	-907.87	-1140.56
	Lukuliro-1	437042	9076079	-831.9	Outside	
	Mihambia-1	524183	8972728	1088.18	-896.87	-191.31
Horizon D	Well	X-value	Y-value	Z-value	Horizon after	Diff after
	Lukuliro-1	437042	9076079	1666.87	Outside	
	Mihambia-1	524183	8972728	1509.35	-896.87	-612.49
Horizon C	Well	X-value	Y-value	Z-value	Horizon after	Diff after
	Mita Gamma-1	518126	9014547	2072.18	-907.87	-1164.31
	Mihambia-1	524183	8972728	1755.61	-896.87	-858.74
Horizon B	Well	X-value	Y-value	Z-value	Horizon after	Diff after
	Mita Gamma-1	518126	9014547	2117.74	-958.17	-1159.57
	Lukuliro-1	437042	9076079	1682.38	Outside	

	Mihambia-1	524183	8972728	1997.59	-1079.56	-918.02
	Kianika-1	512437.1	9073566	1357.67	-941.21	-416.46
Horizon A	Well	X-value	Y-value	Z-value	Horizon after	Diff after
	Mita Gamma-1	518126	9014547	2298.37	-1039.03	-1259.35
	Lukuliro-1	437042	9076079	2218.64	Outside	
	Mihambia-1	524183	8972728	2050.97	-2334.94	283.97
	Kianika-1	512437.1	9073566	1631.07	-1031.92	-599.15